

# **Impairment of endothelial TRPV4 channel signaling in obesity**

Matteo Ottolini

Cremona, Italy

Master of Science in Biomedical Science

University of Virginia, 2019

Doctor of Pharmacy (PharmD),

University of Parma, Italy, 2014

A Dissertation presented to the Graduate Faculty of the University of Virginia in Candidacy for  
the Degree of Doctor of Philosophy

Department of Pharmacology

University of Virginia

In the memory of  
Nonna Linda and Zio Alberto

*“Consciousness begins when brains acquire the power, the simple power I must add, of telling a  
story”*

Antonio Damasio

## Table of Contents

### **Chapter 1: The Calcium Signaling Mechanisms in Arterial Endothelial Cells** 8

1.1 Abstract

1.2 Introduction

1.3 Methodologies for recording  $\text{Ca}^{2+}$  signals

1.4 Endothelial cell  $\text{Ca}^{2+}$  signals in small arteries and arterioles

1.4.1  $\text{Ca}^{2+}$  influx from extracellular compartment

1.4.2  $\text{Ca}^{2+}$  release from intracellular compartments

1.5 Signaling targets of  $\text{Ca}^{2+}$  in ECs

1.6 Abnormal  $\text{Ca}^{2+}$  signaling in vascular disorders

1.7 Conclusion

### **Chapter 2: Materials and Methods** 47

2.1 Materials and Methods for Chapter 3

2.2 Materials and Methods for Chapter 4

2.3 Material and Methods for Chapter 5

### **Chapter 3: Mechanisms for Selective Coupling of Endothelial $\text{Ca}^{2+}$ Signals** 74

**with eNOS or IK/SK Channels in Systemic and Pulmonary Arteries**

3.1 Abstract

3.2 Introduction

3.3 Results

3.4 Discussion

**Chapter 4: Local Peroxynitrite Impairs Endothelial Transient Receptor** 104

**Potential Vanilloid 4 (TRPV4) Channels and Elevates Blood Pressure in Obesity**

4.1 Abstract

4.2 Introduction

4.3 Results

4.4 Discussion

**Chapter 5: Smooth muscle-derived TNF $\alpha$  creates pathological** 134

**inflammatory micro-domains which alter endothelial function in obesity**

5.1 Introduction

5.2 Results

5.3 Discussion

**Chapter 6: Future Directions** 163

**Chapter 7: Acknowledgments** 178

**Chapter 8: References** 181

## List of Figures

### **Chapter 1: The Calcium Signaling Mechanisms in Arterial Endothelial Cells**

Figure 1. The contrasting effects of smooth muscle cell (SMC) and endothelial cell (EC)  $Ca^{2+}$  on vascular contractility

Figure 2.  $Ca^{2+}$  signaling networks at myoendothelial projections (MEPs).

Figure 3. Signaling mechanisms at myoendothelial projections (MEPs) that control the communication between endothelial and smooth muscle cells (SMCs) and SMC contractility.

Figure 4. The molecular mechanism underlying selective activation of IK/SK channels in mesenteric arteries versus eNOS in pulmonary arteries.

Figure 5. The contribution of endothelial P2X purinergic receptor, PIEZO1, TRPP1, and TRPV4 channels to flow-induced vasodilation.

Figure 6. Sarco-endoplasmic reticulum  $Ca^{2+}$ -ATPase (SERCA) transporting cycle.

### **Chapter 3: Mechanisms for Selective Coupling of Endothelial $Ca^{2+}$ Signals with eNOS or IK/SK Channels in Systemic and Pulmonary Arteries**

Figure 1. TRPV4<sub>EC</sub> channels control resting diameter in resistance PAs and MAs.

Figure 2. Whole-cell, but not localized, increases in intracellular  $Ca^{2+}$  activate IK/SK currents in PAs.

Figure 3. GSK101 induces similar TRPV4<sub>EC</sub> channel activity in ECs from MAs and PAs.

Figure 4. TRPV4<sub>EC</sub> channels act through IK/SK channel activation to dilate MAs and through eNOS-NO signaling to dilate PAs.

Figure 5. TRPV4<sub>EC</sub>-IK/SK channels localize at MEPs in MAs but not in PAs.

Figure 6. Hba co-localizes with eNOS at MEPs in MAs but not in PAs.

Figure 7. Schematic depicting the mechanisms underlying preferential TRPV4<sub>EC</sub> sparklet-eNOS versus TRPV4<sub>EC</sub> sparklet-IK/SK channel coupling in resistance PAs and MAs.

## **Chapter 4: Local Peroxynitrite Impairs Endothelial Transient Receptor Potential Vanilloid 4 (TRPV4) Channels and Elevates Blood Pressure in Obesity**

Figure 1. Endothelium-specific TRPV4 (TRPV4<sub>EC</sub><sup>-/-</sup>) and AKAP150 (AKAP150<sub>EC</sub><sup>-/-</sup>) knockout mice show elevated resting blood pressure.

Figure 2. Diet-induced obesity impairs AKAP150<sub>EC</sub>-PKC-TRPV4<sub>EC</sub> signaling and vasodilation.

Figure 3. Elevation of endothelial peroxynitrite (PN) impairs TRPV4<sub>EC</sub> channel activity in obesity.

Figure 4. Localized NOX1 and iNOS upregulation underlies PN-induced impairment of TRPV4<sub>EC</sub> channel activity in obesity.

Figure 5. Peroxynitrite (PN) causes cysteine oxidation of AKAP150<sub>EC</sub> to inhibit AKAP150<sub>EC</sub>-PKC-TRPV4<sub>EC</sub> signaling.

Figure 6. Peroxynitrite (PN) impairs AKAP150<sub>EC</sub> anchoring of PKC in obesity.

## **Chapter 5: Smooth muscle-derived TNF $\alpha$ creates pathological micro-inflammatory domains which alter endothelial function in obesity**

Figure 1. Smooth muscle cells of systemic resistance arteries are an active source of  $\text{TNF}\alpha$  in obesity

Figure 2. Interaction between SMC- $\text{TNF}\alpha$  and  $\text{TNF}\alpha\text{RI}$  at the MEPs underlies the formation of pathological inflammatory micro-domains in obesity

Figure 3. Selectively blockage of  $\text{TNF}\alpha\text{RI}$  signaling normalizes blood pressure in obesity

Figure 4. Selectively blockage of  $\text{TNF}\alpha$ - $\text{TNF}\alpha\text{RI}$  signaling reduces iNOS and NOX1 expression at the MEPs in obesity

Figure 5. Selectively blockage of  $\text{TNF}\alpha$ - $\text{TNF}\alpha\text{RI}$  signaling in obesity rescues TRPV4 sparklets and restores endothelial dependent vasodilation

Figure 6. Schematic representing the formation of pathological MEPs in obesity driven by  $\text{TNF}\alpha$ - $\text{TNF}\alpha\text{RI}$  signaling.

Supplemental Figure 1. HFD mice are glucose intolerant and hypertensive

Supplemental Figure 2.  $\text{TNF}\alpha$ - $\text{TNF}\alpha\text{RI}$  signaling does not influence smooth muscle  $\text{TNF}\alpha$  expression in obesity

Supplemental Table 1. Plasma inflammatory cytokines levels are not different between HFD and Normal mice

## **Chapter 6: Future Directions**

Figure 1.  $\text{NF-}\kappa\text{B}$  inhibition prevents NOX1 expression at the MEPs in obesity

Figure 2. High pressure drives increase expression of smooth muscle  $\text{TNF}\alpha$

Figure 3. Schematic representing hypothetical molecular mechanisms underlying obesity-induced smooth muscle  $\text{TNF}\alpha$  expression

## **Chapter 1: The Calcium Signaling Mechanisms in Arterial Endothelial Cells**

## 1.1 Abstract

The contractile state of resistance arteries and arterioles is a crucial determinant of blood pressure and blood flow. Physiological regulation of arterial contractility requires constant communication between endothelial and smooth muscle cells. Various  $\text{Ca}^{2+}$  signals and  $\text{Ca}^{2+}$ -sensitive targets ensure dynamic control of intercellular communications in the vascular wall. The functional effect of a  $\text{Ca}^{2+}$  signal on arterial contractility depends on the type of  $\text{Ca}^{2+}$ -sensitive target engaged by that signal. Recent studies using advanced imaging methods have identified the spatiotemporal signatures of individual  $\text{Ca}^{2+}$  signals that control arterial and arteriolar contractility. Broadly speaking, intracellular  $\text{Ca}^{2+}$  is increased by ion channels and transporters on the plasma membrane and endoplasmic reticular membrane. Physiological roles for many vascular  $\text{Ca}^{2+}$  signals have already been confirmed, while further investigation is needed for other  $\text{Ca}^{2+}$  signals. This review focuses on endothelial  $\text{Ca}^{2+}$  signaling mechanisms in resistance arteries and arterioles. We discuss the  $\text{Ca}^{2+}$  entry pathways at the plasma membrane,  $\text{Ca}^{2+}$  release signals from the intracellular stores, the functional and physiological relevance of  $\text{Ca}^{2+}$  signals, and their regulatory mechanisms. Finally, we describe the contribution of abnormal endothelial  $\text{Ca}^{2+}$  signals to the pathogenesis of vascular disorders.

## 1.2 Introduction

Vascular resistance is a crucial determinant of blood pressure and blood flow to target organs. The contractile state of small arteries and arterioles determines vascular resistance. Smooth muscle cells (SMCs) and endothelial cells (ECs) are the two main cell-types involved in the dynamic regulation of vascular contractility. Both SMCs and ECs recruit various  $\text{Ca}^{2+}$  signaling mechanisms to regulate vascular contractility (Figure 1) (291). The canonical view is that endothelial and smooth muscle cell  $\text{Ca}^{2+}$  has opposite effects on vascular diameter. While increases in endothelial  $\text{Ca}^{2+}$  cause vasodilation, increases in SMC  $\text{Ca}^{2+}$  have mostly been linked to vasoconstriction, except for  $\text{Ca}^{2+}$  sparks, which can cause vasodilation. Moreover, intracellular

Ca<sup>2+</sup> plays a central role in EC-SMC communication, which is pivotal for physiological regulation of vascular contractility.

Cytosolic Ca<sup>2+</sup> levels can increase via the influx of extracellular Ca<sup>2+</sup> or release of Ca<sup>2+</sup> from intracellular stores, including endoplasmic (ER) or sarcoplasmic (SR) reticulum and lysosomes. The majority of Ca<sup>2+</sup> signals in the arteriolar walls occur in a spatially restricted manner, with the diffusion of Ca<sup>2+</sup> limited by numerous Ca<sup>2+</sup> binding proteins and high viscosity of the cytosol. The spatially restricted nature of Ca<sup>2+</sup> signals confers the specificity of targets/functional effects and limits toxicity to the cell. Moreover, signaling microdomains that localize Ca<sup>2+</sup> signals with their signaling targets ensure specific activation of the targets. Such signaling microdomains also provide efficient Ca<sup>2+</sup> signal-target coupling, whereby smaller increases in Ca<sup>2+</sup> can activate a small number of nearby target molecules to achieve physiological effects. EC projections to SMCs, or myoendothelial projections (MEPs), are prime examples of signaling microdomains enabled by specialized microstructures. The majority of endothelial Ca<sup>2+</sup> signals occur at MEPs, and Ca<sup>2+</sup>-sensitive targets also localize to MEPs. The Ca<sup>2+</sup> signal-target proximity at MEPs facilitates efficient and precise communication between ECs and SMCs. Similarly, signaling nanodomains involving localization of proteins inside the caveolae have been shown in ECs and SMCs. In this review, we discuss the Ca<sup>2+</sup> signal-target linkages in arteries and arterioles, regulatory mechanisms, and abnormalities in Ca<sup>2+</sup> signaling that contribute to the pathogenesis of vascular disorders.

### 1.3 Methodologies for recording Ca<sup>2+</sup> signals

Ca<sup>2+</sup> signals within the cells have unique spatiotemporal properties that translate into numerous cellular functions (20). Therefore, the diversity of Ca<sup>2+</sup> signals cannot be captured with one technique. However, over the last two decades, the use of sensitive fluorescent Ca<sup>2+</sup> indicators and fast, high-resolution imaging techniques (confocal, total internal reflection fluorescence or TIRF, and multi-photon imaging) have enabled effective spatiotemporal resolution of individual Ca<sup>2+</sup> signals. Fluorescent indicators are synthesized as membrane-permeable acetoxymethyl (AM) esters. Cytosolic esterases release the anionic cell impermeable form, which remains in the cytosol (394). Fluorescent Ca<sup>2+</sup> indicators can be classified into ratiometric (dual-wavelength) and non-ratiometric (single wavelength) indicators. Ratiometric indicators show a shift in their excitation (Fura-2) or emission (Indo-1) spectrum upon Ca<sup>2+</sup> binding. A classic example of ratiometric indicators is Fura-2, which presents two excitation wavelengths (Ca<sup>2+</sup>-free form/ Ca<sup>2+</sup>-bound form = 380 nm/340 nm). Elevation in cytosolic Ca<sup>2+</sup> levels increases Fura-2 fluorescence at 340 nm (Ca<sup>2+</sup>-bound form) and decreases the fluorescence at 380 nm (Ca<sup>2+</sup>-free form). Therefore, the ratio of the emission intensity at 340 nm to that at 380 nm is proportional to cytosolic Ca<sup>2+</sup> concentration. Ratiometric dyes have mostly been used for quantification of whole-cell changes in Ca<sup>2+</sup> concentration. Non-ratiometric indicators (fluo- indicators), on the contrary, do not show a shift in excitation/emission wavelengths upon Ca<sup>2+</sup> binding. Instead, the fluorescence intensity increases upon Ca<sup>2+</sup> binding (128). Usually, fluorescence values of non-ratiometric indicators are presented as a ratio between the fluorescent value during the occurrence of a Ca<sup>2+</sup> signal (F) and that at the baseline (F<sub>0</sub>, no Ca<sup>2+</sup> activity) (251). The use of ratiometric indicators is not associated with loading and photobleaching issues that are commonly experienced with non-ratiometric indicators. The drawbacks of ratiometric indicators are- 1) they are not suitable for capturing fast, spatially restricted Ca<sup>2+</sup> signals; 2) they require excitation with ultraviolet light, which is harmful to biological samples; and 3) they cannot be used for studies of individual fast Ca<sup>2+</sup> signals.

Moreover, ultraviolet light is not effectively transmitted through most high numerical aperture objectives. Therefore, non-ratiometric indicators are the “gold standard” for studying fast, spatially restricted  $\text{Ca}^{2+}$  signals (sparks, sparklets, etc.). The main drawbacks of these indicators are uneven sample loading, photobleaching, and leakage issues. Photobleaching occurs when the indicator, in the excited form, undergoes oxidation by interacting with molecular oxygen. Therefore, lowering the laser intensity can prevent photobleaching (382). Non-ratiometric indicators can compartmentalize to specific intracellular organelles. Blocking of anionic-organic cellular transporters has been used as a strategy to reduce this phenomenon (72). Moreover, determining the optimum duration for dye-loading can lower the risk of uneven loading or overloading of the sample.

The selection criteria for  $\text{Ca}^{2+}$  indicators should include the concentration range of  $\text{Ca}^{2+}$  signals being recorded. In an ideal scenario, the mid-point of  $\text{Ca}^{2+}$  concentration range is close to the dissociation constant ( $K_d$ ) of the indicator. Indicators with high  $K_d$  (low  $\text{Ca}^{2+}$  affinity) are suitable for detecting large increases in  $\text{Ca}^{2+}$ . In contrast, indicators with low  $K_d$  (high  $\text{Ca}^{2+}$  affinity) are better suited for detecting lower levels of  $\text{Ca}^{2+}$  and become saturated at high  $\text{Ca}^{2+}$  concentrations. Indeed, some localization studies of  $\text{Ca}^{2+}$  entry events have used a combination of low- and high-affinity  $\text{Ca}^{2+}$  indicators. A combination of Fluo-5 ( $K_d=2.3 \mu\text{M}$ ) and an excess of non-fluorescent EGTA ( $K_d=150 \text{ nM}$ ) was used to study the initiation sites of LTCC sparklets (269). The  $\text{Ca}^{2+}$ -binding rate ( $K_{on}=K_{off}/K_d$ ) of Fluo-5 is 100-times faster than that of EGTA. Therefore, Fluo-5 can detect the more recent  $\text{Ca}^{2+}$  ions that have entered into the cell before ceding them to EGTA. The combination of Fluo-5 and EGTA allowed the identification of  $\text{Ca}^{2+}$  entry sites, which are expected to be within 50 and a few hundred nanometers from the fluorescence signal (91, 246, 269, 446). The combination of Fluo-4 ( $K_d=335 \text{ nM}$ ) and EGTA was used by Sonkusare and colleagues to decipher  $\text{Ca}^{2+}$ -dependent potentiation of endothelial

TRPV4 channels in a cluster. EGTA chelates intracellular  $\text{Ca}^{2+}$  and was found to disrupt  $\text{Ca}^{2+}$ -dependent channel to channel communication (355).

Genetically encoded  $\text{Ca}^{2+}$  indicators (GECI) have proved immensely helpful for studying  $\text{Ca}^{2+}$  signals in biological systems. GECI are encoded by engineered DNA sequences that can be incorporated into the cell genome. Indeed, combining GECI with cell-specific promoters results in cell-specific expression of the  $\text{Ca}^{2+}$  biosensor proteins, which constitutes an enormous advantage over the use of fluorescent indicators.  $\text{Ca}^{2+}$  indicators can show undesirable compartmentalization to intracellular organelles and get pumped out from the cell by ATPases at the cell membrane. GECI are devoid of these disadvantages. The most popular GECI is GCaMP. Briefly, GCaMP protein is formed by a circularly permuted version of GFP (cpGFP) fused with CaM and CaM-interacting MLCK M13 peptide.  $\text{Ca}^{2+}$  binding with CaM causes a conformational change in cpGFP and results in a substantial increase in fluorescence. Point mutations on the GCaMP amino acid sequence have yielded different GCaMP generations with improved dynamic range, kinetic properties, and  $\text{Ca}^{2+}$  sensitivity. In the vascular field, mice expressing GCaMP under the connexin40 (Cx40) promoter or acta2 promoter have been engineered to study  $\text{Ca}^{2+}$  events restricted to endothelium (199, 354, 378) or SMCs (345), respectively.

## **1.4 Endothelial cell $\text{Ca}^{2+}$ signals in small arteries and arterioles**

The endothelium is a single cell layer of cells that lines the inner walls of all the blood vessels. ECs are constantly exposed to the mediators in the blood and mechanical forces exerted by the bloodstream. Endothelial function in arteries and arterioles is also modulated by stimuli from SMCs (112, 147, 268, 392). In this section, we will focus on the physiological  $\text{Ca}^{2+}$  signaling mechanisms that alter EC function. ECs in resistance-sized arteries send out projections, across the internal elastic lamina, to the SMC layer. The sites of contact between ECs and SMCs are enriched with connexin proteins (Cx37, Cx40, and Cx43) that form myoendothelial gap junctions (MEGJs) (131, 160, 322). MEGJ are characterized by two

hemichannels, one each on the EC and SMC membranes. Each hemichannel is a hexamer composed of six connexins (22). MEGJs allow the passage of second messengers and electrical signals (75, 87, 147, 239), and serve as a crucial communication site for ECs and SMCs. ECs can influence the contractile state of the adjacent SMCs via endothelium-derived hyperpolarization (EDH) or by releasing substances that activate vasodilatory signaling in SMCs in a paracrine manner. The preferential activation of one pathway over another may be determined by the vascular bed under consideration (286) and the size of the artery (342, 396). Recent studies show that neighboring ECs are heterogeneous with respect to  $\text{Ca}^{2+}$  signaling mechanisms (201). Indeed, McCarron and colleagues demonstrated that neighboring ECs are organized into  $\text{Ca}^{2+}$  signaling clusters, and communication amongst these clusters is essential for normal vascular function (201). Here, we elaborate on the  $\text{Ca}^{2+}$  signaling pathways that initiate EC to SMC, SMC to EC, and EC to EC communications in the vascular wall, and the target proteins that transduce the  $\text{Ca}^{2+}$  signals into a physiological response.

### **1.4.1 $\text{Ca}^{2+}$ influx from extracellular compartment**

#### **TRPA1 channel**

In the past decade, TRPA1 channels have emerged as a crucial  $\text{Ca}^{2+}$  influx pathway in ECs from specialized vascular beds. TRPA1 channels show a unitary conductance of  $\sim 96$  pS at  $-60$  mV (266), and a higher permeability to  $\text{Ca}^{2+}$  than  $\text{Na}^+$  ( $P_{\text{Ca}^{2+}}/P_{\text{Na}^+} = 7.9$ ) (169). TRPA1 channels are activated by several pungent natural compounds in food such as allicin (garlic) (234), allyl isothiocyanate (mustard), and cinnamon (cinnamaldehyde) (161). TRPA1 channels are gated by extracellular  $\text{Ca}^{2+}$  in a voltage-dependent manner. In patch clamp studies, TRPA1 channels displayed slow activation at a holding potential of  $-80$  mV and in the absence of extracellular  $\text{Ca}^{2+}$ . However, in the presence of extracellular  $\text{Ca}^{2+}$  and EGTA-buffered intracellular  $\text{Ca}^{2+}$ , holding potential of  $-80$  mV caused fast channel activation followed by fast

inactivation. Notably, fast channel inactivation did not occur at a more depolarized membrane potential (-20 mV) (266).

Earley and colleagues provided the first evidence for vasodilatory effects of endothelial TRPA1 channel activation in cerebral arteries. TRPA1 channels co-localized with intermediate-conductance  $\text{Ca}^{2+}$ -activated  $\text{K}^+$  (IK) channels at MEPs (Figure 2).  $\text{Ca}^{2+}$  influx through TRPA1 channels activated nearby IK channels, resulting in EC membrane hyperpolarization and vasodilation. Moreover, the vasodilatory effect of TRPA1-IK channels was boosted by inward-rectifier potassium (Kir) channels on SMC membranes (82). In a subsequent study, TRPA1 channels were shown to promote IP3R  $\text{Ca}^{2+}$  release from the ER. Furthermore, endothelial TRPA1 channel activation inhibited the formation of  $\text{Ca}^{2+}$  waves in SMCs, providing additional evidence supporting the inhibitory effect of endothelial TRPA1 channels on SMC contraction (306).

ROS and products formed by lipid peroxidation, including 4-hydroxynonenal (4-HNE), are the main endogenous modulators of endothelial TRPA1 channel activity (81, 393). ROS generating enzyme NADPH oxidase 2 (NOX2) was present in nanometer proximity with TRPA1 channel in cerebral arteries. NOX2-generated ROS induced membrane lipid peroxidation and 4-HNE formation, thereby increasing TRPA1 channel activity and causing vasodilation. This effect was blunted in the arteries from endothelium-specific TRPA1<sup>-/-</sup> mice (368). Studies by Pires and colleagues suggested that endothelial TRPA1 channels are neuroprotective under hypoxic conditions. Under hypoxic conditions, mitochondrial ROS production enhanced TRPA1 channel-mediated dilation of cerebral arteries. In support of this concept, endothelium-specific TRPA1<sup>-/-</sup> mice showed larger cerebral damage following stroke-induced hypoxia (301). Overall, the current evidence suggests a central role for endothelial TRPA1 channels in mediating  $\text{Ca}^{2+}$  influx in the cerebral vasculature.

## TRPV4 channel

High unitary conductance and permeability for  $\text{Ca}^{2+}$  are characteristic properties of TRPV channels. TRPV channels show a range of selectivity for  $\text{Ca}^{2+}$ , although most TRPV channels are more selective for  $\text{Ca}^{2+}$  over  $\text{Na}^+$ . The unitary conductances of TRPV4 channels are 50-60 pS at -60 mV, and 90-100 pS at +60 mV (365, 414, 415). TRPV4 channels display higher permeability for  $\text{Ca}^{2+}$  over  $\text{Na}^+$  ( $P_{\text{Ca}^{2+}}/P_{\text{Na}^+} = 6-10$ ) (68, 404), and can be activated by temperature, mechanical stimuli, and neurohumoral mediators. TRPV4 is one of the most studied  $\text{Ca}^{2+}$  influx pathways in the intact endothelium. Until recently, the physiological roles of endothelial TRPV4 channels was not known (reviewed in (51)). Systemic administration of a potent and selective TRPV4 channel agonist evoked a dose-dependent drop in blood pressure in dogs, rats, and mice (422). Moreover, acetylcholine-induced decrease in blood pressure was attenuated in global TRPV4<sup>-/-</sup> mice (448). However, global TRPV4<sup>-/-</sup> mice showed unaltered resting blood pressure (147, 448), possibly due to a compensatory upregulation of other ion channels or the absence of TRPV4 channels from multiple cell types in these mice. Ottolini and colleagues, in a recent study, demonstrated the importance of endothelial TRPV4 channels and its regulation by AKAP150 in lowering the resting blood pressure. In this study, tamoxifen-inducible, endothelium-specific TRPV4<sup>-/-</sup> or AKAP150<sup>-/-</sup> mice showed higher resting blood pressures, confirming the pivotal role of endothelial AKAP150-TRPV4 signaling in blood pressure regulation (288).

Multimodal physiological stimuli can activate endothelial TRPV4 channels. Early studies supported a mechanosensory role of endothelial TRPV4 channels, although recent evidence suggests that TRPV4 channels are not direct mechanosensors (274). An alternative explanation for mechanoactivation of TRPV4 channels is that the channels can be activated by mechanical stimuli via signaling pathways involving the activation of cytochrome P450 epoxygenases and EET production (85, 220). Kohler and colleagues demonstrated that sheer stress-induced

vasodilation in rat gracilis arteries is reduced by ruthenium red (RuR), a non-selective TRPV4 channel blocker (185). Flow-induced, TRPV4 channel-mediated vasodilation was also reported in carotid arteries (139) and mesenteric arteries (245) (Figure 5). Inhibiting AA metabolism eliminated shear stress-induced vasodilation, suggesting that AA metabolites are necessary for mechanotransduction by TRPV4 channels. In cremaster arteries, shear stress increased the functional coupling of M3 muscarinic receptors with endothelial TRPV4 channels for vasodilation (64). Bagher and colleagues showed that low intravascular pressure (5-50 mmHg) enhances the activity of endothelial TRPV4 channels, further supporting the activation of endothelial TRPV4 channels by mechanical stimuli (14). Studies by Saliez et al. in EC culture demonstrated that TRPV4 channels co-immunoprecipitate with caveolin-1 (318). Moreover, endothelial  $Ca^{2+}$  influx was impaired in the absence of caveolin-1. Although a direct interaction between caveolin-1 and TRPV4 channel appears likely, the functional evidence on caveolin-1 regulation of TRPV4 channel activity is lacking. Studies using EC-specific caveolin-1 knockout mice will be crucial for unraveling the functional and physiological significance of caveolin-1-TRPV4 channel interaction in the endothelium.

Multiple endogenous modulators of endothelial TRPV4 channels have been identified. TRPV4 channel activity is heavily influenced by GqPCR-PLC signaling in both arterial and capillary endothelium (136, 354, 355). PLC-DAG-activated PKC can phosphorylate TRPV4 channels and potentiate their activity (93). Moreover, PLC-mediated decrease in PIP<sub>2</sub>, a negative modulator of TRPV4 channels, increases TRPV4 channel activity (136, 376). Furthermore, IP<sub>3</sub> was shown to bind to TRPV4 channels and increase their activity (147, 376). As described with SMC TRPV4 channels,  $Ca^{2+}$  itself has a biphasic effect on TRPV4 channel activity. In ECs,  $Ca^{2+}$  influx through TRPV4 channels potentiated the activity of the neighboring TRPV4 channels in a cluster, resulting in cooperative channel openings (354, 355). On the contrary, NO impaired the cooperative openings of TRPV4 channels via activation of endothelial

GC-PKG pathway (238, 442) and reduced channel activity. Hong and colleagues described the presence of a myoendothelial feedback mechanism whereby  $\alpha$ 1AR stimulation-induced vasoconstriction was limited by endothelial TRPV4 channels (Figure 3). PE activated SMC  $\alpha$ 1ARs and increased the levels of IP3, which diffused across the MEGJs to ECs and activated TRPV4 channels at MEPs (147). H<sub>2</sub>S, a gasotransmitter molecule produced by ECs, was shown to activate endothelial TRPV4 channels in a study by Naik and colleagues. H<sub>2</sub>S-activation of TRPV4 channels increased endothelial BK channel currents (267). The authors also showed that H<sub>2</sub>S induces sulfhydration of endothelial TRPV4 channels. Further studies to identify the precise site of action for H<sub>2</sub>S on the TRPV4 channel are awaited.

The detrimental effects of excessive TRPV4 channel activity in pulmonary endothelium are well-known (7, 371, 384, 442), although the physiological roles of pulmonary endothelial TRPV4 channels have not been resolved. Marziano et al. showed that ATP activates endothelial TRPV4 channels via P2 purinergic receptor signaling in resistance pulmonary arteries (238). However, global TRPV4<sup>-/-</sup> mice showed unaltered mean pulmonary arterial pressure (PAP) (432). In this regard, TRPV4 channels are also expressed in SMCs from pulmonary arteries (237), where they promote vasoconstriction (352). Therefore, lack of a PAP phenotype in TRPV4<sup>-/-</sup> mice could be due to the activation of compensatory mechanisms in SMCs and ECs. Future studies in EC-specific TRPV4<sup>-/-</sup> (288) and SMC-specific TRPV4<sup>-/-</sup> are warranted to separate the contributions of endothelial and SMC TRPV4 channels to the regulation of pulmonary arterial pressure.

Unitary Ca<sup>2+</sup> influx signals through TRPV4 channels, called TRPV4 Ca<sup>2+</sup> sparklets, have been recorded in the intact endothelium from resistance arteries and in endothelial cell culture (354, 367). Notably, TRPV4 sparklets are not randomly distributed throughout the EC membrane. Instead, the majority of TRPV4 sparklet activity was observed at MEPs (Figure 2) (147, 354, 355). It was later proposed that MEP-localized AKAP150 anchors PKC in the vicinity

of TRPV4 channels and facilitates the coupling among TRPV4 channels (355). IK and SK channels also localize to MEPs (14, 199, 322), explaining the preferential activation of IK/SK channels by TRPV4 sparklets in systemic resistance arteries (286). Contrary to the systemic arteries, TRPV4 sparklets selectively activated eNOS to dilate resistance pulmonary arteries (238). Very recently, Ottolini et al. provided evidence that spatial coupling determines the TRPV4 sparklets-target linkage in different vascular beds (Figure 4). In this study, the authors showed that TRPV4 channels co-localize with IK/SK channels at MEPs in resistance mesenteric arteries. MEPs in this vascular bed are also enriched with hemoglobin  $\alpha$  (Hb $\alpha$ ) (364), a protein that limits NO release and diffusion (364). TRPV4 channels also localize at MEPs in resistance pulmonary arteries. However, Hb $\alpha$  is absent from MEPs in resistance pulmonary arteries. Additionally, IK/SK channels do not localize at MEPs in this vascular bed. These differences in spatial coupling favor TRPV4-IK/SK channel signaling in resistance mesenteric arteries and TRPV4-eNOS signaling in resistance pulmonary arteries (286).

### **TRPV3 channel**

Consistent with other ion channels of TRPV subfamily, TRPV3 channels show high unitary conductance ( $\sim 170$  pS at +60 mV) and  $\text{Ca}^{2+}$  permeability ( $P_{\text{Ca}^{2+}}/P_{\text{Na}^{+}} = 12$ ). An increase in temperature from 25 C $^{\circ}$  to 37 C $^{\circ}$  increases the outward currents through TRPV3 channels nearly 4-fold (434). TRPV3 channels are also activated by dietary monoterpenes, including carvacrol, thymol, vanillin, and ethyl-vanillin (433). Earley and colleagues provided the first evidence for the functional expression of TRPV3 channels in ECs from cerebral arteries (Figure 2). Endothelial TRPV3 channel activation by carvacrol dilated cerebral arteries through IK/SK channels (83). In a more recent study, Pires et al. recorded unitary  $\text{Ca}^{2+}$  influx events through TRPV3 channels (TRPV3 sparklets) in ECs from cerebral parenchymal arterioles. The authors reported that TRPV3 sparklets show higher single-channel amplitudes when compared to TRPA1 sparklets (302), results that are consistent with a higher unitary conductance of TRPV3 channels.

Endothelium-specific knockout for TRPV3 channels has not been generated; therefore, the physiological roles of endothelial TRPV3 channels remain unclear.

### **TRPV1 channel**

TRPV1 channel has a unitary conductance of 35-70 pS and higher permeability for divalent over monovalent cations ( $P_{Ca^{2+}}/P_{Na^{+}} = 10$ ) (44, 319). TRPV1 channel agonist, capsaicin, constricted canine denervated mesenteric arteries, supporting a contractile role of TRPV1 channels (304). The expression and function of TRPV1 channels in endothelial cells are controversial. Several studies have relied upon TRPV1 channel antibodies to assess its endothelial expression, although the specificity of these antibodies has not been verified using knockout tissue (389). In two recent studies on transgenic TRPV1-LacZ and TRPV1-Cre:tdTomato mice, TRPV1 channels were expressed in the SMC layer but not in the endothelial layer (45). Nevertheless, some studies have proposed an important role for TRPV1 channels in endothelium-dependent vasodilation. Yang and colleagues suggested that TRPV1 channel agonist capsaicin activated eNOS and dilated mesenteric arteries, effects that were absent in the arteries from TRPV1<sup>-/-</sup> mice (437). TRPV1-eNOS signaling in the vasculature has also been proposed by other studies (31, 388). It should be noted that capsaicin can activate TRPV1 channels in sensory nerves to release calcitonin gene-related peptide (CGRP) and substance P (SP) (236), which could affect the endothelium. Therefore, a definitive assessment of the role of endothelial TRPV1 channels in vasodilation awaits the development of endothelium-specific TRPV1<sup>-/-</sup> mice.

### **TRPC channel**

Multiple studies have reported significant roles for endothelial TRPC channels as Ca<sup>2+</sup> influx pathways in resistance arteries. TRPC1 channels formed heteromeric complexes with TRPV4 channels in freshly dissociated endothelial cells from rabbit mesenteric arteries.

Furthermore, TRPC1-TRPV4 complex activated eNOS and caused vasodilation (125). Ma and colleagues indicated that the TRPC1-TRPV4 channel complex plays a crucial role in shear stress-induced increase in endothelial  $\text{Ca}^{2+}$  and vasodilation (229). In a study by Senadheera and colleagues, TRPC3 channels were found to be localized with IK/SK channels at MEPs of rat mesenteric arteries (Figure 2). Moreover, TRPC3-IK/SK channel signaling mediated acetylcholine-induced dilation in these arteries (335). Co-localization of TRPC3 channels with SK/IK channels at MEPs was also observed in rat popliteal arteries (335). Additionally, rat mesenteric arteries treated with TRPC3 antisense oligonucleotides showed impaired relaxation to bradykinin (214), further supporting a role for TRPC3 channels in endothelium-dependent vasodilation. In a recent study, ATP-induced endothelial cell hyperpolarization was shown to have two components: an early hyperpolarization through IK channels; and a sustained hyperpolarization through TRPC3-SK channel signaling, revealing a central role for TRPC3 channels in ATP-induced endothelial hyperpolarization (183).

### **TRPM2 channel**

The unitary conductances of TRPM2 channel are 58 pS and 76 pS at negative and positive voltages, respectively. TRPM2 channel is equally permeable to divalent and monovalent cations (324). The activity of TRPM2 channels was shown to be increased by hydrogen peroxide ( $\text{H}_2\text{O}_2$ ), an important redox signaling molecule with a vasodilatory activity (188, 223). A recent study in cremaster arteries showed that  $\text{H}_2\text{O}_2$ -induced vasodilation is impaired by an antibody against TRPM2 channels, and by inhibiting SK/IK channels (53). Therefore, endothelial TRPM2-SK/IK signaling may underlie  $\text{H}_2\text{O}_2$ -dependent vasodilation, although further studies are required to confirm the role of TRPM2 channels in controlling endothelial function.

## TRPP1 channel

TRPP1 channel is encoded by PKD2, a gene mutated in patients with autosomal-dominant polycystic kidney disease (253). The outward unitary conductances of TRPP1 channel for  $\text{Ca}^{2+}$ ,  $\text{Na}^{+}$  and  $\text{K}^{+}$  are 90 pS, 99 pS, and 117 pS, and inward conductances are 4 pS, 89 pS, and 144 pS, respectively. TRPP1 channels conduct ionic currents with permeability ratios of  $P_{\text{K}^{+}}:P_{\text{Na}^{+}}:P_{\text{Ca}^{2+}}$  of 1:0.4:0.025 (218). In a recent study, MacKay and colleagues demonstrated the importance of endothelial TRPP1 channel in mediating flow-induced dilation of mesenteric arteries (Figure 5). Pressurized mesenteric arteries from endothelium specific TRPP1  $^{-/-}$  mice showed impaired dilation to shear stress. Moreover, endothelium-specific TRPP1  $^{-/-}$  mice had higher diastolic and systolic blood pressures. Thus, endothelial TRPP1 channels appear to be a key element in endothelial cell mechanosensing and vasodilation (230).

## Purinergic P2X receptor ion channels (P2XR)

Evidence in the literature supports a functional role for P2X1, P2X3, and P2X4 purinergic receptors in endothelial cells. P2X1 receptor was found to be expressed on the endothelium of mesenteric arteries from rats (138) and mice (137) (Figure 5). Endogenous purinergic receptor agonist ATP induced a dilation of mesenteric arteries; an effect that was blunted by inhibition of SK/IK channels (138). Importantly, ATP failed to dilate mesenteric arteries from P2X1  $^{-/-}$  mice, supporting the idea that ATP activates P2X1 receptors in this vascular bed (137).

Immunohistochemistry analysis by Glass and colleagues showed that P2X3 receptor is expressed in the endothelium from thymus arteries (116). Moreover, Yamamoto et al. found that ATP- and flow-induced vasodilation is markedly reduced in cremaster and mesenteric arteries from P2X4  $^{-/-}$  mice. Furthermore, P2X4  $^{-/-}$  mice had a hypertensive phenotype accompanied by a reduction in nitrite and nitrate production. These results led the authors to postulate that impaired eNOS activity and NO production may be partially responsible for increasing blood pressure in the P2X4  $^{-/-}$  mice (436).

## PIEZO1 channel

PIEZO channels in vascular cells have been a topic of intense research in recent times. PIEZO proteins are mechanosensitive, non-selective cation channels that show a slight preference for  $\text{Ca}^{2+}$  over monovalent cations. Two PIEZO channel isoforms have been identified: PIEZO1 and PIEZO2 (59). Mammalian PIEZO1 channel shows a unitary conductance of  $\sim 30$  pS, about ten times higher than the *Drosophila* PIEZO1 channel (60). Mammalian PIEZO1 channel is a large protein composed of 2547 amino acids. Cryo-EM at 4.8 Å resolution revealed a trimeric three-bladed propeller-like structure of  $\sim 900$  kDa for PIEZO1 channel. Each subunit has 14 transmembrane  $\alpha$ -helices. The channel pore is formed by two helices, outer (OH) and inner (IH) helix, located close to the C-terminal intracellular tail. The remaining 12 peripheral transmembrane helices (PH) of each subunit contain the N-terminal tail, and function as mechanosensor units (113, 455). PIEZO1 channel is expressed at low levels in conduit arteries but is highly expressed in resistance arteries (78, 310). Endothelium-dependent vasodilation in response to blood flow/shear stress is well-established; however, the exact endothelial mechanosensor underlying this effect has remained elusive. PIEZO1 channel on endothelial cell membrane has recently emerged as the mechanosensor for flow/shear stress-induced changes in vascular resistance (Figure 5). Wang and colleagues showed that PIEZO1 channels mediate the dilation to flow/shear stress via eNOS activation in U46619 pre-constricted third- and fourth-order mesenteric arteries (411). Mesenteric arteries from endothelial PIEZO1<sup>-/-</sup> mice (EC-PIEZO1<sup>-/-</sup>) showed impaired flow-induced vasodilation. Furthermore, PIEZO1 channel promoted extracellular ATP release via Pannexin1/2 channels in response to flow. ATP, in turn, activated eNOS via P2Y2 purinergic receptor signaling. Consistent with impaired vasodilation, EC-PIEZO1<sup>-/-</sup> mice showed higher resting systolic blood pressures (411). On the contrary, Rode and colleagues reported that endothelial PIEZO1 channels cause flow-induced vasoconstriction of second-order mesenteric arteries during whole-body exercise. EC-PIEZO1<sup>-/-</sup> mice on a running

wheel showed lower systolic and diastolic blood pressures. Moreover, endothelial PIEZO1 deletion did not affect the reactivity of larger arteries (saphenous and carotid arteries). The discrepancy in results between the two studies could be explained by blood pressure recordings during exercise versus resting conditions, and studies of vascular function using pressure myography versus wire myography. In a recent study, Lhomme and colleagues demonstrated the importance of endothelial PIEZO1 channels in triggering relaxation of pulmonary arteries via NO production. Furthermore, endothelial PIEZO1 channel-induced vasorelaxation was not impaired in a mouse model of pulmonary hypertension (204). Thus, regardless of the conflicting reports, strong evidence supports the functional significance of endothelial PIEZO1 channels.

### **Na<sup>+</sup>/Ca<sup>2+</sup> exchanger (NCX)**

A recent study demonstrated that NCX contributes to acetylcholine-induced dilation of mesenteric resistance arteries (209). Lillo et al. showed that during acetylcholine-activation of endothelial muscarinic receptor signaling, NCX works in reverse mode (NCX<sub>rm</sub>), enhancing Ca<sup>2+</sup> entry in the endothelium and facilitating endothelium-dependent vasodilation. Moreover, NCX was concentrated within the caveolae, in nanometer proximity to eNOS (209). This result may suggest NCX<sub>rm</sub>-eNOS signaling during acetylcholine-induced vasodilation. Most other studies have used cell culture systems or conduit arteries (115, 121, 329). Overall, the involvement of NCX in influencing endothelial Ca<sup>2+</sup> signaling in resistance arteries and arterioles remains poorly understood.

## **1.4.2 Ca<sup>2+</sup> release from intracellular compartments**

### **Inositol trisphosphate receptors (IP3Rs)**

All three isoforms of IP3Rs (IP3R1-3) have been reported in endothelial cells. Ledoux and colleagues described spatially restricted IP3R Ca<sup>2+</sup> release from the ER at MEPs. These events were termed “Ca<sup>2+</sup> pulsars”. The kinetic properties of Ca<sup>2+</sup> pulsars allow a clear distinction from

Ca<sup>2+</sup> puffs and Ca<sup>2+</sup> waves. When compared to Ca<sup>2+</sup> sparks, Ca<sup>2+</sup> pulsars showed slower rise times and longer durations. Consistent with the occurrence of Ca<sup>2+</sup> pulsars at MEPs, IP3Rs were also shown to localize at MEPs. Ca<sup>2+</sup> pulsars signaled through IK channels to induce endothelial cell hyperpolarization and vasodilation (Figure 2) (199). In a recent study, conditional endothelial IP3R1 deletion did not alter vascular dynamics. However, endothelium-specific triple IP3R<sup>-/-</sup> mice (ECTKO) resulted in higher resting blood pressures. Second-order mesenteric arteries from ECTKO mice also showed impaired acetylcholine-induced dilation (211).

As described for SMCs, EC IP3R activity is also influenced by Ca<sup>2+</sup> influx pathways. Heathcote and colleagues explained that Ca<sup>2+</sup> influx through endothelial TRPV4 channels triggers IP3R opening. Ca<sup>2+</sup> release via IP3Rs amplifies the initial increase in Ca<sup>2+</sup> through TRPV4 channel activation, resulting in long and sustained Ca<sup>2+</sup> waves that lower vascular contractility (141). The focal application of acetylcholine on cremasteric arteries resulted in the formation of Ca<sup>2+</sup> waves that propagated for over 1 mm with a velocity of 116 μm/s. Interestingly, the initial vasodilatory responses to acetylcholine preceded the propagation of Ca<sup>2+</sup> waves. The authors described two temporally distinct vasodilatory phases- an early “electrically-conducted vasodilation” occurring through the transmission of hyperpolarizing signal and a later “Ca<sup>2+</sup> wave-dependent vasodilation”(15, 378). Communication through gap junctions was found to be pivotal for the propagation of Ca<sup>2+</sup> waves between neighboring endothelial cells (88).

IP3 and Ca<sup>2+</sup> play crucial roles in the myoendothelial feedback mechanism that limits α1AR-induced SMC contraction (Figure 3). Garland and colleagues recently demonstrated phenylephrine-induced increase in SMC Ca<sup>2+</sup> and diffusion of SMC Ca<sup>2+</sup> to MEPs via MEGJs, giving rise to the signals called VECTors (VDCC-dependent Endothelial cell Ca<sup>2+</sup> Transients). VECTors activated endothelial IP3Rs and facilitated the formation of Ca<sup>2+</sup> puffs and Ca<sup>2+</sup> waves in the endothelium. In summary, the study by Garland and colleagues suggested that the diffusion of Ca<sup>2+</sup> from SMCs to ECs across MEGJ can counteract α1AR -induced

vasoconstriction (112). In another study, endothelial TRPV4 sparklets were implicated as an essential element of the myoendothelial feedback mechanism. Phenylephrine-induced vasoconstriction was counterbalanced by the diffusion of IP3 from SMCs to ECs across MEGJs and subsequent activation of TRPV4 channels at MEPs. Interestingly, the authors observed that endothelial TRPV4 channel activity is influenced only by diffusion of IP3 and not  $Ca^{2+}$  from SMCs to ECs (147). Tran and colleagues provided further evidence for IP3 diffusion from SMCs to ECs during phenylephrine-induced vasoconstriction.  $\alpha$ 1AR signaling resulted in IP3R activation at MEPs and formation of distinct  $Ca^{2+}$  events termed “ $Ca^{2+}$  wavelets”.  $Ca^{2+}$  wavelets could be distinguished from  $Ca^{2+}$  puffs based on their longer duration and larger spatial spread.  $Ca^{2+}$  wavelets activated nearby IK/SK channels at MEPs to limit  $\alpha$ 1AR-induced vasoconstriction (392). Similarly, Nausch et al. suggested that sympathetic nerve stimulation activates IP3R  $Ca^{2+}$  pulsars at MEPs and limits sympathetic vasoconstriction (268). Finally, the  $Ca^{2+}$ -binding chaperon protein calreticulin (Calr) was also shown to play an important role in myoendothelial feedback mechanism. Calr was highly localized at MEPs in mesenteric arteries.  $\alpha$ 1AR-induced increase in endothelial  $Ca^{2+}$  signals at MEPs was absent in the arteries from endothelial Calr<sup>-/-</sup> mice, which resulted in higher  $\alpha$ 1AR-induced vasoconstriction. Moreover, endothelial Calr<sup>-/-</sup> mice showed higher blood pressure, further supporting the role of endothelial Calr in blood pressure regulation (24).

### **$Ca^{2+}$ -ATPase (SERCA)**

SERCA is encoded by three different genes, SERCA1-3 (297), and different splice variants of these genes have been documented. In SMCs, the predominant isoform is SERCA2b, followed by SERCA2a and SERCA3 (425). SERCA is a P-type ATPase that was discovered by Nobel laureate Jens Skou in the year 1957. A common feature of P-type pumps is to undergo two main conformational changes (E1 and E2), with the formation of a phosphorylated (P) aspartyl intermediate (E1-E2), which gives the family its name. E1 state has

a high affinity for  $\text{Ca}^{2+}$ , and E2 state has a low affinity for  $\text{Ca}^{2+}$  (308). The transition from E1 to E2 is ATP-dependent (Figure 6). In each cycle, SERCA uses one molecule of ATP to pump 2  $\text{Ca}^{2+}$  into the SR in exchange for 2-3  $\text{H}^+$  released into the cytosol (425).

X-ray crystallography studies showed that SERCA comprises three cytoplasmic domains (A, N, and P) and a transmembrane domain. The transmembrane domain is characterized by ten transmembrane helices (TM1-10). TM4 and TM5 are longer and protrude from the SR membrane to the cytosol. Two putative  $\text{Ca}^{2+}$  binding sites have been identified on the transmembrane domains- site I between TM5 and TM6, and site II on TM4. The N (nucleotide) domain is essential for ATP binding, and ATP-dependent phosphorylation of domain P. Asp<sup>351</sup> found in domain P is highly conserved across species, and is pivotal for the formation of high energy phosphorylated- aspartyl intermediate. The A domain transduces the conformational change of domain P to TM domain (282, 391) (Figure 6). At low cytosolic  $\text{Ca}^{2+}$  concentrations, SERCA is inhibited by phospholamban. Phospholamban is a 52-amino acids membrane integral protein that binds to the low  $\text{Ca}^{2+}$  affinity E2 state and inhibits the activity of the pump. Inhibition is relieved either by an increase in cytosolic  $\text{Ca}^{2+}$  or by phosphorylation of phospholamban by PKA (419) or  $\text{Ca}^{2+}$ -CaM-dependent protein kinase II (CaMKII) (231).

Two isoforms of SERCA (SERCA2 and 3) were shown to be expressed in freshly dissociated endothelial cells from coronary arteries and aorta (174), with SERCA3 described as the predominant isoform (261). In an early study, Liu et al. generated SERCA3<sup>-/-</sup> mice and showed that endothelium-dependent vasodilation is impaired in these mice, although blood pressure was not affected (216). S100A1 is an intracellular  $\text{Ca}^{2+}$  binding protein known to regulate SERCA activity (259, 260). S100A1<sup>-/-</sup> mice showed reduced nitric oxide production, impaired endothelium-dependent vasodilation, and higher blood pressure (303), suggesting that SERCA may be an essential regulator of eNOS activity and blood pressure. Consistent with this postulate, adenovirus-mediated SERCA2 delivery into coronary arteries of Yorkshire-Landrace

swine increased eNOS activity. Similarly, an increase in eNOS activity was observed in cultured ECs from human coronary arteries infected with SERCA2-adenovirus (132). Li and colleagues demonstrated that epicardial and endocardial endothelial cells from mice treated with SERCA2-adenovirus are protected against  $\text{Ca}^{2+}$  overload-induced necroptosis known to occur during cardiac ischemia/reperfusion injury (205). Interestingly, a recent study by Zhang et al. revealed a physical interaction between SERCA2 and PIEZO1 channel that results in suppression of PIEZO1 mechanosensation. The disruption of SERCA2-PIEZO1 interaction resulted in increased endothelial cell migration (453). It should be noted that the studies described above have been performed either in conduit arteries or in cell culture systems. Therefore, further investigation is needed to confirm the potential roles of different SERCA isoforms in regulating endothelial cell function in resistance arteries. In this regard, possible interactions between SERCA and other sources of  $\text{Ca}^{2+}$  in the endothelium will be particularly interesting.

## **1.5 Signaling targets of $\text{Ca}^{2+}$ in ECs**

### **Intermediate and small conductance $\text{Ca}^{2+}$ activated $\text{K}^+$ channels (IK/SK)**

IK and SK channels have mostly been described in endothelial cells. The unitary conductance of SK channels is ~10 pS, and that of IK channels is 20-30 pS. SK channel family is composed of four isoforms. SK1 (KCa2.1), SK2 (KCa2.2), and SK3 (KCa2.3) are encoded by KCNN1-3 genes, respectively. The fourth isoform, SK4 (IK or KCa3.1), shows higher conductance and is encoded by KCNN4 (3, 200). Functional SK/IK channel consists of four homologous subunits, each containing six transmembrane segments (S1-6). Segments 5 and 6 line the pore-forming unit of the channel. S1 and S6 are connected to intracellular N- and C-terminal domains, respectively. SK/IK channels share a similar structure to voltage-gated  $\text{K}^+$  channels (Kv), but do not exhibit voltage-dependence. This difference appears to be due to the diverse amino acid sequence of the S4 segment.  $\text{Ca}^{2+}$ -dependent activation of SK/IK channels does not rely on  $\text{Ca}^{2+}$  binding directly onto the channel. Xia and colleagues demonstrated that  $\text{Ca}^{2+}$  sensitivity of the channel is

imparted by interaction with  $\text{Ca}^{2+}$ -CaM (431). The C-terminal lobe (C-lobe) of CaM associates with the C-terminal tail of SK channels in a  $\text{Ca}^{2+}$ -independent manner. The channel gate opens upon  $\text{Ca}^{2+}$  binding to the CaM N-lobe (332). Moreover, CaM binding to SK/IK channels is essential for channel assembly and trafficking to the plasma membrane (166). SK/IK channels show half-maximal activation response at similar  $\text{Ca}^{2+}$  concentrations ( $\text{EC}_{50}$ = 300-500 nM). Moreover, SK/IK channels display a fast time constant for activation (5-15ms) (145, 431). This feature makes SK/IK channels an ideal target for coupling with distinct  $\text{Ca}^{2+}$  signals. Indeed, numerous studies have demonstrated that IK/SK channels are concentrated at MEPS in endothelial cells, where the majority of localized  $\text{Ca}^{2+}$  signals also occur (14, 286, 288, 354, 355). Spatial proximity between SK/IK channels and  $\text{Ca}^{2+}$  signals at MEPS ensures selective activation of SK/IK channels by  $\text{Ca}^{2+}$  signals. SK/IK channel activation, in turn, results in endothelial cell membrane hyperpolarization, which is transmitted to SMC via MEGJs, causing vasodilation. SK and IK channel currents have been recorded in freshly isolated endothelial cells from mesenteric (354), cerebral (134), and pulmonary resistance (286) arteries. Taylor and colleagues reported that SK3 channel deletion depolarizes endothelial cell membrane in mesenteric arteries and increases vasoconstriction and blood pressure (381). A subsequent study showed that inhibition of SK or IK channels depolarizes endothelial cells from mesenteric arteries by ~ 8 mV and 3 mV, respectively (198). These results suggest that SK/IK channels might be constitutively activated by spontaneously occurring  $\text{Ca}^{2+}$  signals in endothelial cells.

### **$\text{Ca}^{2+}$ -CaM-dependent protein kinase II (CaMKII)**

Ser or Thr residues are the target sites of phosphorylation by  $\text{Ca}^{2+}$ -CaM kinase family (CaMK); therefore, CaMKs are also known as Ser/Thr kinases. CaMKs share a conserved structure with three characteristic domains: catalytic, autoinhibitory, and CaM-binding domains. CaMK family is divided into two main groups- multifunctional CaMKs (CaMKI, CaMKII, and CaMKIV), which have multiple downstream intracellular targets; and substrate-specific CaMKIII,

which has only one downstream target (295). CaMKII has recently emerged as an essential vasoregulatory mechanism. CaMKII is expressed as one of the four isoforms ( $\alpha$ ,  $\beta$ ,  $\delta$ , and  $\gamma$ ), with  $\alpha$  and  $\beta$  isoforms occurring primarily in the brain and  $\delta$  and  $\gamma$  isoforms expressed in blood vessels (387). CaMKII, unlike other CaMKs, does not exist in a monomeric state. Indeed, CaMKII has a peculiar association domain that allows the multimeric association of 6 to 12 monomers, which is partly responsible for the ability of CaMKII to respond to diverse intracellular  $\text{Ca}^{2+}$  oscillations (374). Activation of CaMKII occurs in multiple steps. The first step ( $\text{Ca}^{2+}$ -CaM-dependent) involves  $\text{Ca}^{2+}$ -CaM binding to CaMKII and disrupts the interaction between the autoinhibitory and catalytic domains. In the second step ( $\text{Ca}^{2+}$ -CaM independent), the  $\text{Ca}^{2+}$ -CaM activated subunit phosphorylates the catalytic subunit and activates it (61).

The significance of CaMKII in orchestrating the functional responses to intracellular  $\text{Ca}^{2+}$  is unclear, mainly due to two reasons- 1) the majority of studies on CaMKII have been performed in cell culture systems and evidence from intact tissue is scarce (390); and 2) numerous studies have used KN-93, a non-specific CaMKII inhibitor (296). Therefore, caution must be used while interpreting the currently available literature on CaMKII. In a recent development, Murthy and colleagues investigated the role of CaMKII *in vivo* using a transgenic mouse model, where AC3-I (CaMKII inhibitory peptide) was conditionally expressed in the endothelium. AC3-I mice showed unaltered circulating NO levels and blood pressure compared to control mice. Furthermore, endothelium-dependent vasodilation of mesenteric arteries was also unchanged in AC3-I mice. However, in culture systems, AC3-I-dependent CaMKII inhibition prevented the increase in intracellular  $\text{Ca}^{2+}$  in response to bradykinin (264). Therefore, further evidence is needed for a definitive assessment of the functional roles of CaMKs in endothelial cells.

### **Protein kinase C (PKC)**

This large family of serine/threonine protein kinases has been divided into four functionally diverse subfamilies according to their enzymatic properties.  $\text{PKC}\alpha$ ,  $\text{PKC}\beta$ , and  $\text{PKC}\gamma$

belong to the conventional family (cPKC). This review will specifically focus on cPKCs as they are activated in a  $\text{Ca}^{2+}$ -dependent manner (244). The remaining families are: novel PKCs (nPKCs) composed of the  $\delta$ ,  $\eta$ ,  $\epsilon$  and  $\theta$  isotypes; atypical PKCs (aPKCs)  $\lambda$  and  $\zeta$ ; and the PRKs family. The enzymatic activity of nPKCs and aPKCs is  $\text{Ca}^{2+}$ - independent (314). PKC is activated by diacylglycerol (DAG) (377), phosphatidylserine (PS) (349), and by phorbol 12-myristate 13-acetate (PMA) (43).

The N-terminal regulatory (36 kDa) and C-terminal catalytic domains (42 kDa) of PKC are separated by a hinge region (178). The regulatory domain contains- 1) a cysteine-rich sequence that coordinates two  $\text{Zn}^{2+}$  ions (361) and is essential for DAG, PMA (284, 348, 361), and PS binding (175, 271); 2) a conserved autoinhibitory sequence (149) that maintains PKC in an inactive state in the cytosol (150); and 3) a  $\text{Ca}^{2+}$ -binding domain (187).  $\text{Ca}^{2+}$  binding is a pivotal step for PKC activation and its membrane association. Binding of cytosolic PKC with two  $\text{Ca}^{2+}$  ions results in a weak association with the plasma membrane, whereas interaction of PKC with the third  $\text{Ca}^{2+}$  ion enables its strong association with the plasma membrane (187). The  $\text{Ca}^{2+}$ -bound form of PKC is also required for its interaction with PIP2 (320). The catalytic domain comprises ATP binding sequence and a region important for PKC-substrate interaction (275). PKC activators, including  $\text{Ca}^{2+}$ , DAG, PS, and PMA, promote complete allosteric activation and translocation to the plasma membrane (312).

### **Protein kinase C (PKC) in ECs**

PKC has been shown to promote EC proliferation by participating in the vascular endothelial growth factor (VEGF) signaling cascade (426). PKC $\beta$  is thought to be the main isoform associated with the mitogenic effects of VEGF (4, 430), although PKC $\alpha$  has also been associated with VEGF-induced angiogenesis (420). Suzuma et al. demonstrated that PKC $\beta$ II

promotes retinal neovascularization in a mouse model of oxygen-induced retinal neovascularization (373). Indeed, retinal neovascularization was diminished in PKC $\beta$ <sup>-/-</sup> mice, whereas a more extensive network of neovascularization was observed in a mouse model overexpressing PKC $\beta$ II (PKC $\beta$ II Tg) (373). On the contrary, a separate study by Spyridopoulos and colleagues reported that specific PKC $\alpha$  and PKC $\beta$  inhibition increases VEGF-induced angiogenesis. In this study, PKC $\alpha$  and PKC $\beta$  inhibition also enhanced the VEGF-dependent increase in vascular permeability via NOS activation (358). The reasons for the conflicting results in the two studies (358, 373) remain unclear.

Adapala et al. demonstrated that PKC $\alpha$  is necessary for acetylcholine-induced Ca<sup>2+</sup> entry via TRPV4 channels (2). Further studies by Sonkusare and colleagues demonstrated that PKC anchoring by AKAP150 is necessary for enhancing Ca<sup>2+</sup> influx through TRPV4 channels at MEPs. In this regard, Fan et al. showed that PKC phosphorylates TRPV4 channels, an effect that is enhanced by the presence of AKAP150 (93). Along similar lines, Ottolini et al. demonstrated that acetylcholine- and PKC-activation of TRPV4 channels was absent in endothelium-specific TRPV4<sup>-/-</sup> mice (289). However, cell-specific knockout mice are needed to obtain an accurate understanding of the relative contributions of different PKC isoforms to vascular function.

### **Myosin light-chain kinase (MLCK)**

MLCK is a Ca<sup>2+</sup>/CaM-dependent kinase that promotes actin-myosin cross-bridge formation and vasoconstriction (351) (Figure 1). PKA-dependent phosphorylation on Ser<sup>512</sup> negatively modulates the Ca<sup>2+</sup>/CaM-sensitivity of MLCK (156, 224) and reduces its affinity for Ca<sup>2+</sup>/CaM (Ca<sup>2+</sup> desensitization) (57). CaMKII also appears to be involved in MLCK

phosphorylation and Ca<sup>2+</sup> desensitization (379, 380). Two different genes encode for MLCKs: smooth muscle MLCK (*mylk1*) (110) and skeletal muscle MLCK (*mylk2*) (144, 168). For this review, we will focus on SMC MLCK and will refer to it as MLCK. Two known isoforms of MLCK are: short MLCK (130–150 kDa), which is expressed in mature SMCs (25); and long MLCK (208–214 kDa), which is expressed mainly in embryonic SMCs (168) and mature ECs (400).

### **Myosin light-chain kinase (MLCK) in ECs**

The phosphorylation status of myosin light chain (MLC) is an essential regulator of EC permeability. MLCK enhances actomyosin contractility and weakens EC-EC adhesion by phosphorylating MLC (80, 385, 386). Thus, MLCK-dependent MLC phosphorylation regulates endothelial barrier function by maintaining a basal degree of permeability. Indeed, MLCK inhibition resulted in reduced vascular permeability (445). Huang et al. showed that MLCK inhibition lowers microvascular hyperpermeability in thermal injury (152). Genetic deletion of the long MLCK isoform (MLCK-210<sup>-/-</sup>) confirmed the importance of long MLCK in increasing the pulmonary microvascular permeability in response to lung injury (405). Moreover, MLCK-210<sup>-/-</sup> mice are protected against microvascular hyperpermeability induced by burn injury (311). Moitra and colleagues generated genetically engineered mice overexpressing the long MLCK isoform in ECs (VE- MLCK-210) (254). VE-MLCK-210 mice showed increased pulmonary microvascular permeability under resting conditions and augmented hyperpermeability following lung injury (254). These findings established a pivotal role for long MLCK in increasing microvascular permeability. Therefore, targeting long MLCK isoform may be a promising therapeutic intervention in pathological conditions characterized by increased microvascular leakage. In this regard, further research on developing isoform-specific MLCK inhibitors is needed to reduce possible side effects with inhibition of long MLCK (338).

### **Endothelial nitric oxide synthase (eNOS)**

Nitric oxide (NO) was first identified as the major endothelium-derived relaxing factor nearly thirty years ago (108, 109, 153, 154, 262). To this date, NO-dependent vasodilation remains the most studied mechanism for endothelium-dependent vasodilation under physiological and pathological conditions. Three different nitric oxide synthases (NOS) catalyze the production of NO from L-arginine- neuronal or nNOS; inducible or iNOS; and endothelial or eNOS (104). Although other NOS can be present in the vascular wall, endothelial NO mainly comes from the activation of endothelial NO synthase (eNOS) or NOS3 (5, 256, 399). Synthesis of NO by eNOS requires the precursor L-arginine, cofactors tetrahydrobiopterin (BH4), flavin adenine dinucleotide (FAD), flavin mononucleotide (FMN), CaM, and iron protoporphyrin IX (Heme Fe). eNOS protein is synthesized as monomers but needs to form homodimers to produce NO. As monomers, the oxygenase domain of eNOS produces superoxide; a phenomenon commonly referred to as eNOS uncoupling that contributes to oxidative stress in diseases (399).

eNOS is localized in the caveolae, which are membrane invaginations rich in caveolin-1 (104, 357). eNOS can be activated in a  $Ca^{2+}$ -dependent manner or through posttranslational modifications.  $Ca^{2+}$  can activate eNOS by inducing CaM binding to the CaM-binding domain on eNOS. Increased  $Ca^{2+}$ -CaM displaces eNOS from caveolin-1 and relieves the inhibitory effect of caveolin-1 on eNOS activity (71). Moreover, the displacement of eNOS from caveolin-1 promotes its translocation to the cytosol, where eNOS can undergo posttranslational modifications that activate it. Association of eNOS with caveolin-1 also localizes it with several other signaling molecules, including ion channels, protein kinases, GPCRs, and tyrosine kinases, thus potentially increasing the chances of eNOS activation by these signaling elements (399).

Phosphorylation can have variable effects on eNOS activity depending on the site of phosphorylation. Phosphorylation at Ser<sup>1177</sup> activates, whereas phosphorylation at Thr<sup>495</sup> inhibits the enzyme (101, 104, 143, 247). PKA, protein kinase B (PKB), AMPK, CaMK, and extracellular

signal-regulated kinases 1 or 2 can phosphorylate eNOS at Ser<sup>1177</sup> (143). On the contrary, Rho kinase and PKC phosphorylate eNOS at Thr<sup>495</sup> and thus inhibit it (48, 366). Moreover, tyrosine kinase can also phosphorylate eNOS on Tyr<sup>657</sup> and lower eNOS activity (100). Phosphorylation of eNOS at Tyr<sup>81</sup> by Src kinase facilitates NO production (106). In addition to phosphorylation, other posttranslational modifications that modify eNOS activity include cysteine palmitoylation, which localizes eNOS to the caveolae and brings it closer to regulatory signaling elements (215); S-nitrosylation at Cys<sup>94</sup> and Cys<sup>99</sup> that inhibits enzyme activity (309); acetylation at Lys<sup>610</sup> and deacetylation at Lys<sup>497</sup> and Lys<sup>507</sup>, which increase the enzyme activity (143); glycosylation at Ser<sup>1177</sup>, which decreases eNOS activity (265); S-glutathionylation at Cys<sup>689</sup> and Cys<sup>908</sup>, which promotes eNOS uncoupling (46, 47).

NO released as a result of eNOS activation can passively diffuse to the SMC layer, where it activates a soluble guanylyl cyclase (GC)-cGMP-PKG signaling pathway to cause vasodilation (69). NO can also activate the endothelial GC-PKG pathway that limits Ca<sup>2+</sup> influx in ECs and endothelium-dependent vasodilation (238). Two main K<sup>+</sup> channels that regulate SMC membrane potential are BK and Kv channels (163). While it is well-established that NO activates both BK and Kv channels, the mechanism of activation appears to be two-fold. Some studies show GC-cGMP-dependent activation of BK channels by NO (11, 313), whereas other studies indicate that NO can activate both BK and Kv channels in a GC-PKG-independent manner (29, 252). The latter mechanism possibly involves post-translational modification of the channel by NO, such as S-nitrosylation, or cAMP-PKA signaling (159). Activation of SMC K<sup>+</sup> channels by NO results in membrane hyperpolarization, which deactivates LTCCs to relax SMCs. PKG also promotes the uptake of Ca<sup>2+</sup> by the SR by phosphorylating phospholamban, which increases SERCA activity (41, 399). IP3R Ca<sup>2+</sup> release from the SR in SMCs is crucial for myogenic vasoconstriction (118, 421). PKG has also been shown to phosphorylate IP3R-associated PKG substrate (IRAG), inhibiting Ca<sup>2+</sup> release from the SR (327, 328) and myogenic vasoconstriction. The NO-GC-

cGMP-PKG-I pathway also activates MLCP in SMCs. PKG-I binds to and phosphorylates the regulatory subunit of MLCP, MYPT1, and prevents the inhibition of MLCP. This MLCP de-inhibition lowers cross-bridge cycling and SMC contraction (212, 372, 424).

Intriguingly, both IK/SK channels and eNOS can be activated by  $Ca^{2+}$ , and yet either eNOS or IK/SK channels play a predominant role in endothelium-dependent vasodilation in each vascular bed. A generally accepted distinction is that eNOS regulates endothelium-dependent vasodilation in larger (conduit) arteries, whereas IK/SK channel mediated hyperpolarization plays a major role in smaller, resistance-sized arteries (342, 396). Moreover, lower level, localized increases in  $Ca^{2+}$  seem to preferentially couple with IK/SK channels (14, 147, 354, 355) except in the case of small pulmonary arteries where they couple with eNOS (238). Ottolini and colleagues recently showed that  $Ca^{2+}$  signal-IK/SK channel co-localization and NO scavenging protein Hb $\alpha$  favor  $Ca^{2+}$ -IK/SK channel signaling in systemic arteries. On the contrary,  $Ca^{2+}$  signal-eNOS co-localization and absence of Hb $\alpha$  facilitated  $Ca^{2+}$  signal-eNOS signaling in the pulmonary circulation (Figure 4) (286). It should be noted that the blood pressure is elevated in eNOS global knockout mice (339, 359, 398). eNOS is also expressed in cell types other than endothelial cells. Therefore, investigations in endothelium-specific eNOS<sup>-/-</sup> are likely to result in interesting findings on endothelium-dependent vasodilation and blood pressure regulation.

## **1.6 Abnormal $Ca^{2+}$ signaling in vascular disorders**

The role of abnormal  $Ca^{2+}$  signaling mechanisms in the pathogenesis of vascular disorders is well-established, particularly in resistance-sized arteries and arterioles. Both endothelial and SMC  $Ca^{2+}$  signaling mechanisms are impaired in various disorders.  $Ca^{2+}$  signals in SMCs have mostly been associated with increased activity, resulting in vasoconstriction and higher vascular resistance. RyR-mediated  $Ca^{2+}$  sparks are an exception to this rule as they are vasodilatory signals, and their activity is decreased in vascular disorders. Impairment of

endothelial  $\text{Ca}^{2+}$  signaling mechanisms attenuates endothelium-dependent vasodilation, contributing to increased vasoconstriction in vascular disorders. Increased activity of SMC and endothelial  $\text{Ca}^{2+}$  signals has also been associated with hyperproliferation, migration, and hyperpermeability in vascular disorders. In this section, we will discuss the studies on  $\text{Ca}^{2+}$  signaling mechanisms in resistance arteries and arterioles in vascular disorders.

In the endothelium, AKAP150 and TRPV4 channels are highly localized at MEPs, where AKAP150 anchors PKC in the vicinity of TRPV4 channels and increases the coupling among TRPV4 channels (355).  $\text{Ca}^{2+}$  influx through endothelial TRPV4 channels causes vasodilation via IK/SK channel activation (14, 354). Sonkusare and colleagues demonstrated that Ang II-induced hypertension disrupts endothelial AKAP150-TRPV4 channel signaling by lowering the expression of AKAP150 at MEPs (355). A recent study by Ottolini et al. proposed the concept of pathological signaling microdomains in obesity, whereby pathological elements localized at MEPs impaired endothelial  $\text{Ca}^{2+}$  signaling (288). The authors first demonstrated the importance of endothelial AKAP150-TRPV4 channel signaling in lowering systemic blood pressure under normal conditions. In obesity, increased expression of inducible nitric oxide synthase (iNOS) and NADPH oxidase 1 (NOX1) at MEPs correlated with elevated levels of nitric oxide (NO) and superoxide radicals ( $\text{O}_2^{\cdot-}$ ), respectively. Interaction of NO and  $\text{O}_2^{\cdot-}$  resulted in localized formation of the oxidant molecule peroxynitrite. Peroxynitrite, in turn, disrupted AKAP150-PKC interaction, thereby reducing TRPV4 channel activity at MEPs. The loss of endothelium-dependent vasodilation, as a result of this pathological signaling, led to increased blood pressure in obesity. In a separate study, Wilson and colleagues indicated that altered  $\text{Ca}^{2+}$  signaling networks of endothelial cells contribute to the loss of endothelial function in obesity (423).  $\text{Ca}^{2+}$  signaling networks of endothelial cells are critical for determining overall vascular resistance (201). While the loss of endothelial function in obesity is well-documented (288, 423), a study by Greenstein and colleagues reported that obesity is not associated with a loss of endothelium-dependent

vasodilation (126). Differences in diet regimens and analytical techniques may be responsible for the divergent findings. Regardless, it should also be noted that obesity-induced vascular dysfunction is multifactorial and likely caused by both endothelial and smooth muscle impairments.

Alterations in  $\text{Ca}^{2+}$  signals through endothelial TRPV4 channels have been demonstrated in multiple disease models. In cerebral arteries from a mouse model of Alzheimer's disease, endothelial TRPV4 channel activity was impaired with a consequent decrease in acetylcholine-evoked vasodilation. The impairment of TRPV4 channel activity was linked to the excessive formation of ROS in this model. Indeed, reducing  $\text{H}_2\text{O}_2$  and  $\text{O}_2^-$  levels rescued the vasodilation to acetylcholine (450). Similarly, Ma et al. observed decreased acetylcholine-induced vasodilation in mesenteric arteries from diabetic mice that was attributed to impaired TRPV4-SK channel signaling (228). Stroke-prone spontaneously hypertensive rats also showed a downregulation of endothelial TRPV4 and SK channels, resulting in impaired acetylcholine-induced vasodilation (334) .

Recent discoveries suggest a detrimental role for excessive  $\text{Ca}^{2+}$  in endothelial cells from arteries or capillaries in the pathogenesis of some vascular disorders. Excessive endothelial  $\text{Ca}^{2+}$  activity in systemic arteries was correlated with elevated histone levels after traumatic brain injury (56). Collier and colleagues found that high levels of histones in the plasma from trauma patients evoked an exaggerated increase in endothelial  $\text{Ca}^{2+}$ . Prolonged exposure to histones led to endothelial  $\text{Ca}^{2+}$  overload, endothelial cell death, and subsequent loss of endothelium-dependent vasodilation (56). Another study by Suresh et al. suggested that higher endothelial  $\text{Ca}^{2+}$  levels, resulting from increased TRPV4 channel activity, underlies capillary endothelial migration in pulmonary hypertension (370). Contrary to these results, a recent study presented an exciting idea that reduced membrane cholesterol content lowers  $\text{Ca}^{2+}$  entry in endothelial cells in pulmonary hypertension (447).

## 1.7 Conclusion

Ca<sup>2+</sup> signals in ECs arise from different sources and couple with disparate targets. Various Ca<sup>2+</sup> signals combined with multiple Ca<sup>2+</sup>-sensitive targets and physiological stimuli result in numerous stimulus-Ca<sup>2+</sup> signal-target linkages and functional effects. Ca<sup>2+</sup> signals in ECs occur in a spatially restricted manner; however, excessive activation of individual signals can result in a whole-cell increase in Ca<sup>2+</sup>. Recent developments in image acquisition speed, combined with confocal, TIRF, and multi-photon imaging, have advanced our understanding of spatial and kinetic properties of the individual Ca<sup>2+</sup> signals in the vasculature. Recent functional studies have also provided the understanding that Ca<sup>2+</sup> signaling pathways are indispensable for intercellular communications that regulate vascular contractility. Moreover, the individual Ca<sup>2+</sup> signaling elements can interact with one another to achieve a finer control of vascular function.

There is remarkable heterogeneity in the Ca<sup>2+</sup> signaling mechanisms among different vascular beds, contributing to functional heterogeneity of ECs. The Ca<sup>2+</sup> signaling elements, their regulatory proteins, and signaling targets vary from large arteries to small arteries and from one vascular bed to another. While the functional effects of most Ca<sup>2+</sup> signaling pathways are well-established at the level of resistance arteries or arterioles, the physiological roles of many pathways at the whole-animal level remain unknown. In some cases, data interpretation is confounded by the presence of an ion channel in both SMCs and ECs. Cell-specific knockout mice will provide a definitive answer to the physiological significance of such pathways in either ECs or SMCs. The Ca<sup>2+</sup> signaling mechanisms ECs can be activated by mechanical (pressure or flow) or neurohumoral (GPCR signaling, nerve-stimulation) stimuli. Although significant progress has been made in understanding the mechanisms for myogenic vasoconstriction and flow-mediated vasodilation, the precise mechanosensor proteins remain unclear. Recent discoveries suggest that TRPP1, TRPML1, and PIEZO1 channels may represent new Ca<sup>2+</sup> signaling pathways contributing to mechanosensation in the vasculature. It is anticipated that future

studies will reveal newer  $\text{Ca}^{2+}$  signaling elements, their physiological roles, and abnormalities in pathological conditions.  $\text{Ca}^{2+}$  signaling mechanisms and signaling organizations of cells have been shown to be abnormal in vascular disorders. Therefore, a major objective of future studies will be to identify “targetable” abnormalities in  $\text{Ca}^{2+}$  signaling mechanisms in vascular disorders.

**Figure 1. The contrasting effects of smooth muscle cell (SMC) and endothelial cell (EC)  $\text{Ca}^{2+}$  on vascular contractility.**

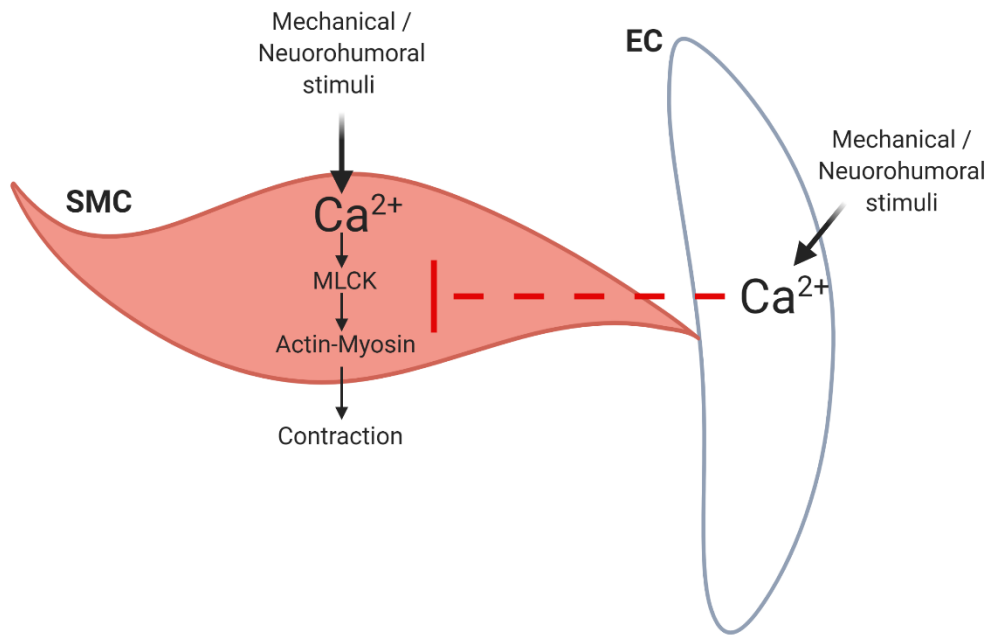


**Figure 1.** Mechanical and neurohumoral stimuli can increase intracellular  $\text{Ca}^{2+}$  in SMCs and ECs. Intracellular  $\text{Ca}^{2+}$  in SMCs and ECs, in general, has opposite effects on vascular resistance. Increase in SMC  $\text{Ca}^{2+}$  activates the contractile machinery in SMCs (myosin light chain kinase or MLCK/Actin-Myosin). In contrast, an increase in EC  $\text{Ca}^{2+}$  inhibits SMC contractile mechanisms. The dotted red line indicates inhibition of SMC contractility.

**Figure 2. Ca<sup>2+</sup> signaling networks at myoendothelial projections (MEPs).**

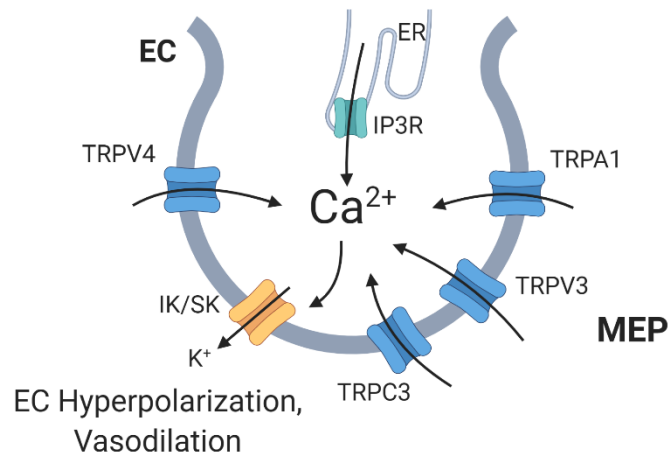


**Figure 2.** Ca<sup>2+</sup> influx via TRPV4/TRPV3/TRPA1/TRPC3 channels or Ca<sup>2+</sup> release from the endoplasmic reticulum (ER) via inositol triphosphate receptors (IP3Rs) at MEPs activates nearby small (SK) and intermediate (IK) conductance Ca<sup>2+</sup>-activated K<sup>+</sup> channels. IK/SK channel activation hyperpolarizes endothelial cells (EC) membrane and results in vasodilation. TRPV/TRPA/TRPC: members of transient receptor potential channel family.

**Figure 3. Signaling mechanisms at myoendothelial projections (MEPs) that control the communication between endothelial and smooth muscle cells (SMCs) and SMC contractility.**

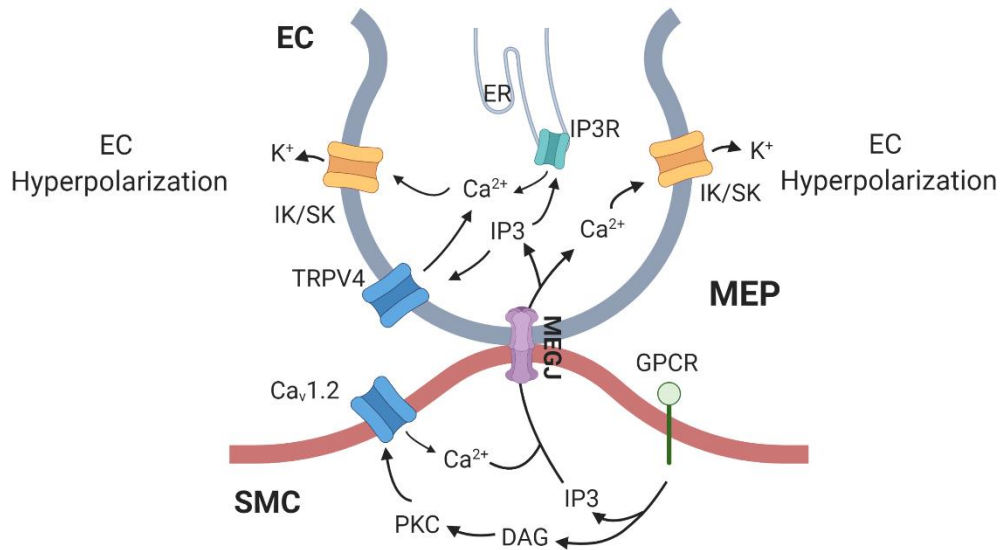


**Figure 3.** Stimulation of Gq-protein coupled receptors (GqPCRs) on SMC membrane leads to the formation of inositol triphosphate (IP3) and diacylglycerol (DAG). DAG activates protein kinase C (PKC), which phosphorylates voltage-gated Ca<sup>2+</sup> (Ca<sub>v</sub>1.2) channel, leading to an increase in SMC Ca<sup>2+</sup> and vasoconstriction. IP3 and Ca<sup>2+</sup> can diffuse to ECs through myoendothelial gap junctions (MEGJ). Elevation of IP3 and Ca<sup>2+</sup> at MEPs limits vasoconstriction by activating TRPV4-IK/SK channel and IP3R-IK/SK channel signaling. TRPV4: transient receptor potential vanilloid channel 4 (TRPV4); SK and IK: small (SK) and intermediate (IK) conductance Ca<sup>2+</sup>-activated K<sup>+</sup> channels.

**Figure 4. The molecular mechanism underlying selective activation of IK/SK channels in mesenteric arteries versus eNOS in pulmonary arteries.**

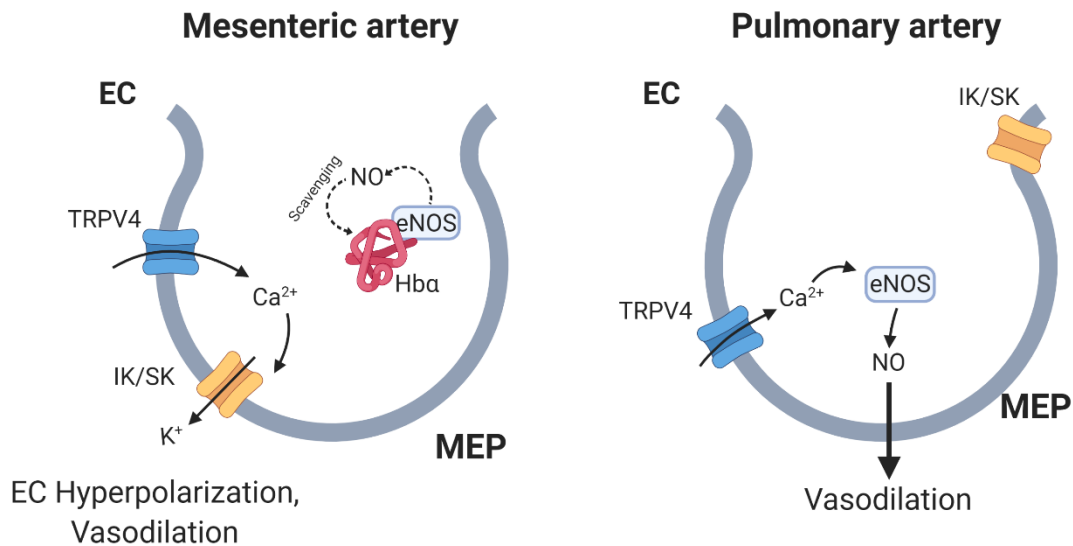


**Figure 4.** In mesenteric arteries,  $Ca^{2+}$  entry through the TRPV4 channel at the myoendothelial projections (MEPs) determines vasodilation via activation of nearby small (SK) and intermediate (IK) conductance  $Ca^{2+}$ -activated  $K^+$  channels. Co-localization of endothelial nitric oxide synthase (eNOS) with hemoglobin alpha (Hb $\alpha$ ), a nitric oxide (NO) scavenging protein, prevents TRPV4-eNOS signaling. On the contrary, in pulmonary arteries, IK/SK channels and Hb $\alpha$  do not localize at MEPs. Therefore,  $Ca^{2+}$  influx via TRPV4 channel activates eNOS causing NO-dependent vasodilation. EC: endothelial cell.

**Figure 5. The contribution of endothelial P2X purinergic receptor, PIEZO1, TRPP1, and TRPV4 channels to flow-induced vasodilation.**

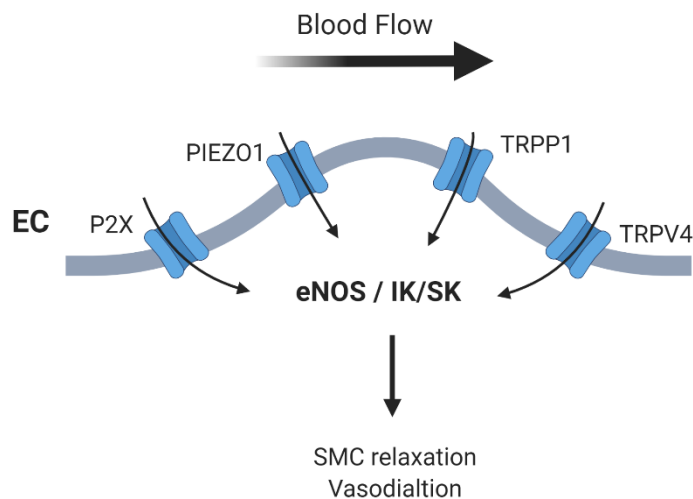


**Figure 5.** Sheer stress-dependent activation of P2X, PIEZO1, TRPP1, and TRPV4 channels increases endothelial  $\text{Ca}^{2+}$ . Shear stress-induced increase in endothelial  $\text{Ca}^{2+}$  can cause vasodilation via one of the two pathways- 1) activation of endothelial nitric oxide synthase (eNOS) and nitric oxide (NO)-mediated vasodilation; and 2) activation of IK/SK channels, leading to endothelium-dependent hyperpolarization and vasodilation. TRPP1: transient receptor potential polycystic 1 channel, TRPV4: transient receptor potential vanilloid 4 channel.

**Figure 6. Sarco-endoplasmic reticulum Ca<sup>2+</sup>-ATPase (SERCA) transporting cycle.**

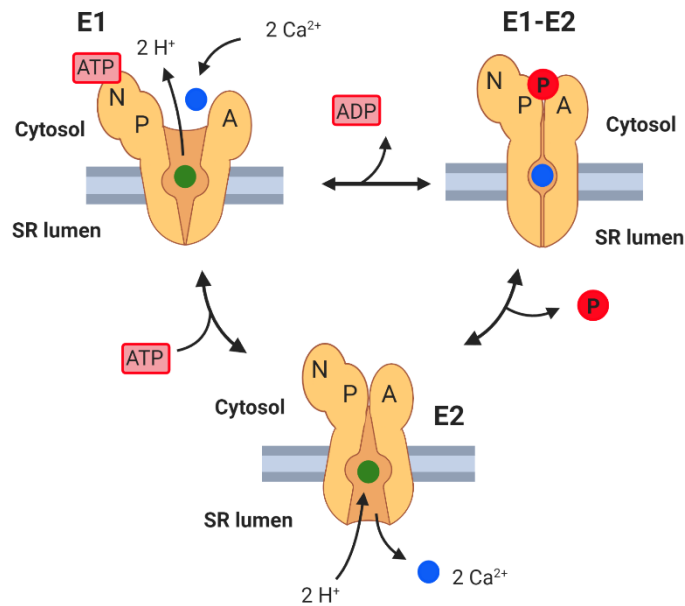


**Figure 6.** E1 indicates SERCA conformation characterized by a high affinity for Ca<sup>2+</sup>. E1-E2 represents a transient high energy state. E2 represents SERCA conformation characterized by a low affinity for Ca<sup>2+</sup>. Two cytosolic Ca<sup>2+</sup> ions bind to SERCA in E1 conformation. Adenosine triphosphate (ATP) tethers to the nucleotide (N) domain and phosphorylates the (P) domain. The phosphorylated (P) domain interacts with the (A) domain resulting in two sequential conformational changes (E1-E2, and E2). SERCA in E2 conformation releases Ca<sup>2+</sup> into the sarcoplasmic reticulum (SR) lumen. Pi: inorganic phosphate; ADP: adenosine diphosphate; H<sup>+</sup>: proton.

## **Chapter 2: Materials and Methods**

## 2.1 Materials and Methods for Chapter 3

**Animal care and use.** Male C57BL6/J, eNOS<sup>-/-</sup> (10–14 weeks old, ~25 g; The Jackson Laboratory, Bar Harbor, ME, USA), and TRPV4<sub>EC</sub><sup>-/-</sup> mice (289) were used in this study (n = 85 mice in total). Mice were housed in an enriched environment and maintained on a 12:12 h light-dark cycle at ~23°C with fresh tap water and standard chow diet available *ad libitum*. Mice were euthanized with pentobarbital (90 mg/kg, intraperitoneal; Diamondback Drugs, Scottsdale, AZ, USA) followed by decapitation for harvesting intestinal and lung tissues. TRPV4<sub>EC</sub><sup>-/-</sup> mice were developed and validated as described earlier (289). Third-order MAs (~100 μm) and fourth order PAs (~100 μm) were dissected in cold Hepes-buffered physiological salt solution (Hepes-PSS; 10 mM Hepes, 134 mM NaCl, 6 mM KCl, 1 mM MgCl<sub>2</sub> hexahydrate, 2 mM CaCl<sub>2</sub> dihydrate, and 7 mM dextrose; pH adjusted to 7.4 using 1 M NaOH).

**Pressure myography.** Isolated PAs and MAs were cannulated on glass pipettes, mounted in an arteriography chamber (Instrumentation and Model Facility, University of Vermont, Burlington, VT, USA) at areas lacking branching points, and pressurized to physiological pressure (15 mm Hg for PAs and 80 mm Hg for MAs). Arteries were superfused with PSS (119 mM NaCl, 4.7 mM KCl, 1.2 mM KH<sub>2</sub>PO<sub>4</sub>, 1.2 mM MgCl<sub>2</sub> hexahydrate, 2.5 mM CaCl<sub>2</sub> dihydrate, 7 mM dextrose, and 24 mM NaHCO<sub>3</sub>) at 37°C and bubbled with 20% O<sub>2</sub>/5% CO<sub>2</sub> to maintain the pH at 7.4. All drugs were added to the superfusing PSS. Arteries were precontracted with 100 nM U46619, a thromboxane A<sub>2</sub> agonist. Endothelial health was assessed by monitoring the response to NS309 (1 μM), a direct opener of endothelial IK/SK channels. Arteries that failed to dilate to NS309 were discarded. In some experiments, the endothelium was denuded by passing an air bubble through the artery for 60 seconds. Complete removal of the endothelial cell layer was verified by the absence of dilation to NS309. Changes in arterial diameter were recorded at a 60-ms frame rate

using a charge-coupled device camera and edge-detection software (IonOptix LLC, Westwood, MA, USA). For all drug treatments, the incubation time was 5–10 minutes. At the end of each experiment, Ca<sup>2+</sup>-free PSS (119 mM NaCl, 4.7 mM KCl, 1.2 mM KH<sub>2</sub>PO<sub>4</sub>, 1.2 mM MgCl<sub>2</sub> hexahydrate, 7 mM dextrose, 24 mM NaHCO<sub>3</sub>, and 5 mM EGTA) was applied to assess the maximum passive diameter. Percent constriction was calculated by

$$\left[ \frac{(Diameter_{before} - Diameter_{after})}{Diameter_{before}} \right] * 100,$$

where *Diameter<sub>before</sub>* is the diameter before drug treatment and *Diameter<sub>after</sub>* is the diameter after drug treatment.

Percent vasodilation was calculated by

$$\left[ \frac{(Diameter_{dilated} - Diameter_{basal})}{(Diameter_{Ca\ free} - Diameter_{basal})} \right] * 100,$$

where *Diameter<sub>basal</sub>* is the diameter before drug treatment, *Diameter<sub>dilated</sub>* is the diameter after drug treatment, and *Diameter<sub>Ca<sub>free</sub></sub>* is the maximum passive diameter.

For a subset of MAs, pressure myography studies were performed in the absence of U46619 at a pressure of 80 mm Hg to induce myogenic tone. Endothelial health was tested with NS309, followed by treatment with the TRPV4 inhibitor GSK2193874.

**Ca<sup>2+</sup> imaging.** Ca<sup>2+</sup>-imaging studies were performed as described previously (147, 238, 354).

Briefly, third-order MAs and fourth-order PAs were surgically opened and pinned down on a SYLGARD block with the endothelium facing up (*en face* preparation). MAs and PAs were incubated with Fluo-4 AM (10 μM) and pluronic acid (0.04%) at 30°C for 45 and 30 minutes, respectively, in the dark. Ca<sup>2+</sup> images were acquired at 30 frames per second using an Andor

Revolution WD (with Borealis) spinning-disk confocal imaging system (Andor Technology, Belfast, UK) comprising an upright Nikon microscope with a 60X water-dipping objective (numerical aperture, 1.0) and an electron multiplying charge-coupled device camera. Arteries were superfused with PSS (119 mM NaCl, 4.7 mM KCl, 1.2 mM KH<sub>2</sub>PO<sub>4</sub>, 1.2 mM MgCl<sub>2</sub> 160 hexahydrate, 2.5 mM CaCl<sub>2</sub> dihydrate, 7 mM dextrose, and 24 mM NaHCO<sub>3</sub>), bubbled with 20% O<sub>2</sub> and 5% CO<sub>2</sub> to maintain the pH at 7.4. All experiments were performed at 37°C. Fluo-4 was excited using a 488-nm solid-state laser, and emitted fluorescence was captured using a 525/36 nm band-pass filter. Arteries were treated with cyclopiazonic acid (CPA; 20 μM), a sarco-endoplasmic reticulum (SR/ER) Ca<sup>2+</sup>-ATPase inhibitor, for 15 minutes at 37°C before imaging to eliminate intracellular Ca<sup>2+</sup>-release signals. CPA does not *per se* alter the activity of endothelial TRPV4 (TRPV<sub>4EC</sub>) sparklets (147). TRPV<sub>4EC</sub> sparklet activity was determined before and 5 minutes after the addition of a given pharmacological agent. Ca<sup>2+</sup> images were analyzed using custom-designed SparkAn software (developed by Dr. Adrian Bonev, University of Vermont). Fractional fluorescence traces (F/F<sub>0</sub>) were obtained by placing a 1.7 μm<sup>2</sup> (5×5 pixels) region of interest (ROI) at the peak event amplitude. Representative F/F<sub>0</sub> traces were filtered using a Gaussian filter and a cutoff corner frequency of 4 Hz.

**Analysis of TRPV<sub>4EC</sub> sparklet activity.** TRPV<sub>4EC</sub> sparklet activity was assessed by measuring increases in fluorescence over an averaged image obtained from 10 images using previously established methods (147, 238, 354). The average TRPV<sub>4EC</sub> sparklet activity is defined as NP<sub>O</sub>, where N is the number of TRPV<sub>4EC</sub> channels per site and P<sub>O</sub> is the open state probability of the channel. NP<sub>O</sub> was calculated with the Single Channel Search module of Clampfit using quantal amplitudes derived from all-points histograms (0.29 ΔF/F<sub>0</sub> for Fluo-4-loaded MAs) by applying the following equation:

$$NP_O = \left[ \frac{(T_{level1} + 2T_{level2} + 3T_{level3} + 4T_{level4})}{T_{total}} \right],$$

where  $T$  represents the dwell time at each quantal level, and  $T_{total}$  is the total recording duration. Average  $NP_O$  per site was obtained by averaging the  $NP_O$  for all sites in a field. The total number of sites per field corresponds to all sparklet sites per field averaged over different arteries.

**Analysis of TRPV4<sub>EC</sub> sparklet localization at MEPs.** TRPV4<sub>EC</sub> sparklet localization at MEPs was measured using Alexa Fluor 633 hydrazide staining of the internal elastic lamina (IEL). After performing  $Ca^{2+}$ -imaging experiments, arteries were incubated with Alexa Fluor 633 hydrazide (10  $\mu$ M) for 5 minutes (147, 238). Images were obtained from the same fields of view (matching X- and Y-coordinates) as used for recording TRPV4<sub>EC</sub> sparklets, using an excitation wavelength of 640 nm and a band-pass emission filter (685/40 nm). Sparklet localization was assessed by overlaying the Fluo-4 image with Alexa Fluor 633 IEL staining. ROIs (1.7  $\mu$ m<sup>2</sup>) corresponding to the peak sparklet fluorescence were placed on the overlaid IEL staining. Sparklet sites were considered to be localized to MEPs if the ROI was within 2  $\mu$ m of the perimeter of holes in the IEL (147, 238). The remaining sparklet sites were considered to be non-MEPs sites.

**Immunostaining.** Immunostaining was performed on *en face* preparations of MAs and PAs. Briefly, arteries were pinned down *en face* on Sylgard blocks and fixed with 4% paraformaldehyde at room temperature for 15 minutes. Fixed arteries were washed three times for 5 minutes with phosphate-buffered saline (PBS). The arteries were then treated with 0.2% Triton-X/PBS for 30 minutes at room temperature on a rocker. Following this permeabilization step, arteries were treated with 5% normal donkey serum or normal goat serum (Abcam plc, Cambridge, MA, USA) for 1 hour at room temperature and subsequently incubated overnight with antibodies against TRPV4, IK, SK, eNOS or H $\beta$  overnight at 4°C. Arteries were then

washed three times with PBS and incubated with Alexa Fluor 568-conjugated donkey anti-rabbit or goat anti-rabbit secondary antibody (1:500; Life Technologies, Carlsbad, CA, USA), as appropriate, at room temperature for 1 hour in the dark. Thereafter, arteries were washed three times with PBS and incubated with 0.3  $\mu$ M 4',6-diamidino-2-phenylindole (DAPI; Invitrogen, Carlsbad, CA, USA) for 10 minutes at room temperature in the dark to stain nuclei. Images were obtained using the Andor imaging system as described previously (147, 238). Consecutive images were taken along the z-axis at a slice thickness of 0.2- $\mu$ m from the top surface of ECs to the bottom surface where they contacted SMCs. DAPI immunostaining was imaged by exciting at 409 nm and collecting the emitted fluorescence with a 447/60-nm band-pass filter. The specificity of the antibody was determined using arteries from endothelial TRPV4<sup>-/-</sup> knockout mice (289) and global eNOS<sup>-/-</sup> mice for TRPV4 and eNOS, respectively. Blocking peptides were used in antibody control experiments for IK channel (REQVNSMVDISKMHMILYDL, Genscript USA Inc., Piscataway, NJ, USA), SK channel (ETQMENYDKHVITYNAERS, Genscript USA Inc.), and Hb $\alpha$  (Abcam plc., ab93083) antibodies. No immunostaining was observed under these conditions.

**Table 1.** List of primary antibodies used for immunostaining.

Protein	Company	ID	Clonality	Concentration	References
TRPV4	LifeSpan BioScience, Inc.	LS_C94498	Polyclonal	1:200	(316)
eNOS	BD Biosciences	610297	Monoclonal	1:100	(197)

IK	Santa Cruz Biotechnology, Inc.	SC 365265	Monoclonal	1:200	(221)
SK	Alomone Labs	APC-028	Monoclonal	1:200	(191)
Hb $\alpha$	Abcam plc.	ab92492	Monoclonal	1:100	(317)

**Automated co-localization analysis.** Imaris 9.3 image analysis software (Bitplane AG, Zurich, Switzerland) was used for automated analyses. Co-localization analyses were performed on three-dimensional (3D) images reconstructed from z-stack images from the top surface of the ECs to the point where MEPs contacted SMCs. The percentage of MEPs (black holes) that coincided with a given protein of interest was determined from automated counts of the total number of holes in each field of view. The green channel, showing the autofluorescence of the IEL, and black holes, indicating MEPs, were inverted so as to render MEPs in green. Background noise was then subtracted, and the image was filtered using a Gaussian filter (filter width, 0.2  $\mu\text{m}$ ). MEPs were automatically detected as green dots  $\geq 2 \mu\text{m}$  in diameter. As a final visual confirmation of the accuracy of the automated detection of MEPs, the original green channel was re-inserted; the detection accuracy for MEPs was found to be  $\sim 95\%$ . MEP detection was followed by automatic detection of the protein of interest, indicated by red immunostaining  $\geq 2 \mu\text{m}$  in diameter. Finally, using a built-in Matlab R2019b co-localization feature in Imaris 9.3, MEPs and the protein of interest were considered to co-localize if the detected protein sites were within a distance of 4  $\mu\text{m}$  from the detected MEPs. A similar procedure was followed for determining the percentage of immunostaining that co-localized with MEPs; immunostaining dots were detected first, followed by MEP detection, and co-localization analysis. To determine the

probability that proteins were randomly distributed to MEPs, we randomly placed ROIs on immunostaining images and performed automated co-localization analyses. This analysis yielded 12% and 22% random co-localization of proteins with MEPs in MAs and PAs, respectively.

**Patch-clamp analysis of freshly isolated ECs.** ECs were freshly isolated from third-order MAs and fourth-order PAs. Briefly, MAs and PAs were digested at 37°C for 60 and 30 minutes, respectively, in dissociation solution (55 mM NaCl, 80 mM Na-glutamate, 6 mM KCl, 2 mM MgCl<sub>2</sub>, 0.1 mM CaCl<sub>2</sub>, 10 mM glucose, 10 mM Hepes, pH 7.3) containing Worthington neutral protease (0.5 mg/mL). For MAs, collagenase (Worthington type 1, 0.5 mg/mL) was added to the enzyme solution after 60 minutes, and digestion was continued for two more minutes. Whole-cell currents were measured at room temperature using the perforated-patch configuration of the whole-cell patch-clamp technique. The bathing solution consisted of 10 mM Hepes, 134 mM NaCl, 6 mM KCl, 2 mM CaCl<sub>2</sub>, 10 mM glucose, and 1 mM MgCl<sub>2</sub> (adjusted to pH 7.4 with NaOH). Patch electrodes were pulled from borosilicate glass (O.D., 1.5 mm; I.D., 1.17 mm; Sutter Instruments, Novato, CA, USA) using a Narishige PC-100 puller (Narishige International USA, Inc., Amityville, NY, USA) and polished using a MicroForge MF-830 polisher (Narishige International USA). The composition of the pipette solution for perforated-patch experiments was 10 mM Hepes, 30 mM KCl, 10 mM NaCl, 110 mM K-aspartate, and 1 mM MgCl<sub>2</sub> (adjusted to pH 7.2 with NaOH). Amphotericin B was dissolved in the intracellular pipette solution to reach a final concentration of 0.3 μM. The pipette resistance was 3–5 MΩ. IK and SK channel currents were elicited by adding 1 μM NS309 (IK/SK channel activator) or 10 and 100 nM GSK101 (TRPV4 channel agonist) to the superfusate. IK/SK channel currents were inhibited by adding TRAM-34 (IK channel inhibitor, 1 μM) and apamin (SK channel inhibitor, 300 nM) to the bath. Current traces obtained from freshly isolated ECs in the presence of TRAM-34 and apamin were subtracted from traces obtained in the presence of NS309 or GSK101 alone to yield TRAM-34 + apamin-sensitive IK/SK channel currents. IK/SK channel currents were recorded by applying

200-ms voltage ramps from -140 mV to +50 mV from a holding potential of -50 mV. The pipette solution for conventional patch clamp consisted of 10 mM HEPES, 123.2 mM KCl, 10 mM NaCl, 5.5 mM MgCl<sub>2</sub>, 0.2 mM CaCl<sub>2</sub>, and 5 mM HEDTA (adjusted to pH 7.2 with 16.8 mM KOH) and contained 3 μM free-Ca<sup>2+</sup> and 1 mM free-Mg<sup>2+</sup>, as calculated using the Max-Chelator program (Chris Patton, Stanford University, CA, USA). TRPV4 channel current was measured in the presence of ruthenium red (1 μM) using the perforated-patch configuration as described previously (354). Currents induced by the TRPV4 channel agonist GSK101 were assessed following application of a 200-ms voltage step from -50 to +100 mV. Data were acquired using a HEKA EPC 10 amplifier and PatchMaster v2X90 software (Harvard Bioscience, Holliston, MA, USA). Patch-clamp data were analyzed using FitMaster v2X73.2 (Harvard Bioscience) and MATLAB R2018a (MathWorks, Natick, MA, USA). TRPV4 channel currents were inhibited by applying 100 nM GSK2193874 (hereafter, GSK219), a selective TRPV4 antagonist, to the bath solution. The effect of each drug was studied 5 minutes after addition.

**Proximity Ligation Assay (PLA).** Third-order MAs and fourth-order PAs were isolated and pinned down *en face* on a Sylgard block. Arteries were fixed in 4% paraformaldehyde for 15 minutes, washed three times with PBS, and then incubated in a solution of 0.2% Triton X for 30 minutes at room temperature. Following this latter permeabilization step, arteries were blocked by incubating with either 5% normal donkey serum (Abcam plc) or 300 mM glycine at room temperature for 1 hour. Arteries were then washed three times with PBS and incubated overnight at 4°C with primary antibodies. The following day, the PLA protocol was performed as described by the manufacturer of the Duolink PLA Technology kit (Sigma-Aldrich, St. Louis, MO, USA). After incubating arteries with 0.3 μM DAPI nuclear stain (Invitrogen, Carlsbad, CA, USA) for 10 minutes at room temperature in the dark, PLA imaging and analysis were performed using an Andor Revolution spinning-disk confocal imaging system and Imaris 9.3 software (Bitplane AG,

Zurich, Switzerland), respectively. Images were obtained along the z-axis at a slice thickness of 0.02  $\mu\text{m}$  from the top surface of ECs to the bottom surface where they contact SMCs.

**NO measurements.** MAs and PAs were pinned down *en face* on a Sylgard block and incubated with 5  $\mu\text{M}$  DAF-FM (4-amino-5 methylamino-2',7'-difluorofluorescein diacetate), prepared in Hepes-PSS containing 0.02% pluronic acid (238) for 20 minutes at 30°C in the dark. DAF-FM forms a fluorescent triazole compound after binding to NO. DAF-FM fluorescence was captured using an Andor Revolution WD (with Borealis) spinning-disk confocal imaging system. DAF-FM fluorescence was recorded using an excitation wavelength of 488 nm, and emitted fluorescence was captured with a 525/36-nm band-pass filter. Images were obtained along the z-axis at a slice thickness of 0.1  $\mu\text{m}$  from the top surface of ECs to the bottom surface where they contact SMCs. For studying GSK101-induced NO release, arteries were treated with GSK101 (or vehicle for a control artery run in parallel) for 5 minutes, followed by GSK101 + DAF-FM (or vehicle + DAF-FM) for 20 minutes. Arteries were then placed in Hepes-PSS for 5 minutes before image acquisition, which was completed within 2 minutes. For studying the effect of Hb $\alpha$ X peptide on GSK101-induced NO release, arteries were treated with Hb $\alpha$ X (or vehicle) for 10 minutes, followed by GSK101 + Hb $\alpha$ X (or vehicle) for 5 minutes and then GSK101 + Hb $\alpha$ X (or vehicle) + DAF-FM for 20 minutes. DAF-FM vials were stored at -20°C and used within two months. Once dissolved in DMSO, DAF-FM solution was stored at -20°C and used within one week. The same DAF-FM solution was used for all comparison groups on each day of experiments.

DAF-FM fluorescence was analyzed using custom-designed SparkAn software. An outline was drawn around each endothelial cell to obtain the arbitrary fluorescence intensity of that cell. The plane with the peak fluorescence intensity was used for quantification. The background (intensity without laser) was then subtracted from the recorded fluorescence. The

fluorescence values from all cells in a field of view were averaged to obtain a single fluorescence number for that field.

**Western blotting.** MAs and PAs were lysed in radioimmunoprecipitation (RIPA) lysis buffer containing protease inhibitors (Life Technologies, Grand Island, NY, USA). Protein concentration was measured using a DC Protein Assay kit (Bio-Rad, CA, USA). Lysates (30  $\mu$ g total protein) were resolved by sodium dodecyl sulfate-polyacrylamide gel electrophoresis on denaturing 4–12% gradient polyacrylamide ready-made gels (NuPAGE Bis-Tris gels; Life Technologies) and transferred onto PVDF (polyvinylidene difluoride) membranes. The membranes were blocked with 10% non-fat dried milk for 1 hour and incubated overnight with rabbit anti-eNOS antibody (NB-300-500, 1:500; Novus Biologicals, Littleton, CO, USA) at 4°C on a rotating shaker. The membranes were then washed three times with PBS containing 0.1% Tween-20 (PBST) and incubated with an anti-rabbit IgG-HRP (1:2500) secondary antibody for 90 minutes at room temperature. Immunoreactive proteins were visualized using enhanced chemiluminescence (ECL) detection reagents (SuperSignal West Femto Maximum Sensitivity Substrate; Life Technologies) as described previously (170). Blots were re-probed for  $\beta$ -actin to ensure equal protein loading. The relative density of bands was analyzed using Image J software.

**Chemicals and reagents.** Cyclopiazonic acid, GSK1016790A, GSK2193874, NS309, apamin, and TRAM-34 were purchased from Tocris Bioscience (Minneapolis, MN, USA). L-NNA, Alexa Fluor 633 hydrazide, and DAF-FM were obtained from Thermo Fisher Scientific Inc. (Waltham, MA, USA). All other chemicals were purchased from Sigma-Aldrich. Hb $\alpha$ X peptide and scrambled control peptide (Scr X) was obtained from Dr. Brant Isakson.

**Statistical analysis.** Results are presented as means  $\pm$  standard deviation. For imaging experiments (Ca<sup>2+</sup> imaging, immunofluorescence, NO measurements, PLA) and pressure myography experiments, n=1 was defined as one artery, and for patch-clamp experiments, n=1

was defined as one cell. Data were obtained from at least three mice in experiments performed on at least two independent batches. All data were presented graphically using CorelDraw Graphics Suite X9 (Ottawa, ON, Canada) and were analyzed statistically using OriginPro 7.5 (Northampton, MA, USA), GraphPad Prism 8 (San Diego, CA, USA), and Matlab R2019b (Natick, MA, USA). The normality of data was determined by performing a Shapiro-Wilk test. Data were analyzed using two-tailed, paired, or independent t-tests for comparison of data collected from two different treatments, or one-way or two-way analysis of variance (ANOVA) for analysis of statistical differences among more than two different treatments. A post hoc Tukey's correction was performed in cases where ANOVA results were significant. *P*-values < 0.05 were considered statistically significant.

## **2.2 Materials and Methods for Chapter 4**

**Animal Protocols.** All animal protocols were approved by the University of Virginia Animal Care and Use Committee (Protocols 4120 and 4051). A total of 210 mice were used in the study. Male C57BL6/J with normal chow (normal fat diet or NFD: 10% kcal fat) or high-fat diet (HFD: 60% kcal fat, Research Diets Inc., New Brunswick, NJ, USA; 14 weeks starting at 6 weeks of age), and endothelium-specific TRPV4 (TRPV4<sub>EC</sub><sup>-/-</sup>) and AKAP150 (AKAP150<sub>EC</sub><sup>-/-</sup>) knockout mice (12-14 weeks old) were used in the present study. Female C57BL6/J mice fed a high-fat diet for 14 weeks did not show endothelial dysfunction, therefore, only male mice were used in this study. Some of TRPV4<sub>EC</sub><sup>-/-</sup> mice were fed HFD for 14 weeks. Mice were euthanized with pentobarbital (90 mg/kg, intraperitoneal) followed by decapitation for harvesting gut tissues. Third-order mesenteric arteries (MAs, ~100 μm) were dissected in cold HEPES-buffered physiological salt solution (HEPES-PSS; 10 mM HEPES, 134 mM NaCl, 6 mM KCl, 1 mM MgCl<sub>2</sub> hexahydrate, 2 mM CaCl<sub>2</sub> dihydrate, and 7 mM dextrose, pH adjusted to 7.4 using 1M NaOH). The perivascular adipose tissue was removed for all the ex vivo experiments. For in vivo experiments, an independent team member performed random assignment of animals to groups

and did not have knowledge of treatment assignment groups. All the in vivo experiments were blinded; information about the groups or treatments was withheld from the experimenter or from the team member who analyzed the data. All the experiments were performed in at least two independent batches. Isolation of human splenius and temporalis muscle tissue. Splenius and temporalis muscle tissue were obtained from non-obese (BMI  $\leq$  25) and obese (BMI  $\geq$  30) individuals during craniotomy surgeries as approved by University of Virginia Institutional Review Board (Protocol # 18699). Informed consents were obtained as per the protocol. Small arteries ( $\sim$  100  $\mu$ m) were dissected out from the muscle tissue in cold Hepes-PSS. Samples from 8 individuals were used in the study (4 non-obese and 4 obese). Generation of TRPV4<sup>EC</sup><sup>-/-</sup> and AKAP150<sup>EC</sup><sup>-/-</sup> mice. TRPV4<sup>EC</sup><sup>-/-</sup> or AKAP150<sup>EC</sup><sup>-/-</sup> mice were generated by crossing TRPV4<sup>lox/lox</sup> or AKAP150<sup>lox/lox</sup> (The Jackson Laboratory, Bar Harbor, ME, USA) mice with tamoxifen-inducible VE-Cadherin (Cdh5) Cre mice. AKAP150<sup>lox/lox</sup> Cre<sup>+</sup> or TRPV4<sup>lox/lox</sup> Cre<sup>+</sup> mice were injected with tamoxifen (Sigma-Aldrich, St. Louis, MO, USA) at 6 weeks of age (40 mg/kg i.p. per day for 10 days), followed by a 2-week washout period. AKAP150<sup>lox/lox</sup> Cre<sup>-</sup> or TRPV4<sup>lox/lox</sup> Cre<sup>-</sup> mice injected with tamoxifen were used as Wild-type (WT) control mice. Immunostaining for TRPV4<sup>EC</sup> or AKAP150<sup>EC</sup> or endothelial cell mRNA levels for TRPV4<sup>EC</sup> or AKAP150<sup>EC</sup> (described below) were compared to confirm endothelial knockout of TRPV4 or AKAP150. Genotyping. Samples of ear tissue were treated with the HotSHOT lysis buffer (25 mM NaOH, 0.2 mM EDTA) and neutralized with an equal volume 40 mM Tris-HCL to extract genomic DNA. Polymerase Chain Reactions were performed using 1 unit Bioline MangoTaq Polymerase and buffer (London, England), 1.5 mM MgCl<sub>2</sub>, 200  $\mu$ M of each dNTP, 1  $\mu$ M 5' and 3' primers, and approximately 100-250 ng genomic DNA, and run on a Bio-Rad T100 Thermal Cycler (Hercules, CA). Reaction products were then run on a 1% agarose gel containing 0.2  $\mu$ g/ $\mu$ L ethidium bromide in TAE Buffer (40 mM Tris Base, 20 mM Acetic Acid, 1 mM EDTA) at 90V using a Bio-Rad PowerPac HC High-Current Power Supply. Gels were visualized by exposing to 302 nm UV light and compared to a New England BioLabs 100 bp DNA Ladder (Ipswich, MA). The genotyping

primers included: Cdh5 Cre, 5' GCCTGCATTACCGGTCGATGCAACGA, 3' GTGGCAGATGGCGCGGCAACACCATT; TRPV4<sup>loxP</sup>, 5' CATGAAATCTGACCTCTTGTCCCC, 3' TTGTGTACTGTCTGCACACCAGGC; AKAP150<sup>loxP</sup>, 5' GAAAGTAGCGCCTCCTTGGT, 3' TGCTCAGATTTTGTGGAGGTC. All primers were ordered from Eurofins Genomics (Louisville, KY).

**Peroxynitrite (PN) preparation and controls.** The concentration of PN in the stock solution was determined spectrophotometrically using the reported extinction coefficient for PN (1670 mol/L<sup>-1</sup> · cm<sup>-1</sup>) (219). The methods for PN preparation and use in vascular experiments were followed as published in Liu et al. (219). PN has a short half-life under physiological conditions. We, therefore, used decomposed PN as a control. Decomposed PN was obtained by leaving PN at room temperature for 2 hours, and the decay of PN was determined spectrophotometrically. Decomposed PN did not affect the activity of endothelial TRPV4 sparklets or vasodilation to carbachol or GSK1016790A.

**Radiotelemetric blood pressure measurement.** Continuous blood pressure measurements were performed using Dataquest A.R.T. 20 software (Data Sciences International, St. Paul, MN), as described previously (24, 356). AKAP150<sup>EC<sup>-/-</sup></sup>, TRPV4<sup>EC<sup>-/-</sup></sup>, and respective WT mice, NFD and HFD mice were anesthetized with isoflurane (1.5%) and radiotelemetry catheter (TA11PA-C10, Data Sciences International, St. Paul, MN) was implanted in the left carotid artery. The catheter was tunneled through to the radiotransmitter, which was placed in a subcutaneous pouch along the flank. Before arterial pressure measurements were initiated, mice were allowed to recover for seven days after surgery to regain normal circadian rhythms. Baseline systolic, diastolic, and mean arterial pressures, and heart rate were recorded continuously over 72 hours (at 1-min intervals) following the recovery period. The values over three days (6 AM to 6 PM) and three nights (6 PM to 6 AM) were averaged to obtain the baseline day- or night-time blood pressures and heart rate. In addition, NFD, HFD, and HFD- TRPV4<sup>EC<sup>-/-</sup></sup>

mice were given a single bolus intraperitoneal injection of uric acid (200 mg/kg), FeTPPS (10 mg/kg), 1400W (10 mg/kg), or LNNA (100 mg/kg) at noon. Sterile saline solution (0.9%) was used as a vehicle, and vehicle only injections were used as control groups for statistical comparisons. Blood pressure and heart rate were recorded for one hour, at 5-min intervals. The blood pressures, at 15-20 minutes after injection, were compared between the groups. The experiments were performed in a blinded manner.

**Immunostaining.** Immunostaining was performed on en face MAs. Briefly, arteries were pinned down en face on SYLGARD blocks and fixed with 4% paraformaldehyde at room temperature for 15-min. Fixed arteries were washed 3 times with phosphate-buffered saline (PBS) solution, each wash lasting for five minutes. The arteries were then treated with 0.2% Triton-X PBS for 30-min at room temperature on a rocker. Following this step, the arteries were treated with 5% normal donkey serum or normal goat serum (Abcam plc, Cambridge, MA, USA) one hour at room temperature and subsequently incubated with antibodies against TRPV4, AKAP150, nitrotyrosine, PKC, iNOS, NOX1, NOX2, NOX4 overnight at 4°C. Following overnight incubation, MAs were washed three times with PBS and then incubated with secondary antibody (1:500; Alexa Fluor® 568-conjugated donkey anti-rabbit, goat anti-rabbit, or goat anti-mouse, Life Technologies, Carlsbad, CA, USA) at room temperature for one hour in the dark room. The MAs were then washed three times with PBS. For nuclear staining, MAs were incubated with 0.3 µM DAPI (Invitrogen, Carlsbad, CA, USA) for 10-min at room temperature in the dark room. Images were obtained using the Andor imaging system described previously. Consecutive images were taken along the z-axis at a slice size of 0.2-µm from the top of the ECs to the bottom of the SMCs. DAPI immunostaining was imaged by exciting at 409 nm and collecting the emitted fluorescence with a 447/60-nm band-pass filter. The 3D rendering was accomplished using Imaris 9.3. For determining the percentage of MEPs that coincided with the immunostaining of interest (TRPV4, AKAP150, NOX, iNOS, nitrotyrosine), the total number of holes was counted for

each field of view. A horizontal x-y plot profile was then obtained for each hole using 5  $\mu\text{m}$  x 50  $\mu\text{m}$  transects encompassing the hole. The holes that coincided with immunostaining intensity that was higher than 2 standard deviations above the baseline fluorescence intensity were counted as MEPs that expressed the protein under consideration. Other holes were grouped as MEPs that did not express the protein under consideration. Knockout mice (TRPV4 and AKAP150), secondary antibody alone control, and blocking peptides (Novus Biologicals NBP2-54670PEP for NOX4, Proteintech Ag5536 for NOX2, custom-synthesized peptide for iNOS from GenScript) at concentration five times higher than that of the antibody were used as negative controls. Primary antibody-specific immunostaining was eliminated in secondary antibody control/blocking peptide control/knockout mice control groups.

### **Imaging for endothelial cysteine oxidation in third-order MAs and HEK293 cells.**

Reversible Cysteine sulfenic acid (CSA) intermediates of cysteine oxidation were trapped by treating the arteries with dimedone (5 mM, 60 minutes at 30°C). The arteries were then washed twice with PBS for five minutes each. Dimedone-tagged CSA containing protein were detected using anti-CSA (2-thiodimedone) antibody (Kerafast, Inc. Boston, MA, USA) (336). The arteries were then fixed with 4% paraformaldehyde, and the standard immunostaining, image acquisition, and analysis protocol was followed as described earlier. For detecting PN-induced cysteine oxidation in HEK293 cells (ATCC, Manassas, VA; passages < 20), the cells were incubated with PN (10  $\mu\text{M}$ ) in DMEM for 5 minutes at 37°C. The cells were washed twice with PBS containing 10 mM dimedone, and then incubated with DMEM containing 10 mM dimedone for 1 hour. The cells were washed three times with PBS, and fixed with 4% paraformaldehyde. The standard immunostaining protocol was followed as explained earlier using the anti-CSA (2-thiodimedone) primary antibody. The mean fluorescence intensity for all the cells in a group was averaged per experiment. Each data point in the scatter plot indicates averaged mean fluorescence intensity per experiment. Each experiment was performed 3-5 times.

**Peroxynitrite imaging.** A peroxynitrite-selective fluorescent indicator coumarin boronic acid (CBA)(456) was used for peroxynitrite imaging. Peroxynitrite oxidizes CBA into the fluorescent product 7-hydroxycoumarin (COH). The arteries were incubated with CBA (20  $\mu$ M) for 30 minutes at room temperature. Endothelial COH at 360 nm (CoolLED Ltd, Andover, UK); emitted fluorescence was captured at room temperature using a 447/60 nm band-pass filter, Nikon fluor 40X objective, and Andor electron multiplying charge coupled device camera. The images were analyzed using the SparkAn program. The average fluorescence intensity for the whole field was compared between the groups. Each data point indicates one field of view. At least three arteries were used for each treatment. CBA reacts with peroxynitrite at exponentially faster rates than H<sub>2</sub>O<sub>2</sub> and hypochlorous acid. Moreover, the endothelial CBA fluorescence was not altered by the presence of PEG catalase (H<sub>2</sub>O<sub>2</sub> decomposer) or taurine.

**Plasmid generation and transfection of HEK293 cells.** The coding sequences for murine TRPV4 and AKAP150 without the stop codons were amplified from a mouse heart cDNA and the coding sequence for EGFP from a commercially available vector. The amplified fragments were introduced into a plasmid backbone which contains a CMV promoter for expression and, in addition, is suitable for lentivirus production (123), by Gibson assembly. For TRPV4, an in-frame FLAG tag was included in the 3'-primer used for amplification. For AKAP150, the EGFP sequence was fused to the 3' of the AKPA150 coding region. All constructs were verified by sequencing the regions, which had been inserted into the vector backbone; complete plasmid sequences are available upon request. Cells were seeded in Dulbecco's Modified Eagle Medium with 10% fetal bovine serum (Thermo Fisher Scientific Inc. Waltham, MA, USA) the day prior to transfection in a 100 mm dish (7 x 10<sup>5</sup> cells per dish). Cells were transfected with 15  $\mu$ g plasmid using LipofectamineLTX (Thermo Fisher Scientific Inc. Waltham, MA, USA) as the transfection reagent. Patch clamp experiments were conducted 48 hours after transfection. The transfection efficiency was tested with AKAP150 or TRPV4 immunostaining. The transfection efficiency with

TRPV4 plasmid was ~ 96%, and that with AKAP150 plasmid was ~ 50%. For patch clamp experiments, the cells carrying AKAP150 were identified by EGFP fluorescence. Site-directed mutagenesis: The mouse AKAP150 sequence inserted into a pLenti CMV GFP plasmid was synthesized as described above. For mutagenesis, cysteine to alanine primers were designed against residue 36 (C36A) using the QuikChange primer design program, and mutagenesis performed using the QuikChange II site-directed mutagenesis kit as per manufacturer instructions (Agilent, Stratagene, Santa Clara, CA). Primers for mutations are as follows: forward 5' ctttctcctctctgaaggcgagtggtgctgttttctct 3' and reverse: 5' agagaaaaacagccacactcgctcaagagaaggaagaaag 3' (IDT, Coralville, IA). Mutants were sequenced (GeneWiz, South Plainfield, NJ), confirmed and maxi prepped for transfection studies. Sequencing confirmed the AKAP150C36A mutation.

**Patch Clamp in freshly isolated ECs and HEK293 cells.** ECs were freshly isolated from thirdorder MAs. Briefly, MAs were digested in dissociation solution (55 mM NaCl, 80 mM Naglutamate, 6 mM KCl, 2 mM MgCl<sub>2</sub>, 0.1 mM CaCl<sub>2</sub>, 10 mM glucose, 10 mM Hepes, pH 7.3) containing Worthington neutral protease (0.5 mg/mL) 60 minutes at 37°C. Collagenase (Worthington type 1, 0.5 mg/mL) was added to the enzyme solution after 60 minutes and digestion was continued for 2 more minutes. Whole-cell currents were measured at room temperature using perforated-patch configuration of whole-cell patch clamp. The bathing solution consisted of 10 mM Hepes, 134 mM NaCl, 6 mM KCl, 2 mM CaCl<sub>2</sub>, 10 mM glucose, and 1 mM MgCl<sub>2</sub> (adjusted to pH 7.4 with NaOH). Patch electrodes were pulled from borosilicate glass (O.D.: 1.5 mm; I.D.: 1.17 mm; Sutter Instruments, Novato, CA, USA) using Narishige PC-100 puller (Narishige International USA, INC., Amityville, NY, USA) and polished using MicroForge MF-830 polisher (Narishige International USA, INC., Amityville, NY, USA). The composition of the pipette solution for perforated-patch experiments was 10 mM Hepes, 30 mM KCl, 10 mM NaCl, 110 mM K-aspartate, and 1 mM MgCl<sub>2</sub> (adjusted to pH 7.2 with NaOH). IK and SK

channels currents were obtained by adding 1  $\mu\text{M}$  NS309 (IK/SK channel activator) to the superfusate. The pipette resistance was (3–5  $\Omega\text{M}$ ). Currents were recorded by applying 200 ms voltage-ramps from  $-140\text{ mV}$  to  $+50\text{ mV}$ . The data were acquired using HEKA EPC 10 amplifier and PatchMaster v2X90 program (Harvard Bioscience, Holliston, MA, USA). The patch clamp data were analyzed using FitMaster v2X73.2 (Harvard Bioscience, Holliston, MA, USA) and MATLAB R2018a (MathWorks, Natick, MA, USA). IK/SK channel currents were inhibited by adding Tram-34 (IK channel inhibitor, 1  $\mu\text{M}$ ) and apamin (SK channel inhibitor, 300 nM) to the bath. Current traces in the presence of Tram-34 and apamin were subtracted from the traces in the presence of NS309 alone to obtain IK/SK channel currents. The effect of each drug was studied 5 minutes after the addition of the drug. Currents through TRPV4 channels in freshly isolated ECs were recorded using perforated patch configuration as described earlier (354). Ruthenium red (RuR, 1  $\mu\text{M}$ ) was applied to block  $\text{Ca}^{2+}$  entry through TRPV4 channels, and thereby prevent IK and SK channel activation and  $\text{Ca}^{2+}$  overload. GSK101-induced outward currents through TRPV4 channels were assessed in response to a 200-ms voltage step from  $-45\text{ mV}$  to  $+100\text{ mV}$ . The cells were exposed to GSK101, PN, or GSK219 for 5 minutes before recording the currents. For HEK293 cells patch clamp, whole-cell currents were measured at room temperature using a conventional whole-cell patch configuration. The bathing solution consisted of 10 mM Hepes, 134 mM NaCl, 6 mM KCl, 2 mM  $\text{CaCl}_2$ , 10 mM glucose, and 1 mM  $\text{MgCl}_2$  (adjusted to pH 7.4 with NaOH). The intracellular solution consisted (in mM) 20 CsCl, 100 Cs-aspartate, 1  $\text{MgCl}_2$ , 4 ATP, 0.08  $\text{CaCl}_2$ , 10 BAPTA, 10 Hepes, pH 7.2 (adjusted with CsOH). Voltage clamped protocol used was voltage-ramp pulses ( $-100\text{ mV}$  to  $+100\text{ mV}$ ) applied over 200 ms with a holding potential of  $-50\text{ mV}$ . TRPV4 currents were measured before or five minutes after the addition of 5  $\mu\text{M}$  peroxyntirite. The effect of TRPV4 inhibitor GSK2193874 (GSK219, 100 nM) was studied by recording currents before and 5 minutes after addition of GSK219.

**Quantitative polymerase chain reaction (qPCR).** Third-order MAs were removed, placed in 500  $\mu$ L RLT buffer (Qiagen RNeasy Mini Kit, Hilden, Germany) with 5  $\mu$ L  $\beta$ -mercapto ethanol, and homogenized using a Standard Microhomogenizer (PRO Scientific Inc., Oxford, CT, USA). For isolation of RNA from endothelial cells, approximately 20 mesenteric arteries from each mouse were used. Arteries were digested in a dissociation solution containing (0.5 mg/mL) 60 minutes at 37°C. Collagenase (Worthington type 1, 0.5 mg/mL) was added to the enzyme solution after 60 minutes and digestion was continued for 2 more minutes. Following the digestion, endothelial cell sheets were gently pushed out of the arterial wall using fine tips of 1 mL syringe needles. Isolated endothelial cell sheets were then placed in a patch clamp chamber, allowed to settle down for 15 minutes at room temperature, and washed three times with enzyme-free dissociation buffer. Endothelial cell sheets were then picked up using a micropipette (~ 100  $\mu$ m tip) under gentle suction, and transferred to a tube with RLT buffer with  $\beta$ -mercapto ethanol for RNA isolation. The steps were repeated in order to pick several endothelial cell sheets. Approximately 20 sheets were used for each sample. Each sheet has approximately 100 cells. The purity of endothelial cells was confirmed with FITC-labelled anti-CD31 antibody. The RLT buffer (with  $\beta$ -mercapto ethanol and endothelial cell sheets) was snap frozen in liquid nitrogen. The samples were thawed, RNA was isolated using a Qiagen RNeasy Mini Kit (Hilden, Germany), treated with Invitrogen DNA-free DNA Removal Kit (Waltham, MA), and converted to cDNA with Bio-Rad iScript cDNA Synthesis Kit. The qPCR reaction mixes were prepared using Bio-Rad 2x SYBR Green Master Mix, 200nM 5' and 3' primers, and 20 nM cDNA, then run in a Bio-Rad CFX96 qPCR Detection System. Results were analyzed using the  $\Delta\Delta$ Ct Method<sup>13</sup>. qPCR primers for TRPV4 and GAPDH (internal control) were ordered from GeneCoepia Inc. (Rockville, MD, USA). The remaining qPCR primers included: AKAP150, 5' GACCTCGGGAGCAGAGC, 3' CTTGAAGCAGAGTGTGGCT; iNOS, TTCACCCAGTTGTGCATCGACCTA, 3' TGGGCTGGGTGTTAGTCTTA; NOX1, 5'

ACCTGCTCATTGCAACCGTA, 3' AGAGATCCATCCATGGCCTGTT, and were ordered from Eurofins Genomics (Louisville, KY).

**Measurement of O<sub>2</sub><sup>-</sup> production in MAs.** Dihydroethidium (DHE, Thermo Fisher Scientific Inc. Waltham, MA, USA) was used for detecting O<sub>2</sub><sup>-</sup> generation in en face MAs on a SYLGARD block. The MAs were incubated with DHE (2 μM) in the dark at 30°C for 30 min. Following the incubation, the arteries were washed three times with Hepes PSS, and then fixed in 4% paraformaldehyde for 20 minutes at room temperature. Images were acquired using the Andor Imaging system described above. Images were obtained along the z-axis at a slice size of 0.05 μm from the top of the endothelial cells to the bottom of the smooth muscle cells. Endothelial cell fluorescence intensity was quantified using custom-made SparkAn software.

**Hypochlorous acid imaging.** A selective fluorescent probe (PIS, Millipore Sigma, Burlington, MA, USA) (435)15 was used for imaging endothelial hypochlorous acid in non-obese and obese mice. The arteries were incubated with PIS for 60 minutes at 30°C. The images were acquired at room temperature by exciting PIS at 385 nm and capturing the emitted fluorescence using 525/36 nm band-pass filter and Andor EMCCD camera.

**Drugs and chemical compounds.** Cyclopiazonic acid, GSK1016790A, GSK2193874, NS309, apamin, charybdotoxin, tempol, Phorbol 12-myristate 13-acetate, and ML-171 were purchased from Tocris Bioscience (Minneapolis, MN, USA). PEG-catalase, L-NNA, CCh, Alexa fluor 633 hydrazide, and DAF-FM were procured from Thermo Fisher Scientific Inc. (Waltham, MA, USA). gp91 ds – tat was obtained from AnaSpec (Fremont, CA, USA). PN, UA, FeTPPS, ML171, and 1400w were purchased from Cayman Chemical (Ann Arbor, MI, USA). All other chemicals were purchased from Sigma-Aldrich (St. Louis, MO, USA).

**Statistical Analysis.** Results are presented as mean ± SEM. N=1 was defined as one artery in the imaging experiments (Ca<sup>2+</sup> imaging, immunofluorescence, PN/NO/superoxide/hypochlorous

acid measurements, PLA, DCP-Rho1), one cell for patch clamp experiments, one mouse for blood pressure measurements, one artery for pressure myography experiments, one sparklet site for coupling coefficient analysis, and one mouse for qPCR experiments. The data were obtained from at least three mice in experiments performed in at least two independent batches. All data are shown in graphical form using CorelDraw Graphics Suite X7 (Ottawa, ON, Canada) and statistically analysed using GraphPad Prism 8.3.0 (Sand Diego, CA). A power analysis to determine group sizes and study power ( $>0.8$ ) was calculated using GLIMPSE software ( $\alpha = 0.05$ ;  $>20\%$  change). Using this method, some experiments required  $n=3$ , while others required  $n\geq 4$ . A Shapiro-Wilk test was performed to determine normality. The data in this article were normally distributed; therefore, parametric statistics were performed. Data were analyzed using two-tailed, paired or independent t-test (for comparison of data collected from two different treatments), one-way ANOVA or two-way ANOVA (to investigate statistical differences among more than two different treatments). Tukey correction was performed for multiple comparisons with one-way ANOVA, and Bonferroni correction was performed for multiple comparisons with two-way ANOVA. Statistical significance was determined as a P value less than 0.05; \*P < 0.05, \*\* P < 0.01, \*\*\* P < 0.001, ## P < 0.01, ### P < 0.001

**Ca<sup>2+</sup> imaging, Pressure myography, and NO measurements: see Materials and Methods for Chapter 3**

## **2.3 Materials and Methods for Chapter 5**

### **Animal Protocols.**

All animal protocols were approved by the University of Virginia Animal Care and Use Committee (Protocols 4120 and 4051). Male C57BL6/J with normal chow (normal fat diet or NFD: 10% kcal fat) or high-fat diet (HFD: 60% kcal fat, Research Diets Inc., New Brunswick, NJ, USA; fed for 14 weeks starting at 6 weeks of age) were used in the study. Mice were euthanized with pentobarbital (90 mg/kg, intraperitoneal) followed by cervical dislocation for harvesting gut

tissues. Third-order mesenteric arteries (MAs, ~100  $\mu$ m) were dissected in cold Hepes-buffered physiological salt solution (Hepes-PSS; 10 mM Hepes, 134 mM NaCl, 6 mM KCl, 1 mM MgCl<sub>2</sub> hexahydrate, 2 mM CaCl<sub>2</sub> dihydrate, and 7 mM dextrose, pH adjusted to 7.4 using 1M NaOH), and cleaned off from the perivascular fat tissue.

### **Radiotelemetric blood pressure measurement.**

Continuous blood pressure measurements were performed using Dataquest A.R.T. 20 software (Data Sciences International, St. Paul, MN), as described previously<sup>3, 4</sup>. NFD and HFD mice were anesthetized with isoflurane (1.5%) and radiotelemetry catheter (TA11PA-C10, Data Sciences International, St. Paul, MN) was implanted in the left carotid artery. The catheter was tunneled through to the radiotransmitter, which was placed in a subcutaneous pouch along the flank. Before arterial pressure measurements were initiated, mice were allowed to recover for seven days after surgery to regain normal circadian rhythms. Baseline systolic, diastolic, and mean arterial pressures, and heart rate were recorded continuously over 24 hours (at 1-min intervals) following the recovery period. The values over one day (6 AM to 6 PM) and one night (6 PM to 6 AM) were averaged to obtain the baseline day- or night-time blood pressures and heart rate. Following, NFD and HFD mice were daily treated for 12 days with intraperitoneal injection of R7050 (10 mg/kg) (177) (MedChemExpress, NJ, USA) and vehicle (10% DMSO, 90% Corn Oil). Blood pressure measurements were taken on day 4, 8, and 12 of treatment. The experiments were performed in a blinded manner.

### **Glucose tolerance test**

Dextrose (1.5 g/kg) was prepared, sterile filtered, and injected intraperitoneal. The glucose excursion was monitored over a 2-hour time course and compared between HFD and NFD mice. Tein vein blood samples were analyzed by glucometer (OneTouch Ultra Mini) at 0, 15, 45, 60,

and 120 minutes following dextrose injection. The cumulative glycemic excursion was evaluated as the area under the curve (AUC).

### **Plasma samples collection.**

Blood was collected from the inferior vena cava using 3.8% sodium citrate coated needles and dispensed into 1.5 mL microcentrifuge tubes with sodium heparin. Tubes were centrifuged at 2,000g for 15 minutes to isolate plasma. Plasma was then flash frozen in liquid nitrogen and stored at -80C until further analysis. Cytokine profiling was performed on isolated plasma by the University of Virginia Flow Cytometry Core Facility using a Luminex MAGPIX instrument and the mouse pro-inflammatory cytokine kit.

### **Flow cytometry.**

Mice were sacrificed using either CO<sub>2</sub> or with pentobarbital (90 mg/kg, intraperitoneal) followed by cervical dislocation. Second and third order mesenteric arteries (MA) and aortae were isolated into ice cold Hepes-buffered physiological salt solution (Hepes-PSS; 10 mM Hepes, 134 mM NaCl, 6 mM KCl, 1 mM MgCl<sub>2</sub> hexahydrate, 2 mM CaCl<sub>2</sub> dihydrate, and 7 mM dextrose, pH adjusted to 7.4 using 1M NaOH). The perivascular tissue was removed from the vessels and the vessels were subsequently added to collagenase digestion solution 2 mg/ml (collagenase type IV, Worthington LS004189) and digestion buffer composition (55 mM NaCl, 80 mM Naglutamate, 6 mM KCl, 2 mM MgCl<sub>2</sub>, 0.1 mM CaCl<sub>2</sub>, 10 mM glucose, 10 mM Hepes, pH 7.3) Vessels were minced in digestion buffer and incubated at 37° C with shaking for 60 minutes for MAs and 80 minutes for aortae. After digestion, enzymatic activity was stopped with fetal bovine serum (FBS) and the cell suspensions were subsequently filtered through a 70 µm mesh cell strainer (Fisher 22-363-548). Cell suspensions were then subjected to red blood cell lysis (Sigma R7757) followed by surface staining on ice to identify immune cells (CD45 - Ebio 17-0451-82, Ebio 47-0451-82, Ebio 45-0451-80, or BioLegend 103116), endothelial cells (VE-Cadherin – BioLegend

138105, CD31 – Biolegend 102420, Biolegend 102410) in the presence of Fc receptor blocking antibodies (eBioscience 16-0161-85). Cells were additionally stained with Live/Dead Fixable Yellow (Thermo L34959). For intracellular staining cells were fixed in 10% formalin overnight at 4° C. After fixation, cells were permeabilized as per manufacturer instructions (eBiosciences 00-8333-56). Antibodies targeting intracellular proteins were added in permeabilization buffer on ice (Smooth muscle actin – Invitrogen 53-9760-82, TNF $\alpha$  – BioLegend – 506318, IL-6 – BioLegend 504507, IL-1 $\beta$  – Invitrogen – 48-7114-80). Cells were then re-suspended in FACS buffer and analyzed by flow cytometry using an Attune NxT flow cytometer (Thermo).

## **Immunostaining.**

Immunostaining was performed on en face MAs. Briefly, MAs were pinned down en face on SYLGARD blocks and fixed with 4% paraformaldehyde at room temperature for 15-min. Fixed arteries were washed 3 times for 5 minutes each with phosphate-buffered saline (PBS) solution. The arteries were then treated with 0.2% Triton-X PBS for 30-min at room temperature on a rocker. Following this step, the arteries were treated with 5% normal donkey serum (Abcam plc, Cambridge, MA, USA) one hour at room temperature. Subsequently, MAs were incubated for an hour at room temperature with primary antibodies against iNOS, NOX1, TNF $\alpha$ , TNF $\alpha$ RI, and CD45 (Table 1). Following the primary staining, MAs were washed three times with PBS and then incubated with secondary antibody (1:500; Alexa Fluor® 568-conjugated donkey anti-rabbit Life Technologies, Carlsbad, CA, USA; Alexa Fluor® 647 donkey anti- mouse Abcam Cambridge, UK) at room temperature for one hour in the dark room. The MAs were then washed three times with PBS. For nuclear staining, MAs were incubated with 0.3  $\mu$ M DAPI (Invitrogen, Carlsbad, CA, USA) for 10-min at room temperature in the dark room. Images were obtained using the Andor imaging systems: Andor Revolution WD (with Borealis) spinning-disk confocal

imaging system (Andor Technology, Belfast, UK) comprising of an upright Nikon microscope with a 60X water dipping objective (numerical aperture 1.0) and an electron multiplying charge coupled device camera. Consecutive images were taken along the z-axis at a slice size of 0.2- $\mu\text{m}$  from the top of the ECs to the bottom of the SMCs. DAPI immunostaining was imaged by exciting at 409 nm and collecting the emitted fluorescence with a 447/60-nm band-pass filter.

**Table 1.** List of primary antibodies used for immunostaining.

Protein	Company	Antibody ID	Clonality	Concentration
iNOS	Novus Biologicals, LLC	NB300-605	Polyclonal	1:500
NOX1	Novus Biologicals, LLC	NBP1-31546	Polyclonal	1:500
TNF $\alpha$	Abcam, UK	Ab-1793	Monoclonal	1:200
TNF $\alpha$ RI	Abcam, UK	Ab-223352	Polyclonal	1:200
CD45	Santa Cruz Biotechnology, Inc.	sc-1178	Monoclonal	1:200

**Statistical Analysis.** Results are presented as mean  $\pm$  SEM. N=1 was defined as one artery in the imaging experiments (Ca<sup>2+</sup> imaging, immunostaining), one artery for pressure myography experiments, one mouse for flow cytometry, plasma cytokines levels, and blood pressure recording. The data were obtained from at least three mice in experiments performed in at least two independent batches. All data are shown in graphical form using CorelDraw Graphics Suite

X7 (Ottawa, ON, Canada) and statistically analyzed using GraphPad Prism 8.3.0 (Sand Diego, CA). Data were analyzed using two-tailed, paired or independent t-test (for comparison of data collected from two different treatments), one-way ANOVA (to investigate statistical differences among more than two different treatments). Tukey correction was performed for multiple comparisons with one-way ANOVA. Statistical significance was determined as a P value less than 0.05. All the P values have been added on the respective figures.

**Ca<sup>2+</sup> imaging, Pressure myography, MEPs co-localization analysis: see Material and Methods for Chapter 3**

**Chapter 3: Mechanisms for Selective Coupling of Endothelial Ca<sup>2+</sup>  
Signals with eNOS or IK/SK Channels in Systemic and Pulmonary  
Arteries**

### 3.1 Abstract

Spatially localized  $\text{Ca}^{2+}$  signals activate  $\text{Ca}^{2+}$ -sensitive intermediate- and small-conductance  $\text{K}^+$  (IK and SK) channels in some vascular beds and endothelial nitric oxide synthase (eNOS) in others. The goal of this study was to uncover the signaling organization that determines selective  $\text{Ca}^{2+}$  signal to vasodilatory target coupling in the endothelium. Resistance-sized mesenteric arteries (MAs) and pulmonary arteries (PAs) were used as prototypes for arteries with predominantly IK/SK channel- and eNOS-dependent vasodilation, respectively.  $\text{Ca}^{2+}$  influx signals through endothelial transient receptor potential vanilloid 4 ( $\text{TRPV4}_{\text{EC}}$ ) channels played an important role in controlling the baseline diameter of both MAs and PAs.  $\text{TRPV4}_{\text{EC}}$  channel activity was similar in MAs and PAs. However, the  $\text{TRPV4}$  channel agonist GSK1016790A (10 nM) selectively activated IK/SK channels in MAs and eNOS in PAs, revealing preferential  $\text{TRPV4}_{\text{EC}}$ -IK/SK channel coupling in MAs and  $\text{TRPV4}_{\text{EC}}$ -eNOS coupling in PAs. IK/SK channels co-localized with  $\text{TRPV4}_{\text{EC}}$  channels at myoendothelial projections (MEPs) in MAs, but lacked the spatial proximity necessary for their activation by  $\text{TRPV4}_{\text{EC}}$  channels in PAs. Additionally, the presence of the NO scavenging protein hemoglobin  $\alpha$  ( $\text{Hb}\alpha$ ) within nanometer proximity to eNOS limits  $\text{TRPV4}_{\text{EC}}$ -eNOS signaling in MAs. In contrast, co-localization of  $\text{TRPV4}_{\text{EC}}$  channels and eNOS at MEPs, and the absence of  $\text{Hb}\alpha$ , favor  $\text{TRPV4}_{\text{EC}}$ -eNOS coupling in PAs. Thus, our results reveal that differential spatial organization of signaling elements determines  $\text{TRPV4}_{\text{EC}}$ -IK/SK versus  $\text{TRPV4}_{\text{EC}}$ -eNOS coupling in resistance arteries.

### 3.2 Introduction

Increases in endothelial cell (EC)  $\text{Ca}^{2+}$  are known to promote vasodilation and thereby reduce vascular resistance and blood pressure. A number of different mechanical stimuli and neurohumoral mediators cause vasodilation by increasing EC  $\text{Ca}^{2+}$ . Intracellular  $\text{Ca}^{2+}$  can activate multiple vasodilator targets in ECs, including intermediate- and small-conductance  $\text{K}^+$  (IK or SK) channels (34, 37, 199, 263, 381), endothelial nitric oxide synthase (eNOS) (35, 155), and

factors that hyperpolarize smooth muscle cells (SMCs) (86). Pressure myography studies in resistance-sized arteries have revealed that increases in endothelial  $\text{Ca}^{2+}$  cause vasodilation mainly via IK/SK channel activation in some vascular beds (14, 82, 199, 302, 354, 381) and eNOS activation in other vascular beds (21, 142, 238). Although the activation of IK/SK channels and eNOS by  $\text{Ca}^{2+}$  has been studied in detail (14, 82, 147, 198, 199, 238, 268, 354, 381), the preferential activation of one target versus the other remains unexplained. The majority of vascular disorders are associated with a loss of IK/SK channel- or eNOS-dependent vasodilation (98, 180, 228, 334). Understanding the molecular basis for preferential coupling of  $\text{Ca}^{2+}$  signals with IK/SK channel or eNOS is therefore essential for deciphering the selective impairment of vasodilatory mechanisms in vascular disorders.

Multiple ion channels increase  $\text{Ca}^{2+}$  levels in native ECs, including ion channels of the transient receptor potential (TRP) family (82, 147, 302, 354, 368) and inositol triphosphate (IP3) receptors (14, 141, 199, 241, 392). The TRP vanilloid 4 (TRPV4) channel has emerged as an important  $\text{Ca}^{2+}$ -influx pathway in ECs from systemic and pulmonary resistance arteries (14, 147, 238, 355). Pharmacological activation of endothelial TRPV4 (TRPV4<sub>EC</sub>) channels is known to dilate systemic and pulmonary arteries (238, 354), and knockout of these channels specifically in the endothelium increases resting blood pressure (289). However, whether TRPV4<sub>EC</sub> channels control resting vascular diameter has not been addressed. Interestingly, activation of TRPV4<sub>EC</sub> channels dilates systemic mesenteric (354), cremaster (14), and cerebral arteries (450) via IK/SK channel activation, and pulmonary arteries via eNOS activation (238). TRPV4<sub>EC</sub> channel-induced activation of IK/SK channels has been attributed to the localization of TRPV4<sub>EC</sub> and IK/SK channels at myoendothelial projections (MEPs), which provide points of contact between ECs and overlying smooth muscle cells (SMCs) (14, 355). However, it is not clear why TRPV4<sub>EC</sub> channels do not activate eNOS in resistance systemic arteries or IK/SK channels in resistance pulmonary arteries. Therefore, we hypothesized that spatial proximity of TRPV4<sub>EC</sub> channels with

eNOS or IK/SK channels determines TRPV4-eNOS or TRPV4-IK/SK coupling in native endothelium.

On the one hand, activation of IK/SK channels causes EC membrane hyperpolarization, which is then transmitted to SMCs via myoendothelial gap junctions (MEGJs) in MEPs (76). SMC hyperpolarization results in deactivation of L-type  $\text{Ca}^{2+}$  channels and vasodilation (182). On the other hand, activation of eNOS releases NO, which diffuses to SMCs and causes vasodilation via guanylyl cyclase-dependent and -independent mechanisms (55). Interestingly, no patch-clamp studies have been performed on arteries that exhibit  $\text{Ca}^{2+}$ -dependent activation of eNOS that would lead to the conclusion that IK/SK channels are present and can be activated in these arteries. It is similarly unknown whether eNOS is expressed and can be activated by  $\text{Ca}^{2+}$  in arteries that show selective  $\text{Ca}^{2+}$  signal-IK/SK channel coupling. Vasodilator effector molecules are a source of endothelial heterogeneity; therefore, it is important to understand the fundamental mechanisms that determine differential  $\text{Ca}^{2+}$  signal-target coupling in ECs.

In the current study, we used third-order mesenteric arteries (MAs) as a model for TRPV4-IK/SK channel coupling (147, 354, 355), and fourth-order pulmonary arteries (PAs) as a prototype for TRPV4-eNOS coupling (238). We provide the first evidence for an essential role of TRPV4<sub>EC</sub> channels in controlling baseline diameter in both MAs and PAs. Functional IK/SK channels and eNOS were present in ECs of both MAs and PAs, and TRPV4<sub>EC</sub> and IK/SK channel current densities were similar between MAs and PAs. Stimulation of TRPV4<sub>EC</sub> channels with the specific agonist GSK1016790A (hereafter, GSK101) selectively activated IK/SK channels in MAs, where TRPV4<sub>EC</sub> and IK/SK channels were found to localize at MEPs; in contrast, stimulation of TRPV4<sub>EC</sub> channels selectively activated eNOS in PAs. Moreover, a lack of TRPV4<sub>EC</sub>-eNOS coupling in MAs correlated with co-localization of the NO-scavenging protein hemoglobin  $\alpha$  (Hb $\alpha$ ) with eNOS in MAs (364) but not in PAs. These results identify novel

mechanisms of  $\text{Ca}^{2+}$  signal-to-vasodilator-target coupling in ECs, and may explain heterogeneity in endothelium-dependent vasodilator mechanisms.

### 3.3 Results

#### **TRPV4<sub>EC</sub> channels control baseline diameter in PAs via eNOS activation and in MAs via IK/SK channel activation.**

Pharmacological activation of TRPV4<sub>EC</sub> channels dilates resistance arteries from multiple vascular beds (14, 238, 354). However, the role of TRPV4<sub>EC</sub> channels in regulating baseline arterial diameter remains unknown. Unlike MAs, which show robust pressure-induced constriction (myogenic tone) at physiological intravascular pressures of 60-80 mm Hg (12), PAs have little to no myogenic tone at their physiological pressure of 15 mm Hg. Therefore, to investigate the contribution of TRPV4 activity to baseline arterial diameter, we tested the effect of the specific TRPV4 inhibitor GSK2193874 (hereafter, GSK219) on baseline diameter in MAs and PAs from wild-type (WT) and TRPV4<sub>EC</sub><sup>-/-</sup> mice pre-constricted with thromboxane receptor agonist U46619 (50 nM). GSK219 (100 nM) constricted both PAs and MAs from WT mice, an effect that was absent in arteries from TRPV4<sub>EC</sub><sup>-/-</sup> mice, providing the first evidence for a dilator effect of TRPV4<sub>EC</sub> channels on basal diameter in systemic and pulmonary resistance arteries (Fig. 1A and B). Interestingly, GSK219-induced constriction of PAs was abolished by NOS inhibition, which had no effect on GSK219-induced constriction of MAs, whereas GSK219-induced constriction of MAs was abolished by IK/SK channel inhibition, which had no effect on PAs (Fig. 1C). In MAs with myogenic tone, GSK219 caused a constriction similar to that in U46619-pre-constricted arteries. This effect was abolished by IK/SK channel inhibition, was unaffected by NOS inhibition and was absent in MAs from TRPV4<sub>EC</sub><sup>-/-</sup> mice (Fig. 1D and E), suggesting that pre-constriction with U46619 did not alter TRPV4<sub>EC</sub> channel-dependent downstream signaling. These results

provide the first evidence for the control of basal diameter by TRPV<sub>4</sub><sub>EC</sub> channel–eNOS signaling in PAs and by TRPV<sub>4</sub><sub>EC</sub> channel–IK/SK channel signaling in MAs.

### **Low-level activation of TRPV<sub>4</sub><sub>EC</sub> channels induces IK/SK channel currents in ECs from MAs, but not PAs.**

Activation of TRPV<sub>4</sub><sub>EC</sub> channels with relatively low concentrations (10 nM) of the specific agonist GSK1016790A (hereafter, GSK101) has been shown to elicit localized Ca<sup>2+</sup> influx signals through TRPV<sub>4</sub><sub>EC</sub> channels, termed TRPV<sub>4</sub><sub>EC</sub> sparklets, without increasing global Ca<sup>2+</sup> levels (238, 354). To determine whether TRPV<sub>4</sub><sub>EC</sub> channel activation induces IK/SK currents, we performed whole-cell patch-clamp studies in freshly isolated ECs from MAs and PAs treated with 10 nM GSK101. GSK101 induced robust IK/SK channel currents in ECs from MAs that were inhibited by TRAM-34 (IK channel inhibitor, 1 μM) + apamin (SK channel inhibitor, 300 nM) (Fig. 2A and B). In sharp contrast, GSK101 failed to evoke IK/SK channel currents in ECs from PAs (Fig. 2A and B). This absence of an effect of GSK101 was not attributable to decreased IK/SK expression in PAs, since direct activation of IK/SK channels with NS309 (1 μM) induced similar IK/SK channel current densities in ECs from MAs and PAs (Fig. 2C and D). These results provide the first direct evidence of functional IK/SK channels in native ECs from resistance PAs and suggest that TRPV<sub>4</sub><sub>EC</sub> sparklet–IK/SK channel coupling occurs in resistance MAs, but not in resistance PAs.

## **Whole-cell increases in intracellular Ca<sup>2+</sup> activate IK/SK channel currents in pulmonary ECs.**

IK/SK channels are primarily activated by increases in intracellular Ca<sup>2+</sup> (200). Both IK and SK channels possess a calmodulin (CaM)-binding site, and Ca<sup>2+</sup>/CaM binding to this site induces a conformational change that opens the channel pore (94, 200). To verify that IK/SK channels in PAs are not sensitive to Ca<sup>2+</sup>/CaM-induced activation, we assessed IK/SK channel activity in ECs in response to increased whole-cell Ca<sup>2+</sup> levels, induced using a high concentration of GSK101 and by increasing the concentration of free Ca<sup>2+</sup> in the patch pipette. At a low concentration (10 nM), GSK101 induced spatially restricted TRPV4<sub>EC</sub> sparklet activity but did not alter whole-cell Ca<sup>2+</sup> fluorescence (Fig. 2E and F). In contrast, excessive TRPV4 channel activation with 100 nM GSK101 increased whole-cell Ca<sup>2+</sup> fluorescence intensity in both PAs and MAs (Fig. 2E and F). These whole-cell increases in endothelial Ca<sup>2+</sup> correlated with an increase in IK/SK channel currents in PAs (Fig. 2G), suggesting that whole-cell increases in Ca<sup>2+</sup> can activate IK/SK channels in PAs. The Ca<sup>2+</sup>-sensitivity of IK/SK channels in ECs from PAs was further tested using the conventional whole-cell patch-clamp configuration under conditions in which the concentration of free Ca<sup>2+</sup> in the patch pipette was increased to 3 μM to cause maximal Ca<sup>2+</sup>-dependent activation of IK/SK channels. Under these conditions, the density of IK/SK channel currents was similar between ECs from PAs and MAs (Fig. 2H and I). These results confirm that increases in intracellular Ca<sup>2+</sup> can activate IK/SK channels in ECs from PAs and that the maximum density of IK/SK channel currents is similar in ECs from resistance PAs and MAs.

## **ECs from MAs and PAs show similar TRPV4<sub>EC</sub> channel activity.**

Lower expression/activity of TRPV4<sub>EC</sub> channels could be one possible explanation for the lack of GSK101-induced IK/SK channel currents in PAs. We addressed this possibility by

recording currents through TRPV4<sub>EC</sub> channels in ECs from MAs and PAs and by recording the activity of TRPV4<sub>EC</sub> sparklets in *en face* preparations of MAs and PAs. Outward currents through TRPV4<sub>EC</sub> channels were recorded in the presence of GSK101 (10 nM) and ruthenium red (RuR, 1  $\mu$ M), the latter of which blocks Ca<sup>2+</sup> influx at negative voltages, preventing Ca<sup>2+</sup> overload and Ca<sup>2+</sup>-dependent activation of IK/SK currents (354). The remaining outward currents were inhibited by the selective TRPV4 channel inhibitor GSK219 (Fig. 3A). GSK101 induced comparable GSK219-sensitive outward currents in ECs from MAs and PAs, suggesting similar TRPV4<sub>EC</sub> channel activity in these arteries (Fig. 3A and B). Furthermore, recordings of elementary Ca<sup>2+</sup> influx through TRPV4<sub>EC</sub> channels (TRPV4<sub>EC</sub> sparklets) in the intact endothelium of MA and PA *en face* preparations in the absence or presence of the TRPV4<sub>EC</sub> channel activator GSK101 (0, 3, 10 nM) showed that TRPV4<sub>EC</sub> sparklet activity was similar between PAs and MAs (Fig. 3C–E). Spatial localization analysis confirmed that TRPV4<sub>EC</sub> sparklet activity was higher at MEPs than non-MEP sites in both PAs and MAs (Fig. 3F), and that overall TRPV4<sub>EC</sub> sparklet activity was similar between PAs and MAs at both MEP and non-MEP locations. These data suggest that TRPV4<sub>EC</sub> channel activity is similar between PAs and MAs and confirm that the absence of TRPV4<sub>EC</sub>-IK/SK channel coupling in PAs is not attributable to diminished TRPV4<sub>EC</sub> channel activity.

### **TRPV4<sub>EC</sub> channels signal through eNOS activation to dilate PAs and through IK/SK channel activation to dilate MAs.**

Previous studies have shown that TRPV4<sub>EC</sub> channel activation causes endothelium-dependent dilation of resistance MAs and PAs (238, 354). Studies using the fluorescent NO indicator DAF-FM showed that TRPV4 channel activation with GSK101 (10 nM) increased endothelial NO levels in PAs, but not MAs (Fig. 4A and B). Moreover, GSK101-induced NO release was absent in PAs from eNOS<sup>-/-</sup> mice, confirming operation of the TRPV4<sub>EC</sub>-eNOS-NO

pathway in these arteries (Fig. 4A and B). In pressurized PAs, vasodilation induced by GSK101 (3-30 nM) was completely abolished by NOS inhibition with L-NNA and was not affected by inhibition of IK/SK channels (Fig. 4C and D). In contrast, GSK101-induced dilation of MAs was largely abolished by IK/SK channel inhibition with TRAM-34 + apamin, but was unaffected by NOS inhibition with L-NNA (Fig. 4C and D). The direct IK/SK channel activator NS309 caused dilation of both PAs and MAs, indicating that communication via myoendothelial junctions occurs in both vascular beds (Fig. 4E). These results, together with our previous demonstration that TRPV4<sub>EC</sub> channel-induced vasodilation is absent in PAs from eNOS<sup>-/-</sup> mice (238), support vasodilatory TRPV4<sub>EC</sub>-eNOS coupling in PAs (but not in MAs) and TRPV4<sub>EC</sub>-IK/SK channel coupling in MAs (but not in PAs).

### **TRPV4<sub>EC</sub> and IK/SK channels localize at MEPs in MAs but not in PAs.**

The activation of IK/SK channels in pulmonary ECs by whole-cell increases in Ca<sup>2+</sup>, but not by TRPV4<sub>EC</sub> sparklets, suggests that the spatial proximity between TRPV4<sub>EC</sub> channels and IK/SK channels necessary for local coupling of TRPV4<sub>EC</sub> sparklets to IK/SK channels is altered in pulmonary ECs. To test whether the spatial proximity of TRPV4<sub>EC</sub> channels with eNOS in PAs and with IK/SK channels in MAs determines the specific TRPV4<sub>EC</sub> sparklet-target coupling, we immunohistochemically assessed co-localization of TRPV4<sub>EC</sub> channels with eNOS and IK/SK channels in PAs and MAs. TRPV4<sub>EC</sub> channels localized mainly at MEPs in PAs and MAs, and almost all MEPs in both vascular beds showed TRPV4<sub>EC</sub> channel expression (Fig. 5A–D), consistent with the localization of TRPV4<sub>EC</sub> sparklets. While the majority of IK and SK channels were localized to MEPs in MAs, only a small fraction of these channels were found at MEPs in PAs, suggesting that IK and SK channels do not co-localize with TRPV4<sub>EC</sub> channels at MEPs in PAs. Interestingly, ~50% of MEPs showed robust eNOS staining in both PAs and MAs, suggesting close proximity of TRPV4<sub>EC</sub> with eNOS in both arteries (Fig. 5A–D). We also detected

eNOS expression at other locations, possibly indicating Golgi/ER localization, as previously reported (Fig. 5A) (107, 122, 333). These results support the concept that the absence of TRPV4<sub>EC</sub>-IK/SK channel coupling in PAs is attributable to the lack of spatial proximity between TRPV4<sub>EC</sub> and IK/SK channels, but do not explain the preferential TRPV4<sub>EC</sub>-eNOS signaling in PAs and its absence in MAs.

### **Hemoglobin $\alpha$ (Hb $\alpha$ ) localizes with eNOS at MEPs in MAs but not in PAs.**

To more precisely compare eNOS levels between PAs and MAs, we studied eNOS expression using western blotting. The expression of eNOS protein was not different between PAs and MAs (Fig. 6A), suggesting that regulation of eNOS activity, rather than its expression, underlies the differential contribution of eNOS in PAs and MAs. Because Hb $\alpha$  has been shown to interact with eNOS and scavenge NO, thereby limiting NO bioavailability (172, 344, 364), we hypothesized that Hb $\alpha$  limits the role of eNOS-NO signaling in MAs. Immunostaining studies showed minimal expression of Hb $\alpha$  in ECs from PAs but confirmed strong expression and localization of Hb $\alpha$  at MEPs in MAs (Fig. 6B-D). Additionally, proximity ligation assays (PLAs) confirmed nanometer proximity between eNOS and Hb $\alpha$  in MAs, but not in PAs (Fig. 6E and F). These results support the concept that the presence of Hb $\alpha$  close to eNOS may be responsible for limiting the role of eNOS in MAs. Inhibiting NOS with L-NNA caused a ~12% constriction in PAs but did not affect the diameter of MAs (Fig. 6G). Hb $\alpha$ X, a peptide that inhibits the interaction of Hb $\alpha$  with eNOS, (172, 344, 363), was used to determine whether Hb $\alpha$ -eNOS interactions limit the role of eNOS in MAs; a scrambled control peptide (Scr X) was used as a control. Both Hb $\alpha$ X and Scr X possess a *tat* tag, which has previously been shown to render these peptides cell permeable (172, 344, 363). Strikingly, MAs treated with Hb $\alpha$ X were capable of constricting in response to L-NNA, suggesting that Hb $\alpha$  and eNOS normally interact in these arteries and that

disruption of Hb $\alpha$ -eNOS interactions with Hb $\alpha$ X disinhibited TRPV4<sub>EC</sub>-eNOS signaling.

Consistent with this, L-NNA was unable to constrict MAs in the presence of Scr X. Neither Hb $\alpha$ X nor Scr X affected L-NNA-induced constriction of PAs (Fig. 6G), supporting the conclusion that Hb $\alpha$  and eNOS do not normally interact in these cells. Interestingly, GSK101-induced increases in NO levels were enhanced in MAs in the presence of Hb $\alpha$ X, but were unaffected by Hb $\alpha$ X in PAs (Fig. 6H). Additionally, the increase in NO in the presence Hb $\alpha$ X was absent in MAs from eNOS<sup>-/-</sup> mice, supporting the eNOS-specific nature of the Hb $\alpha$ X effect in MAs. These results confirm that the spatial proximity of TRPV4<sub>EC</sub> channels with IK/SK/eNOS and of eNOS with Hb $\alpha$  determines the vasodilatory signaling target of TRPV4<sub>EC</sub> channels in resistance arteries (Fig. 7).

### 3.4 Discussion

Heterogeneity in endothelial vasodilatory mechanisms is well known; however, the preferential activation of one vasodilatory pathway over others remains poorly understood. Pressure myography studies have shown that IK/SK channel-induced hyperpolarization is the predominant mechanism for dilation of systemic resistance arteries (14, 82, 199, 302, 354, 368, 381, 392), whereas Ca<sup>2+</sup> signal-eNOS coupling dominates in resistance PAs (238). The current study advances our understanding of heterogeneity in endothelial vasodilatory pathways via three main findings: 1) TRPV4<sub>EC</sub> channels control the basal diameter of resistance PAs and MAs; 2) although functional IK/SK channels and eNOS are present in ECs from both PAs and MAs, TRPV4<sub>EC</sub> channels preferentially activate eNOS in PAs and IK/SK channels in MAs; and 3) spatial proximity of TRPV4<sub>EC</sub> channels with IK/SK channels or eNOS and that of eNOS with Hb $\alpha$  determines the vasodilatory target activated by TRPV4<sub>EC</sub> channels. Moreover, the dilatory effect of TRPV4<sub>EC</sub> channels on baseline diameter may underlie the higher resting blood pressure in TRPV4<sub>EC</sub><sup>-/-</sup> mice (289). Distinct factors regulate systemic and pulmonary arterial pressures; therefore, understanding the different mechanisms that control endothelial function in systemic

and pulmonary microcirculations is a crucial first step in achieving selective regulation of one versus the other. Additionally, many cardiovascular disorders have been associated with selective impairment of either eNOS-mediated or IK/SK channel-mediated vasodilation (103, 180, 228, 334, 355). Spatial uncoupling of TRPV4<sub>EC</sub> channels from IK/SK channels or eNOS, or of eNOS and Hb $\alpha$ , can be explored as a potential mechanism for endothelial dysfunction in vascular disorders.

Although IK/SK channel currents have been reported in cultured pulmonary ECs (210), whether functional IK/SK channels are present in native ECs from the pulmonary circulation had remained unknown. Our results represent the first recordings of IK/SK channel currents in freshly isolated ECs from resistance PAs. Moreover, vasodilation in response to direct IK/SK channel activation (Fig. 4E) provides functional evidence for endothelial-to-smooth muscle communication via MEGJs in PAs. It is important to note that the number of functional IK/SK channels per EC is comparable between MAs and PAs. While TRPV4<sub>EC</sub> channel-dependent activation of IK/SK channels in PAs requires whole-cell increases in endothelial Ca<sup>2+</sup>, localized TRPV4<sub>EC</sub> sparklets are sufficient to activate IK/SK channels in MAs. These findings, together with immunostaining results showing that IK/SK channels localize at MEPs in MAs but not in PAs (Fig. 5A-D), suggest that the absence of TRPV4<sub>EC</sub>-IK/SK channel coupling in PAs is attributable to the lack of proximity between TRPV4<sub>EC</sub> and IK/SK channels.

TRPV4<sub>EC</sub> sparklets do not couple with IK/SK channels in PAs, which begs the question: what is the role of endothelial IK/SK channels in PAs? IK/SK channels may be activated by another localized Ca<sup>2+</sup> signal in PAs, possibly pointing to a physiological stimulus–Ca<sup>2+</sup> signal–IK/SK channel linkage that is unique to PAs. The exact physiological stimulus or Ca<sup>2+</sup> signal that activates IK/SK channels in PAs remains unknown. Pulmonary arterial pressure (PAP) is regulated by a plethora of factors, and there is likely to be some redundancy in the mechanisms that can maintain PAP homeostasis. The presence of IK/SK channels in the PA endothelium

could be a redundant mechanism that comes into play in response to pathological stimuli. eNOS regulates basal PA diameter (Fig. 4C and D) and resting PAP (90, 238), and NO signaling is known to be impaired in pulmonary vascular disorders, including pulmonary arterial hypertension (PAH) (180). Interestingly, it has been shown that expression of endothelial H $\alpha$  is increased in pulmonary hypertension, which may explain the loss of NO signaling (8). A reasonable speculation is that a change in the localization of IK/SK channels at MEPs can, to a certain extent, offset the loss of NO signaling under pathological conditions.

Pressure myography studies are thought to more closely resemble physiological conditions compared with wire myography or tension recording studies (36, 92, 164, 331). Indeed, profound differences in endothelial vasodilatory pathways have been observed between pressure myography and wire-myography/tension recording experiments (26). Resistance-sized systemic arteries are known to develop pressure-induced constriction (myogenic tone) (16, 65)—a physiological autoregulatory mechanism. Because all MAs developed myogenic tone at 80 mmHg and only a small fraction of PAs showed myogenic tone at their physiological pressure of 15 mmHg, vascular reactivity was studied under conditions in which both MAs and PAs were pre-constricted with U46619. GSK219-induced, IK/SK channel-dependent constriction was similar in MAs with myogenic tone and those pre-constricted with U46619. Moreover, previous studies in pressurized MAs have shown that the IK/SK channel-dependent nature of TRPV4<sub>EC</sub> channel-induced vasodilation is preserved in the presence of U46619 (238). Thus, it can be assumed that the presence of U46619 alone did not affect the downstream targets of TRPV4<sub>EC</sub> channels.

Anchoring proteins that influence the activity of TRPV4 channels, IK/SK channels, and eNOS may also contribute to the heterogeneity of vasodilatory endothelial signaling. For example, the activity of TRPV4<sub>EC</sub> channels at MEPs is enhanced by A kinase anchoring protein 150 (AKAP150) in MAs (355); however, AKAP150 is not detected in ECs from PAs (238). The

activity of TRPV4<sub>EC</sub> channels in PAs is likely controlled by other scaffolding proteins. In this regard, caveolin-1 (Cav-1), a crucial protein in the pulmonary circulation, has been shown to interact with both TRPV4 channels and eNOS in ECs (117, 318); (19, 52, 167). The possibility that Cav-1–enriched membrane invaginations provide a signaling scaffold for TRPV4<sub>EC</sub>-eNOS signaling in PAs remains to be tested.

The mechanisms underlying the differential spatial coupling between TRPV4<sub>EC</sub> channels and IK/SK channels or eNOS, and between eNOS and Hb $\alpha$  are not known. Compared to systemic resistance arteries, pulmonary resistance arteries are exposed to a lower pressure, higher flow, and a lower dissolved oxygen content. It is plausible that chronic exposure to vastly different environments ultimately results in the differential signaling organization observed in this study. Moreover, the functional consequences of differential coupling of TRPV4<sub>EC</sub> channels with eNOS or IK/SK channels are not known. In PAs, TRPV4<sub>EC</sub> channel-induced NO was shown to limit TRPV4<sub>EC</sub> sparklet activity (NP<sub>O</sub> per site) (238). This NO-dependent negative feedback loop was absent in MAs, and inhibition of IK/SK channels did not alter the activity of TRPV4<sub>EC</sub> sparklets in MAs ( $0.048 \pm 0.003$  and  $0.054 \pm 0.04$  in the presence of 3 nM GSK101 before and after the addition of TRAM-34 and apamin;  $n=3$ ,  $P=0.098$ ), possibly reflecting tighter regulation of TRPV4<sub>EC</sub> channel activity and its functional consequences in the pulmonary microcirculation.

One of the limitations of our study is that it used autofluorescence of the IEL as a marker of endothelial projections. While this commonly used approach allows localization analyses of Ca<sup>2+</sup> signals and proteins, it should be noted that the presence of a hole in the IEL is not a direct indicator of the presence of MEGJs. Other matrix proteins, including collagen, fibronectin and laminin, may be present in the areas of the IEL that lack elastin, potentially complicating localization analyses. Our automatic detection of co-localization suggested that ~90% of holes in the IEL are sites of TRPV4<sub>EC</sub> channel co-localization, supporting the presence of endothelial

projections in most of the holes. However, the lengths of endothelial projections inside these holes, and the percentage of projections that go on to form MEGJs, is not known.

In conclusion, our results demonstrate that selective TRPV4<sub>EC</sub> channel-IK/SK channel coupling in resistance MAs is made possible by the spatial proximity of TRPV4<sub>EC</sub> channels with IK/SK channels and by the presence of Hb $\alpha$ , which serves to limit eNOS-NO signaling (Fig. 7). In contrast, preferential TRPV4<sub>EC</sub> channel-eNOS signaling in PAs can be explained by the spatial proximity between TRPV4<sub>EC</sub> channels and eNOS, the absence of Hb $\alpha$ , and the lack of proximity between TRPV4<sub>EC</sub> channels and IK/SK channels in this vascular bed. Thus, our studies reveal the unique spatial organizations that underlie endothelial heterogeneity in vasodilatory signaling pathways. Notable in this context, systemic hypertension has been associated with a loss of IK/SK-channel dependent vasodilation in MAs (186, 355), whereas pulmonary hypertension has been associated with a loss of eNOS-mediated vasodilation in PAs (180). Impaired Ca<sup>2+</sup> signal-target coupling may provide a potential mechanism for endothelial dysfunction in vascular disorders.

**Figure 1. TRPV4<sub>EC</sub> channels control resting diameter in resistance PAs and MAs.**

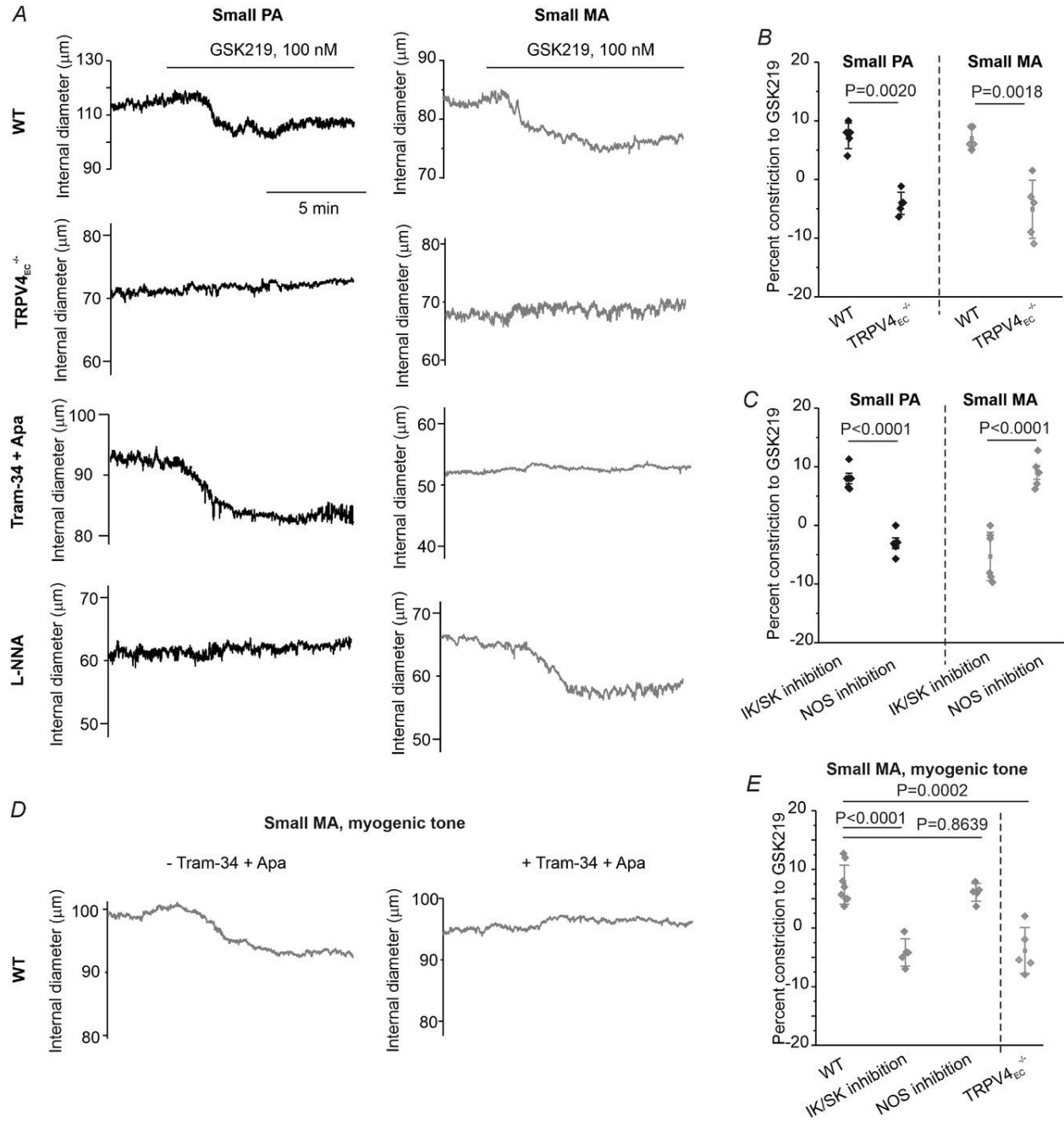


**Figure 1.** *A*, representative diameter traces showing effects of the TRPV4 channel inhibitor GSK219 (100 nM) on PAs (left) and MAs (right) isolated from WT and TRPV4<sub>EC</sub><sup>-/-</sup> mice, and on WT PAs and MAs in the presence of IK/SK channel inhibitors (1 μM TRAM-34, 300 nM apamin) or NOS inhibitor L-NNA (100 μM). Fourth-order PAs (pressurized to 15 mm Hg) and third-order MAs (pressurized to 80 mm Hg) were pre-constricted with the thromboxane analog U46619 (50 nM). *B*, percentage GSK219 (100 nM)-induced constriction of PAs and MAs isolated from WT and TRPV4<sub>EC</sub><sup>-/-</sup> mice (n=5; one-way ANOVA). *C*, percentage GSK219 (100 nM)-induced constriction of PAs and MAs in the presence of IK/SK channel inhibitors (1 μM TRAM-34 + 300 nM apamin) or NOS inhibitor (100 μM L-NNA) (n=5; one-way ANOVA). *D*, representative diameter traces of GSK219-induced constriction of MAs with myogenic tone in the absence (*left*) and presence (*right*) of IK/SK channel inhibitors. *E*, percentage GSK219 (100 nM)-induced constriction of MAs with myogenic tone in the presence of IK/SK channel inhibitors or NOS inhibitor in WT mice, or in MAs from TRPV4<sub>EC</sub><sup>-/-</sup> mice (n=5-7; one-way ANOVA). The vehicle itself (DMSO) did not alter the diameter of PAs and MAs (n=5; t-test, paired; P=0.5349 for PAs and 0.6079 for MAs).

**Figure 2. Whole-cell, but not localized, increases in intracellular  $Ca^{2+}$  activate IK/SK currents in PAs.**

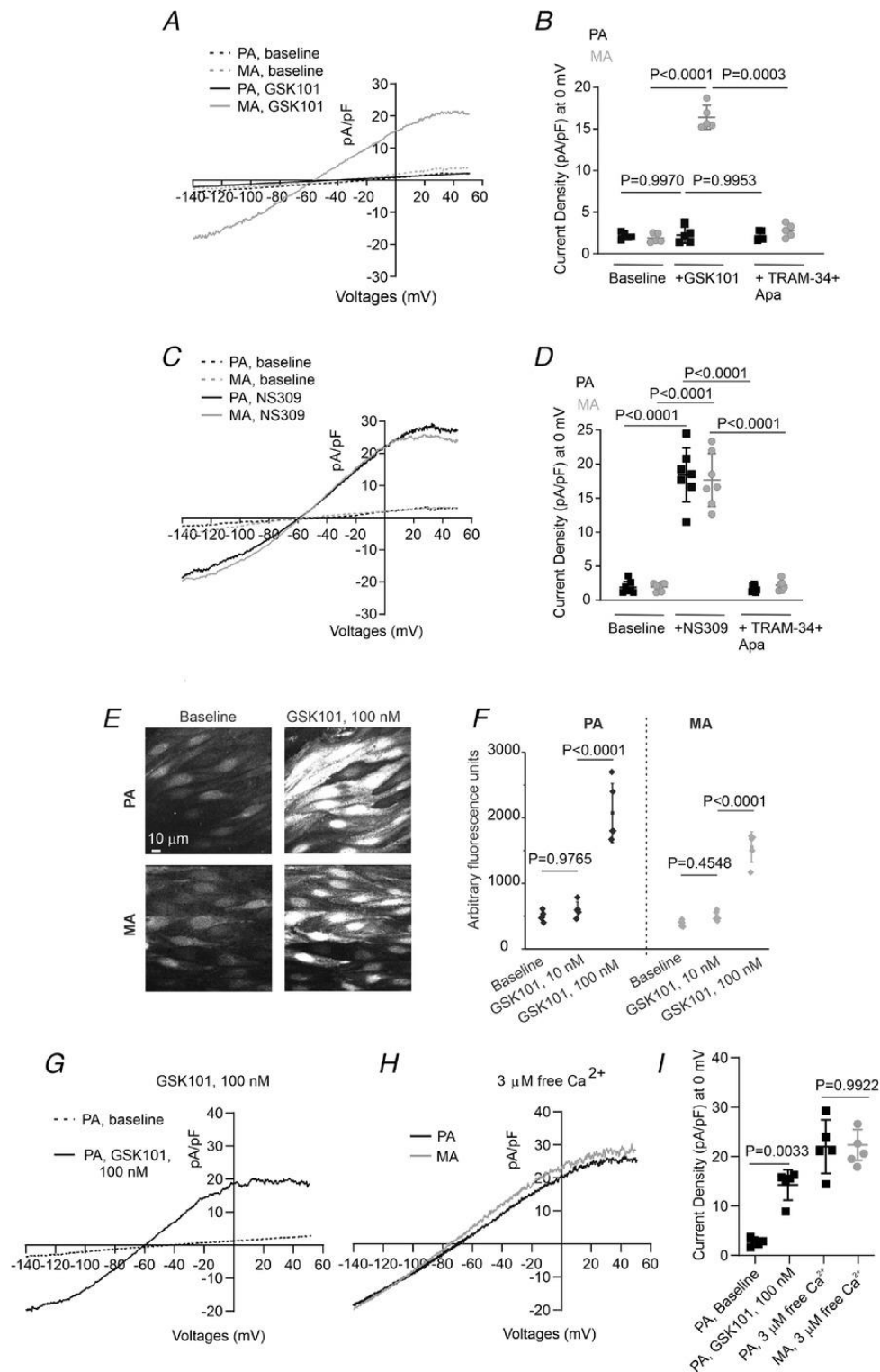


**Figure 2.** *A*, representative traces for ionic currents in freshly isolated ECs from MAs and PAs under baseline conditions, in the presence of GSK101 (10 nM), and GSK101 + TRAM-34 (1  $\mu$ M)/apamin (Apa, 300 nM), recorded in the perforated-patch configuration. *B*, current density plot of outward currents at 0 mV under baseline conditions, in the presence of GSK101 (10 nM), and GSK101 + TRAM-34/apamin (n=5; t-test, unpaired). *C*, representative traces for ionic currents under baseline conditions, in the presence of NS309 (1  $\mu$ M), and NS309 + TRAM-34/apamin in ECs from MAs and PAs in the perforated-patch configuration. *D*, current density plot of outward currents at 0 mV under baseline conditions, in the presence of NS309, and NS309 + TRAM-34/apamin (n=7; t-test, unpaired). *E*, grayscale images of *en face* preparations of PAs and MAs loaded with Fluo-4AM before (left) and after the addition of GSK101 (100 nM) (right). *F*, averaged whole-cell Fluo-4AM fluorescence in ECs from PAs and MAs before (Baseline) and after the addition of GSK101 (10 and 100 nM, n=5, one-way ANOVA). *G*, representative traces for baseline currents and GSK101 (100 nM)-activated, TRAM-34 (1  $\mu$ M)/apamin (300 nM)-sensitive IK/SK channel currents in freshly isolated ECs from PAs in the perforated patch-clamp configuration. *H*, representative traces of TRAM-34/apamin-sensitive IK/SK currents evoked by 3  $\mu$ M free  $\text{Ca}^{2+}$  in freshly isolated ECs from PAs and MAs in the whole-cell configuration. *I*, density plots for outward currents at 0 mV under baseline conditions, and TRAM-34/apamin-sensitive IK/SK channel currents activated by GSK101 (100 nM) or 3  $\mu$ M free  $\text{Ca}^{2+}$  (n=5; one-way ANOVA).

**Figure 3. GSK101 induces similar TRPV4<sub>EC</sub> channel activity in ECs from MAs and PAs.**

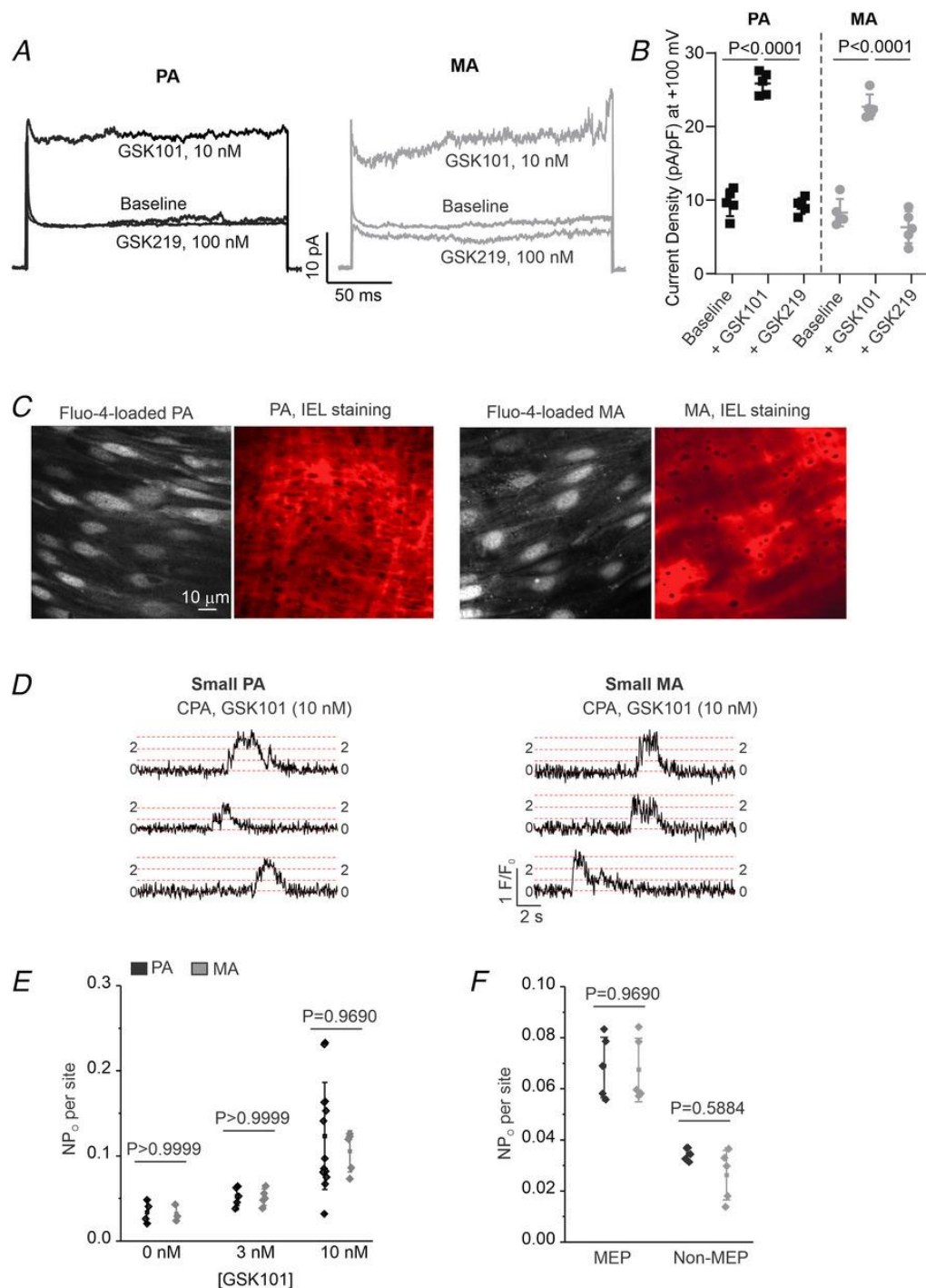


**Figure 3.** A, representative traces for GSK101 (10 nM)-induced outward TRPV4<sub>EC</sub> currents in freshly isolated ECs from PAs (left) and MAs (right). Application of the TRPV4 channel inhibitor

GSK219 (100 nM) attenuated TRPV4<sub>EC</sub> currents. TRPV4<sub>EC</sub> currents were evoked by a 200-ms pulse from -50 mV to +100 mV. Ruthenium red (1  $\mu$ M) was present throughout the experiment to inhibit Ca<sup>2+</sup>-induced IK/SK channel currents and prevent Ca<sup>2+</sup> overload. *B*, scatter plot showing GSK101-induced outward currents at +100 mV, and inhibition by GSK219 (n=5; one-way ANOVA). *C*, representative images for *en face* preparations of PAs (left) and MAs (right) loaded with Fluo-4AM and counterstained with Alexa Fluor 633 hydrazide (10  $\mu$ M). TRPV4<sub>EC</sub> sparklet sites localized at holes in the IEL were indicative of MEPs. *D*, representative F/F<sub>0</sub> traces for TRPV4<sub>EC</sub> sparklets in PAs (left) and MAs (right) in the presence of 10 nM GSK101, to activate TRPV4<sub>EC</sub> channels, and cyclopiazonic acid (CPA, 20  $\mu$ M), to eliminate Ca<sup>2+</sup> release from intracellular stores. *E*, baseline (CPA alone) and GSK101 (3 and 10 nM)-induced TRPV4<sub>EC</sub> sparklet activity in PAs and MAs, expressed as NP<sub>O</sub> per site, where N is the number of channels and P<sub>O</sub> is open state probability (n=5; one-way ANOVA). *F*, GSK101 (3 nM)-induced TRPV4<sub>EC</sub> sparklet activity at MEP and non-MEP sites in PAs and MAs (n=5-13, one-way ANOVA).

**Figure 4. TRPV4<sub>EC</sub> channels act through IK/SK channel activation to dilate MAs and through eNOS-NO signaling to dilate PAs.**

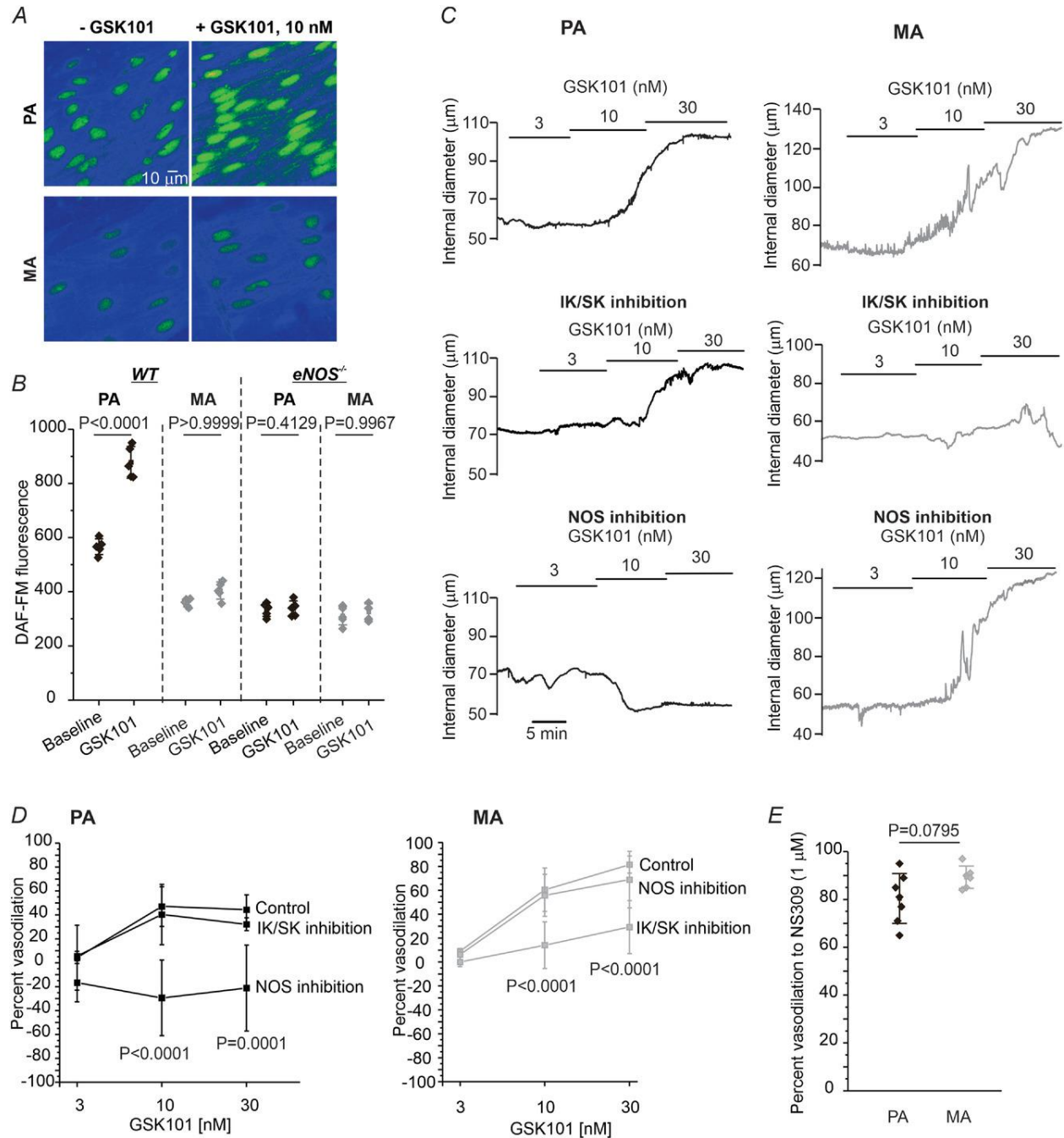


**Figure 4.** *A*, representative images for DAF-FM fluorescence in ECs of PAs and MAs under basal conditions (*left*) and in the presence of the TRPV4 channel agonist GSK101 (10 nM) (*right*). *B*, averaged DAF-FM fluorescence in ECs from PAs and MAs of WT and eNOS<sup>-/-</sup> mice in the absence or presence of 10 nM GSK101 (n=5, one-way ANOVA). *C*, representative diameter traces for GSK101 (3-30 nM)-induced dilation of PAs (*left*) and MAs (*right*) pre-constricted with the thromboxane analog U46619 (50 nM), and effects of TRAM-34 (1 μM) + apamin (300 nM) and the NOS inhibitor L-NNA (100 μM). Third-order MAs were pressurized to 80 mm Hg, and fourth-order PAs were pressurized to 15 mm Hg. *D*, percent dilation of PAs (*left*) and MAs (*right*) in response to GSK101 (3-30 nM) under control conditions, in the presence of TRAM-34 + apamin, and in the presence of L-NNA (n=5, P value vs Control, two-way ANOVA). *E*, scatter plot for NS309 (1 μM)-induced dilation of PAs and MAs (n=6-7; t-test, unpaired).

**Figure 5. TRPV4<sub>EC</sub>-IK/SK channels localize at MEPs in MAs but not in PAs.**

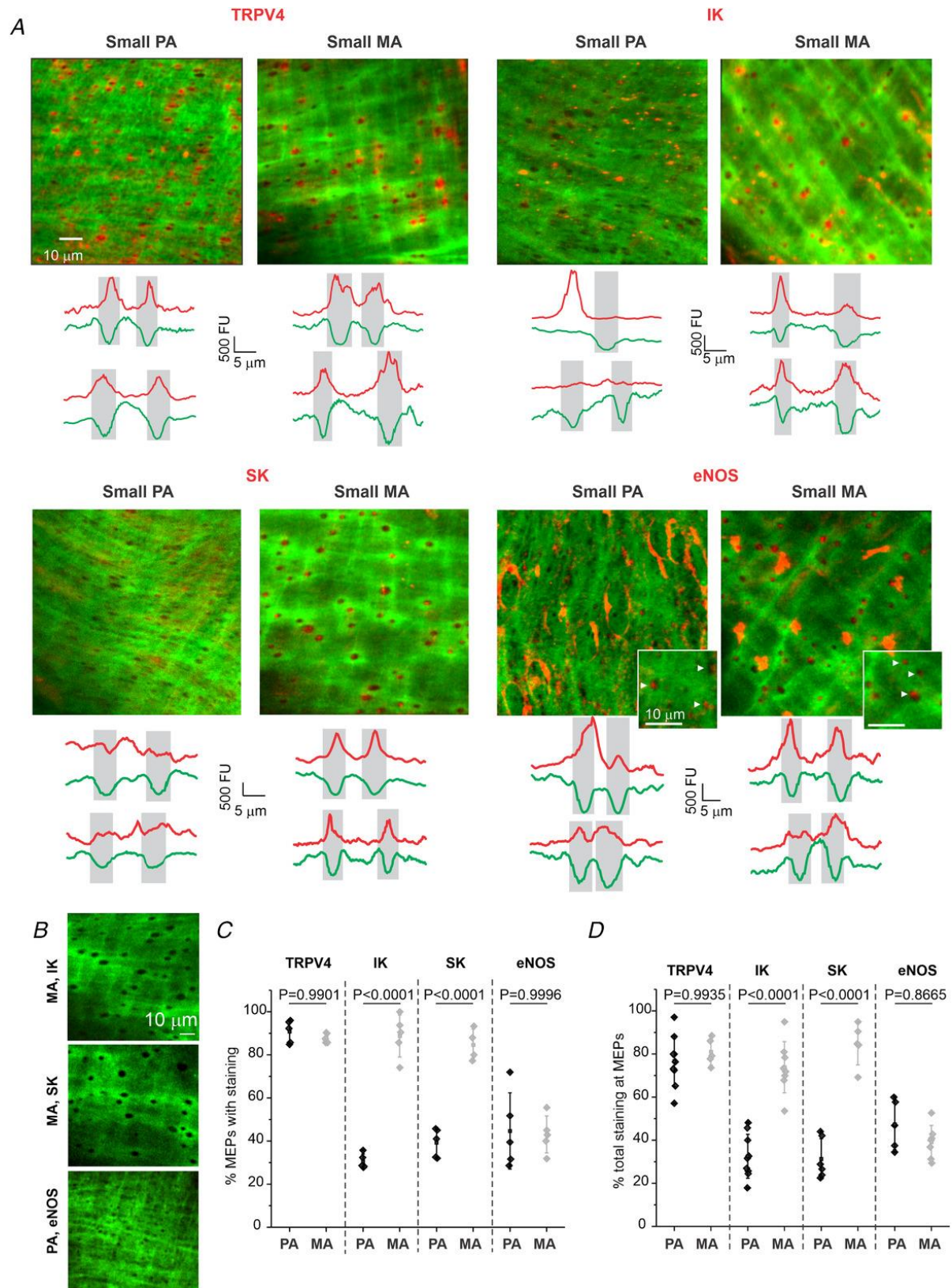


**Figure 5.** *A*, representative merged images from *en face* preparations of fourth-order PAs (left) and third-order MAs (right) showing IEL autofluorescence (green) and TRPV4<sub>EC</sub>, IK, SK, or eNOS immunofluorescence (red). Black holes represent MEPs. Traces under each image indicate representative fluorescence intensity plot profiles for 0.2- $\mu$ m-thick lines across MEPs. Green line, IEL; red line, protein of interest; gray rectangles, MEPs. White arrows in the inset images indicate eNOS localization at MEPs; scale= 10  $\mu$ m. *B*, representative antibody control images for IK and SK channel antibodies (using blocking peptides in MAs) and eNOS antibody (PAs from eNOS<sup>-/-</sup> mice). TRPV4 antibody has previously been validated using TRPV4<sub>EC</sub><sup>-/-</sup> mice (289). *C*, percent of MEPs localized with immunofluorescence (n=6; one-way ANOVA). *D*, percentage of immunofluorescence staining localized with MEPs (n=5-9; one-way ANOVA).

**Figure 6. Hba co-localizes with eNOS at MEPs in MAs but not in PAs.**

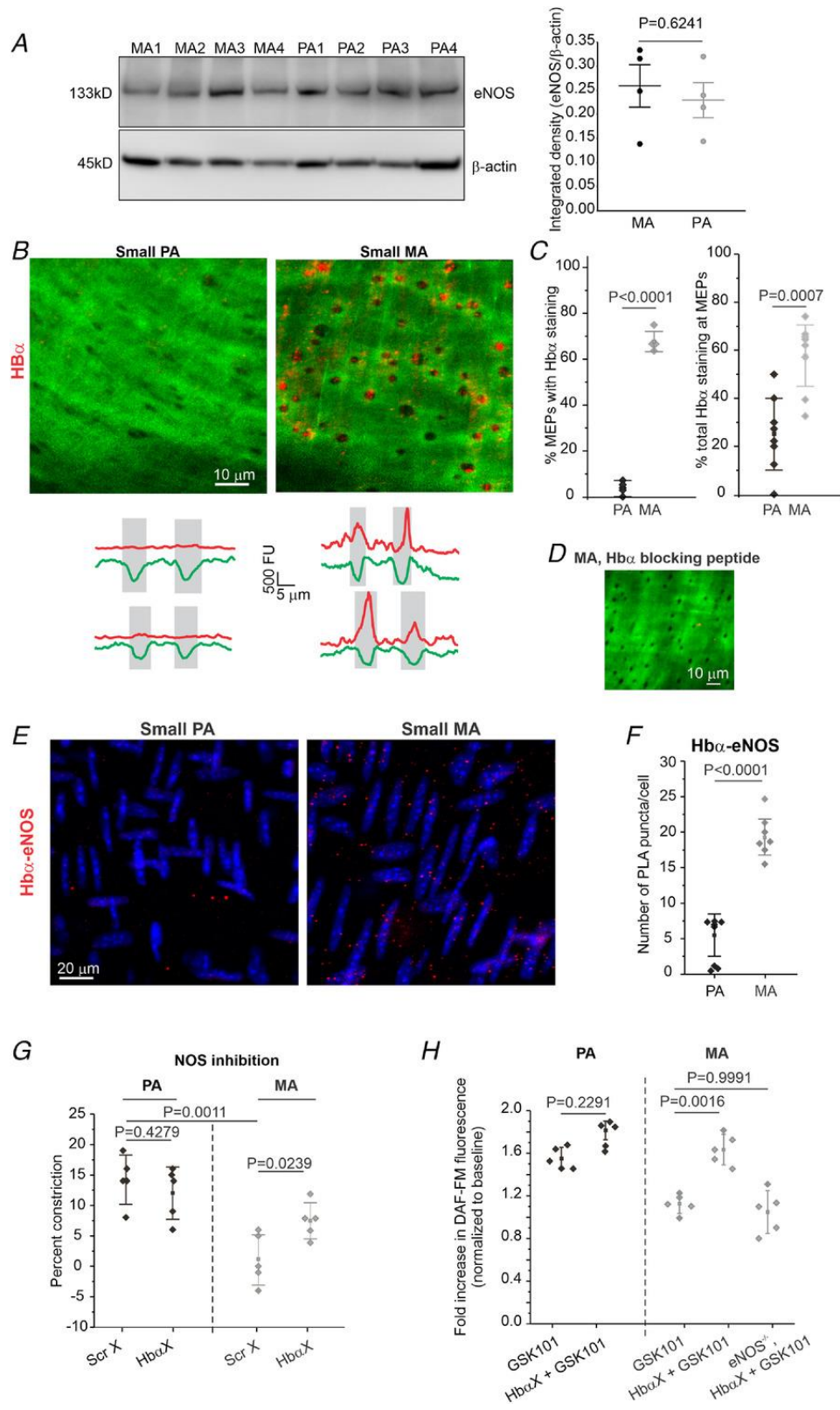


**Figure 6.** *A*, Western blot (*left*) and densitometric analysis (*right*) of eNOS levels showing similar eNOS expression in both MAs and PAs (n=4; t-test, unpaired). *B*, representative merged images from *en face* preparations of PAs (*left*) and MAs (*right*) showing IEL autofluorescence (green) and Hb $\alpha$  immunofluorescence (red). Black holes represent MEPs. Traces under each image are fluorescence intensity plot profiles for 0.2- $\mu$ m-thick lines across MEPs. Green line, IEL; red line, protein of interest. *C*, percent of MEPs localized with red immunofluorescence (*left*) (n=5; t-test, unpaired) and percentage of total immunofluorescence (red) staining at MEPs (*right*) (n=5-8, t-test, unpaired). *D*, representative Hb $\alpha$  immunostaining image from an antibody control experiment using a blocking peptide in MA. *E*, representative PLA merged images showing EC nuclei (blue) and red puncta for eNOS:Hb $\alpha$  co-localization in *en face* preparations of PAs (*left*) and MAs (*right*). *F*, quantification of eNOS:Hb $\alpha$  PLA puncta in PAs and MAs (n=8-9; t-test, unpaired). *G*, percent constriction to L-NNA (100  $\mu$ M) in the absence or presence of the control scrambled peptide Scr X (5  $\mu$ M) or inhibitory peptide Hb $\alpha$ X (5  $\mu$ M) in PAs and MAs (n=5; one-way ANOVA). *H*, averaged fold increase in GSK101 (10 nM)-induced DAF-FM fluorescence in the presence or absence of Hb $\alpha$ X (5  $\mu$ M) in PAs and MAs from WT mice and in MAs from eNOS<sup>-/-</sup> mice (n=5, one-way ANOVA).

**Figure 7. Schematic depicting the mechanisms underlying preferential TRPV4<sub>EC</sub> sparklet-eNOS versus TRPV4<sub>EC</sub> sparklet-IK/SK channel coupling in resistance PAs and MAs.**

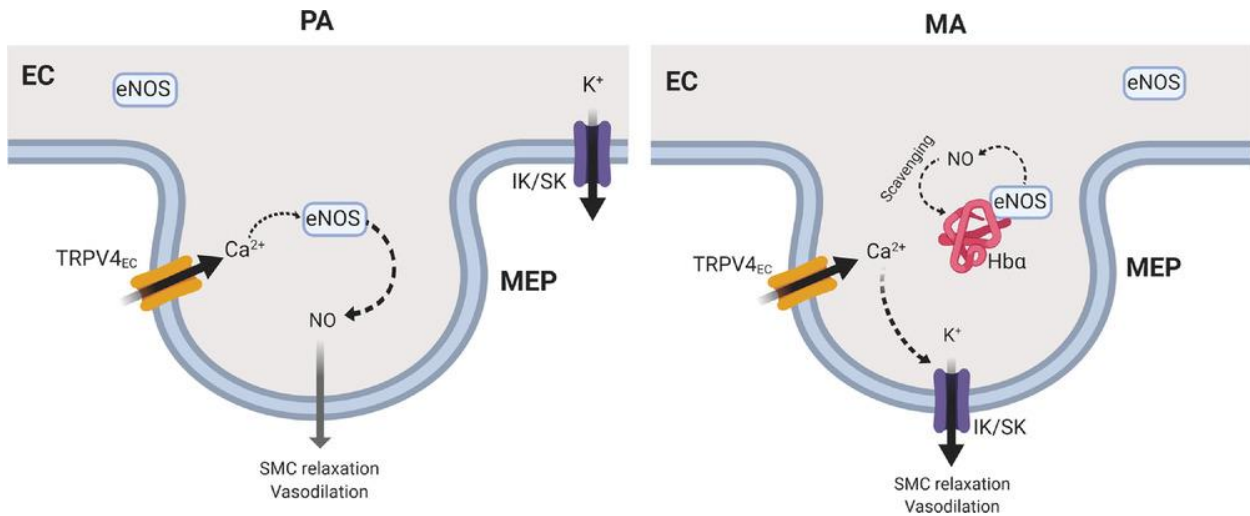


**Figure 7.** Endothelial projections to SMCs in PAs and MAs are shown. EC: endothelial cell; eNOS: endothelial nitric oxide synthase; NO: nitric oxide; SMC: smooth muscle cell; TRPV4<sub>EC</sub>: endothelial cell transient receptor potential vanilloid 4 channel; IK/SK: intermediate and small conductance Ca<sup>2+</sup>-sensitive K<sup>+</sup> channels; Hba: hemoglobin alpha; MEP: myoendothelial projection.

**Chapter 4: Local Peroxynitrite Impairs Endothelial Transient  
Receptor Potential Vanilloid 4 (TRPV4) Channels and Elevates  
Blood Pressure in Obesity**

## 4.1 Abstract

Impaired endothelium-dependent vasodilation is a hallmark of obesity-induced hypertension. The recognition that  $\text{Ca}^{2+}$  signaling in endothelial cells promotes vasodilation has led to the hypothesis that endothelial  $\text{Ca}^{2+}$  signaling is compromised during obesity, but the underlying abnormality is unknown. In this regard, TRPV4 ion channels are a major  $\text{Ca}^{2+}$  influx pathway in endothelial cells, and regulatory protein AKAP150 enhances the activity of TRPV4 channels. We show that  $\text{Ca}^{2+}$  influx through TRPV4 channels at myoendothelial projections (MEPs) to smooth muscle cells decreases resting blood pressure in non-obese mice, a response that is diminished in obese mice. Counterintuitively, release of the vasodilator molecule NO attenuated endothelial TRPV4 channel activity and vasodilation in obese animals. Increased activities of iNOS and NOX1 enzymes at MEPs in obese mice generated higher levels of NO and superoxide radicals, resulting in increased local peroxynitrite formation and subsequent oxidation of the regulatory protein AKAP150 at cysteine 36, to impair AKAP150-TRPV4 channel signaling at MEPs. Strategies that lowered peroxynitrite levels prevented cysteine 36 oxidation of AKAP150, and rescued endothelial AKAP150-TRPV4 signaling, vasodilation, and blood pressure in obesity. Importantly, peroxynitrite-dependent impairment of endothelial TRPV4 channel activity and vasodilation was also observed in the arteries from obese patients. These data suggest that a spatially restricted impairment of endothelial TRPV4 channels contributes to obesity-induced hypertension, and imply that inhibiting peroxynitrite might represent a strategy for normalizing endothelial TRPV4 channel activity, vasodilation, and blood pressure in obesity.

## 4.2 Introduction

According to the World Health Organization, the incidence of obesity worldwide has nearly tripled since 1975, affecting ~650 million adults in 2016(285). Obesity has become a life-threatening health concern and a major risk factor for cardiovascular disease, including

hypertension and stroke(67, 133). Loss of endothelium-dependent vasodilation is commonly observed in human patients(38, 325) and animal models of obesity(39, 190), and is thought to be a major contributor to obesity-induced hypertension(67). Therefore, identifying the molecular mechanisms of obesity-induced endothelial dysfunction may help to realize new strategies for therapeutic intervention that offer the promise of improved global health.

Endothelial cell (EC)  $Ca^{2+}$  signaling is a key regulator of vascular function(290). In small, resistance arteries, spatially localized  $Ca^{2+}$  signals cause endothelium-dependent vasodilation and diminished vascular resistance(14, 147, 368). These  $Ca^{2+}$  signals can occur through  $Ca^{2+}$  release from the endoplasmic reticulum (ER) and/or  $Ca^{2+}$  influx through ion channels at the EC membrane. Notably, elementary  $Ca^{2+}$ -influx signals through endothelial transient receptor potential vanilloid 4 (TRPV4<sub>EC</sub>) channels localized at EC projections to smooth muscle cells (SMCs), termed myoendothelial projections (MEPs), activate nearby  $Ca^{2+}$ -sensitive, intermediate- or small-conductance  $K^+$  (IK and SK, respectively) channels to hyperpolarize the EC plasma membrane(290). This hyperpolarization is subsequently transmitted to surrounding SMCs via myoendothelial gap junctions (MEGJs) that electrically couple ECs and SMCs(76, 323). SMC hyperpolarization, in turn, inactivates voltage-dependent  $Ca^{2+}$  channels to attenuate  $Ca^{2+}$  influx, resulting in vasodilation. Importantly, TRPV4<sub>EC</sub> channels exhibit cooperative gating, an effect that is enhanced for channels localized to MEP sites. A-kinase anchoring protein 150 (AKAP150), which anchors protein kinase C (PKC) and protein kinase A (PKA)(66, 96) and is preferentially localized to MEPs in resistance arteries(355), is a crucial enhancer of TRPV4 channel activity in multiple cell types(246, 355). However, whether the endothelial AKAP150 (AKAP150<sub>EC</sub>)-TRPV4<sub>EC</sub> signaling cascade exerts a tonic influence on resting blood pressure, and how this cascade might operate in obesity, remain unknown.

Resistance arteries control the blood pressure, however, the mechanisms for obesity-induced endothelial dysfunction in resistance arteries remain unknown. In large conduit arteries,

obesity is associated with excessive formation in ECs of reactive oxygen species (ROS), including the superoxide radical ( $O_2^{\cdot-}$ )(227, 346). This abnormality, together with the finding of elevated vascular inducible nitric oxide synthase (iNOS) activity(276, 350), may catalyze the reaction of  $O_2^{\cdot-}$  with nitric oxide (NO) to form peroxynitrite (PN)(307), which has been linked to endothelial dysfunction in conduit arteries(32, 42). Thus, the common vasodilator molecule NO may have deleterious effects on vasodilation and blood pressure in obesity via PN formation.

Here, we postulated that PN impairs endothelial AKAP150<sub>EC</sub>-TRPV4<sub>EC</sub> signaling at MEPs to curtail endothelium-dependent vasodilation and elevate blood pressure in obesity. Using newly developed endothelium-specific AKAP150 (AKAP150<sub>EC</sub><sup>-/-</sup>) and TRPV4 (TRPV4<sub>EC</sub><sup>-/-</sup>) knockout mice, we provide the first evidence for a role of AKAP150<sub>EC</sub>-TRPV4<sub>EC</sub> channel signaling in modulating resting blood pressure. Moreover, PN formation at the MEPs underlies the specific impairment of AKAP150<sub>EC</sub>-TRPV4<sub>EC</sub> channel signaling in obesity, which contributes to obesity-induced loss of endothelium-dependent vasodilation and elevated blood pressure. Spatially localized PN targets AKAP150<sub>EC</sub> to decrease  $Ca^{2+}$  influx through TRPV4<sub>EC</sub> channels in obesity, an abnormality that is reversed by PN and  $O_2^{\cdot-}$  inhibitors. Our studies implicating dysregulated TRPV4<sub>EC</sub> channels in defective endothelium-dependent vasodilation in obesity provide a rationale for designing PN-based therapeutics to restore TRPV4<sub>EC</sub> channel function and normalize blood pressure in obese individuals.

### 4.3 Results

#### **Endothelium-specific TRPV4- and AKAP150-knockout mice show elevated blood pressure.**

AKAP150 enhances TRPV4 channel activity via PKC anchoring in multiple cell-types(246, 355). It is unclear whether the AKAP150<sub>EC</sub>-TRPV4<sub>EC</sub> signaling mechanism impacts blood pressure, since EC-specific knockout of these proteins has not been accomplished to date. Accordingly, we developed and validated two new inducible mouse models, TRPV4<sub>EC</sub><sup>-/-</sup> and AKAP150<sub>EC</sub><sup>-/-</sup>, in which TRPV4 and AKAP150, respectively, were specifically knocked out in ECs. Endothelial knockout of TRPV4 channels or AKAP150 was confirmed by a decrease in TRPV4 and AKAP150 immunostaining in ECs (Figure 1A; Supplementary Figures 1A-1D), and a decrease in endothelial mRNA for TRPV4 channels and AKAP150 (Figure 1B, Supplementary Figure 1E) in the corresponding knockout models. Unitary Ca<sup>2+</sup> influx signals through individual TRPV4<sub>EC</sub> channels, termed TRPV4<sub>EC</sub> sparklets(354), were recorded in resistance mesenteric arteries (MAs) and confirmed by their sensitivity to the highly selective TRPV4 antagonist, GSK2193874 (GSK219, 100 nM; Supplementary Figure 1F). Baseline TRPV4<sub>EC</sub> sparklet activity (recorded in the presence of 20 μM cyclopiazonic acid [CPA] to eliminate interfering inositol 1,4,5-trisphosphate receptor-mediated Ca<sup>2+</sup> signals(354)) as well as that induced by the TRPV4 agonist GSK1016790A (GSK101; 3–30 nM), was markedly reduced in MAs from TRPV4<sub>EC</sub><sup>-/-</sup> mice compared with that in MAs from wild-type (WT) mice (Figure 1C).

The classical muscarinic receptor agonist carbachol (CCh) increases TRPV4<sub>EC</sub> channel activity in an AKAP150/PKC-dependent manner to promote vasodilation(14, 354, 355). In *en face* preparations of MAs from WT mice, AKAP150<sub>EC</sub> was concentrated mainly at MEPs, identifiable as black holes in the internal elastic lamina (IEL) (Figure 1A; Supplementary Figure 1E). Notably, a spatial localization analysis indicated that baseline TRPV4<sub>EC</sub> sparklet activity at MEPs, but not at other (non-MEP) sites, was reduced in MAs from AKAP150<sub>EC</sub><sup>-/-</sup> mice compared with WT mice

(Figures 1D, 1E; Supplementary Figures 2A, 2B). Moreover, CCh enhanced TRPV4<sub>EC</sub> sparklet activity only at MEPs, an effect that was not observed in MAs from AKAP150<sub>EC</sub><sup>-/-</sup> mice (Figure 1E; Supplementary Figures 2A, 2B). PKC-mediated activation of TRPV4<sub>EC</sub> sparklets, induced by the PKC activator PMA (phorbol 12-myristate 13-acetate), also showed a similar AKAP150<sub>EC</sub>-dependence and localization at MEPs (Supplementary Figures 2B, 2C). Thus, AKAP150<sub>EC</sub> is required for the activation of TRPV4<sub>EC</sub> channels at MEPs. Only the direct TRPV4 channel agonist GSK101 (10 nM) was able to increase TRPV4<sub>EC</sub> sparklet activity in MAs from AKAP150<sub>EC</sub><sup>-/-</sup> mice (Figure 1E). TRPV4<sub>EC</sub> sparklets represent coupled openings of individual TRPV4<sub>EC</sub> channels at a given site(354, 355). An analysis of cooperative gating among TRPV4<sub>EC</sub> channels, measured as coupling coefficient (k) value, which varies from 0 (no coupling or independent gating) to 1 (complete coupling), indicated that coupling was weaker at MEPs in MAs from AKAP150<sub>EC</sub><sup>-/-</sup> mice (Figure 1F; Supplementary Figure 3), supporting a critical role of AKAP150<sub>EC</sub> in functional coupling of TRPV4<sub>EC</sub> channels. Furthermore, TRPV4 channel agonist - and CCh-induced dilation of MAs were dramatically decreased in MAs from TRPV4<sub>EC</sub><sup>-/-</sup> and AKAP150<sub>EC</sub><sup>-/-</sup> mice (Figure 1G-1J; Supplementary Figure 4), indicating impaired endothelium-dependent vasodilation in these mice. Importantly, resting systolic, diastolic, and mean arterial pressure (MAP), recorded using radiotelemetry, were elevated in both TRPV4<sub>EC</sub><sup>-/-</sup> and AKAP150<sub>EC</sub><sup>-/-</sup> mice compared with the respective WT mice (Figure 1K; Supplementary Figure 5). Resting heart rate, however, was not different between WT and knockout mice (Supplementary Figures 5A, 5C). Pressure-induced constriction at 80 mm Hg was higher in both TRPV4<sub>EC</sub><sup>-/-</sup> and AKAP150<sub>EC</sub><sup>-/-</sup> mice compared to respective WT mice (Figure 1L), suggesting higher baseline vascular tone in these mice. These new findings provide initial evidence that AKAP150<sub>EC</sub>-TRPV4<sub>EC</sub> signaling at MEPs promotes endothelium-dependent vasodilation and contributes to the regulation of resting blood pressure.

## **Diet-induced obesity is associated with impaired TRPV4<sub>EC</sub> sparklet activity and endothelium-dependent vasodilation.**

Diet-induced obesity caused by excessive intake of energy-dense foods is often accompanied by a rise in blood pressure and defective endothelium-dependent vasodilation(67, 133). Here, we explored whether disrupted TRPV4<sub>EC</sub> Ca<sup>2+</sup> signaling is a feature of defective endothelium-dependent vasodilation in mice fed a high-fat diet (HFD) for 14 weeks. Body weight of these HFD mice (44 ± 2 g) was significantly higher than that of mice fed a normal-fat diet (NFD; 28 ± 1 g, n = 13; *P* < 0.05, t-test). HFD mice also showed higher resting systolic, diastolic, and MAP (Figure 2A; Supplementary Figures 6A, 6B), and a higher pressure-induced vasoconstriction at 80 mm Hg (Supplementary Figures 6C) compared to NFD mice. CCh-induced, endothelium-dependent dilation was markedly blunted in MAs from HFD mice (Figure 2B). Similarly, dilation of MAs in response to the TRPV4 channel agonist GSK101 was also impaired in HFD mice (Figure 2C). TRPV4<sub>EC</sub> sparklets activate IK and SK channels to mediate membrane hyperpolarization of ECs, a response that propagates to adjacent SMCs to induce their relaxation and cause dilation of MAs(354). In the presence of IK/SK channel inhibitors, there was no significant difference in vasodilation to CCh and GSK101 between NFD and HFD mice (Supplementary Figures 7A, 7B). Moreover, in the presence of 60 mM extracellular K<sup>+</sup> to inhibit IK/SK channel-mediated hyperpolarization, there was no difference in vasodilation to CCh or GSK101 between NFD and HFD mice (Supplementary Figures 7C-F), further suggesting a specific impairment of TRPV4<sub>EC</sub>-IK/SK channels in obesity. Conceptually, the loss of TRPV4-mediated vasodilation could be related to reduced expression and/or function of TRPV4<sub>EC</sub> channels or IK/SK channels. We found that the dilatory response to the IK/SK channel activator NS309 was not altered in MAs from HFD mice (Supplementary Figure 8A), suggesting that the impairment in endothelial function in obesity lies upstream of IK/SK channels, possibly at the level of TRPV4<sub>EC</sub> channels, and that the communication across MEGJs is not impaired.

Notably, TRPV<sub>4EC</sub> sparklets were scarce in HFD mice (Figure 2E), a decrease that was spatially restricted to sparklet sites at MEPs (Figures 2E, 2F; Supplementary Figure 8B). Both CCh- and PKC-induced activation of TRPV<sub>4EC</sub> sparklets, which requires AKAP150<sub>EC</sub>, was markedly reduced in MAs from HFD mice (Supplementary Figure 8C). Moreover, the AKAP150<sub>EC</sub>-dependent enhancement of coupling strength among TRPV<sub>4EC</sub> channels at MEPs was also attenuated in obesity (Supplementary Figure 9A). The quantal level (unitary channel amplitude, reflecting stepwise openings of 1–4 TRPV4 channels at a site(354)) of TRPV<sub>4EC</sub> sparklets at MEPs was not altered in AKAP150<sub>EC</sub><sup>-/-</sup> or HFD mice compared with respective controls (Supplementary Figure 9B). Collectively, these findings raise the possibility of defective AKAP150<sub>EC</sub> enhancement of TRPV<sub>4EC</sub> channel function at MEPs in obesity.

Clinical relevance of our findings was established by studying TRPV<sub>4EC</sub>-mediated vasodilation and TRPV<sub>4EC</sub> sparklet activity in splenius/temporalis muscle arteries from non-obese and obese individuals. Both CCh and GSK101 dilated the arteries from non-obese individuals, and the vasodilation was absent in the arteries from obese individuals (Figures 2G-J). Moreover, GSK219-sensitive TRPV<sub>4EC</sub> sparklet activity was attenuated in the arteries from obese individuals when compared to those from non-obese individuals (Figures 2K, 2L). Thus, TRPV<sub>4EC</sub> channel activity and vasodilation are also impaired in the arteries from obese patients.

### **Inhibition of NOS or PN restores TRPV<sub>4EC</sub> channel activity, vasodilation, and blood pressure in obesity.**

TRPV<sub>4EC</sub>-IK/SK channel signaling is the major effector pathway for muscarinic receptor signaling-induced dilation of resistance MAs, whereas TRPV<sub>4EC</sub> channel-independent endothelial NOS (eNOS) activation plays a minor role(14, 354, 355). We hypothesized that NOS inhibition would eliminate the residual vasodilation to CCh in obese mice. Surprisingly, NOS inhibition with L-NNA (L-N<sup>G</sup>-nitroarginine; 100 μM) restored the vasodilation to both CCh and GSK101 (Figures

3A, 3B) in HFD mice. L-NNA had only a slight inhibitory effect on vasodilation to CCh and no effect on vasodilation to GSK101 in NFD mice (Figures 3A, 3B; Supplementary Figure 10A). L-NNA was unable to rescue the vasodilation to CCh or GSK101 in obese TRPV4<sub>EC</sub><sup>-/-</sup> or AKAP150<sub>EC</sub><sup>-/-</sup> mice (Figures 3A, 3B), suggesting the AKAP150<sub>EC</sub>-TRPV4<sub>EC</sub>-dependent rescue of vasodilation by L-NNA in obesity. Moreover, L-NNA rescued TRPV4<sub>EC</sub> sparklet activity in MAs from HFD mice, but had no effect on TRPV4<sub>EC</sub> sparklet activity or TRPV4<sub>EC</sub>-induced vasodilation in NFD mice (Supplementary Figure 10B). NOS-generated NO can react with O<sub>2</sub><sup>-</sup> radicals to form PN(307), which is known to have deleterious effects on endothelial function(42, 181, 416). O<sub>2</sub><sup>-</sup> and NO levels were elevated in ECs from HFD mice (Supplementary Figures 11A, 11B). On the basis of these findings, we postulated that PN is the signaling molecule that reduces TRPV4<sub>EC</sub> sparklet activity in obesity. A PN-selective fluorescent indicator, coumarin boronic acid (CBA), showed a concentration-dependent increase in fluorescence with PN and PN generator SIN-1 (Supplementary Figure 12), and a higher PN fluorescence in ECs from obese patients and mice when compared to respective non-obese controls (Figures 3C, 3D). Using PEG-catalase to decompose H<sub>2</sub>O<sub>2</sub> and taurine to scavenge hypochlorous acid did not lower the CBA fluorescence in obese mice, suggesting that H<sub>2</sub>O<sub>2</sub> or hypochlorous acid did not contribute to increased CBA fluorescence (Supplementary Figure 13). Moreover, immunostaining for 3-nitrotyrosine (NT), a commonly used biomarker of PN formation, revealed very low levels of 3-NT in MAs from NFD mice, but increased 3-NT formation at MEPs in HFD mice (Supplementary Figure 14). Uric acid (UA; 200 μM) and ebselen (1 μM), PN scavengers(347), Fe<sup>III</sup>-tetra-(4-sulfonatophenyl)-porphyrin (FeTPPs; 1 μM), a PN decomposer(193), and tempol (200 μM), a superoxide dismutase (SOD) mimetic that decreases O<sub>2</sub><sup>-</sup>, all rescued TRPV4<sub>EC</sub> sparklet activity at MEPs in MAs from HFD mice and in the arteries from obese individuals (Figures 3E; Supplementary Figures 15, 16). However, none of these agents affected sparklet activity at non-MEP sites in HFD mice or overall

sparklet activity in MAs of NFD mice (Supplementary Figures 15D-G), pointing to a spatially localized elevation in PN levels at MEPs in obesity.

PN inhibitors UA and FeTPPS also rescued CCh- and PKC-induced activation of TRPV4<sub>EC</sub> sparklets in HFD mice, restored coupling coefficients to NFD levels (Supplementary Figure 17A-C) and, like tempol and ebselen, restored dilation to CCh and GSK101 in MAs from HFD mice (Figure 3F; Supplementary Figure 17D). In TRPV4<sub>EC</sub><sup>-/-</sup> mice or AKAP150<sub>EC</sub><sup>-/-</sup> mice fed a HFD, UA was unable to rescue TRPV4<sub>EC</sub> sparklet activity and vasodilation to CCh (Supplementary Figures 17D, 17E), supporting the concept that PN inhibitors specifically rescued AKAP150<sub>EC</sub>-TRPV4<sub>EC</sub>-dependent vasodilation in obesity. Administration of UA (200 mg/kg, i.p.) or FeTPPS (10 mg/kg, i.p.) failed to affect resting blood pressure in NFD mice, but significantly lowered MAP in HFD mice 15 minutes after injection (Figure 3G). Neither compound altered heart rate in HFD mice (Supplementary Figure 18). Moreover, these PN inhibitors had no effect on resting MAP in TRPV4<sub>EC</sub><sup>-/-</sup> mice fed a HFD (Figure 3G), further confirming that inhibition of PN accumulation restored the ability of TRPV4<sub>EC</sub> channels to decrease MAP.

### **MEP-localized NADPH oxidase 1 (NOX1) and iNOS underlie PN-induced TRPV4<sub>EC</sub> channel dysregulation in obesity.**

NOX activity is a major source of cytosolic O<sub>2</sub><sup>-</sup> generation in the vasculature(79), and both NOX and vascular iNOS activity are increased in obesity(276). Three NOX isoforms—NOX1, NOX2 and NOX4—have been reported in rodent ECs(79). In MAs from NFD mice, the predominant NOX isoform detected at MEPs was NOX1 (Figure 4A). Interestingly, the expression of NOX1 at MEPs was increased in MAs from obese mice, whereas expression of NOX2 and NOX4 persisted at low levels (Figure 4A; Supplementary Figures 19, 20). Similarly, expression of iNOS was also elevated at MEPs in MAs from obese mice (Figures 4B, 4C). Consistent with these data, NOX1 and iNOS mRNA levels were elevated in MAs from obese

mice compared with NFD mice (Figure 4D). The specific NOX1 inhibitors NoxA1ds and ML-171, and iNOS inhibitor, 1400W, restored TRPV4<sub>EC</sub> sparklet activity to normal levels at MEPs in MAs from obese mice (Figures 4E-G; Supplementary Figure 21A). However, these compounds had no effect on sparklet activity at non-MEP sites (Figures 4E-G; Supplementary Figure 21A) and failed to affect sparklet activity in MAs from NFD mice (Supplementary Figure 21B). In contrast, the gp91phox blocking peptide, gp91 ds-tat (1  $\mu$ M), which specifically inhibits NOX2, did not alter TRPV4<sub>EC</sub> sparklet activity in obese mice (Supplementary Figure 22). Both NOX1 and iNOS inhibitors restored vasodilator responses to CCh and TRPV4 agonist in MAs from obese mice (Figures 4H, 4I; Supplementary Figure 23), an effect that was absent in the arteries from HFD TRPV4<sup>-/-</sup> mice or HFD AKAP150<sub>EC</sub><sup>-/-</sup> mice (Figures 4H, 4I; Supplementary Figure 24), and lowered the CBA fluorescence in the arteries from obese mice (Supplementary Figure 25). Moreover, 1400W or L-NNA administration also lowered MAP in obese mice (Figure 4J; Supplementary Figure 26). Collectively, these results suggest that elevated NOX1 and iNOS expression at vascular MEPs increases PN formation in obesity, which impairs TRPV4<sub>EC</sub> sparklet activity and endothelium-dependent vasodilation.

### **PN inhibits AKAP150<sub>EC</sub>-mediated enhancement of TRPV4<sub>EC</sub> sparklet activity at MEPs.**

To test whether exogenous PN attenuates TRPV4<sub>EC</sub> sparklet activity, we exposed MAs from WT mice to either PN (1  $\mu$ M) or the PN donor SIN-1 (50  $\mu$ M) for 5 minutes. Both PN and SIN-1 decreased TRPV4<sub>EC</sub> sparklet activity at MEPs, but had no effect on TRPV4<sub>EC</sub> sparklets at non-MEP sites (Figure 5A; Supplementary Figure 27A). SIN-1 generates NO and O<sub>2</sub><sup>-</sup>, which react to form PN. In the presence of the NO scavenger carboxy-PTIO (50  $\mu$ M) or tempol, SIN-1 was unable to inhibit TRPV4<sub>EC</sub> sparklet activity, indicating that neither O<sub>2</sub><sup>-</sup> nor NO *per se* alter TRPV4<sub>EC</sub> sparklet activity (Supplementary Figure 27B). Both UA and FeTPPS inhibited PN-induced 3-NT formation as well as the effect of PN on TRPV4<sub>EC</sub> sparklet activity at MEPs

(Supplementary Figure 28). In patch clamp studies on freshly isolated ECs from WT mice, exogenous PN reduced the currents through TRPV4<sub>EC</sub> channels (Figure 5B), supporting PN-induced inhibition of channel activity. TRPV4 agonist- and CCh-induced vasodilation was also inhibited in the presence of PN (Figures 5C, 5D; Supplementary Figure 29A). Decomposed PN, however, was unable to impair TRPV4<sub>EC</sub> sparklet activity or vasodilation (Supplementary Figures 29B-D). Furthermore, both CCh- and PKC-induced (PMA) increases in TRPV4<sub>EC</sub> sparklet activity were abolished in the presence of PN (Supplementary Figure 30A), and coupling strength among TRPV4<sub>EC</sub> channels at MEPs was lower in the presence of exogenous PN (Supplementary Figure 30B). Collectively, these findings suggest that PN impairs AKAP150<sub>EC</sub>-mediated enhancement of TRPV4<sub>EC</sub> channel activity. Indeed, in MAs from AKAP150<sub>EC</sub><sup>-/-</sup> mice, PN was unable to alter TRPV4<sub>EC</sub> sparklet activity evoked by TRPV4 agonist (10 nM, Figure 5E), confirming that PN does not directly target the TRPV4<sub>EC</sub> channel, but instead impairs AKAP150<sub>EC</sub>-mediated regulation of the channel.

### **PN-induced cysteine oxidation of AKAP150 lowers TRPV4<sub>EC</sub> channel activity.**

Dithiothreitol (DTT; 1 mM), which is used as a reducing agent to reverse cysteine oxidation, rescued TRPV4<sub>EC</sub> sparklet activity in HFD mice but not in HFD AKAP150<sub>EC</sub><sup>-/-</sup> mice (Supplementary Figure 31), suggesting that PN-induced cysteine oxidation may be responsible for AKAP150<sub>EC</sub>-TRPV4<sub>EC</sub> dysfunction in obesity. Ascorbic acid, which is a selective inhibitor of S-nitrosylation(279), did not alter TRPV4<sub>EC</sub> sparklet activity in obese mice suggesting that S-nitrosylation may not be responsible for TRPV4<sub>EC</sub> channel in obesity (Supplementary Figure 32). A 2-thiodimedone antibody to detect cysteine sulfenic acid (CSA) intermediates of cysteine oxidation showed higher CSA levels at MEPs in obese mice when compared to normal mice (Figure 5F). MAs from obese AKAP150<sub>EC</sub><sup>-/-</sup> mice showed minimal CSA staining at MEPs (Figure 5F). Moreover, CSA levels at MEPs in MAs from obese mice were lowered by pretreatment with DTT or PN scavenger UA (Supplementary Figure 33). Overall, these data support the idea that

PN causes cysteine oxidation of AKAP150<sub>EC</sub> in obesity to lower AKAP150<sub>EC</sub>-TRPV4<sub>EC</sub> signaling at MEPs.

In HEK293 cells, TRPV4 inhibitor-sensitive currents were increased in the presence of AKAP150 (Figure 5G). Moreover, PN did not alter TRPV4 currents in HEK293 cells expressing TRPV4 channel alone, but did inhibit such currents in cells expressing the TRPV4 channel and AKAP150 (Figure 5G), suggesting that PN decreases TRPV4 channel activity by targeting AKAP150. There is only one cysteine residue (Cys36) in the PKC-binding region (residues 31-52) of AKAP150(96). Substituting Cys36 of AKAP150 with alanine in HEK293 cells resulted in the loss of PN-inhibition of TRPV4 currents and PN-induced formation of cysteine sulfenic acid, an intermediate in disulfide bond formation (Figure 5G, Supplementary Figure 34). Taken together, these results indicate that PN causes oxidation of Cys36 on AKAP150 to lower TRPV4 channel activity.

TRPV4<sub>EC</sub> sparklets dilate MAs by activating IK/SK channels(354, 355). In freshly isolated ECs, PN did not alter IK/SK currents induced by the direct IK/SK channel activator, NS309 (Supplementary Figure 35A). Furthermore, NS309-induced vasodilation was unaffected by PN (Supplementary Figure 35B), confirming that PN-induced impairment in endothelium-dependent vasodilation occurs upstream of IK/SK channels.

### **PN impairs AKAP150<sub>EC</sub>:PKC localization in obesity.**

The expression of AKAP150<sub>EC</sub> at MEPs was unaltered in obesity (Figures 6A, 6B), and TRPV4<sub>EC</sub> and AKAP150<sub>EC</sub> transcript levels were also unchanged (Figure 6C). We further hypothesized that PN-induced impairment of AKAP150<sub>EC</sub>-PKC-TRPV4<sub>EC</sub> signaling in obesity reflects impaired localized coupling of AKAP150<sub>EC</sub> to PKC and/or TRPV4<sub>EC</sub>. Proximity ligation assays (PLAs) in MAs from NFD mice indicated that AKAP150<sub>EC</sub> exists within nanometer proximity of both PKC and TRPV4<sub>EC</sub> (Figures 6D, 6E). Moreover, AKAP150<sub>EC</sub>:TRPV4<sub>EC</sub> localization was not altered in

MAs from HFD mice (Figures 6D, 6F). However, we observed less AKAP150<sub>EC</sub>:PKC localization, suggesting impaired PKC anchoring by AKAP150<sub>EC</sub> in obesity (Figures 6E, 6F). Therefore, we hypothesized that PN inhibits the anchoring of PKC by AKAP150<sub>EC</sub> in obesity. Treatment of MAs from obese mice with UA for 5 minutes restored the localization of AKAP150<sub>EC</sub> with PKC to NFD levels (Figure 6F). Moreover, the PN donor SIN-1 decreased AKAP150<sub>EC</sub>:PKC localization in WT arteries (Figure 6G). These results support the idea that PN disrupts AKAP150<sub>EC</sub>-PKC-TRPV4<sub>EC</sub> vasodilator signaling at MEPs in obesity by specifically inhibiting anchoring of PKC by AKAP150<sub>EC</sub> (Figure 6H).

#### 4.4 Discussion

Using inducible, endothelium-specific knockout mice, we provide the first demonstration of a physiological role for TRPV4<sub>EC</sub> channels and the regulatory protein AKAP150<sub>EC</sub> in lowering resting blood pressure. Moreover, we show that increased PN at vascular MEPs targets AKAP150<sub>EC</sub> and lowers AKAP150<sub>EC</sub>-mediated enhancement of TRPV4<sub>EC</sub> channel activity, thereby blunting endothelium-dependent vasodilation and increasing blood pressure in diet-induced obesity. Studies in human arteries establish the clinical relevance of PN-induced impairment of TRPV4<sub>EC</sub> channels in obesity. Our results further suggest that increased levels of NOX1 and iNOS at vascular MEPs contribute to enhanced formation of PN in obesity, and demonstrate that prevention of PN formation restores AKAP150<sub>EC</sub>-PKC-TRPV4<sub>EC</sub> channel vasodilatory signaling (Figure 6H). Thus, our studies lay the foundation for PN-based therapeutic strategies for rescuing TRPV4<sub>EC</sub> channel function, and thereby improving endothelium-dependent vasodilator responses and lowering blood pressure in obese individuals.

The contribution of TRPV4<sub>EC</sub> channels to resting blood pressure has been difficult to define. Although numerous studies have identified TRPV4<sub>EC</sub> channels as a key Ca<sup>2+</sup> influx pathway for endothelium-dependent vasodilation, only global TRPV4<sup>-/-</sup> mice have been available for such studies(354, 448). These mice show no change in resting blood pressure(147, 448), an

observation in stark contrast to the higher blood pressure observed in the TRPV4<sup>EC-/-</sup> mice developed for the current study. The role of vascular smooth muscle AKAP150-TRPV4 signaling in regulating arterial diameter remains uncertain, with reports linking TRPV4 signaling in this compartment to both vasodilation and vasoconstriction(84, 246, 432). Thus, a definitive answer to the questions of how smooth muscle AKAP150-TRPV4 signaling influences blood pressure await the development of SMC-specific TRPV4<sup>-/-</sup> and AKAP150<sup>-/-</sup> mice.

An increase in iNOS activity at vascular MEPs contributed to PN formation in obesity, however, higher iNOS levels did not result in vasodilation, a finding that could be explained by the instantaneous reaction of NO with NOX1-generated O<sub>2</sub><sup>-</sup>, thus reducing NO bioavailability. In this regard, NOX1 deletion has previously been shown to lower O<sub>2</sub><sup>-</sup> levels in a mouse model of metabolic disease(383). Importantly, iNOS activity has mainly been associated with immune cells(28). Our z-stack images indicate that iNOS upregulation is restricted to MEPs in obesity, and immunostaining for pan-leucocyte marker CD45 revealed that immune cells were not present at the level of IEL in obese mice (Supplementary Figure 36), further supporting the concept that endothelial iNOS contributed to PN formation in obesity. Importantly, we confirmed the clinical relevance of iNOS and NOX1 overexpression in arteries isolated from obese patients (Supplemental Figure 43). iNOS has been implicated in drastic lowering of blood pressure in sepsis (232). It is conceivable that differential mechanisms downstream of iNOS lead to distinct functional effects in obesity and sepsis.

While our data support the role of NOX1 and iNOS in obesity-induced PN formation at MEPs, the mechanisms for sub-cellular compartmentalization of iNOS and NOX1 within the MEPs were not clear. We postulated that the anchoring protein AKAP150, highly enriched at the MEPs, could be a candidate for this role. However, MAs isolated from HFD AKAP150<sup>EC-/-</sup> mice showed similar iNOS and NOX1 immunostaining to control mice (Supplemental Figure 44) ruling out this hypothesis. Recently, in a mouse model of pulmonary hypertension iNOS and NOX1

were shown to co-localize with endothelial caveolin-1 (Cav-1) (63), a key structural protein that is well known to associate with endothelial nitric-oxide synthase (eNOS) at the endothelial plasma membrane (167). Moreover, Cav-1 directly interacts with NOX1 (9). Therefore, Cav-1 is a strong candidate responsible for anchoring iNOS and NOX1 at the MEPs in obesity. Indeed, obesity drives an increase in endothelial and smooth muscle plasma membrane expression of Cav-1 impairing eNOS signaling (124). Future studies implementing endothelial specific Cav-1 knockout mice (63) in obesity will provide a definitive answer whether Cav-1 could be involved in promoting the localization of NOX1 and iNOS at MEPs.

Although several endogenous oxidant molecules can cause cysteine oxidation(270, 298), AKAP150<sub>EC</sub>-TRPV4<sub>EC</sub> channel impairment in obesity can be attributed specifically to PN-induced cysteine oxidation of AKAP150<sub>EC</sub>. We show that PEG-catalase and taurine are unable to rescue TRPV4<sub>EC</sub> sparklet activity or vasodilation in obese mice (Supplementary Figure 37), suggesting that H<sub>2</sub>O<sub>2</sub> or hypochlorous acid do not play a major role in obesity-induced impairment of TRPV4<sub>EC</sub> channels. Interestingly, addition of high concentration of exogenous H<sub>2</sub>O<sub>2</sub>, but not hypochlorous acid, lowered TRPV4<sub>EC</sub> sparklet activity in MAs from normal mice (Supplementary Figure 38), although the mechanism for this effect is not known. Superoxide and NO radicals have also been commonly associated with cysteine modifications(40). Using the hypoxanthine/xanthine oxidase system, we observed that superoxide radicals inhibited vasodilation to CCh in normal mice, but had no effect on TRPV4<sub>EC</sub> sparklet activity (Supplementary Figure 39). Thus, superoxide radicals are not directly responsible for impairing TRPV4<sub>EC</sub> channel activity in obesity. Moreover, NO donor spermine NONOate (100 μM) also inhibited TRPV4<sub>EC</sub> sparklet activity(238) (Supplementary Figure 40), however, this effect was previously attributed to the activation of endothelial guanylyl cyclase-protein kinase G pathway(238).

Cysteine modifications have a short half-life(412), which may explain the restoration of AKAP150<sub>EC</sub>-TRPV4<sub>EC</sub> signaling within five minutes in obesity. It is plausible that lowering PN levels allows the endogenous glutaredoxins, thioredoxins, and/or peroxiredoxins to reduce oxidized cysteines on AKAP150<sub>EC</sub>(135). PN may also lead to S-nitrosation, however, treatment with ascorbic acid was unable to rescue TRPV4<sub>EC</sub> channel activity in obesity. While a lack of response to ascorbic acid does not definitively exclude a role for S-nitrosothiols, this result together with the detection of cysteine oxidation of AKAP150<sub>EC</sub> support thiol oxidation as the primary mechanism impairing AKAP150<sub>EC</sub>-TRPV4<sub>EC</sub> signaling in obesity. PN may also cause cysteine oxidation of PKC, which is known for its redox regulation(360). However, preventing Cys36 oxidation of AKAP150 alone was sufficient to abolish the effect of PN on TRPV4<sub>EC</sub> channel activity, suggesting that PN-induced thiol oxidation of PKC may not play a role in obesity-induced loss of endothelial function.

Exogenously applied PN has been shown to have varying effects on vascular diameter(33, 280). We observed that PN (5  $\mu$ M) caused a slight and transient vasodilation that was similar to that caused by 100 nM spermine NONOate (Supplementary Figures 41A, 41B). However, NONOate did not alter the vasodilation to CCh or TRPV4<sub>EC</sub> sparklet activity at this concentration (Supplementary Figures 41C, 41D). It should be noted that the effect of exogenously applied PN on vascular diameter is likely an integral of its effects in multiple cell types including smooth muscle cells, and could be different from the effect of locally formed PN in ECs during obesity.

While obesity is a significant risk factor for cardiovascular abnormalities in both sexes, obese female mice did not show a loss of endothelium-dependent vasodilation (Supplementary Figure 42). The risk of hypertension is known to be more in men than women at young ages(95), a trend that is reversed post-menopause. It is plausible that estrogen has a beneficial effect on endothelial function during obesity(158). Future studies on endothelial dysfunction in obese

female mice are needed to address a significant health concerns of obesity-induced hypertension in women.

A recent study supported a key role for perivascular adipose tissue (PVAT) in NO generation and vasodilation(114). Moreover, obesity was shown to be associated with uncoupling of eNOS from PVAT in obesity(428). Therefore, it is plausible that NO/superoxide radicals generated in PVAT contribute to PN formation and endothelial dysfunction. PVAT can also release inflammatory cytokines(28) that may elevate iNOS and NOX1 levels in ECs, thereby having a long-term effect on endothelial function. However, PVAT was cleaned off for all the *ex vivo* experiments in this study, thus, obesity-induced effects on TRPV4<sub>EC</sub> channel activity and vasodilation were independent of PVAT in the current study.

In conclusion, iNOS-generated NO can react with NOX1-generated superoxide to have deleterious effects on vasodilation under pathological conditions. A localized elevation in PN levels at vascular MEPs appears to be sufficient to decrease AKAP150<sub>EC</sub>-mediated enhancement of TRPV4<sub>EC</sub> channel activity without affecting the expression of AKAP150<sub>EC</sub> or TRPV4<sub>EC</sub> channels. Although reactive oxygen and nitrogen species have been implicated in hypertension, results presented here identify specific signaling mechanisms that could be therapeutically targeted for rescuing endothelium-dependent vasodilation and blood pressure in obesity.

**Figure 1. Endothelium-specific TRPV4 (TRPV4<sub>EC</sub><sup>-/-</sup>) and AKAP150 (AKAP150<sub>EC</sub><sup>-/-</sup>) knockout mice show elevated resting blood pressure.**

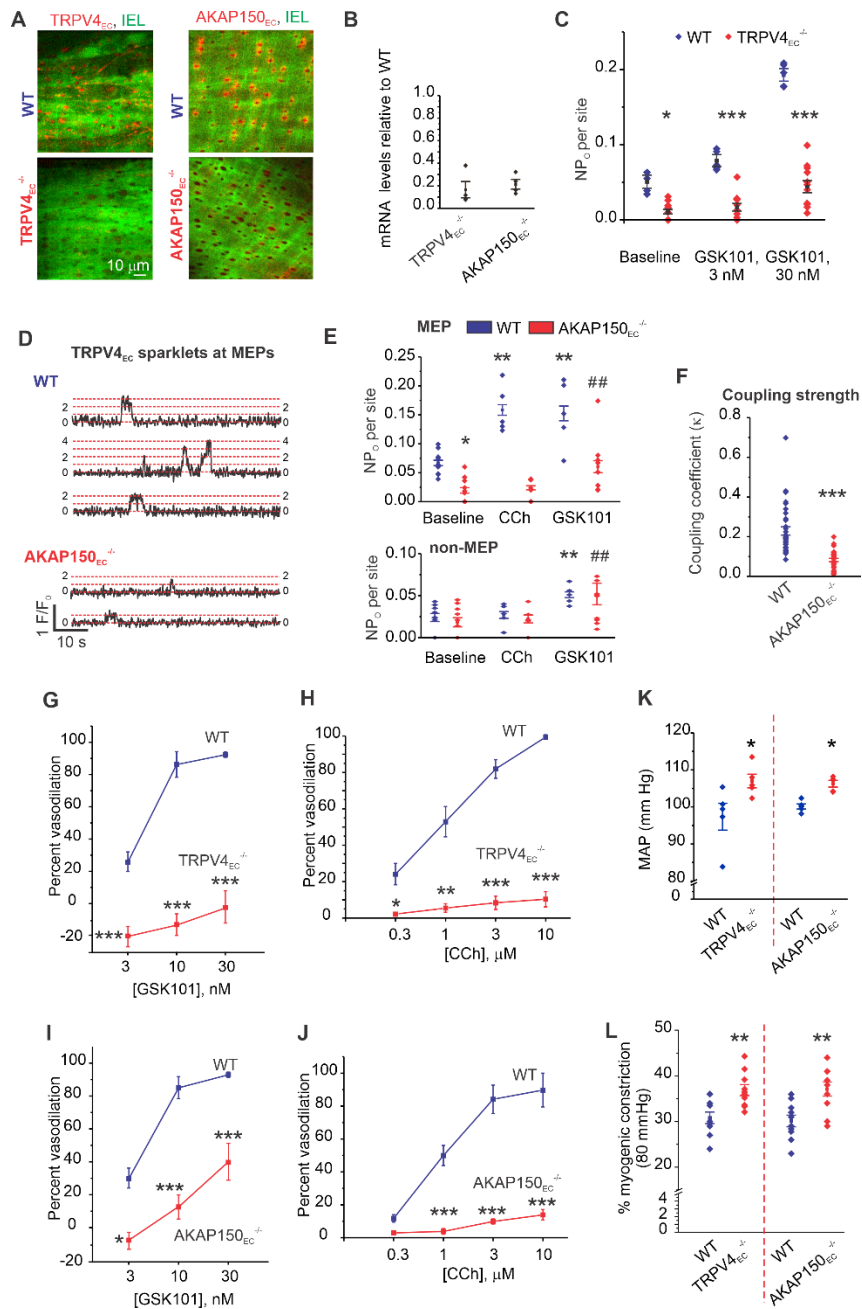


**Figure 1.** (A) Representative merged images from *en face* preparations of third-order MAs showing IEL autofluorescence (green) and TRPV4<sub>EC</sub> or AKAP150<sub>EC</sub> immunofluorescence (red) in WT (*top*), and TRPV4<sub>EC</sub><sup>-/-</sup> or AKAP150<sub>EC</sub><sup>-/-</sup> (*bottom*) mice. (B) Relative TRPV4 and AKAP150

mRNA levels in ECs from TRPV4<sub>EC</sub><sup>-/-</sup> and AKAP150<sub>EC</sub><sup>-/-</sup> mice, respectively, relative to those in WT mice ( $P < 0.01$  for TRPV4<sub>EC</sub><sup>-/-</sup> or AKAP150<sub>EC</sub><sup>-/-</sup> mice vs. respective WT mice;  $n=4$ ;  $***P < 0.001$ ; t-test). (C) TRPV4<sub>EC</sub> sparklet activity per site (NP<sub>O</sub>) in *en face* preparations of MAs from WT and TRPV4<sub>EC</sub><sup>-/-</sup> mice under baseline conditions (i.e., 20  $\mu$ M CPA) or in response to 3 and 10 nM GSK101 ( $n = 5-11$ ;  $*P < 0.05$  [baseline],  $<0.001$  [3 nM GSK101] and  $< 0.001$  [30 nM GSK101] for WT vs. TRPV4<sub>EC</sub><sup>-/-</sup>; one-way ANOVA). (D) Representative baseline F/F<sub>0</sub> traces from TRPV4<sub>EC</sub> sparklet sites at MEPs in Fluo-4-loaded MAs from WT (*top*) and AKAP150<sub>EC</sub><sup>-/-</sup> (*bottom*) mice. Dotted red lines indicate quantal levels(354) derived from an all-points histogram (Extended Data Fig. 7). (E) TRPV4<sub>EC</sub> sparklet activity at MEP (*top*) and non-MEP (*bottom*) sites in MAs from WT and AKAP150<sub>EC</sub><sup>-/-</sup> mice under baseline conditions, and following treatment with 10  $\mu$ M CCh or 10 nM GSK101 ( $n = 5$ ;  $P < 0.05$  for WT baseline vs. TRPV4<sub>EC</sub><sup>-/-</sup> baseline,  $** < 0.01$  for WT CCh vs. WT baseline,  $< 0.01$  for WT GSK101 vs. WT baseline;  $###P < 0.01$  for AKAP150<sub>EC</sub><sup>-/-</sup> GSK101 vs. AKAP150<sub>EC</sub><sup>-/-</sup> baseline; one-way ANOVA). (F) Coupling coefficient ( $k$ ) values for TRPV4<sub>EC</sub> sparklet sites at MEPs indicating the coupling strength among TRPV4<sub>EC</sub> channels at a given site in MAs from AKAP150<sub>EC</sub><sup>-/-</sup> and WT mice ( $P < 0.001$ , t-test,  $n = 25-31$  sites). (G) Averaged data for GSK101-induced dilation of MAs from WT and TRPV4<sub>EC</sub><sup>-/-</sup> mice ( $n = 5$ ;  $P < 0.01$  [3 nM GSK101],  $< 0.001$  [10 nM GSK101] and  $< 0.001$  [30 nM GSK101] for WT vs. TRPV4<sub>EC</sub><sup>-/-</sup> mice; two-way ANOVA). (H) Percent dilation of MAs from WT and TRPV4<sub>EC</sub><sup>-/-</sup> mice in response to CCh (0.3–10  $\mu$ M) ( $n = 5$ ;  $P < 0.05$  [0.3  $\mu$ M CCh] and  $< 0.001$  [1, 3, and 10  $\mu$ M CCh] for WT vs. TRPV4<sub>EC</sub><sup>-/-</sup> mice; two-way ANOVA). (I) Percent dilation of MAs from WT and AKAP150<sub>EC</sub><sup>-/-</sup> mice in response to GSK101 (3–30 nM) ( $n = 5-6$ ;  $P < 0.05$  [3 nM GSK101],  $< 0.01$  [10 nM GSK101] and  $< 0.001$  [30 nM GSK101] for WT vs. AKAP150<sub>EC</sub><sup>-/-</sup> mice; two-way ANOVA). (J) Percent dilation of MAs from WT and AKAP150<sub>EC</sub><sup>-/-</sup> mice in response to CCh (0.3–10  $\mu$ M) ( $n = 5$ ;  $P < 0.05$  [0.3  $\mu$ M CCh] and  $< 0.001$  [1, 3, and 10  $\mu$ M CCh] for WT vs. AKAP150<sub>EC</sub><sup>-/-</sup> mice; two-way ANOVA). (K) Scatter plot of resting MAP (mm Hg) averaged over 3 days in TRPV4<sub>EC</sub><sup>-/-</sup>

and AKAP150<sup>EC-/-</sup> mice and the respective WT mice ( $P < 0.01$  for TRPV4<sup>EC-/-</sup> vs. WT mice,  $P < 0.05$  for AKAP150<sup>EC-/-</sup> vs. WT mice; t-test,  $n=5$ ). (L) Percent myogenic constriction at 80 mm Hg in MAs from TRPV4<sup>EC-/-</sup> and AKAP150<sup>EC-/-</sup>, and respective WT mice ( $P < 0.01$  vs. WT, t-test,  $n=10$ ).

## Figure 2. Diet-induced obesity impairs AKAP150<sup>EC</sup>-PKC-TRPV4<sup>EC</sup> signaling and vasodilation.

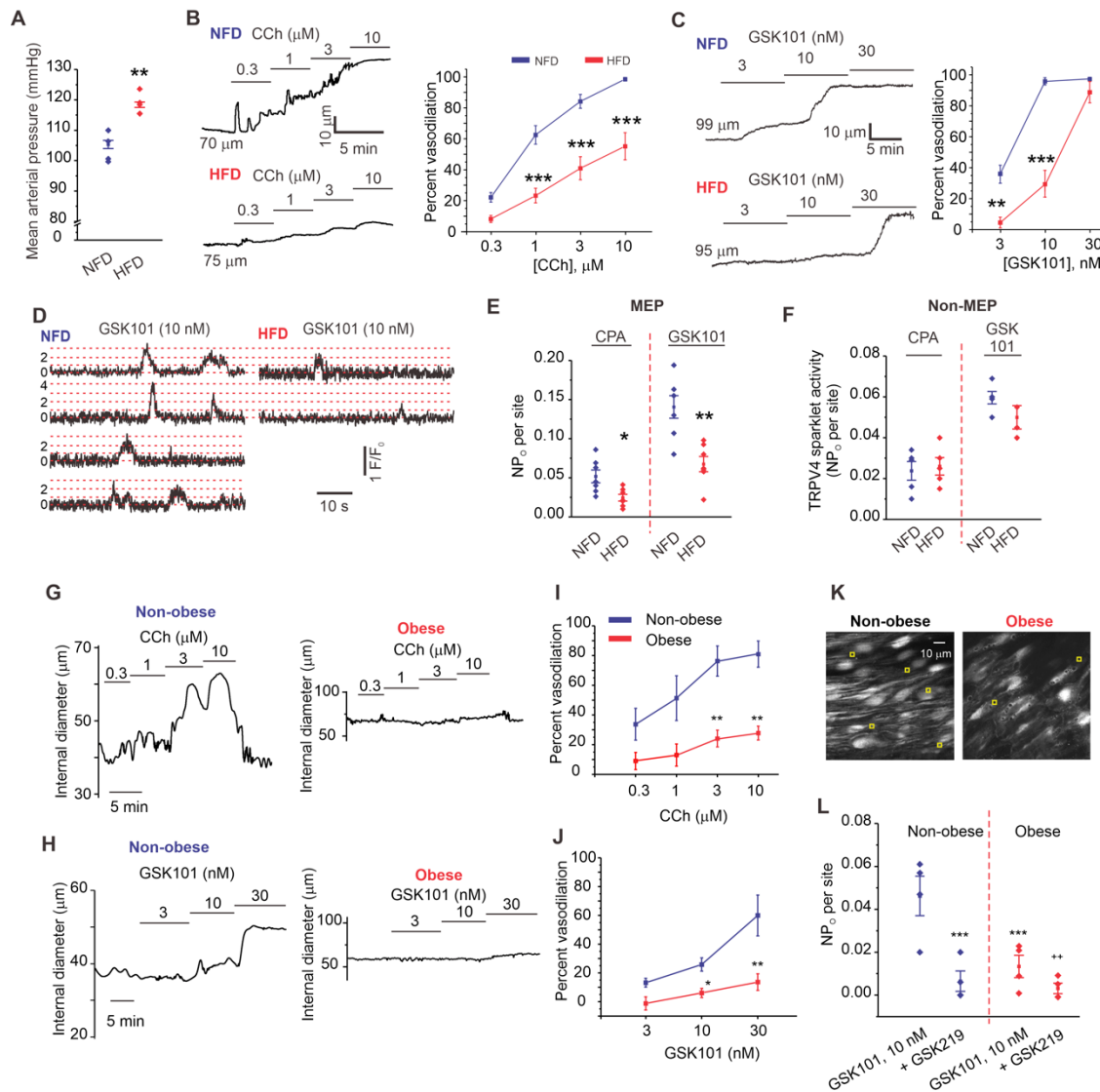


**Figure 2.** (A) Resting MAP (mm Hg) averaged over 3 days in HFD and NFD mice ( $n = 5$ ; \*\* $P < 0.01$  for HFD vs. NFD; t-test). (B) Representative diameter traces (*left*) and averaged

diameter data (*right*) for CCh (0.3–10  $\mu$ M)-induced dilation of MAs from NFD and HFD mice (n = 8–11; \*\*\* $P$  < 0.001 for 1  $\mu$ M, 3  $\mu$ M, and 10  $\mu$ M CCh for NFD vs. HFD mice; two-way ANOVA). (C) Representative diameter traces (*left*) and averaged diameter data (*right*) for GSK101 (3–30 nM)-induced vasodilation in NFD and HFD mice (n = 5–9;  $P$  < 0.01 [3 nM GSK101] and < 0.001 [10 nM GSK101]; two-way ANOVA). (D) Representative  $F/F_0$  traces from TRPV4<sub>EC</sub> sparklet sites (20  $\mu$ M CPA + GSK101, 10 nM) at MEPs in Fluo-4-loaded *en face* preparations of MAs from NFD (*left*) and HFD (*right*) mice. Dotted red lines indicate quantal levels. (E) Averaged TRPV4<sub>EC</sub> sparklet activity (NP<sub>O</sub>) at MEPs in MAs from NFD and HFD mice under baseline conditions (20  $\mu$ M CPA) or in response to GSK101 (10 nM) (n = 7; sparklet activity: \* $P$  < 0.05 [CPA] and < 0.01 [GSK101] for NFD vs. HFD). (F) Averaged TRPV4<sub>EC</sub> sparklet activity in MAs from NFD and HFD mice under baseline conditions (20  $\mu$ M CPA) and in response to GSK101 (10 nM) (n = 7). (G) Representative diameter traces for CCh (0.3–10  $\mu$ M)-induced dilation of splenius muscle arteries from non-obese and obese individuals. (H) Representative diameter traces for GSK101 (3–30 nM)-induced dilation of splenius muscle arteries from obese and non-obese individuals. (I) Averaged diameter data for CCh -induced vasodilation in human splenius and temporalis muscle arteries from obese and non-obese individuals (n = 6;  $P$  < 0.01 vs. non-obese; two-way ANOVA). (J) Averaged diameter data for GSK101-induced vasodilation in human splenius and temporalis muscle arteries from obese and non-obese individuals (n = 6;  $P$  < 0.01, < 0.01, vs. non-obese; two-way ANOVA). (K) Greyscale image of a field of view with ~20 ECs from an *en face* preparation of Fluo-4 loaded splenius muscle artery (SMA) from a non-obese individual; yellow squares indicate sparklet sites in with CPA + GSK101 (10 nM). (L) TRPV4<sub>EC</sub> sparklet activity (NP<sub>O</sub>) at MEP in SMAs from non-obese and obese individuals in response to GSK101 (10 nM) and in the presence of GSK219 (100 nM) (n = 4;  $P$  < 0.001 [GSK101] for non-obese vs. obese and  $P$  < 0.01 [GSK101] vs. [GSK219]; one-way ANOVA).

**Figure 3. Elevation of endothelial peroxynitrite (PN) impairs TRPV4<sub>EC</sub> channel activity in obesity.**

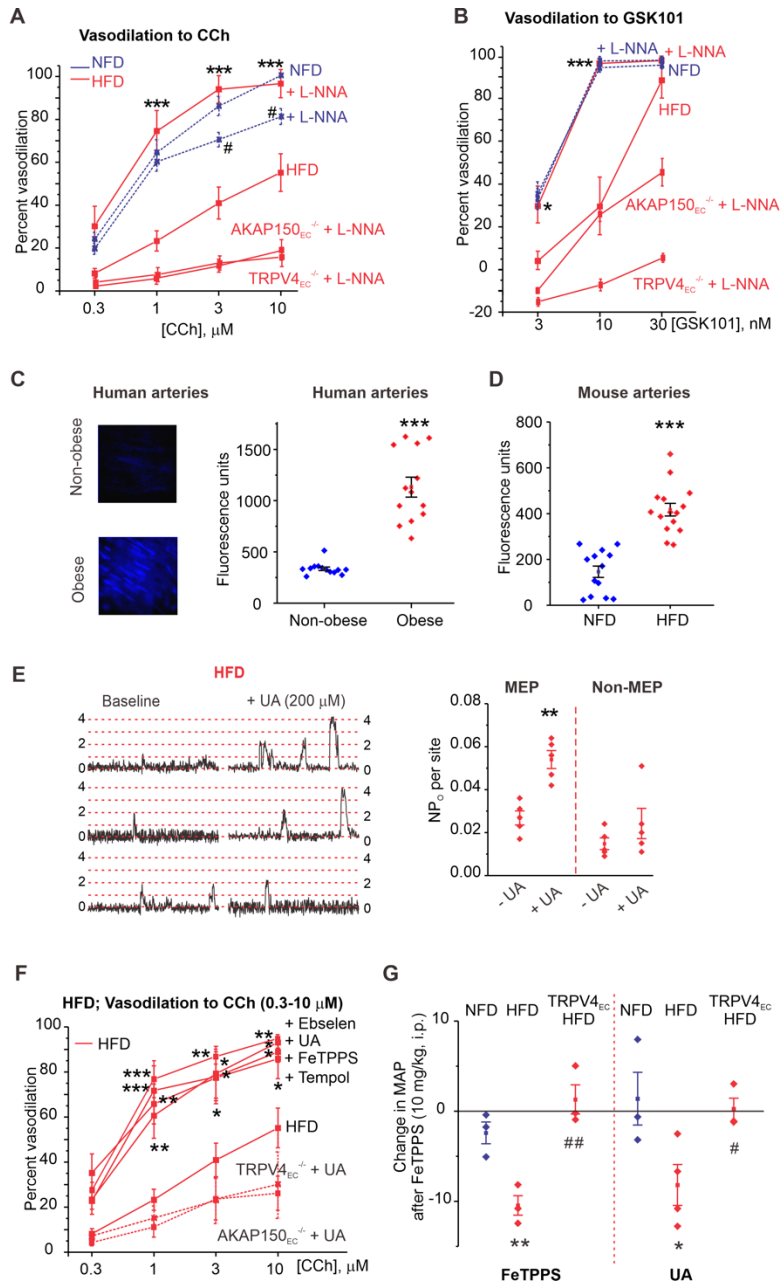


**Figure 3.** (A) Percent dilation of MAs from NFD, HFD, HFD AKAP150<sub>EC</sub><sup>-/-</sup>, and HFD TRPV4<sub>EC</sub><sup>-/-</sup> mice in response to CCh (0.3–10 μM) in the presence or absence of L-NNA (100 μM) (n = 5–9; #*P*<0.05 [3 and 10 μM CCh] for NFD vs. NFD + L-NNA; \*\*\**P* < 0.001 [1, 3, and 10 μM CCh] for

HFD vs. HFD + L-NNA; two-way ANOVA). (B) Percent dilation of MAs from NFD, HFD, HFD AKAP150<sup>EC-/-</sup>, and HFD TRPV4<sup>EC-/-</sup> mice in response to GSK101 (3–30 nM) in the presence or absence of L-NNA (100  $\mu$ M) (n = 5; \* $P$  < 0.05 at 3 nM GSK101 and < 0.001 at 10 nM GSK101 for HFD vs. HFD + L-NNA; two-way ANOVA). (C) Representative images for CBA fluorescence in ECs of splenius muscle arteries from non-obese (*top-left*) and obese (*bottom-left*) individuals; scatter plot of CBA fluorescence intensity (*right*) in ECs from non-obese and obese patients ( $P$  < 0.001; n = 12 fields from 3 arteries; t-test). (D) CBA fluorescence intensity in ECs of MAs from NFD and HFD mice ( $P$  < 0.001; n = 13–15 fields from 3 arteries; t-test). (E) Representative F/F<sub>0</sub> traces (*left*) and scatter plot of TRPV4<sup>EC</sup> sparklet activity (*right*) from MEP and non-MEP sites in fluo-4-loaded MAs from HFD mice in the absence or presence of UA (200  $\mu$ M) (n = 5;  $P$  < 0.01 for MEP sites with vs. without UA; one-way ANOVA). Dotted red lines indicate quantal levels. (F) Effects of UA (200  $\mu$ M), FeTPPS (1  $\mu$ M), tempol (200  $\mu$ M), and Ebselen (1  $\mu$ M) on CCh (0.3–10  $\mu$ M)-induced dilation of MAs from HFD mice (WT), TRPV4<sup>EC-/-</sup> HFD, and AKAP150<sup>EC-/-</sup> HFD mice (n = 5–8;  $P$  < 0.05; < 0.01; < 0.001 vs. HFD only; two-way ANOVA). (G) Changes in resting MAP (mm Hg) in NFD and HFD mice following i.p. injection of FeTPPS (10 mg/kg; *left*) (n = 3–4;  $P$  < 0.01 for FeTPPS-treated NFD vs. FeTPPS-treated HFD,  $^{##}P$  < 0.01 for FeTPPS-treated HFD vs. FeTPPS-treated TRPV4<sup>EC-/-</sup> HFD; one-way ANOVA) or UA (200 mg/kg; *right*) (n = 3;  $P$  < 0.05 for UA-treated NFD vs. UA-treated HFD,  $^{\#}P$  < 0.05 for UA-treated HFD vs. UA-treated TRPV4<sup>EC-/-</sup> HFD; one-way ANOVA).

**Figure 4. Localized NOX1 and iNOS upregulation underlies PN-induced impairment of TRPV4<sub>EC</sub> channel activity in obesity.**

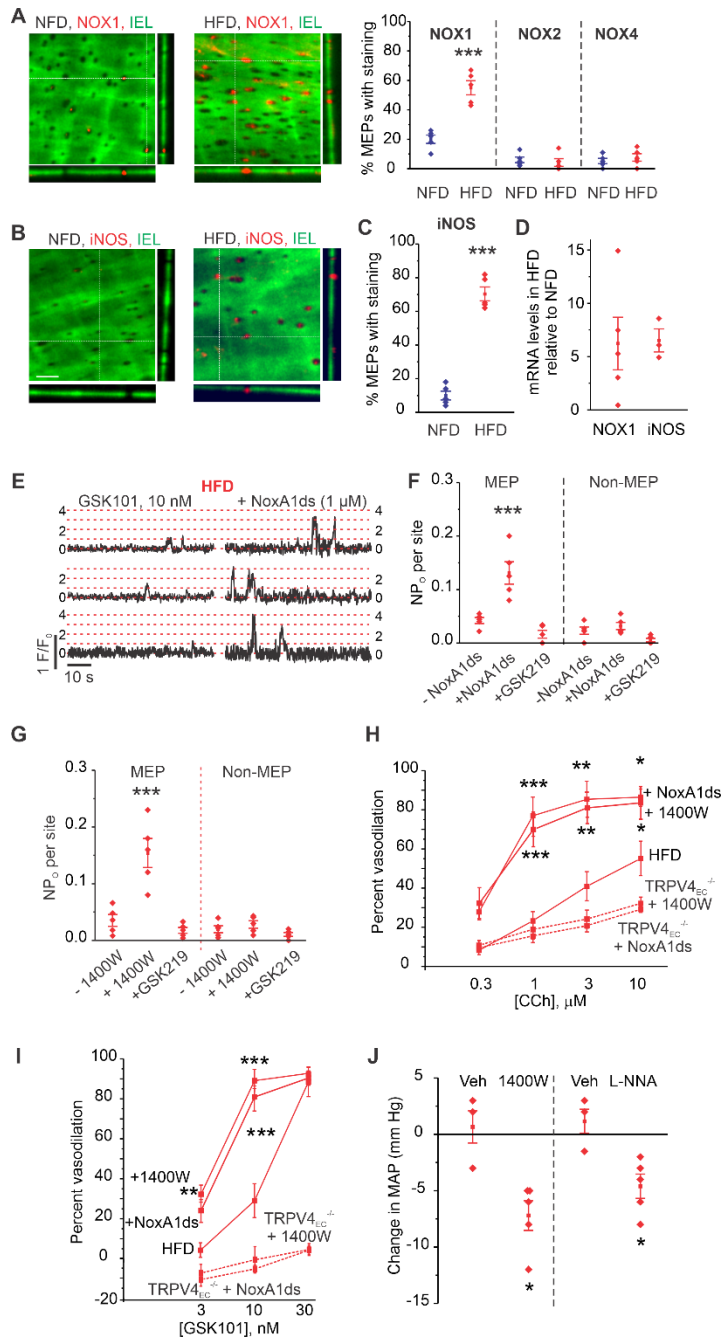


**Figure 4.** (A) *Left*, representative merged z-stack images from *en face* preparations of third-order MAs showing IEL autofluorescence (green) and NOX1 immunofluorescence (red) in NFD (*left panel*) and HFD mice (*right panel*). *Right*, quantification of NOX1, NOX2, and NOX4 localization

at MEPs in NFD and HFD mice ( $n = 5$ ;  $***P < 0.001$  for NOX1 in HFD vs. NFD; one-way ANOVA). (B) Representative merged z-stack images of iNOS staining. (C) Quantification of iNOS localization at MEPs in NFD and HFD mice ( $n = 5$ ;  $P < 0.001$  for iNOS in HFD vs. NFD, t-test). (D) Relative NOX1 and iNOS mRNA levels in homogenates of whole MAs from HFD mice expressed relative to those from NFD mice ( $**P < 0.01$  vs. NFD, one-way ANOVA,  $n = 4-5$ ). (E) Representative  $F/F_0$  traces showing the effect of the NOX1 inhibitor peptide NoxA1ds ( $1 \mu\text{M}$ ) on TRPV4<sub>EC</sub> sparklet activity (GSK101,  $10 \text{ nM}$ ) in MAs from HFD mice. Dotted red lines indicate quantal levels. (F) Effects of NoxA1ds or negative control peptide (-NoxA1ds) on TRPV4<sub>EC</sub> sparklet activity at MEP and non-MEP sites in fluo-4-loaded MAs from HFD mice ( $n = 5$ ;  $P < 0.001$  for sparklet activity at MEP sites in the presence vs. absence of NoxA1ds; one-way ANOVA). (G) TRPV4<sub>EC</sub> sparklet activity (GSK101,  $10 \text{ nM}$ ) at MEP sites in MAs from NFD and HFD mice in the absence or presence of the iNOS inhibitor 1400W ( $1 \mu\text{M}$ ,  $n = 5$ ;  $P < 0.001$  for sparklet activity at MEP sites in the presence vs. absence of 1400W; one-way ANOVA). (H) Effects of NoxA1ds or 1400W on CCh ( $0.3-10 \mu\text{M}$ )-induced dilation of MAs from HFD, TRPV4<sub>EC</sub><sup>-/-</sup> HFD, or AKAP150<sub>EC</sub><sup>-/-</sup> HFD mice ( $n = 5-8$ ;  $*P < 0.05$ ;  $< 0.01$ ;  $< 0.001$  vs. HFD only; two-way ANOVA). (I) Effects of NoxA1ds or 1400W on GSK101 ( $3-10 \text{ nM}$ )-induced dilation of MAs from HFD, TRPV4<sub>EC</sub><sup>-/-</sup> HFD, or AKAP150<sub>EC</sub><sup>-/-</sup> HFD mice ( $n = 5-9$ ;  $P < 0.05$ ;  $< 0.01$ ;  $< 0.001$  vs. HFD only; two-way ANOVA). (J) Change in mean arterial pressure (MAP) following i.p. injection of 1400W ( $10 \text{ mg/kg}$ ) or L-NNA ( $100 \text{ mg/kg}$ ) compared to HFD mice treated with vehicle (Veh, saline;  $n = 3-5$ ;  $P < 0.05$  for 1400W-treated HFD vs. Vehicle-treated [Veh, saline] HFD,  $P < 0.05$  for L-NNA-treated HFD vs. Vehicle-treated HFD; t-test).

**Figure 5. Peroxynitrite (PN) causes cysteine oxidation of AKAP150<sub>EC</sub> to inhibit AKAP150<sub>EC</sub>-PKC-TRPV4<sub>EC</sub> signaling.**

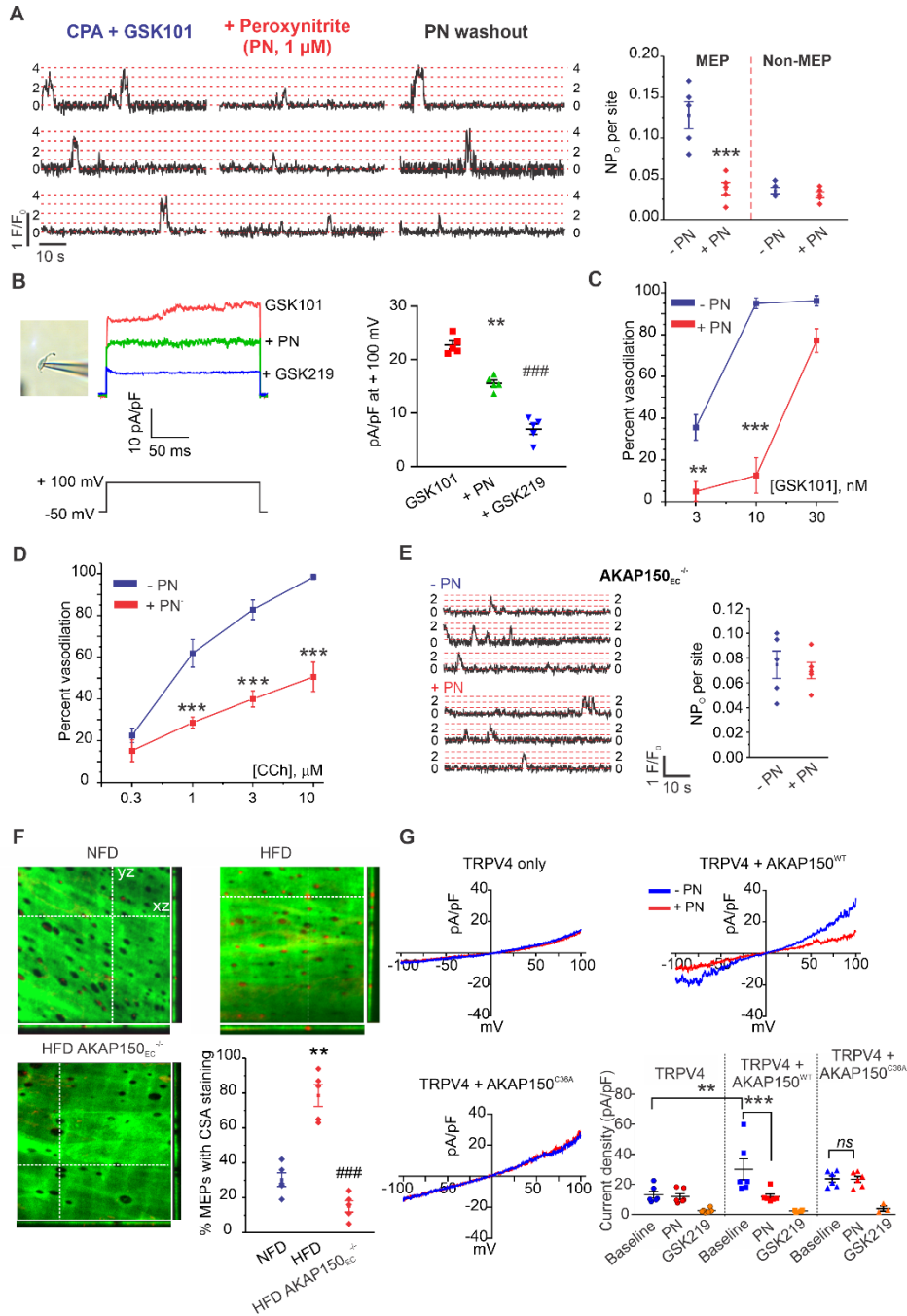


**Figure 5.** (A) Representative traces (*left*) and TRPV4<sub>EC</sub> sparklet activity (NP<sub>O</sub>) per site (*right*) indicating the effect of PN (1  $\mu$ M) on TRPV4<sub>EC</sub> sparklets at MEP and non-MEP sites in Fluo-4-loaded MAs from WT mice in the presence of CPA and GSK101 (10 nM). Dotted red lines indicate quantal levels. Data are presented as means  $\pm$  SEM ( $n = 5$ ;  $***P < 0.001$  for NP<sub>O</sub> at MEP sites in the presence vs. absence of PN; one-way ANOVA). (B) *Left*, an image of EC in perforated patch configuration, *middle*, representative GSK101 (10 nM)-induced outward TRPV4<sub>EC</sub> currents in freshly isolated ECs from WT mice and the effect of PN (5  $\mu$ M) and GSK219 (100 nM), a single pulse from a holding potential of -50 mV to +100 mV was applied in the presence of ruthenium red (1  $\mu$ M) to inhibit Ca<sup>2+</sup>-induced IK/SK currents, *right*, scatter plot showing TRPV4<sub>EC</sub> currents in the presence of GSK101 alone, GSK101 + PN, and GSK101 + PN + GSK219 ( $n=5$ ,  $**P < 0.01$  for GSK101 vs. PN;  $####P < 0.001$  for GSK101 vs. GSK219, one-way ANOVA). (C) Percent dilation in response to GSK101 (3–30 nM) in MAs from WT mice in the absence or presence of PN ( $n = 5–8$ ;  $P < 0.01$  [3 nM GSK101] and  $< 0.001$  [10 nM GSK101] for percent dilation in the presence vs. absence of PN; two-way ANOVA). (D) Percent dilation of MAs from WT mice in response to CCh (0.3–10  $\mu$ M) in the absence or presence of PN ( $n = 5–8$ ;  $P < 0.001$  [1  $\mu$ M, 3  $\mu$ M, and 10  $\mu$ M CCh] in the presence vs. absence of PN; two-way ANOVA). (E) Representative F/F<sub>0</sub> traces (*left*) and scatter plot of TRPV4<sub>EC</sub> sparklet activity (*right*, CPA + GSK101, 10 nM) in Fluo-4-loaded MAs from AKAP150<sub>EC</sub><sup>-/-</sup> mice in the absence or presence of PN (1  $\mu$ M,  $n = 5$ ). (F) Representative merged images from *en face* preparations of third-order MAs showing IEL autofluorescence (green) and cysteine sulfenic acid (CSA) immunofluorescence (red) in NFD (*top-left*), HFD (*top-right*), and AKAP150<sub>EC</sub><sup>-/-</sup> HFD (*bottom-left*) mice; quantification of CSA localization at MEPs (*bottom-right*) in NFD, HFD, and AKAP150<sub>EC</sub><sup>-/-</sup> HFD mice ( $n=3$ ;  $P < 0.01$  for HFD vs. NFD;  $P < 0.001$  for AKAP150<sub>EC</sub><sup>-/-</sup> HFD vs. HFD; one-way ANOVA). (G) Representative current traces of GSK219-sensitive TRPV4 currents in HEK293 cells transfected with TRPV4 only (*top-left*), TRPV4+AKAP150<sup>WT</sup> (*top-right*), and

TRPV4+AKAP150<sup>C36A</sup> (bottom-left) recorded in the whole-cell patch-clamp configuration. Current density plot (bottom-right) of GSK219-sensitive TRPV4 currents ( $n = 6$ ;  $P < 0.01$  for TRPV4 baseline vs. TRPV4+AKAP150<sup>WT</sup> baseline,  $P < 0.001$  for TRPV4+AKAP150<sup>WT</sup> baseline vs. TRPV4+AKAP150<sup>WT</sup> with PN; *ns* for TRPV4+AKAP150<sup>C36A</sup> baseline vs. TRPV4+AKAP150<sup>C36A</sup> with PN; one-way ANOVA).

**Figure 6. Peroxynitrite (PN) impairs AKAP150<sub>EC</sub> anchoring of PKC in obesity.**

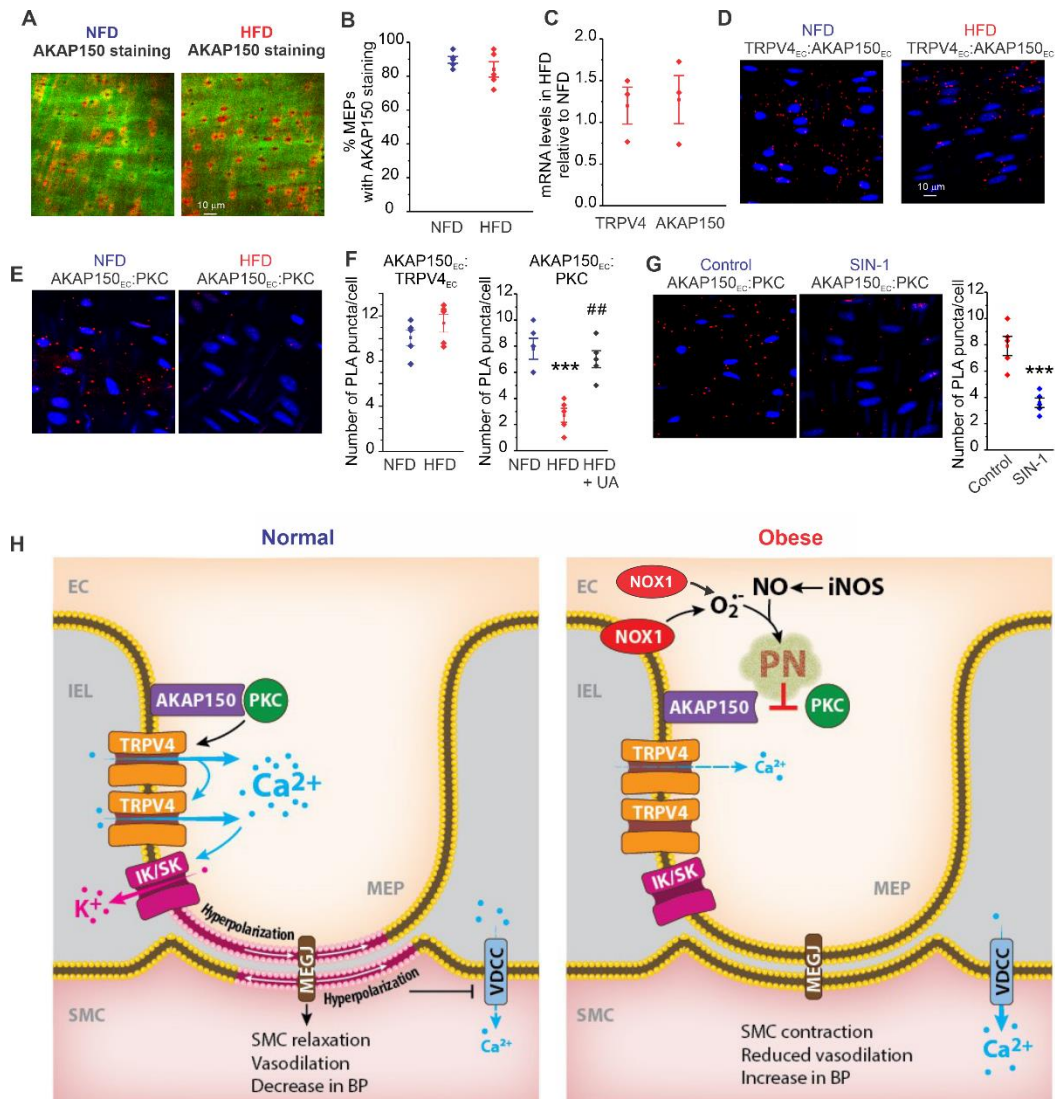
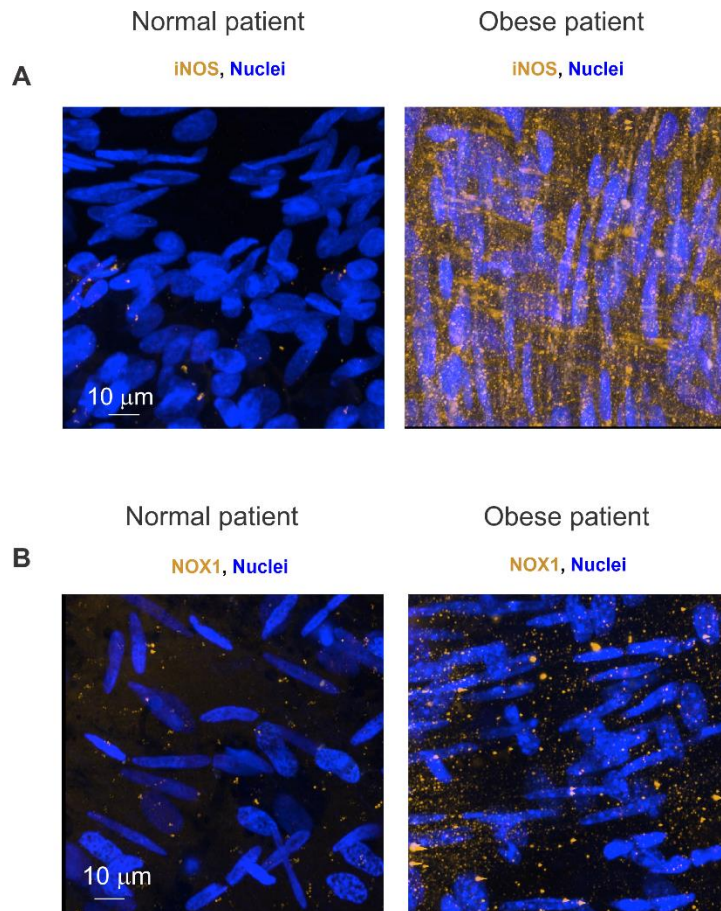


**Figure 6.** (A) Representative merged images from *en face* preparations of third-order MAs showing IEL autofluorescence (green) and AKAP150<sub>EC</sub> immunofluorescence (red) in NFD (*left*) and HFD mice (*right*). (B) Quantification of AKAP150<sub>EC</sub> staining at MEPs in NFD and HFD mice (n = 5). (C) Quantification of TRPV4 and AKAP150 mRNA levels in homogenates of third-order MAs from HFD mice, expressed relative to those in NFD mice (n = 3). (D) Representative PLA merged images of EC nuclei (*blue*) and AKAP150<sub>EC</sub>:TRPV4<sub>EC</sub> co-localization (red puncta) in *en face* preparations of third-order MAs from NFD (*left*) and HFD (*right*) mice. (E) Representative PLA merged images of EC nuclei (*blue*) and AKAP150<sub>EC</sub>:PKC co-localization (red puncta) in third-order *en face* preparations of MAs from NFD (*left*) and HFD (*right*) mice. (F) Quantification of AKAP150<sub>EC</sub>:TRPV4<sub>EC</sub> co-localization (*left*) and AKAP150<sub>EC</sub>:PKC co-localization (*right*) in NFD and HFD mice. AKAP150<sub>EC</sub>:PKC co-localization was rescued by uric acid (UA, 200  $\mu$ M) in HFD mice (n = 5; \*\*\* $P$  < 0.001 for HFD only vs. NFD only, # $P$  < 0.01 for UA-treated HFD vs. HFD only; one-way ANOVA). (G) *Left*, representative PLA merged images of EC nuclei (*blue*) and AKAP150<sub>EC</sub>:PKC co-localization (red) in MAs from WT mice in the absence or presence of 50  $\mu$ M SIN-1. *Right*, quantification of AKAP150<sub>EC</sub>:PKC co-localization (*right*) in WT mice in the absence or presence of SIN-1 (n = 5;  $P$  < 0.001 vs. Control; t-test). (H) Schematic depicting the PN-dependent signaling mechanism that impairs endothelial function and elevates blood pressure in obesity.

**For Supplemental Figures 1 to 42. go to:**

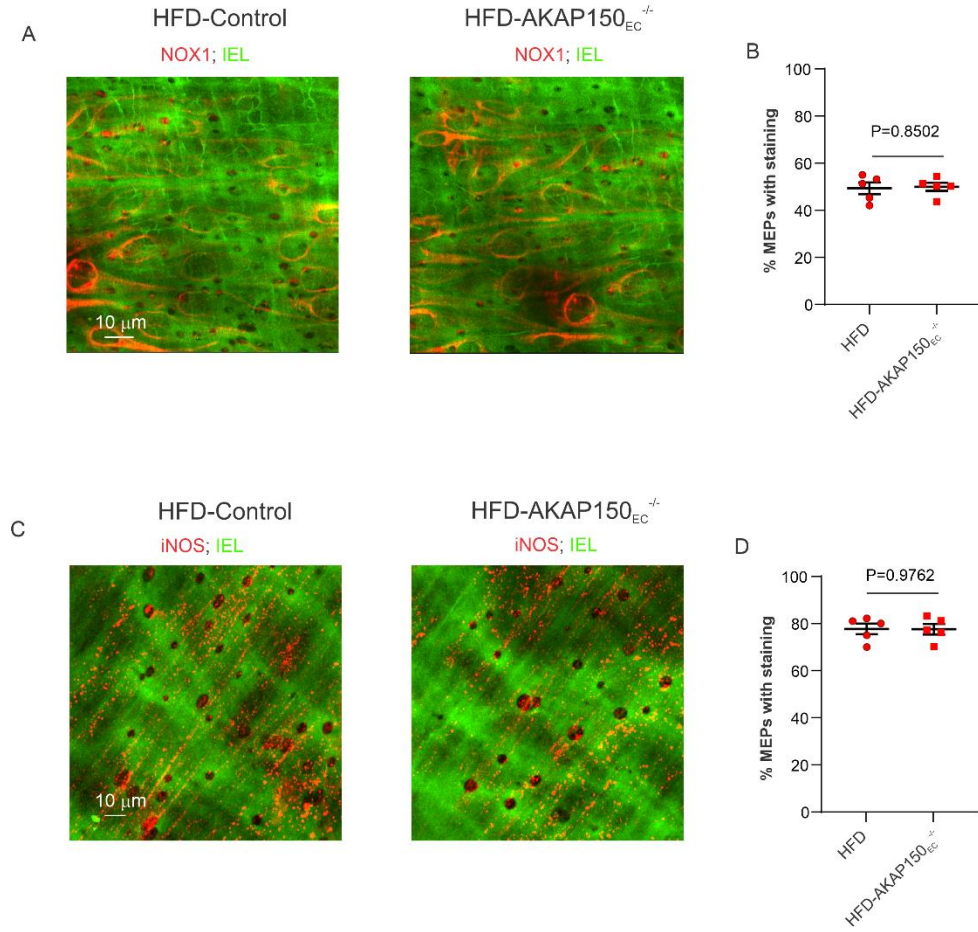
<https://www.ahajournals.org/doi/suppl/10.1161/CIRCULATIONAHA.119.043385>

**Supplemental Figure 43. iNOS and NOX1 are overexpressed in splenius and temporalis muscle arteries (STMA) isolated from obese patients**



**Supplemental Figure 43.** (A) z-stack merged images showing iNOS immunostaining (yellow) in STMA isolated from normal (*left*) and obese (*right*) patients. Nuclei (blue). (B) z-stack merged images showing NOX1 immunostaining (yellow) in STMA isolated from normal (*left*) and obese (*right*) patients. Nuclei (blue).

**Supplemental Figure 44. AKAP150<sub>EC</sub> does not anchor iNOS and NOX1 at the MEPs in obesity**



**Supplemental Figure 44.** (A) z-stack merged images showing NOX1 immunostaining (red) in MAs isolated from HFD-Control (*left*) and HFD-AKAP150<sub>EC</sub><sup>-/-</sup> (*right*) patients. IEL (green). (B) Percentage of MEPs stained with NOX1 (C) z-stack merged images showing iNOS immunostaining (red) in MAs isolated from HFD-Control (*left*) and HFD-AKAP150<sub>EC</sub><sup>-/-</sup> (*right*) patients. IEL (green). (D) Percentage of MEPs stained with iNOS.

**Chapter 5: Smooth muscle-derived TNF $\alpha$  creates pathological inflammatory micro-domains which alter endothelial function in obesity**

## 5.1 Introduction

Obesity a significant cause of morbidity and mortality in the industrialized world. Recent statistical forecast alarms us that the number of obese adults will continue to rise by nearly one in two adults by 2030 in the U.S. (413). The estimated annual health care costs of obesity-derived diseases correspond to almost 20% of the U.S. annual medical expenditure. There is a strong correlation between the pathogenesis of obesity and the progression of cardiovascular diseases (305). Ample evidence suggests that endothelial dysfunction plays a pivotal role in microvascular dysfunction and the underlying cause for obesity-derived hypertension (194, 288). Chronic systemic inflammation is a crucial feature of obesity and underscores the development of endothelial dysfunction (194). However, the link between specific inflammatory cytokines and loss of endothelial function is still unclear. Therefore, identifying inflammatory mediators responsible for endothelial dysfunction in obesity could provide a target against vascular inflammation and high blood pressure.

In resistance arteries, local endothelial calcium ( $\text{Ca}^{2+}$ ) signals occurring through TRPV4 channel ( $\text{Ca}^{2+}$ sparklets) in specialized microdomains, named myoendothelial projections (MEP) that are essential regulators of endothelial function (147, 287, 354, 355). Under obesity conditions, overexpression of pro-inflammatory enzymes iNOS and NOX1 at the MEPs causes oxidative stress that impairs  $\text{Ca}^{2+}$  sparklets leading to high blood pressure (288). However, the nature and source of the inflammatory stimuli underlying pathological expression of endothelial iNOS and NOX1 have yet to be determined.

Tumor necrosis factor-alpha ( $\text{TNF}\alpha$ ) is an inflammatory cytokine that plays a pivotal role in sustaining inflammation in several chronic inflammatory conditions, including obesity (401).  $\text{TNF}\alpha$  signals act via two receptors,  $\text{TNF}\alpha\text{RI}$  and  $\text{TNF}\alpha\text{RII}$ .  $\text{TNF}\alpha$  dependent inflammatory events are primarily translated by  $\text{TNF}\alpha\text{RI}$  signaling, whereas  $\text{TNF}\alpha$  signaling via  $\text{TNF}\alpha\text{RII}$

seems to have protective effects (406, 439) . A large body of evidence demonstrates that  $\text{TNF}\alpha$  induces endothelial dysfunction through oxidative stress (17, 111, 233, 299). Adipose tissue (148, 173, 258) and perivascular fat tissue (PVAT) (127, 402, 429) are known to be pivotal sources of  $\text{TNF}\alpha$  during chronic overnutrition. However, recent findings have added the vascular wall as another critical source of  $\text{TNF}\alpha$  in metabolic disorders (299, 326, 403) . Nonetheless, the question of whether the vasculature only remains a mere target of  $\text{TNF}\alpha$ -induced inflammation or it also becomes an essential source of  $\text{TNF}\alpha$  remains unanswered.

Pathological levels of other inflammatory cytokines such as IL-6 and IL-1 $\beta$  have been linked to obesity (418). However,  $\text{TNF}\alpha$  has been upstream and drives IL-6 and IL-1 $\beta$  expression (293, 395). Indeed, cytokines work in networks, and  $\text{TNF}\alpha$ , based on its high position in the network hierarchy, might play a unique role in mediating obesity-derived inflammation. Therefore, the successful demonstration that in obesity  $\text{TNF}\alpha$ - $\text{TNF}\alpha\text{RI}$  mediated inflammation alters the molecular events underlying healthy endothelial function would provide a novel insight for developing therapies targeting  $\text{TNF}\alpha$ - $\text{TNF}\alpha\text{RI}$  signaling pathway. Indeed, this could result in novel therapeutic avenues directed against obesity-related vascular dysfunction and hypertension.

In this report, we hypothesize that in obesity vascular derived- $\text{TNF}\alpha$  signaling via  $\text{TNF}\alpha\text{RI}$  plays a significant role in generating and sustaining local inflammation of microvascular endothelium. We show that  $\text{TNF}\alpha$  is highly expressed in smooth muscle cells (SMC) and at the MEPs of small mesenteric arteries (MA) isolated from obese mice. The discovery that  $\text{TNF}\alpha\text{RI}$  is highly enriched on the endothelial plasma membrane side at the MEPs strengthened our hypothesis of  $\text{TNF}\alpha$ - $\text{TNF}\alpha\text{RI}$  generated pathological microdomains as a pivotal cause of obesity-induced endothelial dysfunction. Moreover, IL-6 and IL-1 $\beta$  levels in the vascular wall were similar between normal

and obese mice underlying the unique role played by  $\text{TNF}\alpha$  in mediating inflammation. Notably, the selective blockade of  $\text{TNF}\alpha$ - $\text{TNF}\alpha\text{RI}$  signaling reduced endothelial overexpression of iNOS and NOX1 and restored TRPV4 channel activity. This led to normalization of vascular reactivity and blood pressure in obesity.

Our current findings highlight the unique role played by  $\text{TNF}\alpha$ - $\text{TNF}\alpha\text{RI}$  signaling in driving the disruption of the finely regulated  $\text{Ca}^{2+}$  sparklets occurring at the MEPs, critical sites of communication between SMC and endothelial cells (EC). Loss of physiological EC to SMC communication translates into abnormal vascular reactivity. Thus, we can conclude that the generation and implementation of specific anti- $\text{TNF}\alpha\text{RI}$  therapies might represent an efficacious way to rescue microvascular dysfunction in obesity.

## 5.2 Results

### **Smooth muscle cells of systemic resistance arteries are an active source of $\text{TNF}\alpha$ in obesity**

Low-grade inflammation associated with obesity and diabetes is responsible for endothelial dysfunction and microvascular complications (18). The importance of perivascular fat tissue and adipose tissue in generating and sustaining inflammation in obesity is well established. In this scenario, the microvasculature has long been identified as one of the targets of inflammatory cytokines released by fat tissue (184). However, it is not clear whether smooth muscle cells and/or endothelial cells could be an essential source of inflammation in obesity. Recent studies in animal models of heart failure (438) and diabetes (326) identified vascular SMCs as the source of  $\text{TNF}\alpha$ . In the light of these findings, we decided to evaluate  $\text{TNF}\alpha$  levels in smooth muscle (SMC) and endothelial cells (EC) freshly isolated from mesenteric arteries (MA), and aorta of high fat (HFD) compared to regular fat diet (Normal) mice. We also measured vascular

wall levels of two other inflammatory cytokines, IL-1 $\beta$  and IL-6, linked with obesity-derived inflammation (97). Flow cytometry was performed to measure TNF $\alpha$  expression within the ECs and SMCs populations. The gating strategy panel (Figure 1. A-D) was designed to separate immune cells (CD-45<sup>+</sup>) from ECs (VE-Cadh<sup>+</sup>) and SMCs (SMC- $\alpha$ Actine<sup>+</sup>). Following overnight cell fixation and membrane permeabilization, TNF $\alpha$  levels were measured in ECs and SMCs.

On the one hand, SMCs freshly isolated from MAs of HFD showed a significant increase in TNF $\alpha$  levels compared to Normal mice (Figure 1. E, F right). On the other hand, ECs freshly isolated from MAs of HFD did not show a statistical difference in TNF $\alpha$  levels compared to Normal mice (Figure 1. G, H right). Interestingly, TNF $\alpha$  levels were not different in SMCs (Figure 1. E, F left) and ECs (Figure 1. G, H left) isolated from the aorta of HFD and Normal mice. This might suggest that the increase in SMC TNF $\alpha$  level is vessel bed-size specific. On the contrary, IL-6 (Figure 1. I, J) and IL-1 $\beta$  (Figure 1. K, L) levels in SMCs and ECs of aorta and MAs were not significantly different between Normal and HFD mice. These observations collectively add one more evidence to the emerging role of SMCs as a source of TNF $\alpha$  in pathology characterized by low-grade chronic inflammatory processes.

### **Interaction between SMC-TNF $\alpha$ and TNF $\alpha$ RI at the MEPs underlies the formation of pathological inflammatory micro-domains in obesity**

The pivotal role of localized intracellular Ca<sup>2+</sup> signals in regulating SMCs and ECs function and ensuring physiological microvascular reactivity has primarily been proven (292). Most of these Ca<sup>2+</sup> events occur in the spatially restricted micro domain, such as myoendothelial projections (MEPs) that are essential for homeostatic ECs-SMCs communication (291). In obesity, these microdomains are the targets of inflammatory enzymes that cause a loss of endothelial function

and impaired vasodilation (288). Based on the observation that  $\text{TNF}\alpha$  expression is significantly increased in SMCs of MAs isolated from HFD mice (Figure 1), we hypothesized that  $\text{TNF}\alpha$  could be responsible for driving the expression of inflammatory enzymes at the MEPs. Therefore, we performed immunostaining experiments on *en face* MAs to evaluate  $\text{TNF}\alpha$  spatial distribution at the MEPs. EC (Figure 2. A, left) and SMC (Figure 2. A, middle) layers of MAs from Normal mice did not show any  $\text{TNF}\alpha$  staining.

On the contrary, the SMC layer (Figure 2. B, mid-panel) of MAs isolated from HFD mice showed strong  $\text{TNF}\alpha$  immunostaining, whereas  $\text{TNF}\alpha$  signal was almost absent on the ECs plane (Figure 2. B, left panel), confirming our findings in Figure 1. High-resolution images clearly show that in HFD mice, strong  $\text{TNF}\alpha$  signal, arising from the SMC layer (SMC- $\text{TNF}\alpha$ ), protrudes towards the MEPs (black holes) (Figure 2. C, right), whereas no signal was detected in Normal mice (Figure 2. C, left). 3D z-stack reconstruction (Figure 2. D, right) and co-localization analysis (Figure 2. E) of  $\text{TNF}\alpha$  immuno-images confirmed that  $\text{TNF}\alpha$  occupied 75% of the MEPs in HFD mice. In contrast, MEPs of Normal mice did not show any  $\text{TNF}\alpha$  staining (Figure 2. D, left; Figure 2. E). The pro-inflammatory cascade generated by  $\text{TNF}\alpha$  is signaled via  $\text{TNF}\alpha\text{RI}$  activation (408). Based on the observation that SMC- $\text{TNF}\alpha$  is strongly compartmentalized at the MEPs of HFD mice (Figure 2 B, D), we evaluated the spatial distribution of  $\text{TNF}\alpha\text{RI}$ . Immunostaining experiments and plot profiles revealed that  $\text{TNF}\alpha\text{RI}$  expression was similar between HFD and NFD mice (Figure 3. F).

Moreover,  $\text{TNF}\alpha\text{RI}$  was spatially distributed at the MEPs (Figure 3. G). Importantly, high-resolution images of MAs isolated from HFD mice (Figure 2. H, right) showed strong co-localization (light purple signal) at the MEPs of SMC- $\text{TNF}\alpha$  (red) and  $\text{TNF}\alpha\text{RI}$  (light blue), which was prevalently expressed on the plane of the endothelial cell. In contrast, no SMC- $\text{TNF}\alpha$  staining was detected in Normal mice (Figure 4. H, left). Interestingly,  $\text{TNF}\alpha$  and  $\text{TNF}\alpha\text{RI}$

fluorescent signals were unaffected by TNF $\alpha$ RI signaling blockade (Supplemental Figure 2. A-D), suggesting that our model of obesity TNF $\alpha$  influences its expression via TNF $\alpha$ RI signaling.

Finally, we ruled out that immune cells, a well-known source of TNF $\alpha$ (82), were infiltrated into the vascular wall. Indeed, CD45 staining of *en face* MAs was negative in both HFD and Normal mice (Supplemental Figure 2. E). These results support the concept that in obesity, the SMC layer is the source of local vascular inflammation by producing pathological levels of TNF $\alpha$ . Importantly, SMC-TNF $\alpha$  interaction with TNF $\alpha$ RI at the MEPs results in the formation of localized pathological inflammatory micro-domains.

### **Selective blockage of TNF $\alpha$ -TNF $\alpha$ RI signaling normalizes blood pressure in obesity**

TNF $\alpha$  plays a pivotal role in initiating and sustaining inflammation and tissue damage, but it is also crucial in modulating immune system activation and tissue regeneration. These pleiotropic biological effects are due to TNF $\alpha$  binding to two TNF $\alpha$  receptors (TNF $\alpha$ RI, TNF $\alpha$ RII) (406). A large body of evidence points to TNF $\alpha$ RI as the mediator of the pro-inflammatory effects of TNF $\alpha$ , whereas TNF $\alpha$ RII has been shown to transduce the beneficial TNF $\alpha$  biological effects (99, 102, 240, 257, 454). Anti-TNF $\alpha$  therapies implemented to normalize vascular function in obesity and diabetes have been giving confounding results (1, 23, 73). Notably, the observation that in obesity SMC-TNF $\alpha$  co-localizes with TNF $\alpha$ RI at MEPs (Figure 2 H, right) directed our decision of using a recently synthesized small molecule, R7050 (130), to selectively block TNF $\alpha$ RI signaling in our mouse model of obesity-induced hypertension (288). Mice, fed for 14 weeks on HFD, developed glucose intolerance (Supplemental Figure 1. A, B) and hypertension (288) (Supplemental Figure 1. C-F). Treatment of HFD mice with a daily intraperitoneal injection of 10 mg/kg R7050 (177, 222) for twelve days resulted in a significant decrease of night-time systolic (Figure 2. A, C), diastolic (Figure 3. D, F), and mean arterial pressure (MAP) (Figure 3.

G, I) compared to vehicle-treated HFD mice. On the contrary, daytime systolic (Figure 3. B, C), diastolic (Figure 3. E, F), and MAP (Figure 3. H, I) did not show significant changes in HFD mice after the twelve days of drug treatment compared to vehicle. Moreover, day and night-time heart rate were not affected by drug treatment (Figure 3. J-L). These findings provide a proof of concept that selectively target  $\text{TNF}\alpha\text{RI}$  signaling represents a potential novel therapeutic avenue in treating obesity-induced hypertension.

### **Selective inhibition of $\text{TNF}\alpha\text{RI}$ signaling reduces iNOS and NOX1 expression at the MEPs in obesity**

In obesity overexpression at the MEPs of NOX1 and iNOS, reactive oxygen species (ROS) generating enzymes disrupts endothelial function (288).  $\text{TNF}\alpha$ , signaling via  $\text{TNF}\alpha\text{RI}$ , is a prominent stimulus for NOX1 and iNOS expression (176, 242, 441). Accordingly, with our previous study (288), NOX1 (Figure 4. C) and iNOS (Figure 4. E) were highly expressed and localized at the MEPs of HFD and absent in Normal mice (Figure 4. D, F). Notably, R7050 treatment of HFD mice amply reduced NOX1 (Figure 4. C, mid-panel) and iNOS (Figure 4. E, mid-panel) expression normalizing them to Normal mice levels (Figure 4. C, E, right panel). These data support the idea that  $\text{TNF}\alpha\text{RI}$  signaling drives NOX1 and iNOS expression at the MEPs impairing ECs and SMCs intercellular communication essential for maintaining vascular homeostasis.

### **Selective inhibition of $\text{TNF}\alpha\text{RI}$ signaling rescues TRPV4 sparklets and restores endothelial function in obesity**

Unitary  $\text{Ca}^{2+}$  influx occurring through endothelial TRPV4 channels, called  $\text{Ca}^{2+}$  sparklets, are key regulators of endothelial function (287, 354). Recently, we demonstrated the importance of TRPV4 channels in lowering blood pressure. Importantly, obesity-derived ROS targeted TRPV4 sparklets at the MEPs resulting in loss of endothelial-dependent vasodilation and high blood

pressure (288). Based on these previous findings, we sought out whether  $\text{TNF}\alpha$ - $\text{TNF}\alpha\text{RI}$  signaling blockage would have resulted in the rescue of endothelial TRPV4 sparklets and endothelial-dependent vasodilation. The highly specific TRPV4 channel activator, GSK1016790A (GSK101; 3 nM), evoked TRPV4 sparklets in Normal mice (Figure 5. A, B). Significant impairment of TRPV4 sparklets was observed in vehicle-treated HFD mice (Figure 5. A, B), confirming our previous results (288). Significantly, the R7050 treatment normalized TRPV4 sparklets activity in HFD mice (Figure 5. A, B). Similar observations were obtained by evoking TRPV4 sparklets with the muscarinic receptor agonist carbachol, well-known for activating endothelial TRPV4 sparklets (355) (Figure 5. C, D). GSK101-induced TRPV4 channel activation promotes vasodilation (354). GSK101-dependent vasodilation, largely impaired in vehicle-treated HFD mice, was significantly rescued in MAs obtained from R7050-treated HFD mice (Figure 5. E). These results confirmed our hypothesis that preventing  $\text{TNF}\alpha\text{RI}$  signaling in obesity normalizes endothelial TRPV4 channel activity and endothelial-dependent vasodilation.

### 5.3 Discussion

We demonstrated the pathological relevance in obesity of  $\text{TNF}\alpha$ - $\text{TNF}\alpha\text{RI}$  signaling in creating inflammatory microenvironments responsible for the loss of local  $\text{Ca}^{2+}$  signals through TRPV4<sub>EC</sub> channels key regulators of endothelial function. Our results identified the vascular SMC layer of MAs isolated from obese mice as an active source of  $\text{TNF}\alpha$ . Furthermore, we observed that  $\text{TNF}\alpha\text{RI}$ 's preferential co-localization with SMC-derived  $\text{TNF}\alpha$  at the MEPs is a key pathological feature of obesity-derived endothelial dysfunction. Indeed, selective blockage of  $\text{TNF}\alpha\text{RI}$  signaling prevented the overexpression of NOX1 and iNOS at the MEPs and rescued TRPV4<sub>EC</sub> channel  $\text{Ca}^{2+}$  signals. Significantly, targeting  $\text{TNF}\alpha\text{RI}$  normalized microvascular function and lowered blood pressure in our mouse model of obesity. Thus, our findings recognize  $\text{TNF}\alpha$ - $\text{TNF}\alpha\text{RI}$ -induced inflammation as a pathophysiological hallmark of obesity-derived endothelial dysfunction. Our data

unveil the effectiveness of selectively blocking TNF $\alpha$ RI signaling in alleviating endothelial dysfunction and lowering blood pressure in obesity. This highlights the need for developing safe and effective anti-TNF $\alpha$ RI therapies.

Expression and activation of iNOS and NOX1 enzymes highly rely upon inflammatory cytokines. Immune cells are a pivotal source of inflammatory cytokines (49). In diseases characterized by chronic inflammation, such as atherosclerosis, immune cells can infiltrate the vascular wall generating vascular damage and endothelial dysfunction (410). Immunostaining MAs obtained from obese mice with pan-leucocyte marker CD-45 (Supplemental Figure 2. E) demonstrated that immune cells were not infiltrated within the internal elastic lamina of the vascular wall.

Adipose tissue and perivascular fat tissue (PVAT) are well known to release vasoprotective molecules, such as adiponectin (429). However, in obesity, hypertrophic PVAT and white adipose tissue become a source of inflammatory cytokines, such as leptin, resistin, and TNF $\alpha$  (184). TNF $\alpha$  negatively modulates adiponectin release (140), leading to increased vascular NOX and iNOS expression responsible for oxidative-stress induced endothelial dysfunction (10, 206). Therefore, fat tissue-derived inflammatory cytokines may contribute to iNOS and NOX1 overexpression at the MEPs of MAs isolated from obese mice. This condition led us to seek out an alternative source of inflammation within the vascular wall. However, all ex vivo experiments in this study were performed on MAs completely cleaned from any fat tissue.

Recently, it was observed that the vascular wall of small arteries obtained from obese patients is a key source of TNF $\alpha$  (403). The biological activity of TNF $\alpha$  induces NOX and iNOS expression within the vascular wall causing microvascular dysfunction (403, 449) . Our flow cytometry data (Figure 1) show high expression of TNF $\alpha$  in SMCs isolated from MAs from obese mice. Thus, we identify the vascular SMC layer of MAs as a significant contributor of local TNF $\alpha$  . Similarly, Yang and colleagues highlighted vascular SMC-derived TNF $\alpha$  as an essential driver of microvascular

dysfunction in a mouse model of heart failure (438) . Importantly, Sauvé et al. show that SMC conditional deletion of  $TNF\alpha$  rescues vasodilation in a mouse model of diabetes (326) .These studies, together with the most recent findings by Kroetsch et al. (192), focus on the importance of  $TNF\alpha$  signaling within SMCs in regulating microvascular contractility. The observation (Figure 2. H, right) that in obesity, SMC- $TNF\alpha$  and  $TNF\alpha$ RI, mainly expressed on the endothelium, co-localize at the MEPs introduces a novel paradigm where local  $TNF\alpha$ - $TNF\alpha$ RI signaling generates inflammatory microdomains responsible for endothelial dysfunction. Moreover, the fact that no significant differences in plasma inflammatory cytokines levels between HFD and Normal mice were detected (Supplemental Table 1) further confirms the importance of localized vascular inflammatory processes in obesity.

$Ca^{2+}$  events localized at the MEPs of MAs are key mediators of endothelium-dependent vasodilation (77).  $TRPV4_{EC}$  channels are an essential  $Ca^{2+}$  entry pathway at the MEPs of MAs (287, 292, 354, 355). Indeed,  $TRPV4_{EC}$  channel-induced activation of nearby  $Ca^{2+}$ -activated potassium  $K^+$  channels (IK/SK channels) is a hallmark of endothelium-dependent vasodilation of MAs (14, 354). In obesity, NOX1 and iNOS derived oxidative stress impairs  $TRPV4_{EC}$  channel activity leading to hypertension (288). *In vivo* treatment of obese mice with a selective inhibitor of  $TNF\alpha$ RI signaling (130) markedly reduced endothelial iNOS and NOX1 expression (Figure 4), which rescued  $TRPV4_{EC}$  channel activity and endothelium-dependent vasodilation (Figure 5). This is the first direct evidence of the pivotal role of  $TNF\alpha$ - $TNF\alpha$ RI signaling in hindering the physiological occurrence of  $TRPV4_{EC}$  channels-dependent  $Ca^{2+}$  events. Although a flow cytometry assay revealed that other prominent pro-inflammatory cytokines (IL-1 $\beta$  and IL-6) linked to obesity (97) were not altered in MAs from obese mice (Figure 1. I-L), we cannot completely exclude the possibility that other inflammatory mediators could contribute to obesity-derived loss of  $TRPV4_{EC}$  channel activity.

Previous studies reporting anti-TNF $\alpha$  therapy with respect to modulation of blood pressure and vascular function have offered conflicting results (70, 321, 443). Here we present convincing data that anti-TNF $\alpha$ RI treatment significantly reduced blood pressure in obese mice, normalizing it to physiological levels (Figure 3). While our results supported a pro-hypertensive role of TNF $\alpha$ RI, a large limitation of anti-TNF $\alpha$  therapies resides in the fact that TNF $\alpha$  mediates different biological functions depending upon signaling via TNF $\alpha$ RI or TNF $\alpha$ RII (406). Some studies reveal a dual activity of TNF $\alpha$ : a pro-inflammatory role of the TNF $\alpha$ -TNF $\alpha$ RI axis and an anti-inflammatory role of the TNF $\alpha$ -TNF $\alpha$ RII axis (277, 452). On the one hand, TNF $\alpha$ RII signaling protects the endothelium by promoting microvascular repair, angiogenesis, and functional flow recovery (225, 226, 409).

On the other hand, TNF $\alpha$ RI signaling enhances arterial wall chemokines and promotes vascular inflammation (451). It is well-established that TNF $\alpha$ RI-mediated proinflammatory signals occur via TNF $\alpha$ RI interaction with the intracellular accessory subunit tumor necrosis factor receptor (TNFR)-associated death domain (TRADD) which, in turn, activates nuclear factor kappa-light-chain-enhancer of activated B cells (NF- $\kappa$ B) (444). Indeed, selective TNF $\alpha$ RI inhibition suppresses arterial SMC inflammation by reducing NF- $\kappa$ B activation (179). TNF $\alpha$ -induced iNOS expression is prevented by knocking down NF- $\kappa$ B expression (58). In a randomized, double-blind study (300) short-term treatment of obese patients with therapeutic doses of NF- $\kappa$ B inhibitor (189) significantly rescued endothelial dysfunction in peripheral conduit arteries by inhibiting endothelial NOX expression. Importantly, anti-NF- $\kappa$ B treatment significantly reduced systolic blood pressure. Interestingly, TNF $\alpha$ RI was shown to be functionally coupled with NOX enzymes at the plasma membrane via two main accessory intracellular subunits, TRADD and riboflavin kinase (RFK) (441). This association is essential for TNF $\alpha$ -induced NOX1-dependent ROS production (176, 441). These studies are in accordance with the protective effects of the anti-TNF $\alpha$ RI therapy against

obesity-induced vascular inflammation and endothelial dysfunction reported in this manuscript. Indeed, R7050, the anti-TNF $\alpha$ RI small molecule used in this study, blocks TNF $\alpha$ RI interaction with TRADD (130). Future studies implementing the recently generated TNF $\alpha$ RI floxed mice (397) will provide definitive insights into the understanding of the pathophysiological role of TNF $\alpha$ RI signaling in SMCs and ECs in health and disease.

In conclusion, the results exposed in this work show that in obesity, a localized elevation of SMC-derived TNF $\alpha$ , signaling via TNF $\alpha$ RI, is responsible for iNOS and NOX1 overexpression at the MEPs of MAs. In obesity, the deleterious effects of iNOS and NOX1 overexpression at the MEPs on blood pressure and TRPV4<sub>EC</sub> channels mediated vasodilation have been previously demonstrated (288) . Notably, anti-TNF $\alpha$ RI therapy rescued TRPV4<sub>EC</sub> channel-mediated vasodilation and lowered blood pressure in obese mice. Currently, only anti-TNF $\alpha$  therapies are approved for clinical use (255) . Unfortunately, blocking TNF $\alpha$ -mediated signaling is often more detrimental than beneficial. The findings presented here identify a need to develop safe and effective anti-TNF $\alpha$ RI therapies as novel treatments against obesity-dependent microvascular dysfunction.

**Figure1. Smooth muscle cells of systemic resistance arteries are an active source of TNF $\alpha$  in obesity**

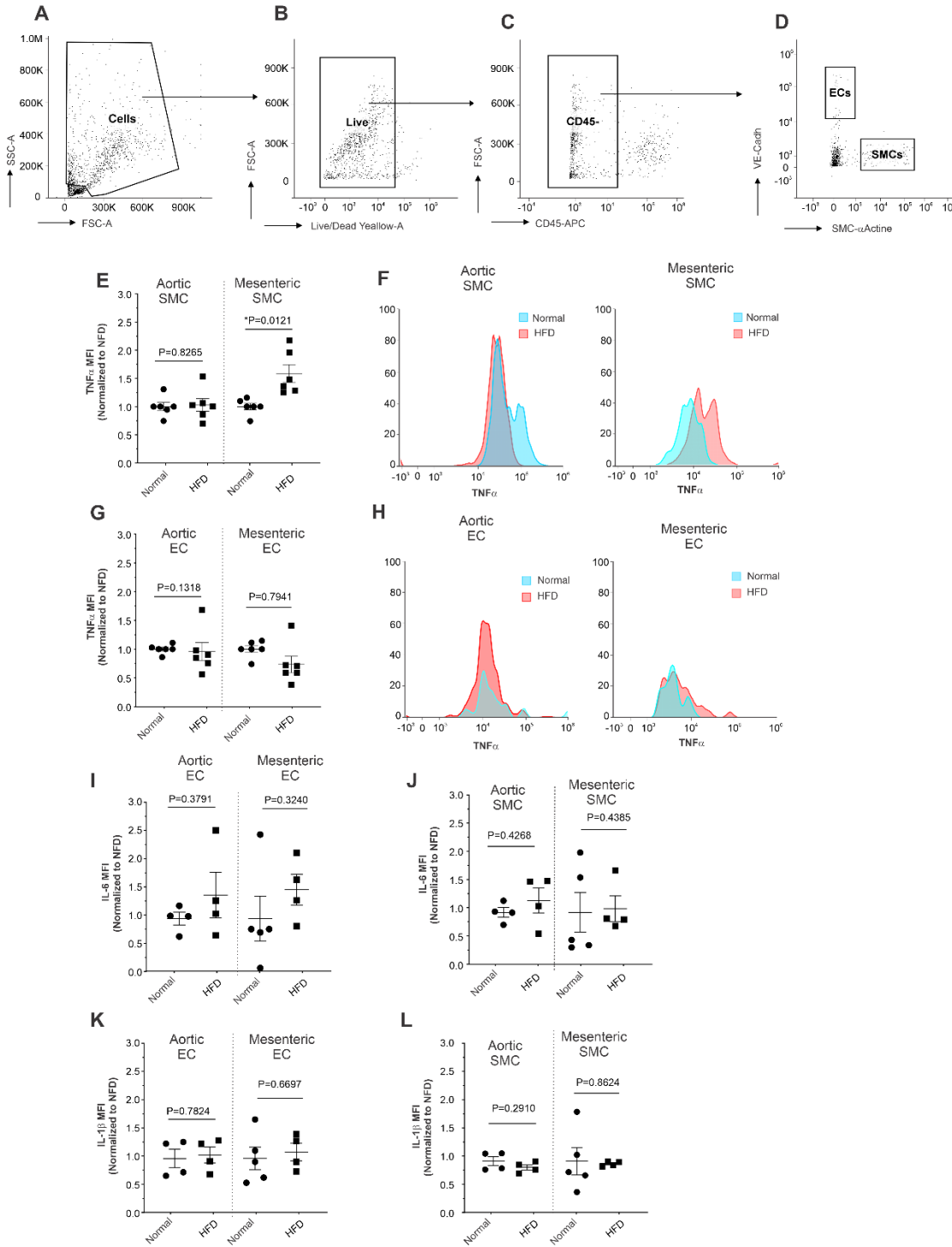


**Figure 1.** Flow cytometry gating strategy for sorting out smooth muscle (SMC) and endothelial (EC) cells freshly isolated from aorta and third order mesenteric arteries of Normal and HFD mice. A, cell population is separated from debris based on forward-scatter area (FSC-A) and side-scatter area (SSC-A) gate. B, Live cells are discriminated from dead cells using a live/dead-yellow stain kit. C, SMCs and ECs are separated from immune cells by using a CD45 gate. D, SMC and EC populations are defined based on expression of smooth muscle  $\alpha$ -actin (SMC  $\alpha$ -actin) and vascular endothelial cadherin (VE-Cadh), respectively. E, scatter plot showing mean fluorescent intensity (MFI) of tumor necrosis factor  $\alpha$  (TNF $\alpha$ ) immunostaining in SMCs freshly isolated from aorta (left) and MAs (right) of Normal and HFD mice. MFI is normalized to Normal mice. Each dot represents a different mouse (n=6, Welch's t-test). F, Representative MFI plot showing TNF $\alpha$  staining intensity in SMCs freshly isolated from aorta (left) and MAs (right) of Normal and HFD mice. G, scatter plot showing MFI of TNF $\alpha$  immunostaining in ECs freshly isolated from aorta (left) and MAs (right) of Normal and HFD mice. MFI is normalized to Normal mice. Each dot represents a different mouse (n=6, Welch's t-test). H, representative MFI plot showing TNF $\alpha$  staining intensity in ECs freshly isolated from aorta (left) and MAs (right) of Normal and HFD mice. I, scatter plot showing mean fluorescent intensity (MFI) of interleukin-6 (IL-6) immunostaining in SMCs freshly isolated from aorta (left) and MAs (right) of Normal and HFD mice. MFI is normalized to Normal mice. Each dot represents a different mouse. (n=4-5, Welch's t-test). J, scatter plot showing MFI of IL-6 immunostaining in ECs freshly isolated from aorta (left) and MAs (right) of Normal and HFD mice. MFI is normalized to Normal mice. Each dot represents a different mouse (n=4-5, Welch's t-test). K, scatter plot showing MFI of interleukin-1 $\beta$  (IL-1 $\beta$ ) immunostaining in SMCs freshly isolated from aorta (left) and MAs (right) of Normal and HFD mice. MFI is normalized to Normal mice. Each dot represents a different mouse (n=4-5, Welch's t-test). L, scatter plot showing MFI of IL-1 $\beta$  immunostaining in ECs freshly isolated from

aorta (left) and MAs (right) of Normal and HFD mice. MFI is normalized to Normal mice. Each dot represents a different mouse (n=4-5, Welch's t-test)

**Figure 2. Interaction between SMC-TNF $\alpha$  and TNF $\alpha$ RI at the MEPs underlies the formation of pathological inflammatory micro-domains in obesity**

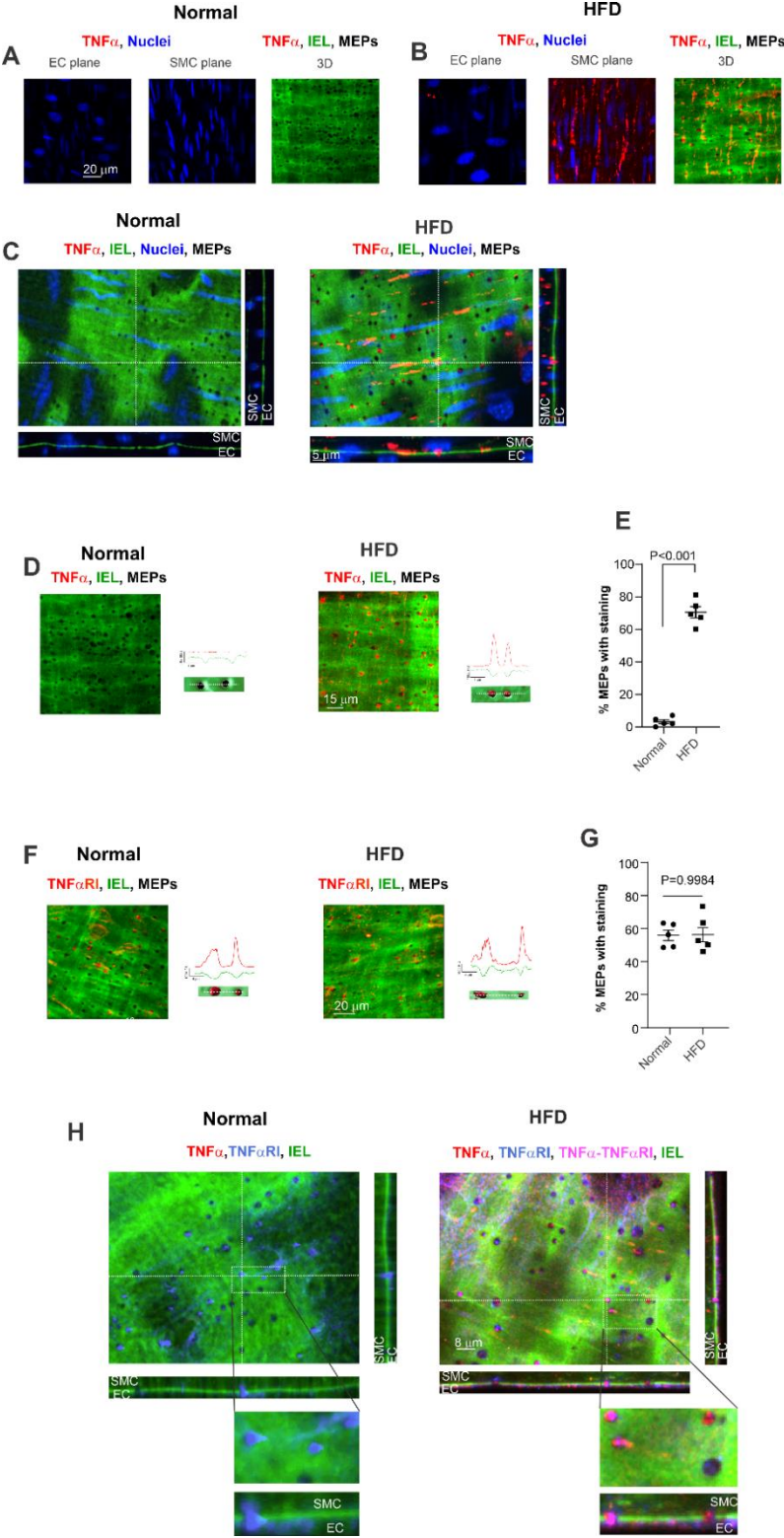


**Figure 2.** A, representative images from *en face* preparations of third-order MAs isolated from Normal mice showing EC plane (left), SMC plane (middle) and merged z-stack (right), black holes represent MEPs. IEL autofluorescence (green) and nuclei (blue). B, representative images from *en face* preparations of third-order MAs isolated from HFD mice showing EC plane (left), SMC plane (middle) and merged z-stack (right), black holes represent MEPs. IEL autofluorescence (green), TNF $\alpha$  (red), and nuclei (blue). C, representative merged z-stack images from *en face* preparations of third-order MAs isolated from Normal (left) and HFD (right) mice showing IEL autofluorescence (green), TNF $\alpha$  (red), nuclei (blue), MEPs (black holes). Insets below and on the right of the images show 3D z-stack view of X and Y axis. D, representative merged z-stack images from *en face* preparations of third-order MAs isolated from Normal (left) and HFD (right) mice showing IEL autofluorescence (green), TNF $\alpha$  (red), nuclei (blue), MEPs (black holes). Small rectangle identifies 2 MEPs within the field of view. The trace above the rectangle indicates a representative fluorescence intensity plot profile for 0.2  $\mu$ m thick line across the 2 MEPs. Green line, IEL; red line, TNF $\alpha$ . E, percentage of MEPs occupied by TNF $\alpha$  ( $n = 5$ ; Welch's t-test). F, representative merged z-stack image from *en face* preparations of third-order MAs isolated from vehicle-treated HFD mice (left) and Normal (right) mice. IEL autofluorescence (green), TNF $\alpha$ RI (red), black holes, MEPs. Small rectangles identify 2 MEPs within the field of views. Traces above the rectangles indicate a representative fluorescence intensity plot profile for 0.2  $\mu$ m thick line across the 2 MEPs. Green line, IEL; red line, TNF $\alpha$ RI. G, percentage of MEPs occupied by TNF $\alpha$ RI ( $n = 5$ ; Welch's t-test). H, representative merged z-stack image from *en face* preparations of third-order MAs isolated from Normal (left) and HFD (right) mice showing IEL autofluorescence (green), TNF $\alpha$  (red), TNF $\alpha$ RI (light blue), TNF $\alpha$ -TNF $\alpha$ RI co-localization (purple), and MEPs (black holes). Insets magnify sites of TNF $\alpha$ -TNF $\alpha$ RI co-localization (purple) at the MEPs of HFD mice (right) and TNF $\alpha$ RI (light blue) expression alone at the MEPs of Normal mice (left).

**Figure 3. Selectively blockage of TNF $\alpha$ RI signaling normalizes blood pressure in obesity**

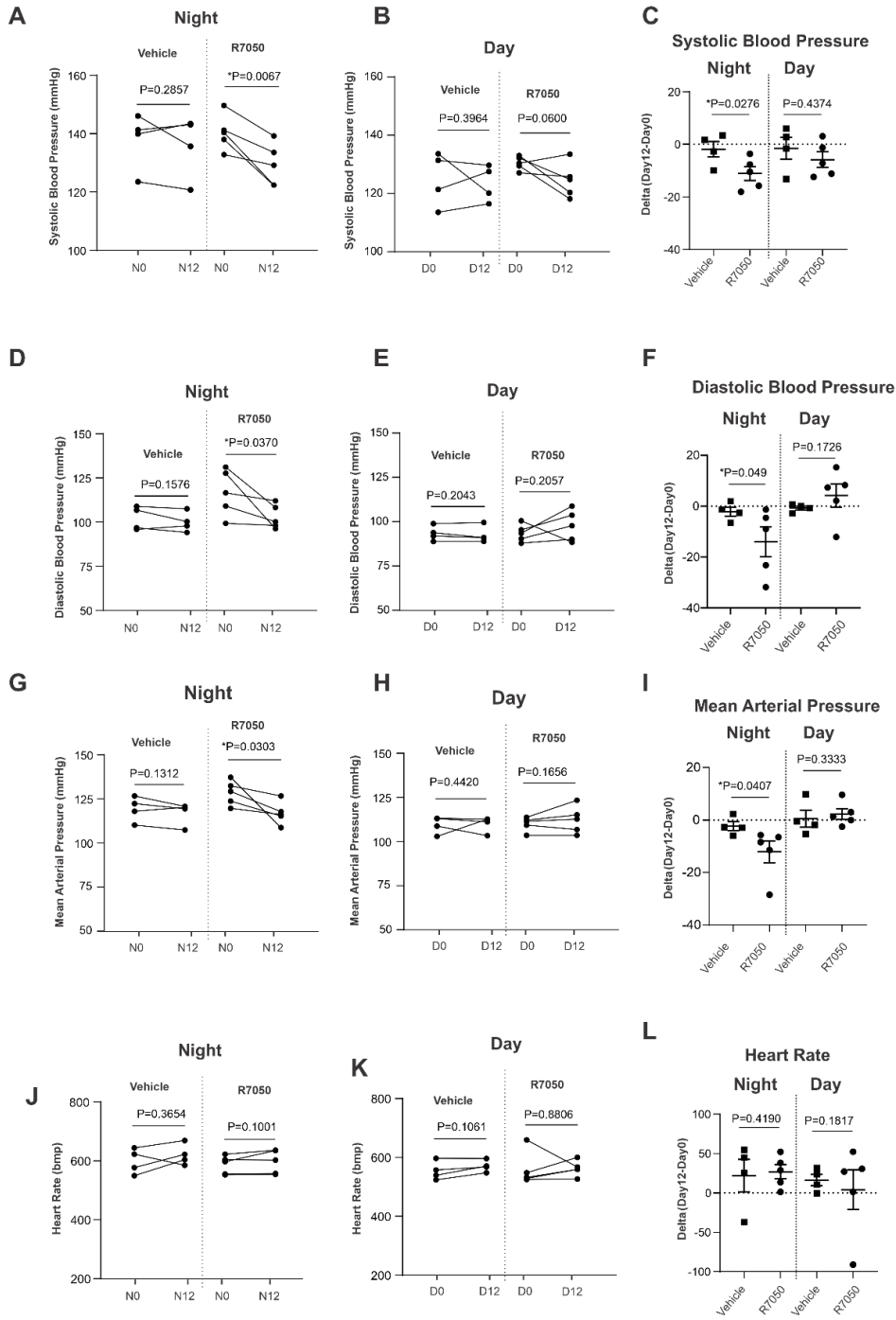


**Figure 3.** A, scatter plot of systolic blood pressure (mmHg) recorded at night (6PM-6AM) in vehicle-treated HFD and R7050-treated HFD mice. N0 and N12 represent systolic blood pressure values at baseline and after twelve days of daily vehicle/R7050 treatment, respectively (n=4, vehicle-treated HFD mice; n=5, R7050-treated HFD mice). B, scatter plot of systolic blood pressure (mmHg) recorded during the day (6AM-6PM) in vehicle-treated HFD and R7050-treated HFD mice. D0 and D12 represent systolic blood pressure values at baseline and after twelve days of daily vehicle/R7050 treatment, respectively (n=4, vehicle-treated HFD mice; n=5, R7050-treated HFD mice). C, changes in systolic blood pressure (night and day) in vehicle-treated HFD and R7050-treated HFD mice after twelve days of daily treatment (n=4, vehicle-treated HFD mice; n=5, R7050-treated HFD mice). D, scatter plot of diastolic blood pressure (mmHg) recorded at night (6 PM-6 AM) in vehicle-treated HFD and R7050-treated HFD mice. N0 and N12 represent diastolic blood pressure values at baseline and after twelve days of daily vehicle/R7050 treatment, respectively (n=4, vehicle-treated HFD mice; n=5, R7050-treated HFD mice). E, scatter plot of diastolic blood pressure (mmHg) recorded during the day (6 AM-6 PM) in vehicle-treated HFD and R7050-treated HFD mice. D0 and D12 represent diastolic blood pressure values at baseline and after twelve days of daily vehicle/R7050 treatment, respectively (n=4, vehicle-treated HFD mice; n=5, R7050-treated HFD mice). F, changes in diastolic blood pressure (night and day) in vehicle-treated HFD and R7050-treated HFD mice after twelve days of daily treatment (n=4, vehicle-treated HFD mice; n=5, R7050-treated HFD mice). G, scatter plot of mean arterial pressure (mmHg) recorded at night (6PM-6AM) in vehicle-treated HFD and R7050-treated HFD mice. N0 and N12 represent mean arterial pressure values at baseline and after twelve days of daily vehicle/R7050 treatment, respectively (n=4, vehicle-treated HFD mice; n=5, R7050-treated HFD mice). H, scatter plot of mean arterial pressure (mmHg) recorded during the day (6AM-6PM) in vehicle-treated HFD and R7050-treated HFD mice. D0 and D12 represent mean arterial pressure values at baseline and after twelve days of daily vehicle/R7050 treatment, respectively (n=4, vehicle-treated HFD mice; n=5, R7050-treated HFD mice). I,

changes in mean arterial pressure (night and day) in vehicle-treated HFD and R7050-treated HFD mice after twelve days of daily treatment (n=4, vehicle-treated HFD mice; n=5, R7050-treated HFD mice). G, scatter plot of heart rate (Bpm) recorded at night (6PM-6AM) in vehicle-treated HFD and R7050-treated HFD mice. N0 and N12 represent heart rate values at baseline and after twelve days of daily vehicle/R7050 treatment, respectively (n=4, vehicle-treated HFD mice; n=5, R7050-treated HFD mice). H, scatter plot of heart rate (Bpm) recorded during the day (6AM-6PM) in vehicle-treated HFD and R7050-treated HFD mice. D0 and D12 represent heart rate values at baseline and after twelve days of daily vehicle/R7050 treatment, respectively (n=4, vehicle-treated HFD mice; n=5, R7050-treated HFD mice). I, changes in heart rate (night and day) in vehicle-treated HFD and R7050-treated HFD mice after twelve days of daily treatment (n=4, vehicle-treated HFD mice; n=5, R7050-treated HFD mice).

**Figure 4. Selectively blockage of TNF $\alpha$ RI signaling reduces iNOS and NOX1 expression at the MEPs in obesity**

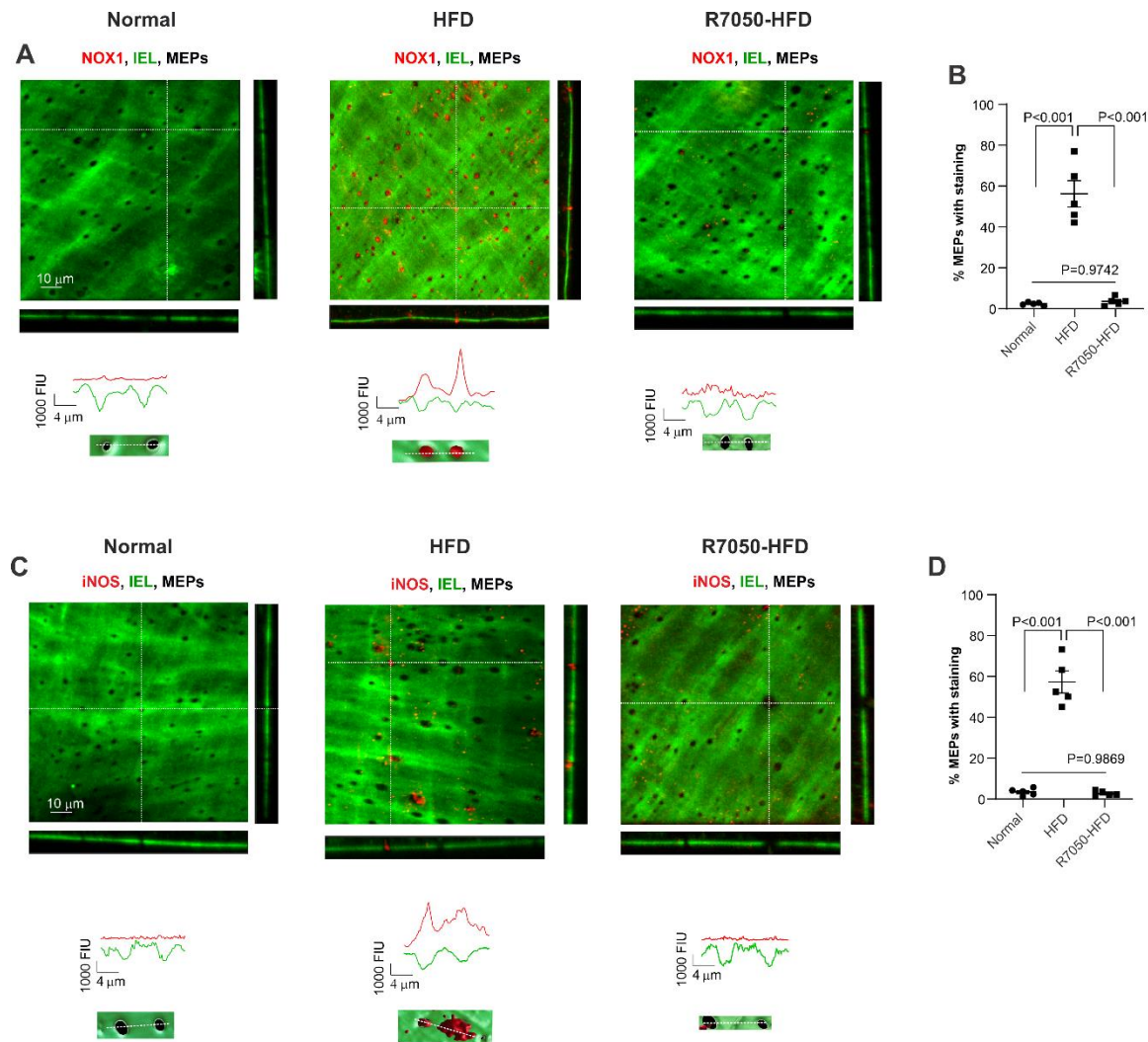


**Figure 4.** A, representative merged z-stack image from *en face* preparations of third-order MAs isolated from HFD (left), R7050-treated HFD (middle), and Normal mice. IEL autofluorescence (green), NOX1 (red), MEPs (black holes). Insets below and on the right of the images show 3D z-stack view of X and Y axis. Small rectangles identify 2 MEPs within the field of views. Traces above the rectangles indicate a representative fluorescence intensity plot profile for 0.2  $\mu$ m thick line across the 2 MEPs. Green line, IEL; red line, NOX1. B, percentage of MEPs occupied by

NOX1 ( $n = 5$ ; one-way ANOVA). C, representative merged z-stack image from *en face* preparations of third-order MAs isolated from vehicle-treated HFD (left), R7050-treated HFD (middle), and Normal mice. IEL autofluorescence (green), iNOS (red), MEPs (black holes). Insets below and on the right of the images show 3D z-stack view of X and Y axis. Small rectangles identify 2 MEPs within the field of views. Traces above the rectangles indicate a representative fluorescence intensity plot profile for 0.2  $\mu\text{m}$  thick line across the 2 MEPs. Green line, IEL; red line, iNOS. D, percentage of MEPs occupied by iNOS ( $n = 5$ ; one-way ANOVA).

### Figure 5. Selectively blockage of $\text{TNF}\alpha\text{RI}$ signaling in obesity rescues TRPV4 sparklets and restores endothelial-dependent vasodilation

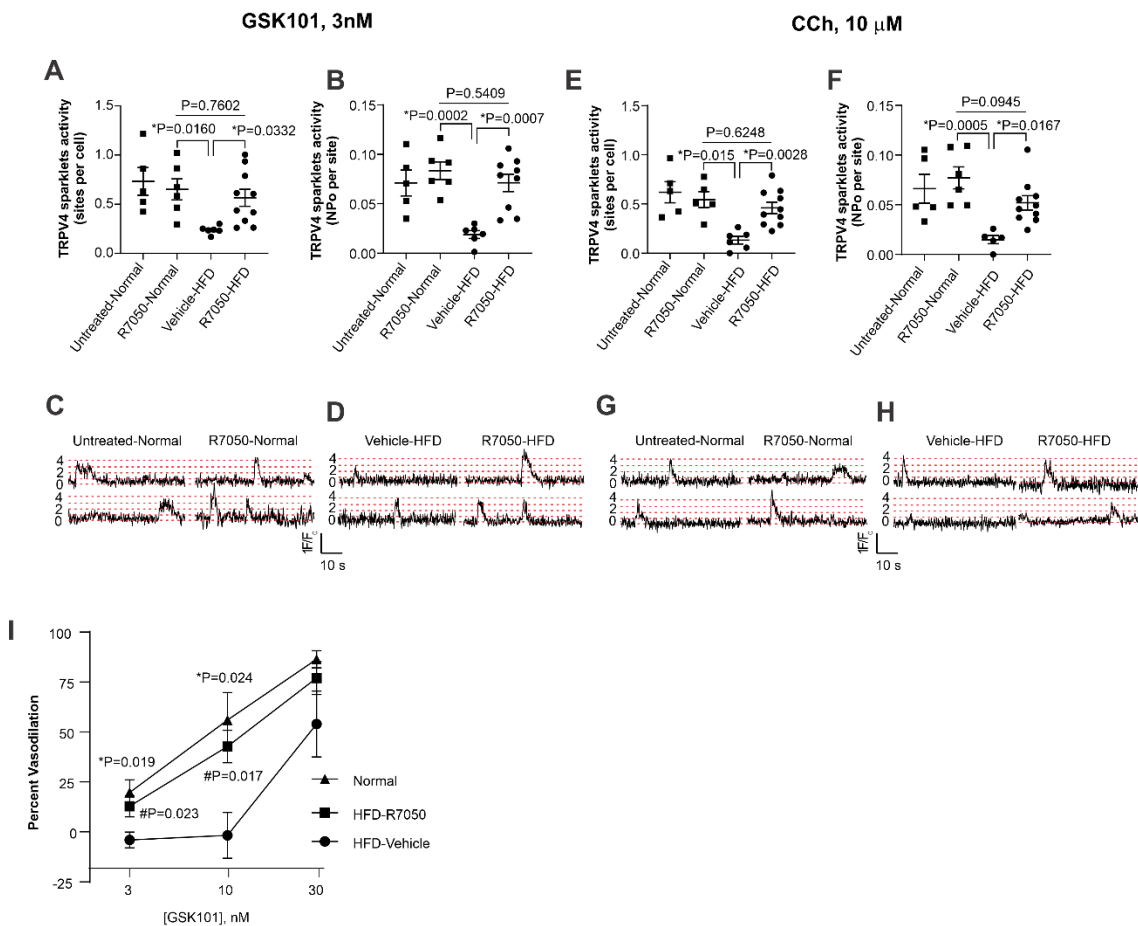
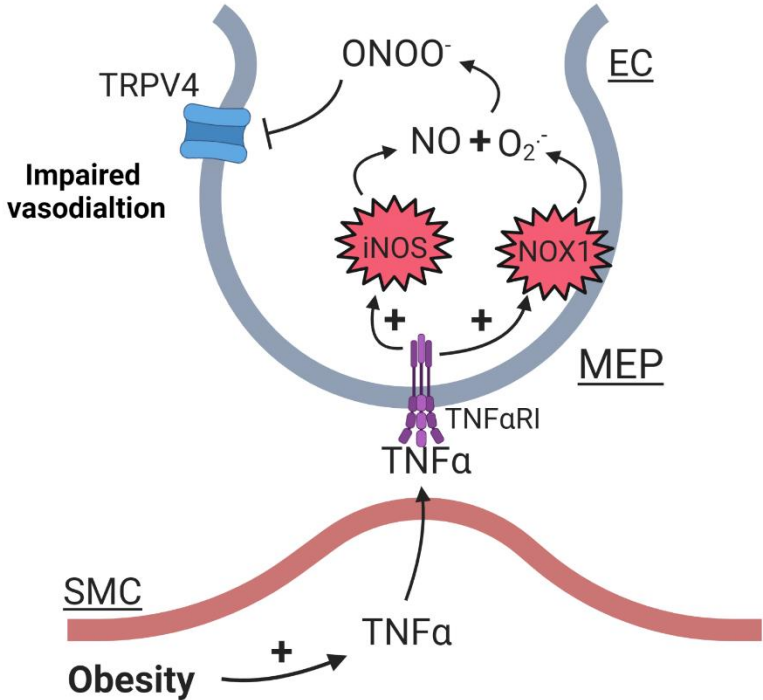


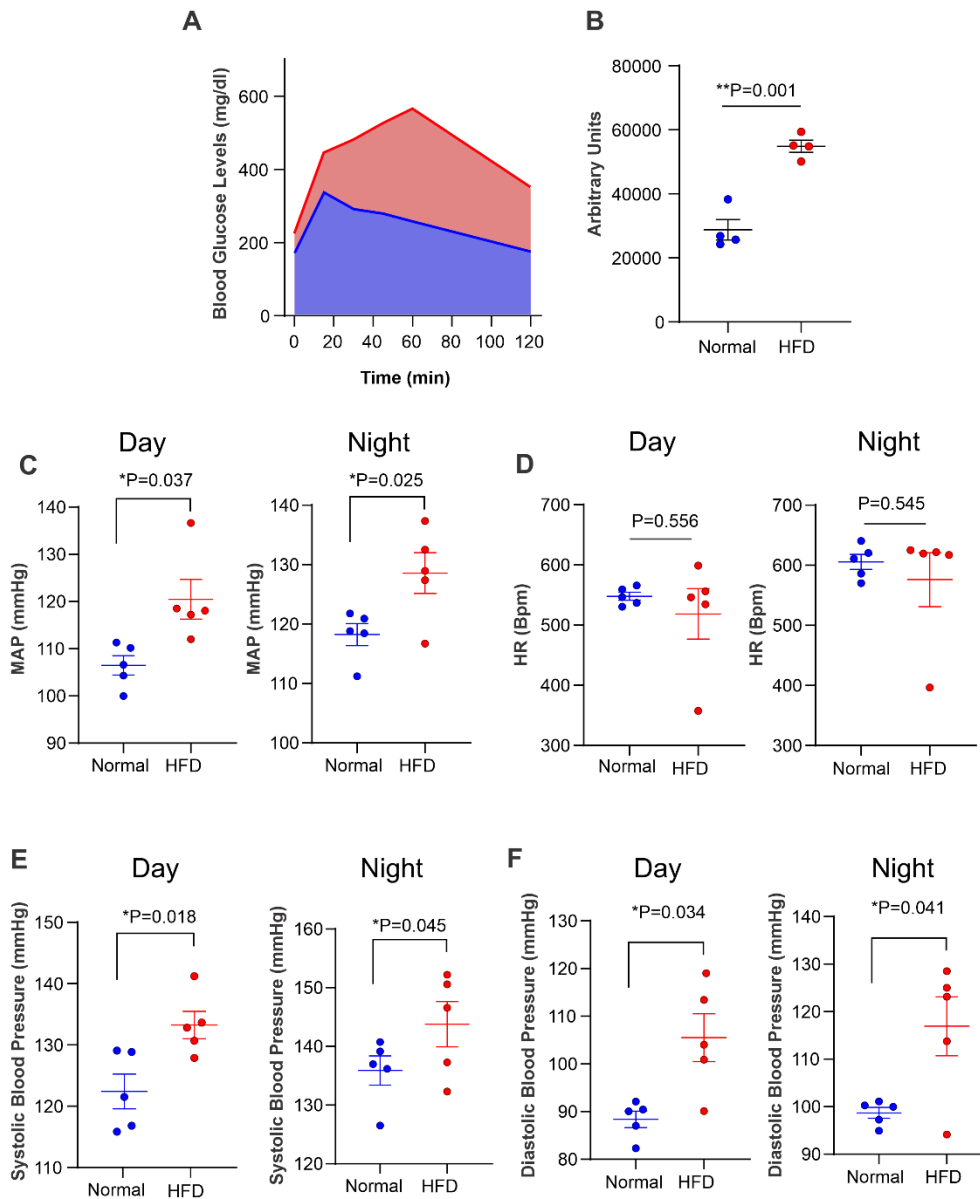
Figure 5. A, GSK101-induced (3 nM) TRPV4<sub>EC</sub> sparklet activity per cell ( $n = 5$ ; one-way

ANOVA); B, GSK101-induced (3 nM) TRPV4<sub>EC</sub> sparklet activity, expressed as NP<sub>o</sub> per site (n = 5; one-way ANOVA). C, representative F/F<sub>0</sub> traces from TRPV4<sub>EC</sub> sparklet sites (20 μM CPA + GSK101, 3 nM) in Fluo-4-loaded *en face* preparations of MAs from Untreated-Normal and R7050-treated Normal mice. Dotted red lines indicate quantal levels. D, representative F/F<sub>0</sub> traces from TRPV4<sub>EC</sub> sparklet sites (CPA, 20 μM + GSK101, 3 nM) in Fluo-4-loaded *en face* preparations of MAs from Untreated-HFD and R7050-treated HFD mice. Dotted red lines indicate quantal levels. E, CCh-induced (10 μM) TRPV4<sub>EC</sub> sparklet activity per cell (n = 5; one-way ANOVA); F, CCh-induced (10 μM) TRPV4<sub>EC</sub> sparklet activity, expressed as NP<sub>o</sub> per site (n = 5; one-way ANOVA). G, representative F/F<sub>0</sub> traces from TRPV4<sub>EC</sub> sparklet sites (CPA, 20 μM + CCh, 10 μM) in Fluo-4-loaded *en face* preparations of MAs from Untreated-Normal and R7050-treated Normal mice. Dotted red lines indicate quantal levels. H, representative F/F<sub>0</sub> traces from TRPV4<sub>EC</sub> sparklet sites (CPA, 20 μM + CCh, 10 μM) in Fluo-4-loaded *en face* preparations of MAs from Untreated-HFD and R7050-treated HFD mice. Dotted red lines indicate quantal levels. I, Percent dilation of MAs in response to GSK101 (3 to 30 nM; n = 5; \*Normal vs. vehicle-HFD; #R7050-HFD vs. vehicle-HFD, one-way Anova).

**Figure 6. Schematic representation of the formation of pathological MEPs in obesity driven by the interaction between SMC-TNF $\alpha$  and TNF $\alpha$ RI.**



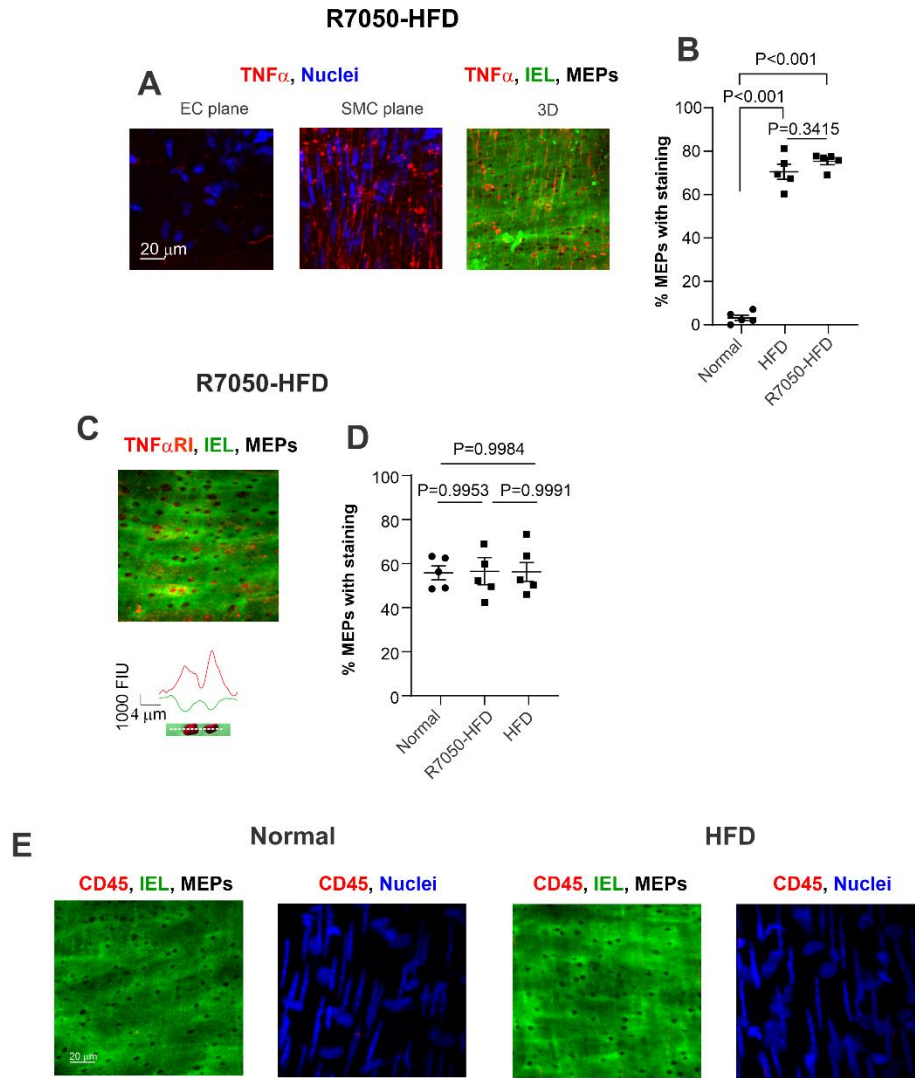
## Supplemental Figure 1. HFD mice are glucose intolerant and hypertensive



**Supplemental Figure 1.** A, plasma glucose concentrations during the intraperitoneal glucose tolerance test (1.5 g/kg) following 24 hours of fasting in Normal (blue) and HFD (red) mice. B, scatter plot of area under the curve (AUC) for glucose calculated using the trapezoidal rule. Each data point represents a mouse (n=4; Welch's t-test). C, scatter plot of baseline mean arterial pressure (mmHg) of Normal and HFD mice recorded during the day (left) and night (right). Each

data point represents a mouse (n=5; Welsh's t-test). D, scatter plot of baseline heart rate (Bpm) of Normal and HFD mice recorded during the day (left) and night (right). Each data point represents a mouse (n=5; Welsh's t-test). E, scatter plot of baseline systolic blood pressure (mmHg) of Normal and HFD mice recorded during the day (left) and night (right). Each data point represents a mouse (n=5; Welsh's t-test). F, scatter plot of diastolic blood pressure (mmHg) of Normal and HFD mice recorded during the day (left) and night (right). Each data point represents a mouse (n=5; Welsh's t-test).

**Supplemental Figure 2. TNF $\alpha$ -TNF $\alpha$ RI signaling does not influence smooth muscle TNF $\alpha$  expression in obesity**



**Supplemental Figure 2.** A, representative images from *en face* preparations of third-order MAs isolated from R7050-treated HFD mice showing EC plane (left), SMC plane (middle) and merged z-stack (right), black holes represent MEPs. IEL autofluorescence (green), TNF $\alpha$  (red), and nuclei (blue). B, percentage of MEPs stained with TNF $\alpha$  ( $n = 5$ ; one-way ANOVA). C, representative merged z-stack image from *en face* preparations of third-order MAs isolated from R7050-treated HFD mice. IEL autofluorescence (green), TNF $\alpha$ RI (red), black holes,

MEPs. Inset images represent volumetric 3D rendering of TNF $\alpha$ RI (red) localization at the MEPs (black holes). Small rectangles identify 2 MEPs within the field of views. Traces above the rectangles indicate a representative fluorescence intensity plot profile for 0.2  $\mu$ m thick line across the 2 MEPs. Green line, IEL; red line, TNF $\alpha$ RI. D, percentage of MEPs stained with TNF $\alpha$ RI ( $n = 5$ ; one-way ANOVA).

**Supplemental Table 1. Plasma inflammatory cytokines levels are not different between HFD and Normal mice**

<b>Cytokine</b>	<b>Normal mice</b>	<b>HFD mice</b>	<b>HFD mice - Vehicle Treated</b>	<b>HFD mice - R7050 Treated</b>
<b>TNF<math>\alpha</math> (pg/ml)</b>	2.71 $\pm$ 0.25	2.51 $\pm$ 0.45	2.84 $\pm$ 0.55	2.41 $\pm$ 0.44
<b>IL-1<math>\alpha</math> (pg/ml)</b>	2.12 $\pm$ 1.86	1.38 $\pm$ 1.12	0.26 $\pm$ 0.06	24.45 $\pm$ 24.19
<b>IL-1<math>\beta</math> (pg/ml)</b>	N/D	N/D	N/D	N/D
<b>IL-6 (pg/ml)</b>	1.66 $\pm$ 1.18	5.08 $\pm$ 2.61	1.39 $\pm$ 0.2	2.58 $\pm$ 1.05
<b>IL-10 (pg/ml)</b>	0.84 $\pm$ 0.01	4.63 $\pm$ 3.31	0.85 $\pm$ 0.01	1.03 $\pm$ 0.2

**Mean  $\pm$  SEM; N/D = Not Detected**

## **Chapter 6: Future Directions**

The importance of endothelial AKAP150-TRPV4 signaling at the MEPs in regulating endothelial function and lowering blood pressure was evident by the increased blood pressure recorded in endothelial specific TRPV4 (TRPV4<sub>EC</sub>) and AKAP150 (AKAP150<sub>EC</sub>) knock out mice (Chapter 4, Figure 1). Importantly, in obesity overexpression at the MEPs of NOX1 and iNOS impairs TRPV4<sub>EC</sub>-AKAP150<sub>EC</sub> signaling resulting in pathological increase of blood pressure (Chapter 4). The well-known pro-inflammatory cytokine TNF $\alpha$ , signaling via TNF $\alpha$ RI, is responsible for NOX1 and iNOS overexpression at the MEPs (Chapter 5, Figure 4). Indeed, selective blockage of TNF $\alpha$ RI lowers NOX1 and iNOS overexpression and blood pressure in obesity (Chapter 5, Figure 3, 4). Our flow cytometry data (Chapter 5, Figure 1) and high-resolution immunostaining images (Chapter 5, Figure 2) reveal that high TNF $\alpha$  expression can be observed within the SMC layer of MAs isolated from obese mice. Interestingly, a few other studies reported a pathological increase of SMC-TNF $\alpha$  expression and its importance in augmenting microvascular contractility under different disease conditions (192, 326). To understand the significance of SMC-TNF $\alpha$  in causing endothelial inflammation in obesity, we have generated conditional SMC-TNF $\alpha$  knockout mice (TNF $\alpha$ <sub>SMC</sub><sup>-/-</sup>). Blood pressure recording, plasma collection, and *ex vivo* experiments will be performed on obese TNF $\alpha$ <sub>SMC</sub><sup>-/-</sup> mice. We are interested in assessing microvascular reactivity, TRPV4<sub>EC</sub> channel function, NOX1, and iNOS expression levels and measuring plasma levels of pro-inflammatory circulating cytokines (IL-6, IL-1 $\beta$ , TNF $\alpha$ , IL-10, INF- $\gamma$ ). If obese TNF $\alpha$ <sub>SMC</sub><sup>-/-</sup> mice display lower blood pressure levels, reduced iNOS and NOX1 expression at the MEPs, and normalized TRPV4<sub>EC</sub> channel activity, these data will indisputably confirm the pathological role of SMC-TNF $\alpha$  in mediating obesity-induced endothelial dysfunction.

Moreover, the pro-inflammatory circulating cytokines panel will give us a clue whether SMC-TNF $\alpha$  can influence plasma levels of other pro-inflammatory cytokines. As already amply discussed in Chapter 5, the proinflammatory effects of TNF $\alpha$  are signaled by TNF $\alpha$ RI. TNF $\alpha$ RI is

highly expressed on the endothelium plane and localized at the MEPs of MAs (Chapter 5, Figure 2. H). From the pivotal discovery that TNF $\alpha$ RI blockage normalizes blood pressure in obesity (Chapter 5, Figure 3) we are planning on generating inducible TNF $\alpha$ RI<sub>EC</sub><sup>-/-</sup> and TNF $\alpha$ RI<sub>SMC</sub><sup>-/-</sup> mice to unravel the importance and role played by TNF $\alpha$ RI<sub>EC</sub> and TNF $\alpha$ RI<sub>SMC</sub> in influencing microvascular homeostasis under pathological as well as physiological conditions.

### **TNF $\alpha$ -TNF $\alpha$ RI-NF- $\kappa$ B signaling in obesity**

The transcriptional factor NF- $\kappa$ B is the main mediator of the inflammatory cascade activated by TNF $\alpha$ -TNF $\alpha$ RI (294, 407). Although TNF $\alpha$ -induced NF- $\kappa$ B activation has been linked with increased NOX1 (235, 427) and iNOS (58, 343) expression and activity, we are interested in confirming this link in our obesity model with two separate sets of experiments:

1. Obese and normal mice, after two weeks of daily treatment with R7050 (TNF $\alpha$ RI inhibitor, Chapter X) or vehicle control, will be sacrificed, and MAs will be collected. Immunostaining for the active form of NF- $\kappa$ B (p65- NF- $\kappa$ B) will be performed. We expect to see increased nuclear translocation of NF- $\kappa$ B in MAs from vehicle-treated obese mice compared to normal and R7050 treated obese mice. Following, we will solidify the findings by implementing a commercially available NF- $\kappa$ B reporter mouse fed a high-fat diet.
2. Obese and normal mice, after two weeks of treatment with the specific NF- $\kappa$ B nuclear translocation inhibitor (JSH-23) (146, 343) or vehicle control, will be sacrificed, and MAs will be collected. We will measure NOX1, iNOS, and TNF $\alpha$  levels via flow cytometry, immunostaining, and RT-PCR. Moreover, we will confirm the inhibition of NF- $\kappa$ B nuclear translocation via immunostaining and western blot. We expect to see higher iNOS,

NOX1, and TNF $\alpha$  levels and strong NF- $\kappa$ B nuclear translocation in MAs from vehicle treated obese mice than normal, and JSH-23 treated obese mice. Preliminary data (Figure 1) show a promising significant reduction in NOX1 staining following JSH-23 treatment of obese mice.

These above-mentioned experiments will enable us to directly link TNF $\alpha$ -TNF $\alpha$ RI dependent NF- $\kappa$ B activation and iNOS and NOX1 endothelial expression in our mouse model of obesity.

### **High intraluminal pressure, SMC Ca<sup>2+</sup> signals, and arterial wall inflammation: missing links**

The nature and source of the stimuli underlying the increase in SMC-TNF $\alpha$  expression in obesity remain unknown. Blood volume has been reported to increase with body mass index (BMI) significantly. Indeed, obese subjects have a larger plasma volume and fluid overload (6, 203, 249) . Fluid overload causes increased arterial intraluminal pressure (417). In small resistance arteries, the intraluminal pressure determines an increase in SMC intracellular Ca<sup>2+</sup>, leading to vasoconstriction (myogenic tone) (182) . While much is known on the role of inflammatory cytokines released by hypertrophic adipose tissue for driving vascular inflammation, far less clear is whether high pressure can directly contribute to inflammation.

Our preliminary data suggest that the high intraluminal pressure triggers SMC-TNF $\alpha$  expression. Indeed, MAs isolated from C57BL/6J mice and pressurized at 120 mmHg for 5 hours show intense SMC-TNF $\alpha$  staining compared to the MAs pressurized at 60 mmHg (Figure 2). Next, we are planning on understanding the molecular mechanism underlying these phenomena.

### **L-type Ca<sup>2+</sup> channels (LTCC) hypothesis**

LTCC is the major SMC  $\text{Ca}^{2+}$  entry pathway responsible for myogenic tone development (292). Pressure-induced LTCC-mediated  $\text{Ca}^{2+}$  influx can modulate gene expression via stimulation of the  $\text{Ca}^{2+}$ /calmodulin-dependent phosphatase calcineurin (CaN) and subsequent activation and nuclear translocation of the transcription factor (NFATc3) (120, 272, 278) . AKAP150 ensures spatial proximity between LTCC-CaN, essential for NFATc3 activation (283). Importantly, NFATc3 promotes  $\text{TNF}\alpha$  expression as macrophages isolated from NFATc3<sup>-/-</sup> obese mice show lower  $\text{TNF}\alpha$  levels (151). Therefore, it is possible that under pressure overload AKAP150/CaN/NFATc3 axis may be critical for the pathophysiological induction of SMC- $\text{TNF}\alpha$  expression.

Furthermore,  $\text{TNF}\alpha$  expression is largely regulated by the transcription factor NF- $\kappa$ B (74) . Intracellular  $\text{Ca}^{2+}$  is known to activate NF- $\kappa$ B via  $\text{Ca}^{2+}$ /calmodulin-dependent protein kinase II (CamKII)-dependent phosphorylation of I $\kappa$ B kinase (IKK) (171, 213), which is responsible for I $\kappa$ B phosphorylation and its subsequent degradation. Indeed, Ikeda and colleagues have demonstrated that  $\text{Ca}^{2+}$  entry through LTCC activates NF- $\kappa$ B via CamKII (157). Therefore, the LTCC-CamKII-NF- $\kappa$ B pathway could also be a key driver of SMC-  $\text{TNF}\alpha$  expression under pressure overload conditions.

To establish the importance of LTCC and downstream activated signaling pathways in possibly regulating SMC- $\text{TNF}\alpha$  expression (Figure 3) we are planning to proceed as follows:

- 1. Establish the importance of LTCC-AKAP150 signaling in driving pressure-induced SMC- $\text{TNF}\alpha$  expression**

- a. LTCC:** MAs, isolated from C57BL6 mice, will be pressurized at 120 mmHg for 4 hours in the presence or absence of the LTCC blocker Nifedipine (375) followed by immunostaining, RT-

PCR, and western blot (WB) for  $\text{TNF}\alpha$ . If LTCC are involved in mediating pressure-induced increase of SMC- $\text{TNF}\alpha$  expression, MAs incubated with Nifedipine will show low  $\text{TNF}\alpha$  signal.

**b. SMC AKAP150:** Recently, we have generated conditional smooth muscle knockout of AKAP150 ( $\text{AKAP150}_{\text{SMC}}^{-/-}$ ) mice in our laboratory. MAs isolated from  $\text{AKAP150}_{\text{SMC}}^{-/-}$  and respectively control (Cre -;  $\text{AKAP150}_{\text{SMC}}^{-/-}$ ) mice will be pressurized at 120 mmHg for 4 hours, followed by immunostaining, RT-PCR, and western blot for  $\text{TNF}\alpha$ . If SMC AKAP150 is essential for the pressure-induced increase of SMC- $\text{TNF}\alpha$  expression, MAs isolated from  $\text{AKAP150}_{\text{SMC}}^{-/-}$  will have low  $\text{TNF}\alpha$  expression compared to control.

**c. LTCC-AKAP150 signaling:** MAs isolated from  $\text{AKAP150}_{\text{SMC}}^{-/-}$  will be pressurized at 120 mmHg for 4 hours in the presence or absence of Nifedipine. Immunostaining, RT-PCR, and WB for  $\text{TNF}\alpha$  will be performed. If the LTCC-AKAP150 axis is a pivotal regulator of pressure-induced SMC- $\text{TNF}\alpha$  expression,  $\text{TNF}\alpha$  levels in MAs of  $\text{AKAP150}_{\text{SMC}}^{-/-}$  will be low and unaffected by Nifedipine treatment.

## **2. Determine whether AKAP150-CaN axis plays a crucial role in driving pressure-induced SMC- $\text{TNF}\alpha$**

**a. CaN :** MAs, isolated from C57BL6, will be pressurized for 4 hours in the presence or absence of calcineurin inhibitors (Cyclosporin A or FK506) (273, 278) , followed by  $\text{TNF}\alpha$  mRNA levels and protein levels will be assessed. If CaN is involved in high pressure-stimulated SMC- $\text{TNF}\alpha$  expression, MAs treated with CaN inhibitors will show lower  $\text{TNF}\alpha$  levels.

**b. AKAP150-CaN signaling:** MAs, isolated from AKAP150<sub>SMC</sub><sup>-/-</sup> mice, will be pressurized at 120 mmHg for 4 hours in the presence of CaN inhibitors. If AKAP150-CaN coupling is essential for pressure-induced SMC-TNF $\alpha$  expression, SMC-TNF $\alpha$  mRNA and protein levels in MAs isolated from AKAP150<sub>SMC</sub><sup>-/-</sup> mice will be low and unaffected by CaN inhibition.

### **3. Establish whether NFATc3 is activated by high pressure and important in driving pressure-induced SMC-TNF $\alpha$ expression**

**a. High-pressure induced NFATc3 activation:** Dephosphorylation of NFATc3 on serine 265 (p-NFATc3<sup>265</sup>) is required for NFATc3 nuclear translocation and gene expression modulation (281). MAs isolated from C57BL6 will be pressurized at 60 and 120 mmHg for 4 hours. We will then measure the difference in p-NFATc3<sup>265</sup> between MAs pressurized at 60 versus 120 mmHg. If high pressure induces NFATc3 nuclear translocation, we expect to detect lower p-NFATc3<sup>265</sup> in MAs at 120 mmHg compared to 60 mmHg.

**b. High-pressure induced SMC-TNF $\alpha$  expression, dependent upon NFATc3 activation:** MAs, isolated from NFATc3<sup>-/-</sup> (commercially available) and C57BL6 mice, will be pressurized at 120 mmHg for 4 hours. TNF $\alpha$  mRNA and protein levels will then be measured. If NFATc3 is directly involved in enhancing pressure-induced SMC-TNF $\alpha$  expression, SMC-TNF $\alpha$  levels will be lower in MAs from NFATc3<sup>-/-</sup> mice compared to C57BL6.

### **4. Determine whether NF- $\kappa$ B is activated by high pressure and responsible for increase SMC-TNF $\alpha$ expression**

**a. High-pressure induced NF- $\kappa$ B activation:** MAs isolated from C57BL6 mice will be pressurized at 60 and 120 mmHg for 4 hours. We will then measure the difference in NF- $\kappa$ B nuclear translocation between MAs pressurized at 60 versus 120 mmHg. If high pressure induces NF- $\kappa$ B nuclear translocation, we expect a higher nuclear NF- $\kappa$ B staining in MAs at 120 mmHg compared to 60 mmHg. We will then further confirm these findings by implementing the commercially available NF- $\kappa$ B luciferase reporter mice.

**b. High-pressure induced SMC-TNF $\alpha$  expression, dependent upon NF- $\kappa$ B activation:** MAs, isolated from C57BL6 mice, will be pressurized at 120 mmHg for 4 hours in the presence or absence of the NF- $\kappa$ B inhibitor (JSH-23). TNF $\alpha$  mRNA and protein levels will then be measured. If NF- $\kappa$ B is directly involved in enhancing pressure-induced SMC-TNF $\alpha$  expression, TNF $\alpha$  levels will be lower in MAs treated with JSH-23.

### **Caveolae-Caveolin1/Piezo1 channel hypothesis**

A recent report by Michell et al. shows that high intraluminal pressure is directly responsible for endothelial inflammation. The authors show that high intraluminal pressure enhances NF- $\kappa$ B activation and vascular inflammation (248) . This process is mediated by the mechanosensory properties of caveolae-caveolin1 microdomains (248, 341) . Caveolae are specialized membrane lipid rafts coated with caveolin scaffolding proteins (Cav1-3), caveolin1 being the main one expressed in SMC (337) . However, the mechanism underlying the mechanosensitive properties of caveolae-caveolin1 and their link with vascular inflammation are still largely unclear. Interestingly, caveolae microdomains harbor the neutral sphingomyelinase enzyme (N-SMase) and its substrate, sphingomyelin (SPH), which have been shown to be essential for caveolae-dependent mechanotransduction (62) . A recent study by Shi et al. purports to reveal the missing

component for explaining the mechanosensory properties of caveolae-caveolin1 microdomains. In fact, Shi and colleagues demonstrated that the gating properties of the mechanically activated non-selective cation channel Piezo1 are highly influenced by N-SMase activity and by the presence of sphingomyelin. Briefly, N-SMase converts sphingomyelin into ceramide (CER), which disables the inactivation gate of Piezo1, ensuring long-lasting Piezo1-dependent  $Ca^{2+}$  entry in response to force (340). Indeed, Piezo1 channels were shown to be expressed within caveolae-caveolin1 microdomains (207) and implicated in mediating SMC remodeling (310) and increased  $TNF\alpha$  expression (13). Piezo1-dependent  $Ca^{2+}$  entry has been linked with  $Ca^{2+}$ /calmodulin-dependent protein kinase II (CaMKII) activation (353, 369), which engages NF- $\kappa$ B via CamKII-dependent phosphorylation of I $\kappa$ B kinase (IKK) (213). As previously mentioned, NF- $\kappa$ B positively modulates  $TNF\alpha$  expression (50, 294).

We are planning on testing the physiological relevance of this hypothetical model (Figure 3) with the following experiments:

- 1. Establish whether SMC Caveolin-1 (Cav-1) is directly involved in promoting pressure-induced SMC- $TNF\alpha$  expression**

In the Sonkusare laboratory, smooth muscle conditional knockout Caveolin-1 ( $Cav-1_{SMC^{-/-}}$ ) mice have been generated. MAs, isolated from  $Cav-1_{SMC^{-/-}}$  and respectively control (Cre -;  $Cav-1_{SMC^{-/-}}$ ) mice, will be pressurized at 120 mmHg for 4 hours. Following, we will perform RT-PCR, Western blot, and immunostaining for  $TNF\alpha$ . If SMC Cav-1 is a crucial element behind the high pressure-induced SMC- $TNF\alpha$  phenomena, we expect to detect low  $TNF\alpha$  levels in the MAs isolated from  $Cav-1_{SMC^{-/-}}$

**2. Determine whether SMC Piezo1-Sphingomyelin/Ceramide signaling is a critical element of the high pressure-induced SMC-TNF $\alpha$  upregulation phenomena**

In the Sonkusare laboratory, smooth muscle conditional knockout Piezo1 (Piezo1<sub>SMC</sub><sup>-/-</sup>) mice have been generated.

**a. SMC Piezo1 channel:** MAs, isolated from Piezo1<sub>SMC</sub><sup>-/-</sup> and respective control (Cre - ; Piezo1<sub>SMC</sub><sup>-/-</sup>) mice, will be pressurized at 120 mmHg for 4 hours. Following, we will measure TNF $\alpha$  mRNA and protein levels. If SMC Piezo1 channels are directly involved in mediating high pressure-induced SMC-TNF $\alpha$  overexpression, we expect to detect lower TNF $\alpha$  levels in MAs of Piezo1<sub>SMC</sub><sup>-/-</sup> compared to control mice.

**b. Sphingomyelin/Ceramide:** MAs, isolated from Piezo1<sub>SMC</sub><sup>-/-</sup> and control (Cre-; Piezo1<sub>SMC</sub><sup>-/-</sup>) mice, will be pressurized at 120 mmHg for 4 hours in the presence or absence of the N-SMase inhibitor, GW4869 (89) . Following, we will perform RT-PCR, Western Blot, and immunostaining for TNF $\alpha$ . If the conversion of sphingomyelin into ceramide, catalyzed by N-SMase, is essential for enabling Piezo1 channel induced SMC-TNF $\alpha$  expression, we expect to measure low TNF $\alpha$  levels in MAs from control mice incubated with GW4869 compared to untreated MAs from control mice. Moreover, TNF $\alpha$  levels in MAs isolated from Piezo1<sub>SMC</sub><sup>-/-</sup> will be low and not affected by GW4869 treatment. We will then further validate the findings with the use of N-SMase<sup>-/-</sup> mice (196)

**c. Sphingomyelin/Ceramide (rescue experiment):** MAs, isolated from Piezo1<sub>SMC</sub><sup>-/-</sup> and control (Cre-; Piezo1<sub>SMC</sub><sup>-/-</sup>) mice, will be pressurized at 120 mmHg for 4 hours in the presence of the N-SMase inhibitor, GW4869, and in the presence or absence of ceramide. Following, we will

perform RT-PCR, Western Blot, and immunostaining for TNF $\alpha$ . If the conversion of sphingomyelin into ceramide, catalyzed by N-SMase, is essential for enabling Piezo1 channel induced SMC-TNF $\alpha$  expression, we expect that TNF $\alpha$  levels will be higher in MAs of control mice incubated with GW4869+ceramide compared to MAs of control mice incubated with GW4869 only. Moreover, TNF $\alpha$  levels in MAs isolated from Piezo1<sub>SMC</sub><sup>-/-</sup> will be low and not be affected by any pharmacological treatment.

### **3. Establish the physiological relevance of the Cav-1-Piezo1 axis in mediating pressure-induced SMC-TNF $\alpha$ expression**

MAs, isolated from Cav-1<sub>SMC</sub><sup>-/-</sup> mice, will be pressurized at 120 mmHg for 4 hours in the presence or absence of the specific Piezo1 channel agonist Yoda1 (30). Following this, we will measure TNF $\alpha$  mRNA and protein levels. If Cav-1 is a necessary component for Piezo 1 channel-mediated increase in SMC-TNF $\alpha$  expression, we expect to detect high TNF $\alpha$  levels in MAs incubated with Yoda1 compared to the untreated MAs.

The experiments listed above represent essential steps for investigating a possible link between the pressure-dependent increase of extracellular calcium influx into SMC and SMC-TNF $\alpha$  expression. Indeed, many other molecular players that we have not considered or described could also be involved in this process. Notably, Gq protein-coupled receptors (GqPCR) have been posited as another critical signaling pathway that can sense and transduce mechanical stretch (243). Pressure-induced GqPCR activation engages phospholipase C (PLC)-diacylglycerol (DAG) - Inositol-3-phosphate (IP3) signaling pathway, which triggers IP3 receptor-dependent Ca<sup>2+</sup> release from endoplasmic-sarcoplasmic reticulum (ER/SR), and likely Ca<sup>2+</sup> entry via TRPC6 channels (119). Therefore, high pressure-dependent upregulation of SMC-TNF $\alpha$  could be mediated by Ca<sup>2+</sup> entry via TRP channels and SR/ER-dependent Ca<sup>2+</sup> release.

Another critical system is the sympathetic nervous system (SNS) which can largely contribute to an increase in SMC intracellular  $Ca^{2+}$ . Indeed, in obesity, the pathological over activation of the SNS has been well documented (129). Different mechanisms have been proposed to explain this phenomenon (129), which still remains largely unknown. Sympathetic stimulation of alpha 1 adrenergic receptor ( $\alpha 1AR$ ) results in increased SMC-intracellular cytosolic  $Ca^{2+}$  levels via LTCC and IP3R activation (217, 250).  $\alpha 1AR$  activation seems to potentiate  $Ca^{2+}$  influx via LTCC through CaMKII stimulation (162). This body of evidence justifies the hypothesis that in obesity, SNS over-activation increases SMC-intracellular  $Ca^{2+}$  and promotes CaMKII activation. These events could be driving SMC inflammation via  $Ca^{2+}$ -dependent NF- $\kappa$ B activation (208). Future studies using the commercially available transgenic mice expressing the light-sensitive effector protein Opto- $\alpha 1AR$  in smooth muscle cells could shed lights on the possible role played by  $\alpha 1AR$  in mediating SMC inflammation.

Finally, the last important aspect that needs to be considered is the emerging role of the adipose tissue as an essential factor in regulating many pathological processes. Indeed, in obesity, there is a significant expansion of the white adipose tissue known to release adipocytokines which are thought to provide a strong link between obesity and inflammatory processes (195, 418). Leptin is one of the more abundant pro-inflammatory adipocytokines released in obesity (105). Indeed, leptin was shown to promote TNF $\alpha$  expression in immune cells (202). SMC cells are known to express leptin receptors (LEP-R) (330). Significantly, SMC-conditional deletion of leptin receptor rescues endothelial-dependent vasodilation in obesity (315). Resistin is another important pro-inflammatory adipocytokine (362) that has been shown to mediate pathological SMC proliferation (27, 54) and to induce TNF $\alpha$  expression (3, 127) strongly. Recently, Jiang et al. demonstrated an essential role of resistin in mediating hypertension and insulin resistance via toll-like receptor 4

(TLR4) activation (165). Activation of TLR4 stimulates the expression of pro-inflammatory cytokines in arterial human and mouse SMC (440), thereby promoting a pro-inflammatory phenotypic switch in SMC. Indeed, overwhelming evidence demonstrate that adipocytokines, such as leptin and resistin, play a crucial role in mediating pro-inflammatory phenomenon. This support the idea that these cytokines might be also involved in promoting the pathological increase in SMC-  $\text{TNF}\alpha$  expression that we have detected in obesity (Chapter 5).

To conclude, it can clearly be stated that obesity is a multifactorial disease characterized by many different dysfunctional cellular mechanisms. The above-described experiments and short literature review (Figure 3) give a solid base on where to begin looking for critical molecular signaling pathways responsible for increased SMC- $\text{TNF}\alpha$  expression. It is reasonable to expect that multiple mechanisms will be involved at once. Therefore, we will focus our effort on the molecular targets that will appear to be the most relevant for normalizing vascular reactivity and blood pressure. These studies could lead to the discovery of novel druggable targets in obesity-derived microvascular dysfunction.

## Figure 1. NF- $\kappa$ B inhibition prevents NOX1 expression at the MEPs in obesity

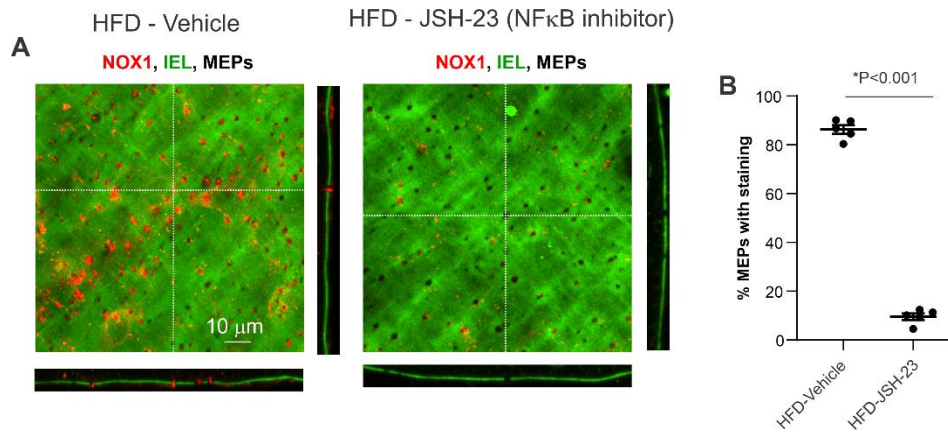


**Figure 1.** A, representative z-stack images of MAs isolated from vehicle-treated HFD (left) and from JSH-23 (5 mg/Kg) treated HFD mice (right). Internal elastic lamina (green); MEPs (Black holes); NOX1 staining (Red). Treatment was administered via intraperitoneal injection once every other day for 15 days. B, scatter plot representing the percentage of MEPs filled with NOX1 staining (Welsh, t-test).

## Figure 2. High-pressure drives increase the expression of smooth muscle TNF $\alpha$

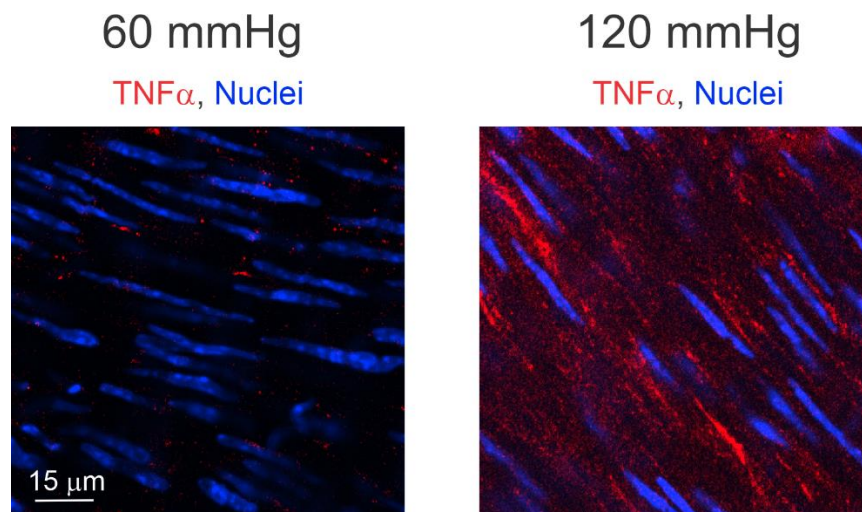
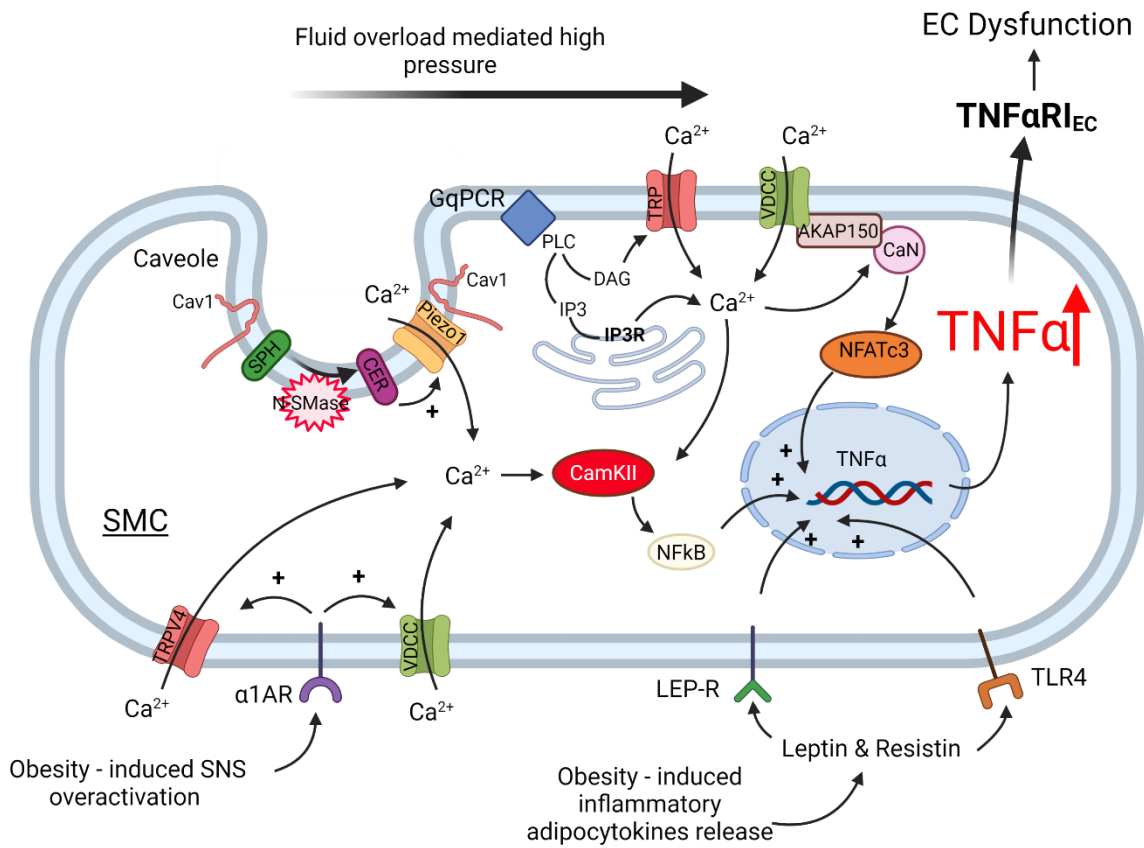


**Figure 2.** Representative immunostaining of the SMC-layer of MAs pressurized for 5 hours at 60 mmHg (left) and at 120 mmHg (right). TNF $\alpha$  staining (red); Nuclei (blue).

**Figure 3. Schematic representing hypothetical molecular mechanisms underlying obesity-induced smooth muscle TNF $\alpha$  expression**



## **Chapter 7: Acknowledgments**

Here I am writing the last page of my Ph.D. thesis work. I feel honored and grateful that life gave me this unique opportunity. At this time, I have many amazing people to thank with open arms. Indeed, words will fall short on describing my feelings towards them like pictures can never do justice to a beautiful panorama.

A deep sense of gratitude goes towards my mentor and guide, Dr. Sonkusare. I would not be here as the person and scientist that I became without him. Our relationship grew stronger with time. Dr. Sonkusare always helped me venture beyond the limits that I was setting up for myself. Indeed, his admirable drive and passion for science have been an incredible aid in moments of difficulties and discomfort. I learned a great deal from him. I will be forever thankful to have encountered him on my life path.

I wish to express many thanks to all the current and former members of the Sonkusare lab. Indeed, science has been done by many and all the work that I have presented in this thesis came to fruition because all of their help and hard work. They have been incredible colleagues and wonderful friends. Thank you guys so much for always being there for me.

A special thanks go to all my committee members, Dr. Brant Isakson, Dr. Thurl Harris, Dr. Paula Barrett, and Dr. Zhen Yan, for all the great insights and suggestions, which improved my scientific acumen and made my work more impactful.

I am thankful to the UVA Pharmacology program for believing in me and giving me a chance to become a UVA Ph.D. student. This changed my life, and so I will be forever grateful.

I do not think I could find any words or sentences that can describe how I feel towards my beloved family. Feelings can only be experienced and felt. The ocean has been between us for several years now, but my love and appreciation for you have only grown stronger. Thank you to the moon and back for all you have done for me.

Last but not least, to all the other people I did not mention here, I met along my life path. A genius once wrote that we meet part of ourselves time and again in other people, I could not agree more.

*“When a summit of life is reached, from the lesser the greater emerges, then the “One becomes two”, and the greater figure, which one always was but which remained invisible, appears to the lesser personality with the force of a revelation”*

C.G. Jung, Collective Work Vol. 9

## **Chapter 8: References**

1. Abdelrahman AM, Al Suleimani YM, Ashique M, Manoj P, Ali BH. Effect of infliximab and tocilizumab on fructose-induced hyperinsulinemia and hypertension in rats. *Biomed Pharmacother* 105: 182-186, 2018.
2. Adapala RK, Talasila PK, Bratz IN, Zhang DX, Suzuki M, Meszaros JG, Thodeti CK. PKC $\alpha$  mediates acetylcholine-induced activation of TRPV4-dependent calcium influx in endothelial cells. *J Biol Chem* 286: H757-765, 2011.
3. Adelman JP, Maylie J and Sah P. Small-conductance Ca $^{2+}$ -activated K $^{+}$  channels: form and function. *Annu Rev Physiol* 74: 245-269, 2012.
4. Aiello LP, Bursell SE, Clermont A, Duh E, Ishii H, Takagi C, Mori F, Ciulla TA, Wachs K, Jirousek M, Smith LE, King GL. Vascular endothelial growth factor-induced retinal permeability is mediated by protein kinase C in vivo and suppressed by an orally effective beta-isoform-selective inhibitor. *Diabetes* 46: 1473-1480, 1997.
5. Alderton WK, Cooper CE and Knowles RG. Nitric oxide synthases: structure, function and inhibition. *Biochem J* 357: 593-615, 2001.
6. Alexander JK, Dennis EW, Smith WG, Amad KH, Duncan WC, Austin RC. Blood volume, cardiac output, and distribution of systemic blood flow in extreme obesity. *Cardiovasc Res Cent Bull* 1: 39-44, 1962.
7. Alvarez DF, King JA, Weber D, Addison E, Liedtke W, Townsley MI. Transient receptor potential vanilloid 4-mediated disruption of the alveolar septal barrier: a novel mechanism of acute lung injury. *Circ Res* 99: 988-995, 2006.
8. Alvarez RA, Miller MP, Hahn SA, Galley JC, Bauer E, Bachman T, Hu J, Sembrat J, Goncharov D, Mora AL, Rojas M, Goncharova E, Straub AC. Targeting Pulmonary Endothelial Hemoglobin  $\alpha$  Improves Nitric Oxide Signaling and Reverses Pulmonary Artery Endothelial Dysfunction. *Am J Respir Cell Mol Biol* 57: 733-744, 2017.
9. Anagnostopoulou A, Camargo LL, Rodrigues D, Montezano AC, Touyz RM. Importance of cholesterol-rich microdomains in the regulation of Nox isoforms and redox signaling in human vascular smooth muscle cells. *Sci Rep* 10: 17818, 2020.
10. Antonopoulos AS, Margaritis M, Coutinho P, Shirodaria C, Psarros C, Herdman L, Sanna F, De Silva R, Petrou M, Sayeed R, Krasopoulos G, Lee R, Digby J, Reilly S, Bakogiannis C, Tousoulis D, Kessler B, Casadei B, Channon KM, Antoniades C. Adiponectin as a link between type 2 diabetes and vascular NADPH oxidase activity in the human arterial wall: the regulatory role of perivascular adipose tissue. *Diabetes* 64: 2207-2219, 2015.
11. Archer SL, Huang JM, Hampf V, Nelson DP, Shultz PJ, Weir EK. Nitric oxide and cGMP cause vasorelaxation by activation of a charybdotoxin-sensitive K channel by cGMP-dependent protein kinase. *Proc Natl Acad Sci U S A* 91: 7583-7587, 1994.
12. Artamonov MV, Sonkusare SK, Good ME, Momotani K, Eto M, Isakson BE, Le TH, Cope EL, Derewenda ZS, Derewenda U, Somlyo AV. RSK2 contributes to myogenic vasoconstriction of resistance arteries by activating smooth muscle myosin and the Na $^{+}$ /H $^{+}$  exchanger. *Sci Signal* 11: 2018.
13. Atcha H, Jairaman A, Holt JR, Meli VS, Nagalla RR, Veerasubramanian PK, Brumm KT, Lim HE, Othy S, Cahalan MD, Pathak MM, Liu WF. Mechanically activated ion channel Piezo1 modulates macrophage polarization and stiffness sensing. *Nat Commun* 12: 3256, 2021.
14. Bagher P, Beleznaï T, Kansui Y, Mitchell R, Garland CJ, Dora KA. Low intravascular pressure activates endothelial cell TRPV4 channels, local Ca $^{2+}$  events, and IKCa channels, reducing arteriolar tone. *Proc Natl Acad Sci U S A* 109: 18174-18179, 2012.
15. Bagher P, Davis MJ and Segal SS. Visualizing calcium responses to acetylcholine convection along endothelium of arteriolar networks in Cx40BAC-GCaMP2 transgenic mice. *Am J Physiol Heart Circ Physiol* 301: H794-802, 2011.
16. Bayliss WM. On the local reactions of the arterial wall to changes of internal pressure. *J Physiol* 28: 220-231, 1902.

17. Bereta J, Bereta M, Allison AC, Kruger PB, Koj A. Inhibitory effect of di-catechol rooperol on VCAM-1 and iNOS expression in cytokine-stimulated endothelium. *Life Sci* 60: 325-334, 1997.
18. Berg AH and Scherer PE. Adipose tissue, inflammation, and cardiovascular disease. *Circ Res* 96: 939-949, 2005.
19. Bernatchez PN, Bauer PM, Yu J, Prendergast JS, He P, Sessa WC. Dissecting the molecular control of endothelial NO synthase by caveolin-1 using cell-permeable peptides. *Proc Natl Acad Sci U S A* 102: 761-766, 2005.
20. Berridge MJ, Lipp P and Bootman MD. The versatility and universality of calcium signalling. *Nat Rev Mol Cell Biol* 1: 11-21, 2000.
21. Beyer AM and Gutterman DD. Regulation of the human coronary microcirculation. *J Mol Cell Cardiol* 52: 814-821, 2012.
22. Beyer EC and Berthoud VM. Gap junction structure: unraveled, but not fully revealed. *F1000Res* 6: 568, 2017.
23. Bilsborough W, O'Driscoll G, Stanton K, Weerasooriya R, Dembo L, Taylor R, Green D. Effect of lowering tumour necrosis factor-alpha on vascular endothelial function in Type II diabetes. *Clin Sci (Lond)* 103: 163-169, 2002.
24. Biwer LA, Good ME, Hong K, Patel RK, Agrawal N, Looft-Wilson R, Sonkusare SK, Isakson BE. Non-Endoplasmic Reticulum-Based Calr (Calreticulin) Can Coordinate Heterocellular Calcium Signaling and Vascular Function. *Arterioscler Thromb Vasc Biol* 38: 120-130, 2018.
25. Blue EK, Goeckeler ZM, Jin Y, Hou L, Dixon SA, Herring BP, Wysolmerski RB, Gallagher PJ. 220- and 130-kDa MLCKs have distinct tissue distributions and intracellular localization patterns. *Am J Physiol Cell Physiol* 282: C451-460, 2002.
26. Boettcher M and de Wit C. Distinct endothelium-derived hyperpolarizing factors emerge in vitro and in vivo and are mediated in part via connexin 40-dependent myoendothelial coupling. *Hypertension* 57: 802-808, 2011.
27. Boettger T, Beetz N, Kostin S, Schneider J, Kruger M, Hein L, Braun T. Acquisition of the contractile phenotype by murine arterial smooth muscle cells depends on the Mir143/145 gene cluster. *J Clin Invest* 119: 2634-2647, 2009.
28. Bogdan C. Nitric oxide synthase in innate and adaptive immunity: an update. *Trends Immunol* 36: 161-178, 2015.
29. Bolotina VM, Najibi S, Palacino JJ, Pagano PJ, Cohen RA. Nitric oxide directly activates calcium-dependent potassium channels in vascular smooth muscle. *Nature* 368: 850-853, 1994.
30. Botello-Smith WM, Jiang W, Zhang H, Ozkan AD, Lin YC, Pham CN, Lacroix JJ, Luo Y. A mechanism for the activation of the mechanosensitive Piezo1 channel by the small molecule Yoda1. *Nat Commun* 10: 4503, 2019.
31. Bratz IN, Dick GM, Tune JD, Edwards JM, Neeb ZP, Dincer UD, Sturek M. Impaired capsaicin-induced relaxation of coronary arteries in a porcine model of the metabolic syndrome. *Am J Physiol Heart Circ Physiol* 294: H2489-2496, 2008.
32. Brodsky SV, Gealekman O, Chen J, Zhang F, Togashi N, Crabtree M, Gross SS, Nasjletti A, Goligorsky MS. Prevention and reversal of premature endothelial cell senescence and vasculopathy in obesity-induced diabetes by ebselen. *Circ Res* 94: 377-384, 2004.
33. Brzezinska AK, Gebremedhin D, Chilian WM, Kalyanaraman B, Elliott SJ. Peroxynitrite reversibly inhibits Ca(2+)-activated K(+) channels in rat cerebral artery smooth muscle cells. *Am J Physiol Heart Circ Physiol* 278: H1883-1890, 2000.
34. Burnham MP, Bychkov R, Feletou M, Richards GR, Vanhoutte PM, Weston AH, Edwards G. Characterization of an apamin-sensitive small-conductance Ca(2+)-activated K(+) channel in porcine coronary artery endothelium: relevance to EDHF. *Br J Pharmacol* 135: 1133-1143, 2002.
35. Busse R and Mulsch A. Calcium-dependent nitric oxide synthesis in endothelial cytosol is mediated by calmodulin. *FEBS Lett* 265: 133-136, 1990.

36. Buus NH, VanBavel E and Mulvany MJ. Differences in sensitivity of rat mesenteric small arteries to agonists when studied as ring preparations or as cannulated preparations. *Br J Pharmacol* 112: 579-587, 1994.
37. Bychkov R, Burnham MP, Richards GR, Edwards G, Weston AH, Feletou M, Vanhoutte PM. Characterization of a charybdotoxin-sensitive intermediate conductance Ca<sup>2+</sup>-activated K<sup>+</sup> channel in porcine coronary endothelium: relevance to EDHF. *Br J Pharmacol* 137: 1346-1354, 2002.
38. Campia U, Tesauro M and Cardillo C. Human obesity and endothelium-dependent responsiveness. *Br J Pharmacol* 165: 561-573, 2012.
39. Candela J, Wang R and White C. Microvascular Endothelial Dysfunction in Obesity Is Driven by Macrophage-Dependent Hydrogen Sulfide Depletion. *Arterioscler Thromb Vasc Biol* 37: 889-899, 2017.
40. Cardey B, Foley S and Enescu M. Mechanism of thiol oxidation by the superoxide radical. *J Phys Chem A* 111: 13046-13052, 2007.
41. Carvajal JA, Germain AM, Huidobro-Toro JP, Weiner CP. Molecular mechanism of cGMP-mediated smooth muscle relaxation. *J Cell Physiol* 184: 409-420, 2000.
42. Cassuto J, Dou H, Czikora I, Szabo A, Patel VS, Kamath V, Belin de Chantemele E, Feher A, Romero MJ, Bagi Z. Peroxynitrite disrupts endothelial caveolae leading to eNOS uncoupling and diminished flow-mediated dilation in coronary arterioles of diabetic patients. *Diabetes* 63: 1381-1393, 2014.
43. Castagna M, Takai Y, Kaibuchi K, Sano K, Kikkawa U, Nishizuka Y. Direct activation of calcium-activated, phospholipid-dependent protein kinase by tumor-promoting phorbol esters. *J Biol Chem* 257: 7847-7851, 1982.
44. Caterina MJ, Schumacher MA, Tominaga M, Rosen TA, Levine JD, Julius D. The capsaicin receptor: a heat-activated ion channel in the pain pathway. *Nature* 389: 816-824, 1997.
45. Cavanaugh DJ, Chesler AT, Jackson AC, Sigal YM, Yamanaka H, Grant R, O'Donnell D, Nicoll RA, Shah NM, Julius D, Basbaum AI. Trpv1 reporter mice reveal highly restricted brain distribution and functional expression in arteriolar smooth muscle cells. *J Neurosci* 31: 5067-5077, 2011.
46. Chen CA, De Pascali F, Basye A, Hemann C, Zweier JL. Redox modulation of endothelial nitric oxide synthase by glutaredoxin-1 through reversible oxidative post-translational modification. *Biochemistry* 52: 6712-6723, 2013.
47. Chen CA, Wang TY, Varadharaj S, Reyes LA, Hemann C, Talukder MA, Chen YR, Druhan LJ, Zweier JL. S-glutathionylation uncouples eNOS and regulates its cellular and vascular function. *Nature* 468: 1115-1118, 2010.
48. Chen F, Kumar S, Yu Y, Aggarwal S, Gross C, Wang Y, Chakraborty T, Verin AD, Catravas JD, Lucas R, Black SM, Fulton DJ. PKC-dependent phosphorylation of eNOS at T495 regulates eNOS coupling and endothelial barrier function in response to G<sup>+</sup>-toxins. *PLoS One* 9: e99823, 2014.
49. Chen L, Deng H, Cui H, Fang J, Zuo Z, Deng J, Li Y, Wang X, Zhao L. Inflammatory responses and inflammation-associated diseases in organs. *Oncotarget* 9: 7204-7218, 2018.
50. Chen LW, Egan L, Li ZW, Greten FR, Kagnoff MF, Karin M. The two faces of IKK and NF-kappaB inhibition: prevention of systemic inflammation but increased local injury following intestinal ischemia-reperfusion. *Nat Med* 9: 575-581, 2003.
51. Chen YL and Sonkusare SK. Endothelial TRPV4 channels and vasodilator reactivity. *Curr Top Membr* 85: 89-117, 2020.
52. Chen Z, S DSO, Zimnicka AM, Jiang Y, Sharma T, Chen S, Lazarov O, Bonini MG, Haus JM, Minshall RD. Reciprocal regulation of eNOS and caveolin-1 functions in endothelial cells. *Mol Biol Cell* 29: 1190-1202, 2018.

53. Chidgey J, Fraser PA and Aaronson PI. Reactive oxygen species facilitate the EDH response in arterioles by potentiating intracellular endothelial Ca(2+) release. *Free Radic Biol Med* 97: 274-284, 2016.
54. Cho Y, Lee SE, Lee HC, Hur J, Lee S, Youn SW, Lee J, Lee HJ, Lee TK, Park J, Hwang SJ, Kwon YW, Cho HJ, Oh BH, Park YB, Kim HS. Adipokine resistin is a key player to modulate monocytes, endothelial cells, and smooth muscle cells, leading to progression of atherosclerosis in rabbit carotid artery. *J Am Coll Cardiol* 57: 99-109, 2011.
55. Cohen RA, Weisbrod RM, Gericke M, Yaghoubi M, Bierl C, Bolotina VM. Mechanism of nitric oxide-induced vasodilatation: refilling of intracellular stores by sarcoplasmic reticulum Ca2+ ATPase and inhibition of store-operated Ca2+ influx. *Circ Res* 84: 210-219, 1999.
56. Collier DM, Villalba N, Sackheim A, Bonev AD, Miller ZD, Moore JS, Shui B, Lee JC, Lee FK, Reining S, Kotlikoff MI, Nelson MT, Freeman K. Extracellular histones induce calcium signals in the endothelium of resistance-sized mesenteric arteries and cause loss of endothelium-dependent dilation. *Am J Physiol Heart Circ Physiol* 316: H1309-H1322, 2019.
57. Conti MA and Adelstein RS. The relationship between calmodulin binding and phosphorylation of smooth muscle myosin kinase by the catalytic subunit of 3':5' cAMP-dependent protein kinase. *J Biol Chem* 256: 3178-3181, 1981.
58. Cortese-Krott MM, Kulakov L, Oplander C, Kolb-Bachofen V, Kroncke KD, Suschek CV. Zinc regulates iNOS-derived nitric oxide formation in endothelial cells. *Redox Biol* 2: 945-954, 2014.
59. Coste B, Mathur J, Schmidt M, Earley TJ, Ranade S, Petrus MJ, Dubin AE, Patapoutian A. Piezo1 and Piezo2 are essential components of distinct mechanically activated cation channels. *Science* 330: 55-60, 2010.
60. Coste B, Xiao B, Santos JS, Syeda R, Grandl J, Spencer KS, Kim SE, Schmidt M, Mathur J, Dubin AE, Montal M, Patapoutian A. Piezo proteins are pore-forming subunits of mechanically activated channels. *Nature* 483: 176-181, 2012.
61. Couchonnal LF and Anderson ME. The role of calmodulin kinase II in myocardial physiology and disease. *Physiology (Bethesda)* 23: 151-159, 2008.
62. Czarny M, Liu J, Oh P, Schnitzer JE. Transient mechanoactivation of neutral sphingomyelinase in caveolae to generate ceramide. *J Biol Chem* 278: 4424-4430, 2003.
63. Daneva Z, Marziano C, Ottolini M, Chen YL, Baker TM, Kuppusamy M, Zhang A, Ta HQ, Reagan CE, Mihalek AD, Kasetti RB, Shen Y, Isakson BE, Minshall RD, Zode GS, Goncharova EA, Laubach VE, Sonkusare SK. Caveolar peroxynitrite formation impairs endothelial TRPV4 channels and elevates pulmonary arterial pressure in pulmonary hypertension. *Proc Natl Acad Sci U S A* 118: 2021.
64. Darby WG, Potocnik S, Ramachandran R, Hollenberg MD, Woodman OL, McIntyre P. Shear stress sensitizes TRPV4 in endothelium-dependent vasodilatation. *Pharmacol Res* 133: 152-159, 2018.
65. Davis MJ and Hill MA. Signaling mechanisms underlying the vascular myogenic response. *Physiol Rev* 79: 387-423, 1999.
66. Dell'Acqua ML and Scott JD. Protein kinase A anchoring. *J Biol Chem* 272: 12881-12884, 1997.
67. DeMarco VG, Aror AR and Sowers JR. The pathophysiology of hypertension in patients with obesity. *Nat Rev Endocrinol* 10: 364-376, 2014.
68. Deng Z, Paknejad N, Maksaev G, Sala-Rabanal M, Nichols CG, Hite RK, Yuan P. Cryo-EM and X-ray structures of TRPV4 reveal insight into ion permeation and gating mechanisms. *Nat Struct Mol Biol* 25: 252-260, 2018.
69. Denninger JW and Marletta MA. Guanylate cyclase and the .NO/cGMP signaling pathway. *Biochim Biophys Acta* 1411: 334-350, 1999.

70. Desai RJ, Solomon DH, Schneeweiss S, Danaei G, Liao KP, Kim SC. Tumor Necrosis Factor-alpha Inhibitor Use and the Risk of Incident Hypertension in Patients with Rheumatoid Arthritis. *Epidemiology* 27: 414-422, 2016.
71. Dessy C, Feron O and Balligand JL. The regulation of endothelial nitric oxide synthase by caveolin: a paradigm validated in vivo and shared by the 'endothelium-derived hyperpolarizing factor'. *Pflugers Arch* 459: 817-827, 2010.
72. Di Virgilio F, Steinberg TH and Silverstein SC. Organic-anion transport inhibitors to facilitate measurement of cytosolic free Ca<sup>2+</sup> with fura-2. *Methods Cell Biol* 31: 453-462, 1989.
73. Dominguez H, Storgaard H, Rask-Madsen C, Steffen Hermann T, Ihlemann N, Baunbjerg Nielsen D, Spohr C, Kober L, Vaag A, Torp-Pedersen C. Metabolic and vascular effects of tumor necrosis factor-alpha blockade with etanercept in obese patients with type 2 diabetes. *J Vasc Res* 42: 517-525, 2005.
74. Dong J, Jimi E, Zeiss C, Hayden MS, Ghosh S. Constitutively active NF-kappaB triggers systemic TNFalpha-dependent inflammation and localized TNFalpha-independent inflammatory disease. *Genes Dev* 24: 1709-1717, 2010.
75. Dora KA, Doyle MP and Duling BR. Elevation of intracellular calcium in smooth muscle causes endothelial cell generation of NO in arterioles. *Proc Natl Acad Sci U S A* 94: 6529-6534, 1997.
76. Dora KA, Sandow SL, Gallagher NT, Takano H, Rummery NM, Hill CE, Garland CJ. Myoendothelial gap junctions may provide the pathway for EDHF in mouse mesenteric artery. *Journal of Vascular Research* 40: 480-490, 2003.
77. Dora KA, Sandow SL, Gallagher NT, Takano H, Rummery NM, Hill CE, Garland CJ. Myoendothelial gap junctions may provide the pathway for EDHF in mouse mesenteric artery. *J Vasc Res* 40: 480-490, 2003.
78. Douguet D, Patel A, Xu A, Vanhoutte PM, Honore E. Piezo Ion Channels in Cardiovascular Mechanobiology. *Trends Pharmacol Sci* 40: 956-970, 2019.
79. Drummond GR and Sobey CG. Endothelial NADPH oxidases: which NOX to target in vascular disease? *Trends Endocrinol Metab* 25: 452-463, 2014.
80. Dudek SM and Garcia JG. Cytoskeletal regulation of pulmonary vascular permeability. *J Appl Physiol (1985)* 91: 1487-1500, 2001.
81. Earley S. TRPA1 channels in the vasculature. *Br J Pharmacol* 167: 13-22, 2012.
82. Earley S, Gonzales AL and Crnich R. Endothelium-dependent cerebral artery dilation mediated by TRPA1 and Ca<sup>2+</sup>-Activated K<sup>+</sup> channels. *Circ Res* 104: 987-994, 2009.
83. Earley S, Gonzales AL and Garcia ZI. A dietary agonist of transient receptor potential cation channel V3 elicits endothelium-dependent vasodilation. *Mol Pharmacol* 77: 612-620, 2010.
84. Earley S, Heppner TJ, Nelson MT, Brayden JE. TRPV4 forms a novel Ca<sup>2+</sup> signaling complex with ryanodine receptors and BKCa channels. *Circ Res* 97: 1270-1279, 2005.
85. Earley S, Pauyo T, Drapp R, Tavares MJ, Liedtke W, Brayden JE. TRPV4-dependent dilation of peripheral resistance arteries influences arterial pressure. *Am J Physiol Heart Circ Physiol* 297: H1096-1102, 2009.
86. Ellinsworth DC, Sandow SL, Shukla N, Liu Y, Jeremy JY, Gutterman DD. Endothelium-Derived Hyperpolarization and Coronary Vasodilation: Diverse and Integrated Roles of Epoxyeicosatrienoic Acids, Hydrogen Peroxide, and Gap Junctions. *Microcirculation* 23: 15-32, 2016.
87. Emerson GG and Segal SS. Electrical coupling between endothelial cells and smooth muscle cells in hamster feed arteries: role in vasomotor control. *Circ Res* 87: 474-479, 2000.
88. Emerson GG and Segal SS. Endothelial cell pathway for conduction of hyperpolarization and vasodilation along hamster feed artery. *Circ Res* 86: 94-100, 2000.

89. Essandoh K, Yang L, Wang X, Huang W, Qin D, Hao J, Wang Y, Zingarelli B, Peng T, Fan GC. Blockade of exosome generation with GW4869 dampens the sepsis-induced inflammation and cardiac dysfunction. *Biochim Biophys Acta* 1852: 2362-2371, 2015.
90. Fagan KA, Fouty BW, Tyler RC, Morris KG, Jr., Hepler LK, Sato K, LeCras TD, Abman SH, Weinberger HD, Huang PL, McMurtry IF, Rodman DM. The pulmonary circulation of homozygous or heterozygous eNOS-null mice is hyperresponsive to mild hypoxia. *J Clin Invest* 103: 291-299, 1999.
91. Fakler B and Adelman JP. Control of K(Ca) channels by calcium nano/microdomains. *Neuron* 59: 873-881, 2008.
92. Falloon BJ, Stephens N, Tulip JR, Heagerty AM. Comparison of small artery sensitivity and morphology in pressurized and wire-mounted preparations. *Am J Physiol* 268: H670-678, 1995.
93. Fan HC, Zhang X and McNaughton PA. Activation of the TRPV4 ion channel is enhanced by phosphorylation. *J Biol Chem* 284: 27884-27891, 2009.
94. Fanger CM, Ghanshani S, Logsdon NJ, Rauer H, Kalman K, Zhou J, Beckingham K, Chandy KG, Cahalan MD, Aiyar J. Calmodulin mediates calcium-dependent activation of the intermediate conductance KCa channel, IKCa1. *J Biol Chem* 274: 5746-5754, 1999.
95. Faulkner JL and Belin de Chantemele EJ. Sex Differences in Mechanisms of Hypertension Associated With Obesity. *Hypertension* 71: 15-21, 2018.
96. Faux MC, Rollins EN, Edwards AS, Langeberg LK, Newton AC, Scott JD. Mechanism of A-kinase-anchoring protein 79 (AKAP79) and protein kinase C interaction. *Biochem J* 343 Pt 2: 443-452, 1999.
97. Febbraio MA. Role of interleukins in obesity: implications for metabolic disease. *Trends Endocrinol Metab* 25: 312-319, 2014.
98. Feletou M. Calcium-activated potassium channels and endothelial dysfunction: therapeutic options? *Br J Pharmacol* 156: 545-562, 2009.
99. Fischer R, Kontermann RE and Pfizenmaier K. Selective Targeting of TNF Receptors as a Novel Therapeutic Approach. *Front Cell Dev Biol* 8: 401, 2020.
100. Fisslthaler B, Loot AE, Mohamed A, Busse R, Fleming I. Inhibition of endothelial nitric oxide synthase activity by proline-rich tyrosine kinase 2 in response to fluid shear stress and insulin. *Circ Res* 102: 1520-1528, 2008.
101. Fleming I. Molecular mechanisms underlying the activation of eNOS. *Pflugers Arch* 459: 793-806, 2010.
102. Fontaine V, Mohand-Said S, Hanoteau N, Fuchs C, Pfizenmaier K, Eisel U. Neurodegenerative and neuroprotective effects of tumor Necrosis factor (TNF) in retinal ischemia: opposite roles of TNF receptor 1 and TNF receptor 2. *J Neurosci* 22: RC216, 2002.
103. Forstermann U and Munzel T. Endothelial nitric oxide synthase in vascular disease: from marvel to menace. *Circulation* 113: 1708-1714, 2006.
104. Forstermann U and Sessa WC. Nitric oxide synthases: regulation and function. *Eur Heart J* 33: 829-837, 837a-837d, 2012.
105. Friedman JM and Halaas JL. Leptin and the regulation of body weight in mammals. *Nature* 395: 763-770, 1998.
106. Fulton D, Church JE, Ruan L, Li C, Sood SG, Kemp BE, Jennings IG, Venema RC. Src kinase activates endothelial nitric-oxide synthase by phosphorylating Tyr-83. *J Biol Chem* 280: 35943-35952, 2005.
107. Fulton D, Fontana J, Sowa G, Gratton JP, Lin M, Li KX, Michell B, Kemp BE, Rodman D, Sessa WC. Localization of endothelial nitric-oxide synthase phosphorylated on serine 1179 and nitric oxide in Golgi and plasma membrane defines the existence of two pools of active enzyme. *J Biol Chem* 277: 4277-4284, 2002.
108. Furchgott RF and Vanhoutte PM. Endothelium-derived relaxing and contracting factors. *FASEB J* 3: 2007-2018, 1989.

109. Furchgott RF and Zawadzki JV. The obligatory role of endothelial cells in the relaxation of arterial smooth muscle by acetylcholine. *Nature* 288: 373-376, 1980.
110. Gallagher PJ and Herring BP. The carboxyl terminus of the smooth muscle myosin light chain kinase is expressed as an independent protein, telokin. *J Biol Chem* 266: 23945-23952, 1991.
111. Gao X, Belmadani S, Picchi A, Xu X, Potter BJ, Tewari-Singh N, Capobianco S, Chilian WM, Zhang C. Tumor necrosis factor-alpha induces endothelial dysfunction in Lepr(db) mice. *Circulation* 115: 245-254, 2007.
112. Garland CJ, Bagher P, Powell C, Ye X, Lemmey HAL, Borysova L, Dora KA. Voltage-dependent Ca(2+) entry into smooth muscle during contraction promotes endothelium-mediated feedback vasodilation in arterioles. *Sci Signal* 10: 2017.
113. Ge J, Li W, Zhao Q, Li N, Chen M, Zhi P, Li R, Gao N, Xiao B, Yang M. Architecture of the mammalian mechanosensitive Piezo1 channel. *Nature* 527: 64-69, 2015.
114. Gil-Ortega M, Stucchi P, Guzman-Ruiz R, Cano V, Arribas S, Gonzalez MC, Ruiz-Gayo M, Fernandez-Alfonso MS, Somoza B. Adaptive nitric oxide overproduction in perivascular adipose tissue during early diet-induced obesity. *Endocrinology* 151: 3299-3306, 2010.
115. Girardin NC, Antigny F and Frieden M. Electrophysiological characterization of store-operated and agonist-induced Ca<sup>2+</sup> entry pathways in endothelial cells. *Pflugers Arch* 460: 109-120, 2010.
116. Glass R, Townsend-Nicholson A and Burnstock G. P2 receptors in the thymus: expression of P2X and P2Y receptors in adult rats, an immunohistochemical and in situ hybridisation study. *Cell Tissue Res* 300: 295-306, 2000.
117. Goedicke-Fritz S, Kaistha A, Kacik M, Markert S, Hofmeister A, Busch C, Banfer S, Jacob R, Grgic I, Hoyer J. Evidence for functional and dynamic microcompartmentation of Cav-1/TRPV4/K(Ca) in caveolae of endothelial cells. *Eur J Cell Biol* 94: 391-400, 2015.
118. Gonzales AL, Amberg GC and Earley S. Ca<sup>2+</sup> release from the sarcoplasmic reticulum is required for sustained TRPM4 activity in cerebral artery smooth muscle cells. *Am J Physiol Cell Physiol* 299: C279-288, 2010.
119. Gonzales AL, Yang Y, Sullivan MN, Sanders L, Dabertrand F, Hill-Eubanks DC, Nelson MT, Earley S. A PLCgamma1-dependent, force-sensitive signaling network in the myogenic constriction of cerebral arteries. *Sci Signal* 7: ra49, 2014.
120. Gonzalez Bosc LV, Wilkerson MK, Bradley KN, Eckman DM, Hill-Eubanks DC, Nelson MT. Intraluminal pressure is a stimulus for NFATc3 nuclear accumulation: role of calcium, endothelium-derived nitric oxide, and cGMP-dependent protein kinase. *J Biol Chem* 279: 10702-10709, 2004.
121. Goto Y, Miura M and Iijima T. Extrusion mechanisms of intracellular Ca<sup>2+</sup> in human aortic endothelial cells. *Eur J Pharmacol* 314: 185-192, 1996.
122. Govers R, van der Sluijs P, van Donselaar E, Slot JW, Rabelink TJ. Endothelial nitric oxide synthase and its negative regulator caveolin-1 localize to distinct perinuclear organelles. *J Histochem Cytochem* 50: 779-788, 2002.
123. Goy C, Czypiorski P, Altschmied J, Jakob S, Rabanter LL, Brewer AC, Ale-Agha N, Dyballa-Rukes N, Shah AM, Haendeler J. The imbalanced redox status in senescent endothelial cells is due to dysregulated Thioredoxin-1 and NADPH oxidase 4. *Exp Gerontol* 56: 45-52, 2014.
124. Grayson TH, Chadha PS, Bertrand PP, Chen H, Morris MJ, Senadheera S, Murphy TV, Sandow SL. Increased caveolae density and caveolin-1 expression accompany impaired NO-mediated vasorelaxation in diet-induced obesity. *Histochem Cell Biol* 139: 309-321, 2013.
125. Greenberg HZE, Carlton-Carew SRE, Khan DM, Zargaran AK, Jahan KS, Vanessa Ho WS, Albert AP. Heteromeric TRPV4/TRPC1 channels mediate calcium-sensing receptor-induced nitric oxide production and vasorelaxation in rabbit mesenteric arteries. *Vascul Pharmacol* 96-98: 53-62, 2017.

126. Greenstein AS, Kadir S, Csato V, Sugden SA, Baylie RA, Eisner DA, Nelson MT. Disruption of Pressure-Induced Ca(2+) Spark Vasoregulation of Resistance Arteries, Rather Than Endothelial Dysfunction, Underlies Obesity-Related Hypertension. *Hypertension* 75: 539-548, 2020.
127. Greenstein AS, Khavandi K, Withers SB, Sonoyama K, Clancy O, Jeziorska M, Laing I, Yates AP, Pemberton PW, Malik RA, Heagerty AM. Local inflammation and hypoxia abolish the protective anticontractile properties of perivascular fat in obese patients. *Circulation* 119: 1661-1670, 2009.
128. Grynkiewicz G, Poenie M and Tsien RY. A new generation of Ca<sup>2+</sup> indicators with greatly improved fluorescence properties. *J Biol Chem* 260: 3440-3450, 1985.
129. Guarino D, Nannipieri M, Iervasi G, Taddei S, Bruno RM. The Role of the Autonomic Nervous System in the Pathophysiology of Obesity. *Front Physiol* 8: 665, 2017.
130. Gururaja TL, Yung S, Ding R, Huang J, Zhou X, McLaughlin J, Daniel-Issakani S, Singh R, Cooper RD, Payan DG, Masuda ES, Kinoshita T. A class of small molecules that inhibit TNF $\alpha$ -induced survival and death pathways via prevention of interactions between TNF $\alpha$ RI, TRADD, and RIP1. *Chem Biol* 14: 1105-1118, 2007.
131. Haddock RE, Grayson TH, Brackenbury TD, Meaney KR, Neylon CB, Sandow SL, Hill CE. Endothelial coordination of cerebral vasomotion via myoendothelial gap junctions containing connexins 37 and 40. *Am J Physiol Heart Circ Physiol* 291: H2047-2056, 2006.
132. Hadri L, Bobe R, Kawase Y, Ladage D, Ishikawa K, Atassi F, Lebeche D, Kranias EG, Leopold JA, Lompre AM, Lipskaia L, Hajjar RJ. SERCA2a gene transfer enhances eNOS expression and activity in endothelial cells. *Mol Ther* 18: 1284-1292, 2010.
133. Hall JE, do Carmo JM, da Silva AA, Wang Z, Hall ME. Obesity-induced hypertension: interaction of neurohumoral and renal mechanisms. *Circ Res* 116: 991-1006, 2015.
134. Hannah RM, Dunn KM, Bonev AD, Nelson MT. Endothelial SK(Ca) and IK(Ca) channels regulate brain parenchymal arteriolar diameter and cortical cerebral blood flow. *J Cereb Blood Flow Metab* 31: 1175-1186, 2011.
135. Hanschmann EM, Godoy JR, Berndt C, Hudemann C, Lillig CH. Thioredoxins, glutaredoxins, and peroxiredoxins--molecular mechanisms and health significance: from cofactors to antioxidants to redox signaling. *Antioxid Redox Signal* 19: 1539-1605, 2013.
136. Harraz OF, Longden TA, Hill-Eubanks D, Nelson MT. PIP2 depletion promotes TRPV4 channel activity in mouse brain capillary endothelial cells. *Elife* 7: 2018.
137. Harrington LS, Evans RJ, Wray J, Norling L, Swales KE, Vial C, Ali F, Carrier MJ, Mitchell JA. Purinergic 2X1 receptors mediate endothelial dependent vasodilation to ATP. *Molecular pharmacology* 72: 1132-1136, 2007.
138. Harrington LS and Mitchell JA. Novel role for P2X receptor activation in endothelium-dependent vasodilation. *Br J Pharmacol* 143: 611-617, 2004.
139. Hartmannsgruber V, Heyken WT, Kacik M, Kaistha A, Grgic I, Harteneck C, Liedtke W, Hoyer J, Kohler R. Arterial response to shear stress critically depends on endothelial TRPV4 expression. *PLoS One* 2: e827, 2007.
140. He Y, Lu L, Wei X, Jin D, Qian T, Yu A, Sun J, Cui J, Yang Z. The multimerization and secretion of adiponectin are regulated by TNF- $\alpha$ . *Endocrine* 51: 456-468, 2016.
141. Heathcote HR, Lee MD, Zhang X, Saunter CD, Wilson C, McCarron JG. Endothelial TRPV4 channels modulate vascular tone by Ca(2+) -induced Ca(2+) release at inositol 1,4,5-trisphosphate receptors. *Br J Pharmacol* 176: 3297-3317, 2019.
142. Hein TW and Kuo L. cAMP-independent dilation of coronary arterioles to adenosine : role of nitric oxide, G proteins, and K(ATP) channels. *Circ Res* 85: 634-642, 1999.
143. Heiss EH and Dirsch VM. Regulation of eNOS enzyme activity by posttranslational modification. *Curr Pharm Des* 20: 3503-3513, 2014.

144. Herring BP, El-Mounayri O, Gallagher PJ, Yin F, Zhou J. Regulation of myosin light chain kinase and telokin expression in smooth muscle tissues. *Am J Physiol Cell Physiol* 291: C817-827, 2006.
145. Hirschberg B, Maylie J, Adelman JP, Marrion NV. Gating of recombinant small-conductance Ca-activated K<sup>+</sup> channels by calcium. *J Gen Physiol* 111: 565-581, 1998.
146. Homme RP, Sandhu HS, George AK, Tyagi SC, Singh M. Sustained Inhibition of NF-kappaB Activity Mitigates Retinal Vasculopathy in Diabetes. *Am J Pathol* 191: 947-964, 2021.
147. Hong K, Cope EL, DeLalio LJ, Marziano C, Isakson BE, Sonkusare SK. TRPV4 (Transient Receptor Potential Vanilloid 4) Channel-Dependent Negative Feedback Mechanism Regulates Gq Protein-Coupled Receptor-Induced Vasoconstriction. *Arterioscler Thromb Vasc Biol* 38: 542-554, 2018.
148. Hotamisligil GS, Arner P, Caro JF, Atkinson RL, Spiegelman BM. Increased adipose tissue expression of tumor necrosis factor-alpha in human obesity and insulin resistance. *J Clin Invest* 95: 2409-2415, 1995.
149. House C and Kemp BE. Protein kinase C contains a pseudosubstrate prototope in its regulatory domain. *Science* 238: 1726-1728, 1987.
150. House C and Kemp BE. Protein kinase C pseudosubstrate prototope: structure-function relationships. *Cell Signal* 2: 187-190, 1990.
151. Hu L, He F, Huang M, Peng M, Zhou Z, Liu F, Dai YS. NFATc3 deficiency reduces the classical activation of adipose tissue macrophages. *J Mol Endocrinol* 61: 79-89, 2018.
152. Huang Q, Xu W, Ustinova E, Wu M, Childs E, Hunter F, Yuan S. Myosin light chain kinase-dependent microvascular hyperpermeability in thermal injury. *Shock* 20: 363-368, 2003.
153. Ignarro LJ. Biosynthesis and metabolism of endothelium-derived nitric oxide. *Annu Rev Pharmacol Toxicol* 30: 535-560, 1990.
154. Ignarro LJ. Signal transduction mechanisms involving nitric oxide. *Biochem Pharmacol* 41: 485-490, 1991.
155. Ignarro LJ, Buga GM, Wood KS, Byrns RE, Chaudhuri G. Endothelium-derived relaxing factor produced and released from artery and vein is nitric oxide. *Proc Natl Acad Sci U S A* 84: 9265-9269, 1987.
156. Ikebe M, Maruta S and Reardon S. Location of the inhibitory region of smooth muscle myosin light chain kinase. *J Biol Chem* 264: 6967-6971, 1989.
157. Ikeda S, Matsushima S, Okabe K, Ikeda M, Ishikita A, Tadokoro T, Enzan N, Yamamoto T, Sada M, Deguchi H, Morimoto S, Ide T, Tsutsui H. Blockade of L-type Ca(2+) channel attenuates doxorubicin-induced cardiomyopathy via suppression of CaMKII-NF-kappaB pathway. *Sci Rep* 9: 9850, 2019.
158. Iorga A, Cunningham CM, Moazeni S, Ruffenach G, Umar S, Eghbali M. The protective role of estrogen and estrogen receptors in cardiovascular disease and the controversial use of estrogen therapy. *Biol Sex Differ* 8: 33, 2017.
159. Irvine JC, Favalaro JL and Kemp-Harper BK. NO- activates soluble guanylate cyclase and Kv channels to vasodilate resistance arteries. *Hypertension* 41: 1301-1307, 2003.
160. Isakson BE, Best AK and Duling BR. Incidence of protein on actin bridges between endothelium and smooth muscle in arterioles demonstrates heterogeneous connexin expression and phosphorylation. *Am J Physiol Heart Circ Physiol* 294: H2898-2904, 2008.
161. Iwasaki Y, Tanabe M, Kobata K, Watanabe T. TRPA1 agonists--allyl isothiocyanate and cinnamaldehyde--induce adrenaline secretion. *Biosci Biotechnol Biochem* 72: 2608-2614, 2008.
162. J OU, Komukai K, Kusakari Y, Obata T, Hongo K, Sasaki H, Kurihara S. alpha1-adrenoceptor stimulation potentiates L-type Ca<sup>2+</sup> current through Ca<sup>2+</sup>/calmodulin-dependent PK II (CaMKII) activation in rat ventricular myocytes. *Proc Natl Acad Sci U S A* 102: 9400-9405, 2005.
163. Jackson WF. Potassium Channels in Regulation of Vascular Smooth Muscle Contraction and Growth. *Adv Pharmacol* 78: 89-144, 2017.

164. Jadeja RN, Rachakonda V, Bagi Z, Khurana S. Assessing Myogenic Response and Vasoactivity In Resistance Mesenteric Arteries Using Pressure Myography. *J Vis Exp* e50997, 2015.
165. Jiang Y, Lu L, Hu Y, Li Q, An C, Yu X, Shu L, Chen A, Niu C, Zhou L, Yang Z. Resistin Induces Hypertension and Insulin Resistance in Mice via a TLR4-Dependent Pathway. *Sci Rep* 6: 22193, 2016.
166. Joiner WJ, Khanna R, Schlichter LC, Kaczmarek LK. Calmodulin regulates assembly and trafficking of SK4/IK1 Ca<sup>2+</sup>-activated K<sup>+</sup> channels. *J Biol Chem* 276: 37980-37985, 2001.
167. Ju H, Zou R, Venema VJ, Venema RC. Direct interaction of endothelial nitric-oxide synthase and caveolin-1 inhibits synthase activity. *J Biol Chem* 272: 18522-18525, 1997.
168. Kamm KE and Stull JT. Dedicated myosin light chain kinases with diverse cellular functions. *J Biol Chem* 276: 4527-4530, 2001.
169. Karashima Y, Prenen J, Talavera K, Janssens A, Voets T, Nilius B. Agonist-induced changes in Ca(2+) permeation through the nociceptor cation channel TRPA1. *Biophys J* 98: 773-783, 2010.
170. Kasetti RB, Maddineni P, Patel PD, Searby C, Sheffield VC, Zode GS. Transforming growth factor beta2 (TGFbeta2) signaling plays a key role in glucocorticoid-induced ocular hypertension. *J Biol Chem* 293: 9854-9868, 2018.
171. Kashiwase K, Higuchi Y, Hirotsu S, Yamaguchi O, Hikoso S, Takeda T, Watanabe T, Taniike M, Nakai A, Tsujimoto I, Matsumura Y, Ueno H, Nishida K, Hori M, Otsu K. CaMKII activates ASK1 and NF-kappaB to induce cardiomyocyte hypertrophy. *Biochem Biophys Res Commun* 327: 136-142, 2005.
172. Keller TC, Butcher JT, Broseghini-Filho GB, Marziano C, DeLalio LJ, Rogers S, Ning B, Martin JN, Chechova S, Cabot M, Shu X, Best AK, Good ME, Simao Padilha A, Purdy M, Yeager M, Peirce SM, Hu S, Doctor A, Barrett E, Le TH, Columbus L, Isakson BE. Modulating Vascular Hemodynamics With an Alpha Globin Mimetic Peptide (HbalphaX). *Hypertension* 68: 1494-1503, 2016.
173. Kern PA, Saghizadeh M, Ong JM, Bosch RJ, Deem R, Simsolo RB. The expression of tumor necrosis factor in human adipose tissue. Regulation by obesity, weight loss, and relationship to lipoprotein lipase. *J Clin Invest* 95: 2111-2119, 1995.
174. Khan I, Sandhu V, Misquitta CM, Grover AK. SERCA pump isoform expression in endothelium of veins and arteries: every endothelium is not the same. *Mol Cell Biochem* 203: 11-15, 2000.
175. Kim HR, Gallant C and Morgan KG. Regulation of PKC autophosphorylation by calponin in contractile vascular smooth muscle tissue. *Biomed Res Int* 2013: 358643, 2013.
176. Kim YS, Morgan MJ, Choksi S, Liu ZG. TNF-induced activation of the Nox1 NADPH oxidase and its role in the induction of necrotic cell death. *Mol Cell* 26: 675-687, 2007.
177. King MD, Alleyne CH, Jr. and Dhandapani KM. TNF-alpha receptor antagonist, R-7050, improves neurological outcomes following intracerebral hemorrhage in mice. *Neurosci Lett* 542: 92-96, 2013.
178. Kishimoto A, Mikawa K, Hashimoto K, Yasuda I, Tanaka S, Tominaga M, Kuroda T, Nishizuka Y. Limited proteolysis of protein kinase C subspecies by calcium-dependent neutral protease (calpain). *J Biol Chem* 264: 4088-4092, 1989.
179. Kitagaki M, Isoda K, Kamada H, Kobayashi T, Tsunoda S, Tsutsumi Y, Niida T, Kujiraoka T, Ishigami N, Ishihara M, Matsubara O, Ohsuzu F, Kikuchi M. Novel TNF-alpha receptor 1 antagonist treatment attenuates arterial inflammation and intimal hyperplasia in mice. *J Atheroscler Thromb* 19: 36-46, 2012.
180. Klinger JR, Abman SH and Gladwin MT. Nitric oxide deficiency and endothelial dysfunction in pulmonary arterial hypertension. *Am J Respir Crit Care Med* 188: 639-646, 2013.

181. Knepler JL, Jr., Taher LN, Gupta MP, Patterson C, Pavalko F, Ober MD, Hart CM. Peroxynitrite causes endothelial cell monolayer barrier dysfunction. *Am J Physiol Cell Physiol* 281: C1064-1075, 2001.
182. Knot HJ and Nelson MT. Regulation of arterial diameter and wall  $[Ca^{2+}]$  in cerebral arteries of rat by membrane potential and intravascular pressure. *J Physiol* 508 ( Pt 1): 199-209, 1998.
183. Kochukov MY, Balasubramanian A, Abramowitz J, Birnbaumer L, Marrelli SP. Activation of endothelial transient receptor potential C3 channel is required for small conductance calcium-activated potassium channel activation and sustained endothelial hyperpolarization and vasodilation of cerebral artery. *J Am Heart Assoc* 3: 2014.
184. Koenen M, Hill MA, Cohen P, Sowers JR. Obesity, Adipose Tissue and Vascular Dysfunction. *Circ Res* 128: 951-968, 2021.
185. Kohler R, Heyken WT, Heinau P, Schubert R, Si H, Kacik M, Busch C, Grgic I, Maier T, Hoyer J. Evidence for a functional role of endothelial transient receptor potential V4 in shear stress-induced vasodilatation. *Arterioscler Thromb Vasc Biol* 26: 1495-1502, 2006.
186. Kohler R, Kaistha BP and Wulff H. Vascular K<sub>Ca</sub>-channels as therapeutic targets in hypertension and restenosis disease. *Expert Opin Ther Targets* 14: 143-155, 2010.
187. Kohout SC, Corbalan-Garcia S, Torrecillas A, Gomez-Fernandez JC, Falke JJ. C2 domains of protein kinase C isoforms alpha, beta, and gamma: activation parameters and calcium stoichiometries of the membrane-bound state. *Biochemistry* 41: 11411-11424, 2002.
188. Kolisek M, Beck A, Fleig A, Penner R. Cyclic ADP-ribose and hydrogen peroxide synergize with ADP-ribose in the activation of TRPM2 channels. *Mol Cell* 18: 61-69, 2005.
189. Kopp E and Ghosh S. Inhibition of NF-kappa B by sodium salicylate and aspirin. *Science* 265: 956-959, 1994.
190. Korda M, Kubant R, Patton S, Malinski T. Leptin-induced endothelial dysfunction in obesity. *Am J Physiol Heart Circ Physiol* 295: H1514-1521, 2008.
191. Kramar EA, Lin B, Lin CY, Arai AC, Gall CM, Lynch G. A novel mechanism for the facilitation of theta-induced long-term potentiation by brain-derived neurotrophic factor. *J Neurosci* 24: 5151-5161, 2004.
192. Kroetsch JT, Levy AS, Zhang H, Aschar-Sobbi R, Lidington D, Offermanns S, Nedospasov SA, Backx PH, Heximer SP, Bolz SS. Constitutive smooth muscle tumour necrosis factor regulates microvascular myogenic responsiveness and systemic blood pressure. *Nat Commun* 8: 14805, 2017.
193. Kumar A, Chen SH, Kadiiska MB, Hong JS, Zielonka J, Kalyanaraman B, Mason RP. Inducible nitric oxide synthase is key to peroxynitrite-mediated, LPS-induced protein radical formation in murine microglial BV2 cells. *Free Radic Biol Med* 73: 51-59, 2014.
194. Kwaifa IK, Bahari H, Yong YK, Noor SM. Endothelial Dysfunction in Obesity-Induced Inflammation: Molecular Mechanisms and Clinical Implications. *Biomolecules* 10: 2020.
195. La Cava A and Matarese G. The weight of leptin in immunity. *Nat Rev Immunol* 4: 371-379, 2004.
196. Lallemand T, Rouahi M, Swiader A, Grazide MH, Geoffre N, Alayrac P, Recazens E, Coste A, Salvayre R, Negre-Salvayre A, Auge N. nSMase2 (Type 2-Neutral Sphingomyelinase) Deficiency or Inhibition by GW4869 Reduces Inflammation and Atherosclerosis in Apoe(-/-) Mice. *Arterioscler Thromb Vasc Biol* 38: 1479-1492, 2018.
197. Laufs U, Endres M, Stagliano N, Amin-Hanjani S, Chui DS, Yang SX, Simoncini T, Yamada M, Rabkin E, Allen PG, Huang PL, Bohm M, Schoen FJ, Moskowitz MA, Liao JK. Neuroprotection mediated by changes in the endothelial actin cytoskeleton. *J Clin Invest* 106: 15-24, 2000.
198. Ledoux J, Bonev AD and Nelson MT. Ca<sup>2+</sup>-activated K<sup>+</sup> channels in murine endothelial cells: block by intracellular calcium and magnesium. *J Gen Physiol* 131: 125-135, 2008.

199. Ledoux J, Taylor MS, Bonev AD, Hannah RM, Solodushko V, Shui B, Tallini Y, Kotlikoff MI, Nelson MT. Functional architecture of inositol 1,4,5-trisphosphate signaling in restricted spaces of myoendothelial projections. *Proc Natl Acad Sci U S A* 105: 9627-9632, 2008.
200. Ledoux J, Werner ME, Brayden JE, Nelson MT. Calcium-activated potassium channels and the regulation of vascular tone. *Physiology (Bethesda)* 21: 69-78, 2006.
201. Lee MD, Wilson C, Saunter CD, Kennedy C, Girkin JM, McCarron JG. Spatially structured cell populations process multiple sensory signals in parallel in intact vascular endothelium. *Sci Signal* 11: 2018.
202. Lee SM, Choi HJ, Oh CH, Oh JW, Han JS. Leptin increases TNF-alpha expression and production through phospholipase D1 in Raw 264.7 cells. *PLoS One* 9: e102373, 2014.
203. Lemmens HJ, Bernstein DP and Brodsky JB. Estimating blood volume in obese and morbidly obese patients. *Obes Surg* 16: 773-776, 2006.
204. Lhomme A, Gilbert G, Pele T, Deweirdt J, Henrion D, Baudrimont I, Campagnac M, Marthan R, Guibert C, Ducret T, Savineau JP, Quignard JF. Stretch-activated Piezo1 Channel in Endothelial Cells Relaxes Mouse Intrapulmonary Arteries. *Am J Respir Cell Mol Biol* 60: 650-658, 2019.
205. Li C, Ma Q, Toan S, Wang J, Zhou H, Liang J. SERCA overexpression reduces reperfusion-mediated cardiac microvascular damage through inhibition of the calcium/MCU/mPTP/necroptosis signaling pathways. *Redox Biol* 36: 101659, 2020.
206. Li R, Wang WQ, Zhang H, Yang X, Fan Q, Christopher TA, Lopez BL, Tao L, Goldstein BJ, Gao F, Ma XL. Adiponectin improves endothelial function in hyperlipidemic rats by reducing oxidative/nitrative stress and differential regulation of eNOS/iNOS activity. *Am J Physiol Endocrinol Metab* 293: E1703-1708, 2007.
207. Liao J, Lu W, Chen Y, Duan X, Zhang C, Luo X, Lin Z, Chen J, Liu S, Yan H, Chen Y, Feng H, Zhou D, Chen X, Zhang Z, Yang Q, Liu X, Tang H, Li J, Makino A, Yuan JX, Zhong N, Yang K, Wang J. Upregulation of Piezo1 (Piezo Type Mechanosensitive Ion Channel Component 1) Enhances the Intracellular Free Calcium in Pulmonary Arterial Smooth Muscle Cells From Idiopathic Pulmonary Arterial Hypertension Patients. *Hypertension* 77: 1974-1989, 2021.
208. Lilienbaum A and Israel A. From calcium to NF-kappa B signaling pathways in neurons. *Mol Cell Biol* 23: 2680-2698, 2003.
209. Lillo MA, Gaete PS, Puebla M, Ardiles NM, Poblete I, Becerra A, Simon F, Figueroa XF. Critical contribution of Na(+)-Ca(2+) exchanger to the Ca(2+)-mediated vasodilation activated in endothelial cells of resistance arteries. *FASEB J* 32: 2137-2147, 2018.
210. Lin MT, Jian MY, Taylor MS, Cioffi DL, Yap FC, Liedtke W, Townsley MI. Functional coupling of TRPV4, IK, and SK channels contributes to Ca(2+)-dependent endothelial injury in rodent lung. *Pulm Circ* 5: 279-290, 2015.
211. Lin Q, Zhao L, Jing R, Trexler C, Wang H, Li Y, Tang H, Huang F, Zhang F, Fang X, Liu J, Jia N, Chen J, Ouyang K. Inositol 1,4,5-Trisphosphate Receptors in Endothelial Cells Play an Essential Role in Vasodilation and Blood Pressure Regulation. *J Am Heart Assoc* 8: e011704, 2019.
212. Lincoln TM. Myosin phosphatase regulatory pathways: different functions or redundant functions? *Circ Res* 100: 10-12, 2007.
213. Ling H, Gray CB, Zambon AC, Grimm M, Gu Y, Dalton N, Purcell NH, Peterson K, Brown JH. Ca2+/Calmodulin-dependent protein kinase II delta mediates myocardial ischemia/reperfusion injury through nuclear factor-kappaB. *Circ Res* 112: 935-944, 2013.
214. Liu CL, Huang Y, Ngai CY, Leung YK, Yao XQ. TRPC3 is involved in flow- and bradykinin-induced vasodilation in rat small mesenteric arteries. *Acta Pharmacol Sin* 27: 981-990, 2006.
215. Liu J, Garcia-Cardena G and Sessa WC. Palmitoylation of endothelial nitric oxide synthase is necessary for optimal stimulated release of nitric oxide: implications for caveolae localization. *Biochemistry* 35: 13277-13281, 1996.

216. Liu LH, Paul RJ, Sutliff RL, Miller ML, Lorenz JN, Pun RY, Duffy JJ, Doetschman T, Kimura Y, MacLennan DH, Hoying JB, Shull GE. Defective endothelium-dependent relaxation of vascular smooth muscle and endothelial cell Ca<sup>2+</sup> signaling in mice lacking sarco(endo)plasmic reticulum Ca<sup>2+</sup>-ATPase isoform 3. *J Biol Chem* 272: 30538-30545, 1997.
217. Liu QY, Karpinski E and Pang PK. The L-type calcium channel current is increased by alpha-1 adrenoceptor activation in neonatal rat ventricular cells. *J Pharmacol Exp Ther* 271: 935-943, 1994.
218. Liu X, Vien T, Duan J, Sheu SH, DeCaen PG, Clapham DE. Polycystin-2 is an essential ion channel subunit in the primary cilium of the renal collecting duct epithelium. *Elife* 7: 2018.
219. Liu Y, Terata K, Chai Q, Li H, Kleinman LH, Gutterman DD. Peroxynitrite inhibits Ca<sup>2+</sup>-activated K<sup>+</sup> channel activity in smooth muscle of human coronary arterioles. *Circ Res* 91: 1070-1076, 2002.
220. Loot AE, Popp R, Fisslthaler B, Vriens J, Nilius B, Fleming I. Role of cytochrome P450-dependent transient receptor potential V4 activation in flow-induced vasodilatation. *Cardiovasc Res* 80: 445-452, 2008.
221. Lu R, Flauaus C, Kennel L, Petersen J, Drees O, Kallenborn-Gerhardt W, Ruth P, Lukowski R, Schmidtko A. KCa3.1 channels modulate the processing of noxious chemical stimuli in mice. *Neuropharmacology* 125: 386-395, 2017.
222. Lucas-Ruiz F, Galindo-Romero C, Salinas-Navarro M, Gonzalez-Riquelme MJ, Vidal-Sanz M, Agudo Barriuso M. Systemic and Intravitreal Antagonism of the TNFR1 Signaling Pathway Delays Axotomy-Induced Retinal Ganglion Cell Loss. *Front Neurosci* 13: 1096, 2019.
223. Lucchesi PA, Belmadani S and Matrougui K. Hydrogen peroxide acts as both vasodilator and vasoconstrictor in the control of perfused mouse mesenteric resistance arteries. *J Hypertens* 23: 571-579, 2005.
224. Lukas TJ, Burgess WH, Prendergast FG, Lau W, Watterson DM. Calmodulin binding domains: characterization of a phosphorylation and calmodulin binding site from myosin light chain kinase. *Biochemistry* 25: 1458-1464, 1986.
225. Luo D, Luo Y, He Y, Zhang H, Zhang R, Li X, Dobrucki WL, Sinusas AJ, Sessa WC, Min W. Differential functions of tumor necrosis factor receptor 1 and 2 signaling in ischemia-mediated arteriogenesis and angiogenesis. *Am J Pathol* 169: 1886-1898, 2006.
226. Luo Y, Xu Z, Wan T, He Y, Jones D, Zhang H, Min W. Endothelial-specific transgenesis of TNFR2 promotes adaptive arteriogenesis and angiogenesis. *Arterioscler Thromb Vasc Biol* 30: 1307-1314, 2010.
227. Lynch CM, Kinzenbaw DA, Chen X, Zhan S, Mezzetti E, Filosa J, Ergul A, Faulkner JL, Faraci FM, Didion SP. Nox2-derived superoxide contributes to cerebral vascular dysfunction in diet-induced obesity. *Stroke* 44: 3195-3201, 2013.
228. Ma X, Du J, Zhang P, Deng J, Liu J, Lam FF, Li RA, Huang Y, Jin J, Yao X. Functional role of TRPV4-KCa2.3 signaling in vascular endothelial cells in normal and streptozotocin-induced diabetic rats. *Hypertension* 62: 134-139, 2013.
229. Ma X, Qiu S, Luo J, Ma Y, Ngai CY, Shen B, Wong CO, Huang Y, Yao X. Functional role of vanilloid transient receptor potential 4-canonical transient receptor potential 1 complex in flow-induced Ca<sup>2+</sup> influx. *Arterioscler Thromb Vasc Biol* 30: 851-858, 2010.
230. MacKay CE, Leo MD, Fernandez-Pena C, Hasan R, Yin W, Mata-Daboin A, Bulley S, Gammons J, Mancarella S, Jaggar JH. Intravascular flow stimulates PKD2 (polycystin-2) channels in endothelial cells to reduce blood pressure. *Elife* 9: 2020.
231. MacLennan DH and Kranias EG. Phospholamban: a crucial regulator of cardiac contractility. *Nat Rev Mol Cell Biol* 4: 566-577, 2003.
232. MacMicking JD, Nathan C, Hom G, Chartrain N, Fletcher DS, Trumbauer M, Stevens K, Xie QW, Sokol K, Hutchinson N, et al. Altered responses to bacterial infection and endotoxic shock in mice lacking inducible nitric oxide synthase. *Cell* 81: 641-650, 1995.

233. MacNaul KL and Hutchinson NI. Differential expression of iNOS and cNOS mRNA in human vascular smooth muscle cells and endothelial cells under normal and inflammatory conditions. *Biochem Biophys Res Commun* 196: 1330-1334, 1993.
234. Macpherson LJ, Geierstanger BH, Viswanath V, Bandell M, Eid SR, Hwang S, Patapoutian A. The pungency of garlic: activation of TRPA1 and TRPV1 in response to allicin. *Curr Biol* 15: 929-934, 2005.
235. Manea A, Tanase LI, Raicu M, Simionescu M. Transcriptional regulation of NADPH oxidase isoforms, Nox1 and Nox4, by nuclear factor-kappaB in human aortic smooth muscle cells. *Biochem Biophys Res Commun* 396: 901-907, 2010.
236. Mapp PI, McWilliams DF, Turley MJ, Hargin E, Walsh DA. A role for the sensory neuropeptide calcitonin gene-related peptide in endothelial cell proliferation in vivo. *Br J Pharmacol* 166: 1261-1271, 2012.
237. Martin E, Dahan D, Cardouat G, Gillibert-Duplantier J, Marthan R, Savineau JP, Ducret T. Involvement of TRPV1 and TRPV4 channels in migration of rat pulmonary arterial smooth muscle cells. *Pflugers Arch* 464: 261-272, 2012.
238. Marziano C, Hong K, Cope EL, Kotlikoff MI, Isakson BE, Sonkusare SK. Nitric Oxide-Dependent Feedback Loop Regulates Transient Receptor Potential Vanilloid 4 (TRPV4) Channel Cooperativity and Endothelial Function in Small Pulmonary Arteries. *J Am Heart Assoc* 6: 2017.
239. Mather S, Dora KA, Sandow SL, Winter P, Garland CJ. Rapid endothelial cell-selective loading of connexin 40 antibody blocks endothelium-derived hyperpolarizing factor dilation in rat small mesenteric arteries. *Circ Res* 97: 399-407, 2005.
240. McCann FE, Perocheau DP, Ruspi G, Blazek K, Davies ML, Feldmann M, Dean JL, Stoop AA, Williams RO. Selective tumor necrosis factor receptor I blockade is antiinflammatory and reveals immunoregulatory role of tumor necrosis factor receptor II in collagen-induced arthritis. *Arthritis Rheumatol* 66: 2728-2738, 2014.
241. McCarron JG, Chalmers S, MacMillan D, Olson ML. Agonist-evoked Ca(2+) wave progression requires Ca(2+) and IP(3). *J Cell Physiol* 224: 334-344, 2010.
242. Medeiros R, Prediger RD, Passos GF, Pandolfo P, Duarte FS, Franco JL, Dafre AL, Di Giunta G, Figueiredo CP, Takahashi RN, Campos MM, Calixto JB. Connecting TNF-alpha signaling pathways to iNOS expression in a mouse model of Alzheimer's disease: relevance for the behavioral and synaptic deficits induced by amyloid beta protein. *J Neurosci* 27: 5394-5404, 2007.
243. Mederos y Schnitzler M, Storch U, Meibers S, Nurwakagari P, Breit A, Essin K, Gollasch M, Gudermann T. Gq-coupled receptors as mechanosensors mediating myogenic vasoconstriction. *EMBO J* 27: 3092-3103, 2008.
244. Mellor H and Parker PJ. The extended protein kinase C superfamily. *Biochem J* 332 ( Pt 2): 281-292, 1998.
245. Mendoza SA, Fang J, Gutterman DD, Wilcox DA, Bubolz AH, Li R, Suzuki M, Zhang DX. TRPV4-mediated endothelial Ca<sup>2+</sup> influx and vasodilation in response to shear stress. *Am J Physiol Heart Circ Physiol* 298: H466-476, 2010.
246. Mercado J, Baylie R, Navedo MF, Yuan C, Scott JD, Nelson MT, Brayden JE, Santana LF. Local control of TRPV4 channels by AKAP150-targeted PKC in arterial smooth muscle. *J Gen Physiol* 143: 559-575, 2014.
247. Michel T and Vanhoutte PM. Cellular signaling and NO production. *Pflugers Arch* 459: 807-816, 2010.
248. Michell DL, Shihata WA, Andrews KL, Abidin NAZ, Jefferis AM, Sampson AK, Lumsden NG, Huet O, Parat MO, Jennings GL, Parton RG, Woollard KJ, Kaye DM, Chin-Dusting JPF, Murphy AJ. High intraluminal pressure promotes vascular inflammation via caveolin-1. *Sci Rep* 11: 5894, 2021.
249. Miller WL and Borlaug BA. Impact of Obesity on Volume Status in Patients With Ambulatory Chronic Heart Failure. *J Card Fail* 26: 112-117, 2020.

250. Minneman KP and Esbenshade TA. Alpha 1-adrenergic receptor subtypes. *Annu Rev Pharmacol Toxicol* 34: 117-133, 1994.
251. Minta A, Kao JP and Tsien RY. Fluorescent indicators for cytosolic calcium based on rhodamine and fluorescein chromophores. *J Biol Chem* 264: 8171-8178, 1989.
252. Mistry DK and Garland CJ. Nitric oxide (NO)-induced activation of large conductance Ca<sup>2+</sup>-dependent K<sup>+</sup> channels (BK(Ca)) in smooth muscle cells isolated from the rat mesenteric artery. *Br J Pharmacol* 124: 1131-1140, 1998.
253. Mochizuki T, Wu G, Hayashi T, Xenophontos SL, Veldhuisen B, Saris JJ, Reynolds DM, Cai Y, Gabow PA, Pierides A, Kimberling WJ, Breuning MH, Deltas CC, Peters DJ, Somlo S. PKD2, a gene for polycystic kidney disease that encodes an integral membrane protein. *Science* 272: 1339-1342, 1996.
254. Moitra J, Evenoski C, Sammani S, Wadgaonkar R, Turner JR, Ma SF, Garcia JG. A transgenic mouse with vascular endothelial over-expression of the non-muscle myosin light chain kinase-2 isoform is susceptible to inflammatory lung injury: role of sexual dimorphism and age. *Transl Res* 151: 141-153, 2008.
255. Monaco C, Nanchahal J, Taylor P, Feldmann M. Anti-TNF therapy: past, present and future. *Int Immunol* 27: 55-62, 2015.
256. Moncada S. Nitric oxide in the vasculature: physiology and pathophysiology. *Ann N Y Acad Sci* 811: 60-67; discussion 67-69, 1997.
257. Monden Y, Kubota T, Inoue T, Tsutsumi T, Kawano S, Ide T, Tsutsui H, Sunagawa K. Tumor necrosis factor-alpha is toxic via receptor 1 and protective via receptor 2 in a murine model of myocardial infarction. *Am J Physiol Heart Circ Physiol* 293: H743-753, 2007.
258. Morin CL, Eckel RH, Marcel T, Pagliassotti MJ. High fat diets elevate adipose tissue-derived tumor necrosis factor-alpha activity. *Endocrinology* 138: 4665-4671, 1997.
259. Most P and Koch WJ. S100A1: a calcium-modulating inotropic prototype for future clinical heart failure therapy. *Future Cardiol* 3: 5-11, 2007.
260. Most P, Remppis A, Pleger ST, Katus HA, Koch WJ. S100A1: a novel inotropic regulator of cardiac performance. Transition from molecular physiology to pathophysiological relevance. *Am J Physiol Regul Integr Comp Physiol* 293: R568-577, 2007.
261. Mountian II, Baba-Aissa F, Jonas JC, Humbert De S, Wuytack F, Parys JB. Expression of Ca(2+) Transport Genes in Platelets and Endothelial Cells in Hypertension. *Hypertension* 37: 135-141, 2001.
262. Murad F. Discovery of some of the biological effects of nitric oxide and its role in cell signaling. *Biosci Rep* 24: 452-474, 2004.
263. Murphy ME and Brayden JE. Apamin-sensitive K<sup>+</sup> channels mediate an endothelium-dependent hyperpolarization in rabbit mesenteric arteries. *J Physiol* 489 ( Pt 3): 723-734, 1995.
264. Murthy S, Koval OM, Ramiro Diaz JM, Kumar S, Nuno D, Scott JA, Allamargot C, Zhu LJ, Broadhurst K, Santhana V, Kutschke WJ, Irani K, Lamping KG, Grumbach IM. Endothelial CaMKII as a regulator of eNOS activity and NO-mediated vasoreactivity. *PLoS One* 12: e0186311, 2017.
265. Musicki B, Kramer MF, Becker RE, Burnett AL. Inactivation of phosphorylated endothelial nitric oxide synthase (Ser-1177) by O-GlcNAc in diabetes-associated erectile dysfunction. *Proc Natl Acad Sci U S A* 102: 11870-11875, 2005.
266. Nagata K, Duggan A, Kumar G, Garcia-Anoveros J. Nociceptor and hair cell transducer properties of TRPA1, a channel for pain and hearing. *J Neurosci* 25: 4052-4061, 2005.
267. Naik JS, Osmond JM, Walker BR, Kanagy NL. Hydrogen sulfide-induced vasodilation mediated by endothelial TRPV4 channels. *Am J Physiol Heart Circ Physiol* 311: H1437-H1444, 2016.
268. Nausch LW, Bonev AD, Heppner TJ, Tallini Y, Kotlikoff MI, Nelson MT. Sympathetic nerve stimulation induces local endothelial Ca<sup>2+</sup> signals to oppose vasoconstriction of mouse mesenteric arteries. *Am J Physiol Heart Circ Physiol* 302: H594-602, 2012.

269. Navedo MF, Amberg GC, Votaw VS, Santana LF. Constitutively active L-type Ca<sup>2+</sup> channels. *Proc Natl Acad Sci U S A* 102: 11112-11117, 2005.
270. Nelson KJ, Bolduc JA, Wu H, Collins JA, Burke EA, Reisz JA, Klomsiri C, Wood ST, Yammani RR, Poole LB, Furdul CM, Loeser RF. H<sub>2</sub>O<sub>2</sub> oxidation of cysteine residues in c-Jun N-terminal kinase 2 (JNK2) contributes to redox regulation in human articular chondrocytes. *J Biol Chem* 293: 16376-16389, 2018.
271. Newton AC and Keranen LM. Phosphatidyl-L-serine is necessary for protein kinase C's high-affinity interaction with diacylglycerol-containing membranes. *Biochemistry* 33: 6651-6658, 1994.
272. Nieves-Cintrón M, Amberg GC, Navedo MF, Molkentin JD, Santana LF. The control of Ca<sup>2+</sup> influx and NFATc3 signaling in arterial smooth muscle during hypertension. *Proc Natl Acad Sci U S A* 105: 15623-15628, 2008.
273. Nieves-Cintrón M, Amberg GC, Nichols CB, Molkentin JD, Santana LF. Activation of NFATc3 down-regulates the beta1 subunit of large conductance, calcium-activated K<sup>+</sup> channels in arterial smooth muscle and contributes to hypertension. *J Biol Chem* 282: 3231-3240, 2007.
274. Nikolaev YA, Cox CD, Ridone P, Rohde PR, Cordero-Morales JF, Vasquez V, Laver DR, Martinac B. Mammalian TRP ion channels are insensitive to membrane stretch. *J Cell Sci* 132: 2019.
275. Nishizuka Y. Intracellular signaling by hydrolysis of phospholipids and activation of protein kinase C. *Science* 258: 607-614, 1992.
276. Noronha BT, Li JM, Wheatcroft SB, Shah AM, Kearney MT. Inducible nitric oxide synthase has divergent effects on vascular and metabolic function in obesity. *Diabetes* 54: 1082-1089, 2005.
277. Nouri Barkestani M, Shamdani S, Afshar Bakshloo M, Arouche N, Bamba B, Uzan G, Naserian S. TNFalpha priming through its interaction with TNFR2 enhances endothelial progenitor cell immunosuppressive effect: new hope for their widespread clinical application. *Cell Commun Signal* 19: 1, 2021.
278. Nystoriak MA, Nieves-Cintrón M, Nygren PJ, Hinke SA, Nichols CB, Chen CY, Puglisi JL, Izu LT, Bers DM, Dell'acqua ML, Scott JD, Santana LF, Navedo MF. AKAP150 contributes to enhanced vascular tone by facilitating large-conductance Ca<sup>2+</sup>-activated K<sup>+</sup> channel remodeling in hyperglycemia and diabetes mellitus. *Circ Res* 114: 607-615, 2014.
279. Oh CK, Sultan A, Platzer J, Dolatabadi N, Soldner F, McClatchy DB, Diedrich JK, Yates JR, 3rd, Ambasudhan R, Nakamura T, Jaenisch R, Lipton SA. S-Nitrosylation of PINK1 Attenuates PINK1/Parkin-Dependent Mitophagy in hiPSC-Based Parkinson's Disease Models. *Cell Rep* 21: 2171-2182, 2017.
280. Ohashi M, Faraci F and Heistad D. Peroxynitrite hyperpolarizes smooth muscle and relaxes internal carotid artery in rabbit via ATP-sensitive K<sup>+</sup> channels. *Am J Physiol Heart Circ Physiol* 289: H2244-2250, 2005.
281. Okamura H, Aramburu J, Garcia-Rodriguez C, Viola JP, Raghavan A, Tahiliani M, Zhang X, Qin J, Hogan PG, Rao A. Concerted dephosphorylation of the transcription factor NFAT1 induces a conformational switch that regulates transcriptional activity. *Mol Cell* 6: 539-550, 2000.
282. Olesen C, Picard M, Winther AM, Gyruup C, Morth JP, Oxvig C, Møller JV, Nissen P. The structural basis of calcium transport by the calcium pump. *Nature* 450: 1036-1042, 2007.
283. Oliveria SF, Dell'Acqua ML and Sather WA. AKAP79/150 anchoring of calcineurin controls neuronal L-type Ca<sup>2+</sup> channel activity and nuclear signaling. *Neuron* 55: 261-275, 2007.
284. Ono Y, Fujii T, Igarashi K, Kuno T, Tanaka C, Kikkawa U, Nishizuka Y. Phorbol ester binding to protein kinase C requires a cysteine-rich zinc-finger-like sequence. *Proc Natl Acad Sci U S A* 86: 4868-4871, 1989.
285. Organization WH. Obesity and overweight. <https://www.who.int/news-room/factsheets/detail/obesity-and-overweight>: World Health Organization, 2018.

286. Ottolini M, Daneva Z, Chen YL, Cope EL, Kasetti RB, Zode GS, Sonkusare SK. Mechanisms underlying selective coupling of endothelial Ca(2+) signals with eNOS vs. IK/SK channels in systemic and pulmonary arteries. *J Physiol* 2020.
287. Ottolini M, Daneva Z, Chen YL, Cope EL, Kasetti RB, Zode GS, Sonkusare SK. Mechanisms underlying selective coupling of endothelial Ca(2+) signals with eNOS vs. IK/SK channels in systemic and pulmonary arteries. *J Physiol* 598: 3577-3596, 2020.
288. Ottolini M, Hong K, Cope EL, Daneva Z, DeLalio LJ, Sokolowski JD, Marziano C, Nguyen NY, Altschmied J, Haendeler J, Johnstone SR, Kalani MY, Park MS, Patel RP, Liedtke W, Isakson BE, Sonkusare SK. Local Peroxynitrite Impairs Endothelial Transient Receptor Potential Vanilloid 4 Channels and Elevates Blood Pressure in Obesity. *Circulation* 141: 1318-1333, 2020.
289. Ottolini M, Hong K, Cope EL, Daneva Z, DeLalio LJ, Sokolowski JD, Marziano C, Nguyen NY, Altschmied J, Haendeler J, Johnstone SR, Kalani MY, Park MS, Patel RP, Liedtke W, Isakson BE, Sonkusare SK. Local Peroxynitrite Impairs Endothelial TRPV4 Channels and Elevates Blood Pressure in Obesity. *Circulation* 2020.
290. Ottolini M, Hong K and Sonkusare SK. Calcium signals that determine vascular resistance. *Wiley Interdiscip Rev Syst Biol Med* e1448, 2019.
291. Ottolini M, Hong K and Sonkusare SK. Calcium signals that determine vascular resistance. *Wiley Interdiscip Rev Syst Biol Med* 11: e1448, 2019.
292. Ottolini M and Sonkusare SK. The Calcium Signaling Mechanisms in Arterial Smooth Muscle and Endothelial Cells. *Compr Physiol* 11: 1831-1869, 2021.
293. Park Y, Capobianco S, Gao X, Falck JR, Dellsperger KC, Zhang C. Role of EDHF in type 2 diabetes-induced endothelial dysfunction. *Am J Physiol Heart Circ Physiol* 295: H1982-1988, 2008.
294. Pasparakis M, Luedde T and Schmidt-Supprian M. Dissection of the NF-kappaB signalling cascade in transgenic and knockout mice. *Cell Death Differ* 13: 861-872, 2006.
295. Pearson RB and Kemp BE. Protein kinase phosphorylation site sequences and consensus specificity motifs: tabulations. *Methods Enzymol* 200: 62-81, 1991.
296. Pellicena P and Schulman H. CaMKII inhibitors: from research tools to therapeutic agents. *Front Pharmacol* 5: 21, 2014.
297. Periasamy M and Kalyanasundaram A. SERCA pump isoforms: their role in calcium transport and disease. *Muscle Nerve* 35: 430-442, 2007.
298. Peskin AV and Winterbourn CC. Kinetics of the reactions of hypochlorous acid and amino acid chloramines with thiols, methionine, and ascorbate. *Free Radic Biol Med* 30: 572-579, 2001.
299. Picchi A, Gao X, Belmadani S, Potter BJ, Focardi M, Chilian WM, Zhang C. Tumor necrosis factor-alpha induces endothelial dysfunction in the prediabetic metabolic syndrome. *Circ Res* 99: 69-77, 2006.
300. Pierce GL, Lesniewski LA, Lawson BR, Beske SD, Seals DR. Nuclear factor-{kappa}B activation contributes to vascular endothelial dysfunction via oxidative stress in overweight/obese middle-aged and older humans. *Circulation* 119: 1284-1292, 2009.
301. Pires PW and Earley S. Neuroprotective effects of TRPA1 channels in the cerebral endothelium following ischemic stroke. *Elife* 7: 2018.
302. Pires PW, Sullivan MN, Pritchard HA, Robinson JJ, Earley S. Unitary TRPV3 channel Ca2+ influx events elicit endothelium-dependent dilation of cerebral parenchymal arterioles. *Am J Physiol Heart Circ Physiol* 309: H2031-2041, 2015.
303. Pleger ST, Harris DM, Shan C, Vinge LE, Chuprun JK, Berzins B, Pleger W, Druckman C, Volkens M, Heierhorst J, Oie E, Remppis A, Katus HA, Scalia R, Eckhart AD, Koch WJ, Most P. Endothelial S100A1 modulates vascular function via nitric oxide. *Circ Res* 102: 786-794, 2008.
304. Porszasz R, Porkolab A, Ferencz A, Pataki T, Szilvassy Z, Szolcsanyi J. Capsaicin-induced nonneural vasoconstriction in canine mesenteric arteries. *European journal of pharmacology* 441: 173-175, 2002.

305. Powell-Wiley TM, Poirier P, Burke LE, Despres JP, Gordon-Larsen P, Lavie CJ, Lear SA, Ndumele CE, Neeland IJ, Sanders P, St-Onge MP, American Heart Association Council on L, Cardiometabolic H, Council on C, Stroke N, Council on Clinical C, Council on E, Prevention, Stroke C. Obesity and Cardiovascular Disease: A Scientific Statement From the American Heart Association. *Circulation* 143: e984-e1010, 2021.
306. Qian X, Francis M, Solodushko V, Earley S, Taylor MS. Recruitment of dynamic endothelial Ca<sup>2+</sup> signals by the TRPA1 channel activator AITC in rat cerebral arteries. *Microcirculation* 20: 138-148, 2013.
307. Radi R. Peroxynitrite, a stealthy biological oxidant. *J Biol Chem* 288: 26464-26472, 2013.
308. Raguimova ON, Smolin N, Bovo E, Bhayani S, Autry JM, Zima AV, Robia SL. Redistribution of SERCA calcium pump conformers during intracellular calcium signaling. *J Biol Chem* 293: 10843-10856, 2018.
309. Ravi K, Brennan LA, Levic S, Ross PA, Black SM. S-nitrosylation of endothelial nitric oxide synthase is associated with monomerization and decreased enzyme activity. *Proc Natl Acad Sci U S A* 101: 2619-2624, 2004.
310. Retailleau K, Duprat F, Arhatte M, Ranade SS, Peyronnet R, Martins JR, Jodar M, Moro C, Offermanns S, Feng Y, Demolombe S, Patel A, Honore E. Piezo1 in Smooth Muscle Cells Is Involved in Hypertension-Dependent Arterial Remodeling. *Cell Rep* 13: 1161-1171, 2015.
311. Reynoso R, Perrin RM, Breslin JW, Daines DA, Watson KD, Watterson DM, Wu MH, Yuan S. A role for long chain myosin light chain kinase (MLCK-210) in microvascular hyperpermeability during severe burns. *Shock* 28: 589-595, 2007.
312. Ringvold HC and Khalil RA. Protein Kinase C as Regulator of Vascular Smooth Muscle Function and Potential Target in Vascular Disorders. *Adv Pharmacol* 78: 203-301, 2017.
313. Robertson BE, Schubert R, Hescheler J, Nelson MT. cGMP-dependent protein kinase activates Ca-activated K channels in cerebral artery smooth muscle cells. *Am J Physiol* 265: C299-303, 1993.
314. Rosse C, Linch M, Kermorgant S, Cameron AJ, Boeckeler K, Parker PJ. PKC and the control of localized signal dynamics. *Nat Rev Mol Cell Biol* 11: 103-112, 2010.
315. Ryan MJ, Coleman TT, Sasser JM, Pittman KM, Hankins MW, Stec DE. Vascular smooth muscle-specific deletion of the leptin receptor attenuates leptin-induced alterations in vascular relaxation. *Am J Physiol Regul Integr Comp Physiol* 310: R960-967, 2016.
316. Ryskamp DA, Witkovsky P, Barabas P, Huang W, Koehler C, Akimov NP, Lee SH, Chauhan S, Xing W, Renteria RC, Liedtke W, Krizaj D. The polymodal ion channel transient receptor potential vanilloid 4 modulates calcium flux, spiking rate, and apoptosis of mouse retinal ganglion cells. *J Neurosci* 31: 7089-7101, 2011.
317. Saha D, Koli S, Patgaonkar M, Reddy KV. Expression of hemoglobin-alpha and beta subunits in human vaginal epithelial cells and their functional significance. *PLoS One* 12: e0171084, 2017.
318. Saliez J, Bouzin C, Rath G, Ghisdal P, Desjardins F, Rezzani R, Rodella LF, Vriens J, Nilius B, Feron O, Balligand JL, Dessy C. Role of caveolar compartmentation in endothelium-derived hyperpolarizing factor-mediated relaxation: Ca<sup>2+</sup> signals and gap junction function are regulated by caveolin in endothelial cells. *Circulation* 117: 1065-1074, 2008.
319. Samways DS and Egan TM. Calcium-dependent decrease in the single-channel conductance of TRPV1. *Pflugers Arch* 462: 681-691, 2011.
320. Sanchez-Bautista S, Marin-Vicente C, Gomez-Fernandez JC, Corbalan-Garcia S. The C2 domain of PKCalpha is a Ca<sup>2+</sup>-dependent PtdIns(4,5)P<sub>2</sub> sensing domain: a new insight into an old pathway. *J Mol Biol* 362: 901-914, 2006.
321. Sandoo A, Panoulas VF, Toms TE, Smith JP, Stavropoulos-Kalinoglou A, Metsios GS, Gasparyan AY, Carroll D, Veldhuijzen van Zanten JJ, Kitas GD. Anti-TNFalpha therapy may lead to blood pressure reductions through improved endothelium-dependent microvascular function in patients with rheumatoid arthritis. *J Hum Hypertens* 25: 699-702, 2011.

322. Sandow SL, Neylon CB, Chen MX, Garland CJ. Spatial separation of endothelial small- and intermediate-conductance calcium-activated potassium channels (K(Ca)) and connexins: possible relationship to vasodilator function? *J Anat* 209: 689-698, 2006.
323. Sandow SL, Tare M, Coleman HA, Hill CE, Parkington HC. Involvement of myoendothelial gap junctions in the actions of endothelium-derived hyperpolarizing factor. *Circ Res* 90: 1108-1113, 2002.
324. Sano Y, Inamura K, Miyake A, Mochizuki S, Yokoi H, Matsushime H, Furuichi K. Immunocyte Ca<sup>2+</sup> influx system mediated by LTRPC2. *Science* 293: 1327-1330, 2001.
325. Sasaki S, Higashi Y, Nakagawa K, Kimura M, Noma K, Sasaki S, Hara K, Matsuura H, Goto C, Oshima T, Chayama K. A low-calorie diet improves endothelium-dependent vasodilation in obese patients with essential hypertension. *Am J Hypertens* 15: 302-309, 2002.
326. Sauve M, Hui SK, Dinh DD, Foltz WD, Momen A, Nedospasov SA, Offermanns S, Husain M, Kroetsch JT, Lidington D, Bolz SS. Tumor Necrosis Factor/Sphingosine-1-Phosphate Signaling Augments Resistance Artery Myogenic Tone in Diabetes. *Diabetes* 65: 1916-1928, 2016.
327. Schlossmann J, Ammendola A, Ashman K, Zong X, Huber A, Neubauer G, Wang GX, Allescher HD, Korth M, Wilm M, Hofmann F, Ruth P. Regulation of intracellular calcium by a signalling complex of IRAG, IP3 receptor and cGMP kinase I $\beta$ . *Nature* 404: 197-201, 2000.
328. Schlossmann J and Desch M. IRAG and novel PKG targeting in the cardiovascular system. *Am J Physiol Heart Circ Physiol* 301: H672-682, 2011.
329. Schneider JC, El Kebir D, Chereau C, Mercier JC, Dall'Ava-Santucci J, Dinh-Xuan AT. Involvement of Na<sup>(+)</sup>/Ca<sup>(2+)</sup> exchanger in endothelial NO production and endothelium-dependent relaxation. *Am J Physiol Heart Circ Physiol* 283: H837-844, 2002.
330. Schroeter MR, Schneiderman J, Schumann B, Gluckermann R, Grimmas P, Buchwald AB, Tirilomis T, Schondube FA, Konstantinides SV, Schafer K. Expression of the leptin receptor in different types of vascular lesions. *Histochem Cell Biol* 128: 323-333, 2007.
331. Schubert R, Wesselman JP, Nilsson H, Mulvany MJ. Noradrenaline-induced depolarization is smaller in isobaric compared to isometric preparations of rat mesenteric small arteries. *Pflugers Arch* 431: 794-796, 1996.
332. Schumacher MA, Rivard AF, Bachinger HP, Adelman JP. Structure of the gating domain of a Ca<sup>2+</sup>-activated K<sup>+</sup> channel complexed with Ca<sup>2+</sup>/calmodulin. *Nature* 410: 1120-1124, 2001.
333. Sehgal PB, Mukhopadhyay S, Xu F, Patel K, Shah M. Dysfunction of Golgi tethers, SNAREs, and SNAPs in monocrotaline-induced pulmonary hypertension. *Am J Physiol Lung Cell Mol Physiol* 292: L1526-1542, 2007.
334. Seki T, Goto K, Kiyohara K, Kansui Y, Murakami N, Haga Y, Ohtsubo T, Matsumura K, Kitazono T. Downregulation of Endothelial Transient Receptor Potential Vanilloid Type 4 Channel and Small-Conductance of Ca<sup>2+</sup>-Activated K<sup>+</sup> Channels Underpins Impaired Endothelium-Dependent Hyperpolarization in Hypertension. *Hypertension* 69: 143-153, 2017.
335. Senadheera S, Kim Y, Grayson TH, Toemoe S, Kochukov MY, Abramowitz J, Housley GD, Bertrand RL, Chadha PS, Bertrand PP, Murphy TV, Tare M, Birnbaumer L, Marrelli SP, Sandow SL. Transient receptor potential canonical type 3 channels facilitate endothelium-derived hyperpolarization-mediated resistance artery vasodilator activity. *Cardiovasc Res* 95: 439-447, 2012.
336. Seo YH and Carroll KS. Profiling protein thiol oxidation in tumor cells using sulfenic acid-specific antibodies. *Proc Natl Acad Sci U S A* 106: 16163-16168, 2009.
337. Shakirova Y, Bonnevier J, Albinsson S, Adner M, Rippe B, Broman J, Arner A, Sward K. Increased Rho activation and PKC-mediated smooth muscle contractility in the absence of caveolin-1. *Am J Physiol Cell Physiol* 291: C1326-1335, 2006.
338. Shen Q, Rigor RR, Pivetti CD, Wu MH, Yuan SY. Myosin light chain kinase in microvascular endothelial barrier function. *Cardiovasc Res* 87: 272-280, 2010.

339. Shesely EG, Maeda N, Kim HS, Desai KM, Krege JH, Laubach VE, Sherman PA, Sessa WC, Smithies O. Elevated blood pressures in mice lacking endothelial nitric oxide synthase. *Proc Natl Acad Sci U S A* 93: 13176-13181, 1996.
340. Shi J, Hyman AJ, De Vecchis D, Chong J, Lichtenstein L, Futers TS, Rouahi M, Salvayre AN, Auge N, Kalli AC, Beech DJ. Sphingomyelinase Disables Inactivation in Endogenous PIEZO1 Channels. *Cell Rep* 33: 108225, 2020.
341. Shihata WA, Michell DL, Andrews KL, Chin-Dusting JP. Caveolae: A Role in Endothelial Inflammation and Mechanotransduction? *Front Physiol* 7: 628, 2016.
342. Shimokawa H, Yasutake H, Fujii K, Owada MK, Nakaike R, Fukumoto Y, Takayanagi T, Nagao T, Egashira K, Fujishima M, Takeshita A. The importance of the hyperpolarizing mechanism increases as the vessel size decreases in endothelium-dependent relaxations in rat mesenteric circulation. *J Cardiovasc Pharmacol* 28: 703-711, 1996.
343. Shin HM, Kim MH, Kim BH, Jung SH, Kim YS, Park HJ, Hong JT, Min KR, Kim Y. Inhibitory action of novel aromatic diamine compound on lipopolysaccharide-induced nuclear translocation of NF-kappaB without affecting IkappaB degradation. *FEBS Lett* 571: 50-54, 2004.
344. Shu X, Ruddiman CA, Keller TCSt, Keller AS, Yang Y, Good ME, Best AK, Columbus L, Isakson BE. Heterocellular Contact Can Dictate Arterial Function. *Circ Res* 124: 1473-1481, 2019.
345. Shui B, Lee JC, Reining S, Lee FK, Kotlikoff MI. Optogenetic sensors and effectors: CHROMus-the Cornell Heart Lung Blood Institute Resource for Optogenetic Mouse Signaling. *Front Physiol* 5: 428, 2014.
346. Silver AE, Beske SD, Christou DD, Donato AJ, Moreau KL, Eskurza I, Gates PE, Seals DR. Overweight and obese humans demonstrate increased vascular endothelial NAD(P)H oxidase-p47(phox) expression and evidence of endothelial oxidative stress. *Circulation* 115: 627-637, 2007.
347. Skinner KA, White CR, Patel R, Tan S, Barnes S, Kirk M, Darley-Usmar V, Parks DA. Nitrosation of uric acid by peroxyxynitrite. Formation of a vasoactive nitric oxide donor. *J Biol Chem* 273: 24491-24497, 1998.
348. Slater SJ, Ho C, Kelly MB, Larkin JD, Taddeo FJ, Yeager MD, Stubbs CD. Protein kinase Calpha contains two activator binding sites that bind phorbol esters and diacylglycerols with opposite affinities. *J Biol Chem* 271: 4627-4631, 1996.
349. Snoek GT, Rosenberg I, de Laat SW, Gitler C. The interaction of protein kinase C and other specific cytoplasmic proteins with phospholipid bilayers. *Biochim Biophys Acta* 860: 336-344, 1986.
350. Soares AG, de Carvalho MHC and Akamine E. Obesity Induces Artery-Specific Alterations: Evaluation of Vascular Function and Inflammatory and Smooth Muscle Phenotypic Markers. *Biomed Res Int* 2017: 5038602, 2017.
351. Somlyo AP and Somlyo AV. Ca<sup>2+</sup> sensitivity of smooth muscle and nonmuscle myosin II: modulated by G proteins, kinases, and myosin phosphatase. *Physiol Rev* 83: 1325-1358, 2003.
352. Song S, Yamamura A, Yamamura H, Ayon RJ, Smith KA, Tang H, Makino A, Yuan JX. Flow shear stress enhances intracellular Ca<sup>2+</sup> signaling in pulmonary artery smooth muscle cells from patients with pulmonary arterial hypertension. *Am J Physiol Cell Physiol* 307: C373-383, 2014.
353. Song Y, Li D, Farrelly O, Miles L, Li F, Kim SE, Lo TY, Wang F, Li T, Thompson-Peer KL, Gong J, Murthy SE, Coste B, Yakubovich N, Patapoutian A, Xiang Y, Rompolas P, Jan LY, Jan YN. The Mechanosensitive Ion Channel Piezo Inhibits Axon Regeneration. *Neuron* 102: 373-389 e376, 2019.
354. Sonkusare SK, Bonev AD, Ledoux J, Liedtke W, Kotlikoff MI, Heppner TJ, Hill-Eubanks DC, Nelson MT. Elementary Ca<sup>2+</sup> signals through endothelial TRPV4 channels regulate vascular function. *Science* 336: 597-601, 2012.

355. Sonkusare SK, Dalsgaard T, Bonev AD, Hill-Eubanks DC, Kotlikoff MI, Scott JD, Santana LF, Nelson MT. AKAP150-dependent cooperative TRPV4 channel gating is central to endothelium-dependent vasodilation and is disrupted in hypertension. *Sci Signal* 7: ra66, 2014.
356. Sorensen I, Adams RH and Gossler A. DLL1-mediated Notch activation regulates endothelial identity in mouse fetal arteries. *Blood* 113: 5680-5688, 2009.
357. Sowa G, Pypaert M and Sessa WC. Distinction between signaling mechanisms in lipid rafts vs. caveolae. *Proc Natl Acad Sci U S A* 98: 14072-14077, 2001.
358. Spyridopoulos I, Luedemann C, Chen D, Kearney M, Chen D, Murohara T, Principe N, Isner JM, Losordo DW. Divergence of angiogenic and vascular permeability signaling by VEGF: inhibition of protein kinase C suppresses VEGF-induced angiogenesis, but promotes VEGF-induced, NO-dependent vascular permeability. *Arterioscler Thromb Vasc Biol* 22: 901-906, 2002.
359. Stauss HM, Godecke A, Mrowka R, Schrader J, Persson PB. Enhanced blood pressure variability in eNOS knockout mice. *Hypertension* 33: 1359-1363, 1999.
360. Steinberg SF. Mechanisms for redox-regulation of protein kinase C. *Front Pharmacol* 6: 128, 2015.
361. Steinberg SF. Structural basis of protein kinase C isoform function. *Physiol Rev* 88: 1341-1378, 2008.
362. Steppan CM and Lazar MA. Resistin and obesity-associated insulin resistance. *Trends Endocrinol Metab* 13: 18-23, 2002.
363. Straub AC, Butcher JT, Billaud M, Mutchler SM, Artamonov MV, Nguyen AT, Johnson T, Best AK, Miller MP, Palmer LA, Columbus L, Somlyo AV, Le TH, Isakson BE. Hemoglobin alpha/eNOS coupling at myoendothelial junctions is required for nitric oxide scavenging during vasoconstriction. *Arterioscler Thromb Vasc Biol* 34: 2594-2600, 2014.
364. Straub AC, Lohman AW, Billaud M, Johnstone SR, Dwyer ST, Lee MY, Bortz PS, Best AK, Columbus L, Gaston B, Isakson BE. Endothelial cell expression of haemoglobin alpha regulates nitric oxide signalling. *Nature* 491: 473-477, 2012.
365. Strotmann R, Harteneck C, Nunnenmacher K, Schultz G, Plant TD. OTRPC4, a nonselective cation channel that confers sensitivity to extracellular osmolarity. *Nat Cell Biol* 2: 695-702, 2000.
366. Sugimoto M, Nakayama M, Goto TM, Amano M, Komori K, Kaibuchi K. Rho-kinase phosphorylates eNOS at threonine 495 in endothelial cells. *Biochem Biophys Res Commun* 361: 462-467, 2007.
367. Sullivan MN, Francis M, Pitts NL, Taylor MS, Earley S. Optical recording reveals novel properties of GSK1016790A-induced vanilloid transient receptor potential channel TRPV4 activity in primary human endothelial cells. *Mol Pharmacol* 82: 464-472, 2012.
368. Sullivan MN, Gonzales AL, Pires PW, Bruhl A, Leo MD, Li W, Oulidi A, Boop FA, Feng Y, Jaggar JH, Welsh DG, Earley S. Localized TRPA1 channel Ca<sup>2+</sup> signals stimulated by reactive oxygen species promote cerebral artery dilation. *Sci Signal* 8: ra2, 2015.
369. Sun W, Chi S, Li Y, Ling S, Tan Y, Xu Y, Jiang F, Li J, Liu C, Zhong G, Cao D, Jin X, Zhao D, Gao X, Liu Z, Xiao B, Li Y. The mechanosensitive Piezo1 channel is required for bone formation. *Elife* 8: 2019.
370. Suresh K, Servinsky L, Jiang H, Bigham Z, Yun X, Kliment C, Huetsch J, Damarla M, Shimoda LA. Reactive oxygen species induced Ca<sup>2+</sup> influx via TRPV4 and microvascular endothelial dysfunction in the SU5416/hypoxia model of pulmonary arterial hypertension. *Am J Physiol Lung Cell Mol Physiol* 314: L893-L907, 2018.
371. Suresh K, Servinsky L, Reyes J, Baksh S, Undem C, Caterina M, Pearse DB, Shimoda LA. Hydrogen peroxide-induced calcium influx in lung microvascular endothelial cells involves TRPV4. *Am J Physiol Lung Cell Mol Physiol* 309: L1467-1477, 2015.
372. Surks HK, Mochizuki N, Kasai Y, Georgescu SP, Tang KM, Ito M, Lincoln TM, Mendelsohn ME. Regulation of myosin phosphatase by a specific interaction with cGMP-dependent protein kinase Ialpha. *Science* 286: 1583-1587, 1999.

373. Suzuma K, Takahara N, Suzuma I, Isshiki K, Ueki K, Leitges M, Aiello LP, King GL. Characterization of protein kinase C beta isoform's action on retinoblastoma protein phosphorylation, vascular endothelial growth factor-induced endothelial cell proliferation, and retinal neovascularization. *Proc Natl Acad Sci U S A* 99: 721-726, 2002.
374. Swulius MT and Waxham MN. Ca<sup>2+</sup>/calmodulin-dependent protein kinases. *Cell Mol Life Sci* 65: 2637-2657, 2008.
375. Tajada S, Moreno CM, O'Dwyer S, Woods S, Sato D, Navedo MF, Santana LF. Distance constraints on activation of TRPV4 channels by AKAP150-bound PKC $\alpha$  in arterial myocytes. *J Gen Physiol* 149: 639-659, 2017.
376. Takahashi N, Hamada-Nakahara S, Itoh Y, Takemura K, Shimada A, Ueda Y, Kitamata M, Matsuoka R, Hanawa-Suetsugu K, Senju Y, Mori MX, Kiyonaka S, Kohda D, Kitao A, Mori Y, Suetsugu S. TRPV4 channel activity is modulated by direct interaction of the ankyrin domain to PI(4,5)P<sub>2</sub>. *Nature communications* 5: 4994, 2014.
377. Takai Y, Kishimoto A, Kikkawa U, Mori T, Nishizuka Y. Unsaturated diacylglycerol as a possible messenger for the activation of calcium-activated, phospholipid-dependent protein kinase system. *Biochem Biophys Res Commun* 91: 1218-1224, 1979.
378. Tallini YN, Brekke JF, Shui B, Doran R, Hwang SM, Nakai J, Salama G, Segal SS, Kotlikoff MI. Propagated endothelial Ca<sup>2+</sup> waves and arteriolar dilation in vivo: measurements in Cx40BAC GCaMP2 transgenic mice. *Circ Res* 101: 1300-1309, 2007.
379. Tansey MG, Luby-Phelps K, Kamm KE, Stull JT. Ca<sup>2+</sup>-dependent phosphorylation of myosin light chain kinase decreases the Ca<sup>2+</sup> sensitivity of light chain phosphorylation within smooth muscle cells. *J Biol Chem* 269: 9912-9920, 1994.
380. Tansey MG, Word RA, Hidaka H, Singer HA, Schworer CM, Kamm KE, Stull JT. Phosphorylation of myosin light chain kinase by the multifunctional calmodulin-dependent protein kinase II in smooth muscle cells. *J Biol Chem* 267: 12511-12516, 1992.
381. Taylor MS, Bonev AD, Gross TP, Eckman DM, Brayden JE, Bond CT, Adelman JP, Nelson MT. Altered expression of small-conductance Ca<sup>2+</sup>-activated K<sup>+</sup> (SK<sub>3</sub>) channels modulates arterial tone and blood pressure. *Circ Res* 93: 124-131, 2003.
382. Thomas D, Tovey SC, Collins TJ, Bootman MD, Berridge MJ, Lipp P. A comparison of fluorescent Ca<sup>2+</sup> indicator properties and their use in measuring elementary and global Ca<sup>2+</sup> signals. *Cell Calcium* 28: 213-223, 2000.
383. Thompson JA, Larion S, Mintz JD, Belin de Chantemele EJ, Fulton DJ, Stepp DW. Genetic Deletion of NADPH Oxidase 1 Rescues Microvascular Function in Mice With Metabolic Disease. *Circ Res* 121: 502-511, 2017.
384. Thorneloe KS, Cheung M, Bao W, Alsaïd H, Lenhard S, Jian MY, Costell M, Maniscalco-Hauk K, Krawiec JA, Olzinski A, Gordon E, Lozinskaya I, Elefante L, Qin P, Matasic DS, James C, Tunstead J, Donovan B, Kallal L, Waszkiewicz A, Vaidya K, Davenport EA, Larkin J, Burgert M, Casillas LN, Marquis RW, Ye G, Eidam HS, Goodman KB, Toomey JR, Roethke TJ, Jucker BM, Schnackenberg CG, Townsley MI, Lepore JJ, Willette RN. An orally active TRPV4 channel blocker prevents and resolves pulmonary edema induced by heart failure. *Science translational medicine* 4: 159ra148, 2012.
385. Tinsley JH, De Lanerolle P, Wilson E, Ma W, Yuan SY. Myosin light chain kinase transference induces myosin light chain activation and endothelial hyperpermeability. *Am J Physiol Cell Physiol* 279: C1285-1289, 2000.
386. Tinsley JH, Yuan SY and Wilson E. Isoform-specific knockout of endothelial myosin light chain kinase: closing the gap on inflammatory lung disease. *Trends Pharmacol Sci* 25: 64-66, 2004.
387. Tobimatsu T and Fujisawa H. Tissue-specific expression of four types of rat calmodulin-dependent protein kinase II mRNAs. *J Biol Chem* 264: 17907-17912, 1989.
388. Torres-Narvaez JC, Mondragon Ldel V, Varela Lopez E, Perez-Torres I, Diaz Juarez JA, Suarez J, Hernandez GP. Role of the transient receptor potential vanilloid type 1 receptor and

stretch-activated ion channels in nitric oxide release from endothelial cells of the aorta and heart in rats. *Exp Clin Cardiol* 17: 89-94, 2012.

389. Toth A, Czikora A, Pasztor ET, Dienes B, Bai P, Csernoch L, Rutkai I, Csato V, Manyine IS, Porszasz R, Edes I, Papp Z, Boczan J. Vanilloid receptor-1 (TRPV1) expression and function in the vasculature of the rat. *J Histochem Cytochem* 62: 129-144, 2014.

390. Toussaint F, Charbel C, Allen BG, Ledoux J. Vascular CaMKII: heart and brain in your arteries. *Am J Physiol Cell Physiol* 311: C462-478, 2016.

391. Toyoshima C, Nakasako M, Nomura H, Ogawa H. Crystal structure of the calcium pump of sarcoplasmic reticulum at 2.6 Å resolution. *Nature* 405: 647-655, 2000.

392. Tran CH, Taylor MS, Plane F, Nagaraja S, Tsoukias NM, Solodushko V, Vigmond EJ, Furstenhaupt T, Brigdan M, Welsh DG. Endothelial Ca<sup>2+</sup> wavelets and the induction of myoendothelial feedback. *Am J Physiol Cell Physiol* 302: C1226-1242, 2012.

393. Trevisani M, Siemens J, Materazzi S, Bautista DM, Nassini R, Campi B, Imamachi N, Andre E, Patacchini R, Cottrell GS, Gatti R, Basbaum AI, Bunnett NW, Julius D, Geppetti P. 4-Hydroxynonenal, an endogenous aldehyde, causes pain and neurogenic inflammation through activation of the irritant receptor TRPA1. *Proc Natl Acad Sci U S A* 104: 13519-13524, 2007.

394. Tsien RY, Pozzan T and Rink TJ. Calcium homeostasis in intact lymphocytes: cytoplasmic free calcium monitored with a new, intracellularly trapped fluorescent indicator. *J Cell Biol* 94: 325-334, 1982.

395. Turner NA, Mughal RS, Warburton P, O'Regan DJ, Ball SG, Porter KE. Mechanism of TNF $\alpha$ -induced IL-1 $\alpha$ , IL-1 $\beta$  and IL-6 expression in human cardiac fibroblasts: effects of statins and thiazolidinediones. *Cardiovasc Res* 76: 81-90, 2007.

396. Urakami-Harasawa L, Shimokawa H, Nakashima M, Egashira K, Takeshita A. Importance of endothelium-derived hyperpolarizing factor in human arteries. *J Clin Invest* 100: 2793-2799, 1997.

397. Van Hauwermeiren F, Armaka M, Karagianni N, Kranidioti K, Vandenbroucke RE, Loges S, Van Roy M, Staelens J, Puimege L, Palagani A, Berghe WV, Victoratos P, Carmeliet P, Libert C, Kollias G. Safe TNF-based antitumor therapy following p53/TNFR reduction in intestinal epithelium. *J Clin Invest* 123: 2590-2603, 2013.

398. Van Vliet BN, Chafe LL and Montani JP. Characteristics of 24 h telemetered blood pressure in eNOS-knockout and C57Bl/6J control mice. *J Physiol* 549: 313-325, 2003.

399. Vanhoutte PM, Zhao Y, Xu A, Leung SW. Thirty Years of Saying NO: Sources, Fate, Actions, and Misfortunes of the Endothelium-Derived Vasodilator Mediator. *Circ Res* 119: 375-396, 2016.

400. Verin AD, Lazar V, Torry RJ, Labarrere CA, Patterson CE, Garcia JG. Expression of a novel high molecular-weight myosin light chain kinase in endothelium. *Am J Respir Cell Mol Biol* 19: 758-766, 1998.

401. Viridis A, Colucci R, Bernardini N, Blandizzi C, Taddei S, Masi S. Microvascular Endothelial Dysfunction in Human Obesity: Role of TNF- $\alpha$ . *J Clin Endocrinol Metab* 104: 341-348, 2019.

402. Viridis A, Duranti E, Rossi C, Dell'Agnello U, Santini E, Anselmino M, Chiarugi M, Taddei S, Solini A. Tumour necrosis factor- $\alpha$  participates on the endothelin-1/nitric oxide imbalance in small arteries from obese patients: role of perivascular adipose tissue. *Eur Heart J* 36: 784-794, 2015.

403. Viridis A, Santini F, Colucci R, Duranti E, Salvetti G, Rugani I, Segnani C, Anselmino M, Bernardini N, Blandizzi C, Salvetti A, Pinchera A, Taddei S. Vascular generation of tumor necrosis factor- $\alpha$  reduces nitric oxide availability in small arteries from visceral fat of obese patients. *J Am Coll Cardiol* 58: 238-247, 2011.

404. Voets T, Prenen J, Vriens J, Watanabe H, Janssens A, Wissenbach U, Bodding M, Droogmans G, Nilius B. Molecular determinants of permeation through the cation channel TRPV4. *J Biol Chem* 277: 33704-33710, 2002.

405. Wainwright MS, Rossi J, Schavocky J, Crawford S, Steinhorn D, Velentza AV, Zasadzki M, Shirinsky V, Jia Y, Haiech J, Van Eldik LJ, Watterson DM. Protein kinase involved in lung injury susceptibility: evidence from enzyme isoform genetic knockout and in vivo inhibitor treatment. *Proc Natl Acad Sci U S A* 100: 6233-6238, 2003.
406. Wajant H, Pfizenmaier K and Scheurich P. Tumor necrosis factor signaling. *Cell Death Differ* 10: 45-65, 2003.
407. Wajant H and Scheurich P. TNFR1-induced activation of the classical NF-kappaB pathway. *FEBS J* 278: 862-876, 2011.
408. Wajant H and Siegmund D. TNFR1 and TNFR2 in the Control of the Life and Death Balance of Macrophages. *Front Cell Dev Biol* 7: 91, 2019.
409. Wan T, Xu Z, Zhou HJ, Zhang H, Luo Y, Li Y, Min W. Functional analyses of TNFR2 in physiological and pathological retina angiogenesis. *Invest Ophthalmol Vis Sci* 54: 211-221, 2013.
410. Wang D, Wang Z, Zhang L, Wang Y. Roles of Cells from the Arterial Vessel Wall in Atherosclerosis. *Mediators Inflamm* 2017: 8135934, 2017.
411. Wang S, Chennupati R, Kaur H, Iring A, Wettschureck N, Offermanns S. Endothelial cation channel PIEZO1 controls blood pressure by mediating flow-induced ATP release. *J Clin Invest* 126: 4527-4536, 2016.
412. Wani R and Murray BW. Analysis of Cysteine Redox Post-Translational Modifications in Cell Biology and Drug Pharmacology. *Methods Mol Biol* 1558: 191-212, 2017.
413. Ward ZJ, Bleich SN, Craddock AL, Barrett JL, Giles CM, Flax C, Long MW, Gortmaker SL. Projected U.S. State-Level Prevalence of Adult Obesity and Severe Obesity. *N Engl J Med* 381: 2440-2450, 2019.
414. Watanabe H, Vriens J, Prenen J, Droogmans G, Voets T, Nilius B. Anandamide and arachidonic acid use epoxyeicosatrienoic acids to activate TRPV4 channels. *Nature* 424: 434-438, 2003.
415. Watanabe H, Vriens J, Suh SH, Benham CD, Droogmans G, Nilius B. Heat-evoked activation of TRPV4 channels in a HEK293 cell expression system and in native mouse aorta endothelial cells. *J Biol Chem* 277: 47044-47051, 2002.
416. Wattanapitayakul SK, Weinstein DM, Holycross BJ, Bauer JA. Endothelial dysfunction and peroxynitrite formation are early events in angiotensin-induced cardiovascular disorders. *FASEB J* 14: 271-278, 2000.
417. Weir MR. Hypervolemia and blood pressure: powerful indicators of increased mortality among hemodialysis patients. *Hypertension* 56: 341-343, 2010.
418. Wellen KE and Hotamisligil GS. Inflammation, stress, and diabetes. *J Clin Invest* 115: 1111-1119, 2005.
419. Wellman GC, Santana LF, Bonev AD, Nelson MT. Role of phospholamban in the modulation of arterial Ca(2+) sparks and Ca(2+)-activated K(+) channels by cAMP. *Am J Physiol Cell Physiol* 281: C1029-1037, 2001.
420. Wellner M, Maasch C, Kupprion C, Lindschau C, Luft FC, Haller H. The proliferative effect of vascular endothelial growth factor requires protein kinase C-alpha and protein kinase C-zeta. *Arterioscler Thromb Vasc Biol* 19: 178-185, 1999.
421. Westcott EB and Jackson WF. Heterogeneous function of ryanodine receptors, but not IP3 receptors, in hamster cremaster muscle feed arteries and arterioles. *Am J Physiol Heart Circ Physiol* 300: H1616-1630, 2011.
422. Willette RN, Bao W, Nerurkar S, Yue TL, Doe CP, Stankus G, Turner GH, Ju H, Thomas H, Fishman CE, Sulpizio A, Behm DJ, Hoffman S, Lin Z, Lozinskaya I, Casillas LN, Lin M, Trout RE, Votta BJ, Thorneloe K, Lashinger ES, Figueroa DJ, Marquis R, Xu X. Systemic activation of the transient receptor potential vanilloid subtype 4 channel causes endothelial failure and circulatory collapse: Part 2. *J Pharmacol Exp Ther* 326: 443-452, 2008.

423. Wilson C, Zhang X, Lee MD, MacDonald M, Heathcote HR, Alorfi NMN, Buckley C, Dolan S, McCarron JG. Disrupted endothelial cell heterogeneity and network organization impair vascular function in prediabetic obesity. *Metabolism* 111: 154340, 2020.
424. Wooldridge AA, MacDonald JA, Erdodi F, Ma C, Borman MA, Hartshorne DJ, Haystead TA. Smooth muscle phosphatase is regulated in vivo by exclusion of phosphorylation of threonine 696 of MYPT1 by phosphorylation of Serine 695 in response to cyclic nucleotides. *J Biol Chem* 279: 34496-34504, 2004.
425. Wu KD, Bungard D and Lytton J. Regulation of SERCA Ca<sup>2+</sup> pump expression by cytoplasmic Ca<sup>2+</sup> in vascular smooth muscle cells. *Am J Physiol Cell Physiol* 280: C843-851, 2001.
426. Wu LW, Mayo LD, Dunbar JD, Kessler KM, Baerwald MR, Jaffe EA, Wang D, Warren RS, Donner DB. Utilization of distinct signaling pathways by receptors for vascular endothelial cell growth factor and other mitogens in the induction of endothelial cell proliferation. *J Biol Chem* 275: 5096-5103, 2000.
427. Wu W, Li L, Su X, Zhu Z, Lin X, Zhang J, Zhuang Z, Cai H, Huang W. Nuclear factor-kappaB regulates the transcription of NADPH oxidase 1 in human alveolar epithelial cells. *BMC Pulm Med* 21: 98, 2021.
428. Xia N, Horke S, Habermeier A, Closs EI, Reifenberg G, Gericke A, Mikhed Y, Munzel T, Daiber A, Forstermann U, Li H. Uncoupling of Endothelial Nitric Oxide Synthase in Perivascular Adipose Tissue of Diet-Induced Obese Mice. *Arterioscler Thromb Vasc Biol* 36: 78-85, 2016.
429. Xia N and Li H. The role of perivascular adipose tissue in obesity-induced vascular dysfunction. *Br J Pharmacol* 174: 3425-3442, 2017.
430. Xia P, Aiello LP, Ishii H, Jiang ZY, Park DJ, Robinson GS, Takagi H, Newsome WP, Jirousek MR, King GL. Characterization of vascular endothelial growth factor's effect on the activation of protein kinase C, its isoforms, and endothelial cell growth. *J Clin Invest* 98: 2018-2026, 1996.
431. Xia XM, Fakler B, Rivard A, Wayman G, Johnson-Pais T, Keen JE, Ishii T, Hirschberg B, Bond CT, Lutsenko S, Maylie J, Adelman JP. Mechanism of calcium gating in small-conductance calcium-activated potassium channels. *Nature* 395: 503-507, 1998.
432. Xia Y, Fu Z, Hu J, Huang C, Paudel O, Cai S, Liedtke W, Sham JS. TRPV4 channel contributes to serotonin-induced pulmonary vasoconstriction and the enhanced vascular reactivity in chronic hypoxic pulmonary hypertension. *Am J Physiol Cell Physiol* 305: C704-715, 2013.
433. Xu H, Delling M, Jun JC, Clapham DE. Oregano, thyme and clove-derived flavors and skin sensitizers activate specific TRP channels. *Nat Neurosci* 9: 628-635, 2006.
434. Xu H, Ramsey IS, Kotecha SA, Moran MM, Chong JA, Lawson D, Ge P, Lilly J, Silos-Santiago I, Xie Y, DiStefano PS, Curtis R, Clapham DE. TRPV3 is a calcium-permeable temperature-sensitive cation channel. *Nature* 418: 181-186, 2002.
435. Xu Q, Heo CH, Kim G, Lee HW, Kim HM, Yoon J. Development of imidazoline-2-thiones based two-photon fluorescence probes for imaging hypochlorite generation in a co-culture system. *Angew Chem Int Ed Engl* 54: 4890-4894, 2015.
436. Yamamoto K, Sokabe T, Matsumoto T, Yoshimura K, Shibata M, Ohura N, Fukuda T, Sato T, Sekine K, Kato S, Isshiki M, Fujita T, Kobayashi M, Kawamura K, Masuda H, Kamiya A, Ando J. Impaired flow-dependent control of vascular tone and remodeling in P2X4-deficient mice. *Nat Med* 12: 133-137, 2006.
437. Yang D, Luo Z, Ma S, Wong WT, Ma L, Zhong J, He H, Zhao Z, Cao T, Yan Z, Liu D, Arendshorst WJ, Huang Y, Tepel M, Zhu Z. Activation of TRPV1 by dietary capsaicin improves endothelium-dependent vasorelaxation and prevents hypertension. *Cell Metab* 12: 130-141, 2010.
438. Yang J, Noyan-Ashraf MH, Meissner A, Voigtlaender-Bolz J, Kroetsch JT, Foltz W, Jaffray D, Kapoor A, Momen A, Heximer SP, Zhang H, van Eede M, Henkelman RM, Matthews

- SG, Lidington D, Husain M, Bolz SS. Proximal cerebral arteries develop myogenic responsiveness in heart failure via tumor necrosis factor-alpha-dependent activation of sphingosine-1-phosphate signaling. *Circulation* 126: 196-206, 2012.
439. Yang S, Wang J, Brand DD, Zheng SG. Role of TNF-TNF Receptor 2 Signal in Regulatory T Cells and Its Therapeutic Implications. *Front Immunol* 9: 784, 2018.
440. Yang X, Coriolan D, Murthy V, Schultz K, Golenbock DT, Beasley D. Proinflammatory phenotype of vascular smooth muscle cells: role of efficient Toll-like receptor 4 signaling. *Am J Physiol Heart Circ Physiol* 289: H1069-1076, 2005.
441. Yazdanpanah B, Wiegmann K, Tchikov V, Krut O, Pongratz C, Schramm M, Kleinridders A, Wunderlich T, Kashkar H, Utermohlen O, Bruning JC, Schutze S, Kronke M. Riboflavin kinase couples TNF receptor 1 to NADPH oxidase. *Nature* 460: 1159-1163, 2009.
442. Yin J, Hoffmann J, Kaestle SM, Neye N, Wang L, Baeurle J, Liedtke W, Wu S, Kuppe H, Pries AR, Kuebler WM. Negative-feedback loop attenuates hydrostatic lung edema via a cGMP-dependent regulation of transient receptor potential vanilloid 4. *Circ Res* 102: 966-974, 2008.
443. Yoshida S, Takeuchi T, Kotani T, Yamamoto N, Hata K, Nagai K, Shoda T, Takai S, Makino S, Hanafusa T. Infliximab, a TNF-alpha inhibitor, reduces 24-h ambulatory blood pressure in rheumatoid arthritis patients. *J Hum Hypertens* 28: 165-169, 2014.
444. Yu H, Lin L, Zhang Z, Zhang H, Hu H. Targeting NF-kappaB pathway for the therapy of diseases: mechanism and clinical study. *Signal Transduct Target Ther* 5: 209, 2020.
445. Yuan Y, Huang Q and Wu HM. Myosin light chain phosphorylation: modulation of basal and agonist-stimulated venular permeability. *Am J Physiol* 272: H1437-1443, 1997.
446. Zenisek D, Davila V, Wan L, Almers W. Imaging calcium entry sites and ribbon structures in two presynaptic cells. *J Neurosci* 23: 2538-2548, 2003.
447. Zhang B, Naik JS, Jernigan NL, Walker BR, Resta TC. Reduced membrane cholesterol limits pulmonary endothelial Ca(2+) entry after chronic hypoxia. *Am J Physiol Heart Circ Physiol* 312: H1176-H1184, 2017.
448. Zhang DX, Mendoza SA, Bubolz AH, Mizuno A, Ge ZD, Li R, Warltier DC, Suzuki M, Gutterman DD. Transient receptor potential vanilloid type 4-deficient mice exhibit impaired endothelium-dependent relaxation induced by acetylcholine in vitro and in vivo. *Hypertension* 53: 532-538, 2009.
449. Zhang H, Park Y, Wu J, Chen X, Lee S, Yang J, Dellsperger KC, Zhang C. Role of TNF-alpha in vascular dysfunction. *Clin Sci (Lond)* 116: 219-230, 2009.
450. Zhang L, Papadopoulos P and Hamel E. Endothelial TRPV4 channels mediate dilation of cerebral arteries: impairment and recovery in cerebrovascular pathologies related to Alzheimer's disease. *Br J Pharmacol* 170: 661-670, 2013.
451. Zhang L, Peppel K, Sivashanmugam P, Orman ES, Brian L, Exum ST, Freedman NJ. Expression of tumor necrosis factor receptor-1 in arterial wall cells promotes atherosclerosis. *Arterioscler Thromb Vasc Biol* 27: 1087-1094, 2007.
452. Zhang L, Sivashanmugam P, Wu JH, Brian L, Exum ST, Freedman NJ, Peppel K. Tumor necrosis factor receptor-2 signaling attenuates vein graft neointima formation by promoting endothelial recovery. *Arterioscler Thromb Vasc Biol* 28: 284-289, 2008.
453. Zhang T, Chi S, Jiang F, Zhao Q, Xiao B. A protein interaction mechanism for suppressing the mechanosensitive Piezo channels. *Nat Commun* 8: 1797, 2017.
454. Zhang Y, Zhao J, Lau WB, Jiao LY, Liu B, Yuan Y, Wang X, Gao E, Koch WJ, Ma XL, Wang Y. Tumor necrosis factor-alpha and lymphotoxin-alpha mediate myocardial ischemic injury via TNF receptor 1, but are cardioprotective when activating TNF receptor 2. *PLoS One* 8: e60227, 2013.
455. Zhao Q, Wu K, Geng J, Chi S, Wang Y, Zhi P, Zhang M, Xiao B. Ion Permeation and Mechanotransduction Mechanisms of Mechanosensitive Piezo Channels. *Neuron* 89: 1248-1263, 2016.

456. Zielonka J, Sikora A, Joseph J, Kalyanaraman B. Peroxynitrite is the major species formed from different flux ratios of co-generated nitric oxide and superoxide: direct reaction with boronate-based fluorescent probe. *J Biol Chem* 285: 14210-14216, 2010.